1977

The dynamical evolution of gas clouds undergoing radiative acceleration near compact luminous objects

Michael Robert Haas
Iowa State University

The dynamical evolution of gas clouds undergoing radiative acceleration near compact luminous objects

by

Michael Robert Haas

A Dissertation Submitted to the
Graduate Faculty in Partial Fulfillment of
The Requirements for the Degree of
DOCTOR OF PHILOSOPHY

Major: Physics

Approved:

Signature was redacted for privacy.

In Charge of Major Work

Signature was redacted for privacy.

For the Major Department

Signature was redacted for privacy.

For the Graduate College

Iowa State University
Ames, Iowa

1977

TABLE OF CONTENTS

LIST OF TABLES

LIST OF FIGURES

NOMENCLATURE

a	Radius of spherical cloud
$\dot{a}$	Rate of cloud expansion, $\dot{a} = da/dt$
A	Ratio of the squares of the cloud expansion time and the acceleration time, $A = t^2_{exp}/t^2_{acc}$ (Equation 2.19)
B	Magnetic field; constant defined by Equation 2.13
c	Speed of light
c_c	Adiabatic speed of sound in cloud
c_{ic}	Adiabatic speed of sound in intercloud medium
c_L	Local adiabatic speed of sound
c_o	Initial adiabatic speed of sound
c_p	Specific heat at constant pressure
c_T	Isothermal speed of sound
C_Q	Constant specifying the strength of the artificial viscous pressures in the gasdynamic computer code
d	Earth-QSO luminosity distance
D	Characteristic dimension of the flow region
e	Specific internal energy; electron electric charge; base of Napierian logarithms
e_{ic}	Specific internal energy of intercloud medium
E	Total energy per unit mass
f	Oscillator strength
F_{ic}	Photon flux produced by radiative cooling of high-temperature intercloud medium
F_{QSO}	Photon flux from QSO continuum source

F_{shock} Photon flux produced by radiative cooling of shock-heated intercloud gas

F_x X-ray flux at the Earth produced by high-temperature intercloud gas

F_ν F_{QSO} as a function of frequency

g Effective acceleration (Equations 6.1 and 6.4)

$\vec{g}$ External accelerations (g_x and g_y are the x- and y-components)

g_{ff} Gaunt factor for free-free emission

G Gravitational constant (6.67×10^{-8} dynes cm^2 g^{-2})

G_{drag} Deceleration due to drag of intercloud medium

G_{grav} Deceleration due to gravitational attraction of mass within sphere of radius r

G_{rad} Radiative acceleration

GC The ratio of the radiative acceleration due to bound-free absorption and electron scattering to the gas density (ρ) for a static, optically thin gas (Figure 4)

GCL The ratio of the total radiative acceleration to the gas density (ρ) for a static, optically thin gas (Figure 4)

h Planck's constant (6.626×10^{-27} erg sec)

HI Neutral hydrogen

k Boltzmann's constant (1.381×10^{-16} ergs $^\circ K^{-1}$)

ℓ Stopping length for drag-decelerated cloud of constant size (cf Equation 3.2)

L Cloud length in radial direction; total photon luminosity of QSO continuum source,

$$L = \int_0^\infty L(\nu)\,d\nu$$

L_{ic} Photon luminosity produced by radiative cooling of the high-temperature intercloud medium

L_{ion} Ionizing photon luminosity of QSO continuum source, $L_{ion} = \int_{\nu_0}^{\infty} L(\nu)d\nu$ where ν_0 = frequency of Lyman continuum edge

L_{QSO} Total photon luminosity of QSO continuum source

$L(\nu)$ QSO photon luminosity as a function of frequency

m Mass of cell in computational grid

m_c Mass of cloud

m_e Electron mass

m_o Mass of 1 amu

m_p Proton mass

M Mach number; central gravitating point mass in Appendix A

M_c Mach number of coherently moving cloud

$\bar{M}_n$ Momentum-averaged Mach number for 5% of cloud by mass (cf Equation 5.4)

M_p Mach number of piston (or cloud) driving a one-dimensional flow

M_{QSO} Mass of QSO (really the mass within a sphere of radius r)

M_∞ Terminal Mach number for drag-decelerated cloud; free stream Mach number

$M_\odot$ Mass of the sun

n Number density in atoms (or positive ions) per cm^3

n_c Number density n in cloud

n_e Electron number density

n_{ic}	Number density n in intercloud medium
P, P_g	Thermal gas pressure
P_c	Thermal gas pressure in cloud
P_{ic}	Thermal gas pressure in intercloud medium
P_r	Radiation pressure
Pe	Peclet number (Equation 3.12)
r	Radial distance, usually from cloud to center of QSO continuum region
R	Radius of high-temperature region in which clouds are embedded
Re	Reynold's number (Equation 3.22)
s	Time measured in units of cloud expansion times, $s = c_c(0)t/a_o$
t	Time in seconds
t_{cool}	Characteristic time for a high-temperature gas to cool to its radiative equilibrium temperature
t_{flow}	Characteristic flow time, $t_{flow} = D/U$
T	Temperature; fluctuation time of QSO continuum in Chapter I
$T(\xi)$	Photoionization equilibrium temperature (cf Figure 6)
T_c	Temperature in cloud
T_e	Electron temperature
T_{ic}	Temperature in intercloud medium
T_s	Stagnation temperature; postshock temperature in one-dimensional flow
u	Eulerian or transverse (x) velocity
U	Characteristic velocity of flow region

v	Radial velocity (Lagrangian (y) velocity in gasdynamic code)
v_c	Radial velocity of coherently moving cloud
$v_\perp$	Velocity perpendicular to direction of magnetic field
v_∞	Terminal velocity
V	Volume of cell in computational grid
x	Eulerian or transverse coordinate in computational grid
y	Lagrangian or radial coordinate in computational grid
z_{abs}	Absorption line redshift, $z_{abs} = \lambda - \lambda_o/\lambda_o$ where λ_o is the rest wavelength of the line
z_{em}	Emission line redshift
α	Spectral index
β	Constant defined by Equation 2.10, $\beta = G_{rad}/n$ ($\beta_{continuum} = \beta/5$ includes only the contribution of bound-free absorption)
γ	Adiabatic index, $\gamma = 5/3$ throughout; $\gamma = (1-v^2/c^2)^{-1/2}$ in Chapter I
ε	Energy radiated per cm^3 per sec by a hot gas
κ	Coefficient of thermal conductivity
λ	Wavelength; mean free path
Λ	Cooling rate or rate of kinetic energy loss per cm^3 of gas per sec
Λ_c	Cutoff factor resulting from the ineffectiveness of particle encounters beyond some critical distance
μ	Mean mass of gas per particle; coefficient of viscosity
μ_i	Mean mass of gas per positive ion

ν	Frequency
ξ	Ratio of photon flux to gas density, $\xi = L_{ion}/nr^2$
ξ_c	ξ in cloud
ξ_{ic}	ξ in intercloud medium
ρ	Mass density in g cm^{-3}
ρ_c	Mass density in g cm^{-3} in cloud
ρ_{ic}	Mass density in g cm^{-3} in intercloud medium
ρ_s	Stagnation mass density in g cm^{-3}; postshock mass density in g cm^{-3} for a one-dimensional flow
$\sigma(\nu)$	Total cross section at frequency ν
σ_o	Cross section for HI at the Lyman continuum edge
$\tau(\nu)$	Optical length at frequency ν, $\tau(\nu) = \int \sigma(\nu)\ n\ dr$
τ_c	Optical depth at the Lyman continuum edge
τ_ℓ	Optical depth at line center (Equation 3.25)
τ_o	Initial optical depth of cloud at Lyman continuum edge
Ω	Scale factor (Chapter III.E)

I. INTRODUCTION

A. General Introduction

The emission lines observed in the spectra of quasi-stellar objects (QSOs) are generally very broad and highly redshifted. The redshift is defined as $z = (\lambda-\lambda_o)/\lambda_o$, where λ is the wavelength observed for a spectral feature whose rest wavelength is λ_o. The most widely accepted interpretation of these redshifts is that they are cosmological and therefore they imply that the QSOs are extremely distant. The widths of these lines, if attributed to Doppler broadening, imply velocity dispersions in excess of 1000 km/sec within the emitting gas. Observations suggest that similar high velocity gas flows occur in other compact, luminous objects (Burbidge 1970; Burbidge 1972; Morgan 1972) such as Seyfert galaxies (Osterbrock and Parker 1965; Oke and Sargent 1968; Walker 1968a; Anderson 1970; Khachikian and Weedman 1974), N-galaxies, and radio galaxies (Osterbrock et al. 1975, 1976).

In addition to these emission features, some QSOs also possess narrow absorption lines. In almost every case, the absorption line redshift (z_{abs}) is less than the emission line redshift (z_{em}). If this is a Doppler effect, then the absorbing gas must be moving away from the center of the emission region at a speed which often exceeds one-tenth the speed of light. Yet the narrow widths of the absorption

lines limit the velocity dispersion in this gas to less than 50 km/sec. Such displaced absorption lines have also been observed in the spectra of two Seyfert galaxies (Anderson and Kraft 1969; Arakelian et al. 1971; Adams 1972; Adams and Weedman 1972). It is difficult to understand how large masses of gas can be coherently accelerated to such high velocities.

The possibility of explaining these observations in terms of radiation-pressure-accelerated gas clouds has received considerable attention in the literature (references in Chapter I.C). However, much of this work consists of equilibrium calculations for one-dimensional, static slabs of gas. The existing dynamical calculations employ extremely simple cloud models. In this thesis, a two-dimensional, gasdynamic computer code is used to study the dynamical evolution of gas clouds undergoing radiative acceleration. It is assumed that the clouds are optically thin and that they are confined by either the ram pressure or the thermal pressure of the external medium. Justification for such a model comes from both the observations (see Chapter I.B) and from theoretical considerations (see Chapter I.C). Whenever specific parameter choices are required, those believed to be representative of QSOs are used because these objects represent the most

severe test of any proposed acceleration mechanism. However, most of the results are equally applicable to other compact, luminous objects. The remainder of this chapter presents a brief review of the QSO observations, their deduced structure, alternate explanations for the wide emission lines and the highly displaced absorption lines, and a review of the past work on radiation pressure.

B. The Morphology of QSOs

Since the QSOs are essentially stellar in appearance, their structure is inferred from observations of the continuous spectrum and the superposed emission and absorption features. For some QSOs the observations range over frequencies from the radio to the optical; for 3C 273 they extend to the X-ray portion of the spectrum. Thus far, few lines have been observed outside of the optical window.[1] Here the emission lines account for approximately ten percent of the flux and the remainder is continuum (Oke et al. 1970). The majority of the QSOs have a strongly polarized optical continuum (Appenzeller and Hiltner 1967; Visvanathan 1973) which can be fit by a power law, $\nu^{-\alpha}$, where α ranges from about 0.2 to 1.6

[1] Paschen-α has recently been detected in the infrared for 3C 273 (Grasdalen 1976) and the 21 cm line of hydrogen has been seen in 3C 286 (Brown and Roberts 1973).

(Oke et al. 1970). This distinctly nonthermal spectrum is generally attributed to electron synchrotron emission.

Some QSOs exhibit large flux variations in both the optical (Goldsmith and Kinman 1965; Kinman et al. 1968; Schmidt 1969; Elliot and Shapiro 1974) and the radio (Kellermann and Pauliny-Toth 1968; Harris 1972; Kellermann 1972) continuum in a time, T, which may be as short as a few days. This sets an upper limit on their radius of $2c\gamma T$, where $\gamma = (1-v^2/c^2)^{-1/2}$, c is the speed of light, and v is the speed of the light emitting surface (Burbidge and Burbidge 1967). Unless these sources are experiencing highly relativistic expansions (Burbidge 1973a), they are most likely only a few light days ($\simeq 10^{16}$ cm) across. Considerably smaller sizes ($\lesssim 10^{14}$ cm) are ruled out by the Schwarzschild limit (Elliot and Shapiro 1974).

The Harvard historical plate collection shows that a number of QSOs have existed for at least 90 years (Angione and Smith 1972). One can argue on the basis of the large scale radio structure and the number of sources that the lifetime of the QSO phenomena is at least 10^6 years. The distance to the QSOs is still uncertain (Burbidge 1973a), but if they are at their cosmological distances, then they are extremely luminous ($\leq 10^{47}$ ergs/sec). Energetics then forces one to set lower limits

on the mass of 10^6 to 10^8 $M_\odot$. The rotation curves of Seyfert galaxies indicate central masses greater than 10^8 $M_\odot$ (references in Eilek (1975)). No generally acceptable model of this central region exists. For a review of early work see Burbidge (1970); for two recent proposals see Arons et al. (1975) and Colgate et al. (1975). In this thesis the continuum source is treated as a "black box" which emits a large flux of ultraviolet photons capable of ionizing and accelerating the surrounding gas.

The gas producing the emission lines is believed to occupy a larger volume than the continuum source. The most direct evidence for this is that in at least some QSOs the emission line strengths remain constant during the continuum fluctuations (Sandage et al. 1966; Burbidge and Burbidge 1967; Oke 1967; see Baldwin et al. (1973) and Chan (1974) for possible counterexamples). If the QSOs are at the cosmological distances given by their redshifts, then direct photographs set the upper limit for the size of this region at about 10 kpc (Kristian 1973; Scargle et al. 1974; Wampler et al. 1975).

Many QSOs have emission line profiles (Burbidge and Burbidge 1967; Baldwin 1975) similar to those observed in class 1 Seyfert galaxies (Khachikian and Weedman 1974). The Balmer lines and other permitted lines

consist of a narrow component superposed on very broad wings. The forbidden line profiles are similar to the permitted line cores. This is generally cited as evidence that the gas distribution is clumpy (Osterbrock and Parker 1965; Oke and Sargent 1968). That is, the narrow lines are formed in a region where the electron density is low and the broad wings are formed in a region of high electron density ($n_e \gtrsim 10^8$ cm^{-3}) where the forbidden lines are suppressed by collisional de-excitation. This latter density is several orders of magnitude larger than the average density derived from the emissivity of the Balmer lines and the size of the emission region (examples in Osterbrock 1971; Blumenthal and Mathews 1975; McKee and Tarter 1975). This also supports the idea of clouds or filaments and suggests that they occupy only a small fraction (10^{-5} to 10^{-2}) of the total volume. The wide range of ionization states observed in any one object also implies that the gas is stratified (Burbidge and Burbidge 1967). Static models are able to reproduce the observed line strengths if the emitting gas is assumed to exist in two distinct phases and to be in photoionization equilibrium with the ultraviolet radiation of the small, central source (Davidson 1972, 1973; MacAlpine 1972; Scargle et al. 1974; Chan and Burbidge 1975; for Seyferts

see Shields and Oke 1975). Finally, in Seyfert nuclei the emission line cores exhibit structure which demonstrates the existence of fast-moving cloud complexes of ionized gas (Walker 1968a,b; Osterbrock 1971; Burbidge 1972).

The forbidden lines and the permitted line cores have Doppler widths of a few 100 km/sec (Khachikian and Weedman 1974; Baldwin 1975). The preferred broadening mechanism is large scale mass motions or turbulence. Significant thermal broadening would require temperatures ($\gtrsim 10^6$ °K) considerably greater than those ($\simeq 2\times10^4$ °K) indicated by the relative line strengths.

The permitted line wings often have widths of 5000 km/sec or more (Khachikian and Weedman 1974; Baldwin 1975; Osterbrock et al. 1975). Electron scattering (Mathis 1970; Weymann 1970) may be responsible for producing these profiles, particularly the smooth, symmetric ones observed for many objects (Adams 1973; Baldwin 1975). However, Blumenthal and Mathews (1975) show that these profiles can be equally well fit by a model which employs a large number of small, confined clouds driven by radiation pressure. This, along with the fact that some of the observed profiles are asymmetric (Walker 1968b; Burbidge 1972; Baldwin 1975; Osterbrock et al. 1975), favors large

scale mass motions as the principal broadening agent. Many other broadening agents have been proposed that can account for a subset of the observed line profiles. The theses by Baldwin (1975) and by Adams (1973) contain excellent discussions and references.

Before moving on to the absorption spectra, it is worth emphasizing once again that the continuum and emission features of QSOs are very similar to those of Seyfert galaxies, N-galaxies, radio galaxies, and other active galactic nuclei. This implies that the physics of all these objects is very similar and the differences only a matter of degree. Many additional references beyond those already cited, as well as excellent discussions, can be found in the published review articles by Burbidge (1967), Kellermann and Pauliny-Toth (1968), Schmidt (1969), Burbidge (1970), and Strittmatter and Williams (1976) and in the conference proceedings edited by Pacholczyk and Weymann (1968), O'Connell (1971), and Evans (1972).

The fraction of QSOs possessing absorption lines and the number of lines per object seems to increase sharply with z_{em} (McCrea 1968; Lynds 1972). However, this may be an observational selection effect because Lyman-α and a number of other strong resonance lines fall in the optical window only for large z_{abs} (Bahcall 1971; Basu 1973). In

the complex absorption spectra of the large redshift QSOs it is often possible to identify five to ten distinct redshift systems (Lowrance et al. 1972; Bahcall and Joss 1973; Baldwin et al. 1974; Aaronson et al. 1975; Carswell et al. 1975; Oemler and Lynds 1975; Wingert 1975). This implies the existence of discrete clouds or filaments along the line of sight. (High velocity shells of gas are presumably less stable and would soon fragment.)

The number of individual clouds may be quite large. Lynds (1971, 1972) has pointed out that many of the lines which remain unidentified in these spectra lie shortward of the Lyman-α emission line and may be due to Lyman-α in separate clouds which lack sufficient optical depth to produce other detectable features (Baldwin et al. 1974; Oemler and Lynds 1975; Wingert 1975). Also, under high resolution many of the lines are found to be double or multiple (Morton and Morton 1972; Morton and Richstone 1973; Boksenberg and Sargent 1975).

Some absorption lines lie in the wings of emission lines and yet are black at line center (Chan and Burbidge 1971; Lowrance et al. 1972; Baldwin et al. 1974; Boksenberg and Sargent 1975). This implies that the corresponding absorption regions are large in size and lie outside of the emission region. Unfortunately, just how

far outside is unknown. The absorbing gas may be relatively near and physically associated with the QSO (the "intrinsic" hypothesis), or it may be far from the QSO and lie in the line of sight only by chance (the "cosmological" or "intervening" hypothesis).

The physical conditions in the absorbing gas give clues as to its location. Bahcall and Wolf (1968) have shown that the presence or absence of excited fine structure states allows limits to be set on the density of the gas if collisionally excited and on the photon flux if the gas is photoionized. Lines from excited fine structure transitions may be present in 3C 191 (Stockton and Lynds 1966; Bahcall et al. 1967; Williams et al. 1975), OQ 172 (Baldwin et al. 1974), PHL 957 (Grewing and Strittmatter 1973; Wingert 1975), 1331 + 170 (Strittmatter et al. 1973), and PKS 0237-23 (Boksenberg and Sargent 1975). This has traditionally been cited as evidence that the absorption is intrinsic, as the inferred gas densities are higher than those expected in intervening matter (Bahcall and Wolf 1968; Morton et al. 1972; Smith 1972; Baldwin et al. 1974; Wingert 1975; but see Bahcall et al. (1973a) and Aaronson et al. (1974)). The inferred distance of the absorbing gas is typically 1 kpc or greater (Bahcall et al. 1967; Williams et al. 1975).

Even though absorption system A of PHL 957 shows evidence for some fine structure levels being populated, it may well be an HI cloud in an intervening spiral galaxy (Grewing and Strittmatter 1973; Wingert 1975). This latter interpretation is supported by observations that the neutral hydrogen column density is unusually large ($N(HI) = 1.0 \pm 0.5 \times 10^{21}$ cm^{-2}) and that the level of excitation is very low. Many neutral species (Grewing and Strittmatter 1973; Aaronson et al. 1975; Wingert 1975) and possibly molecular hydrogen (Aaronson et al. 1974) are present.

There is a wide range of ionization observed in any one absorption line system and conditions seem to vary significantly from one to the next. Low, moderate, and high excitation systems have been identified, but there appears to be no correlation with the redshift difference, $z_{em}-z_{abs}$ (Cohen 1973). McKee et al. (1973) have calculated the line strengths expected for an optically thin gas which is either in photoionization equilibrium in a specified radiation field or in collisional equilibrium at a given temperature. Comparing their results with observations of 4C 05.34, they conclude that the absorption regions are photoionized and that they lie at distances of a few hundred kiloparsecs from the QSO. Cohen (1973) has argued that the almost universal presence of Lyman-α as the

strongest line suggests that photoionization is generally the dominant excitation mechanism (see also Bahcall et al. 1973b). She concludes that the absorbing gas must be within 1 Mpc of the QSOs.

If the redshift difference, $z_{em}-z_{abs}$, is due to the Doppler effect, then the implied velocity of separation of absorber and emitter is given by the standard relativistic formula (Bahcall et al. 1967)

$$v = c \frac{(1+z_{em})^2-(1+z_{abs})^2}{(1+z_{em})^2+(1+z_{abs})^2} . \qquad (1.1)$$

This velocity is plotted in Figure 1 for the well-established systems as recently compiled by Burbidge and Burbidge (1975). The two Seyfert galaxies possessing absorption lines have been included. As already noted, these velocities are extremely large compared to the narrow widths ($\lesssim$ 50 km/sec) (Chan and Burbidge 1971; Morton and Morton 1972; Boksenberg and Sargent 1975; Oemler and Lynds 1975; Wingert 1975) of the lines. This small dispersion is a much more severe constraint for the intrinsic models than for the intervening ones.

If the absorption regions are intrinsic to the QSOs, then the interpretation of the redshift difference as a Doppler effect is almost certainly correct, as the requisite

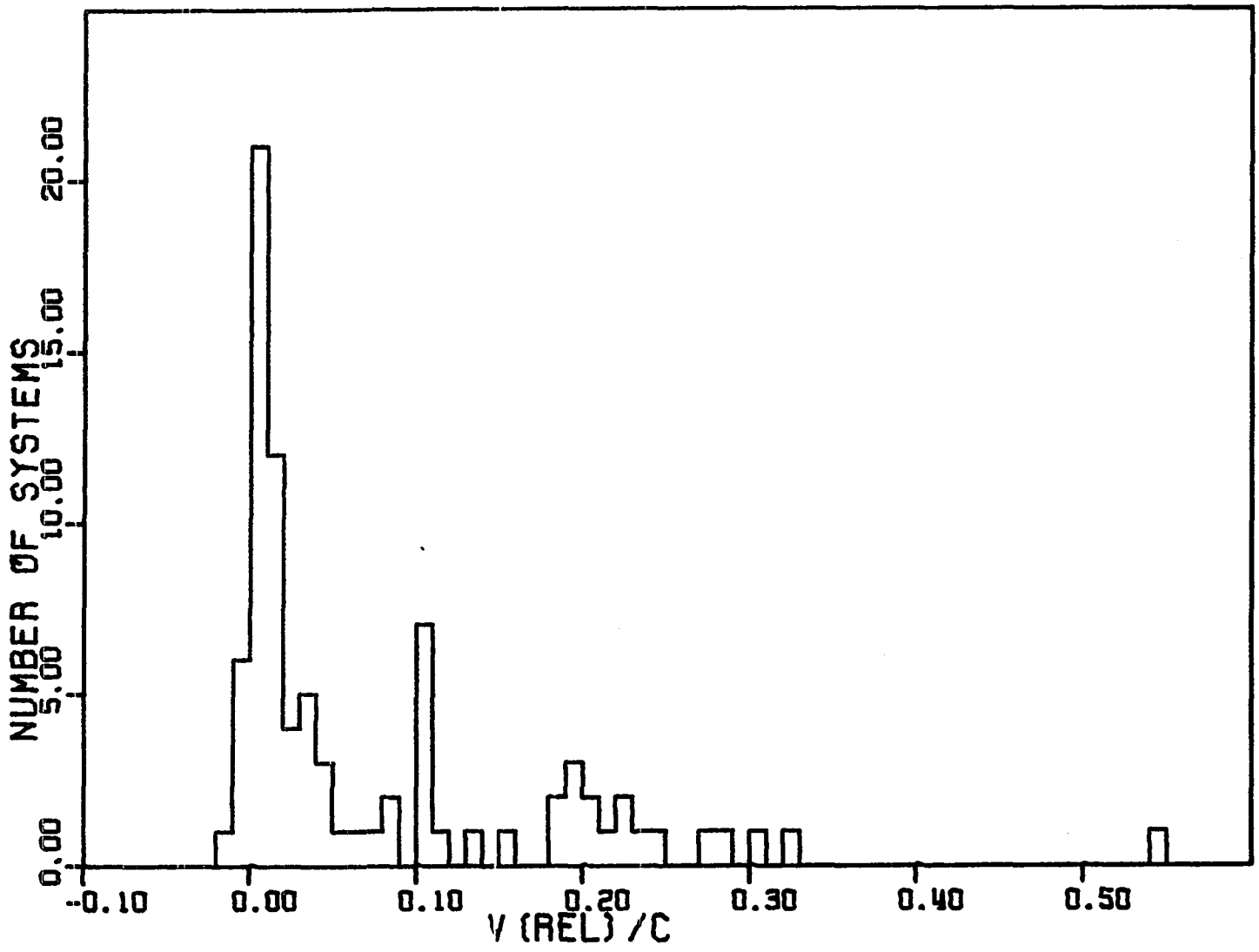

Figure 1. A histogram displaying the relative velocities of the absorption and emission regions as implied by their redshifts (normalized to c, the speed of light)

gravitational redshifts seem untenable (Fackerell 1968; Ipser and Thorne 1968; Ipser 1969a,b; Bisnovatyi-Kogan and Zel'dovich 1969; but see Ross (1973) for another alternative). In the event that the absorption regions are intervening, the difference in redshifts is probably a result of the cosmological expansion of the universe, or possibly the relative motion within a cluster of galaxies containing the QSO (Bahcall 1971). Proposed sources of intervening matter are the interstellar medium in normal galaxies (Shklovsky 1967; Wagoner 1967; Roeder and Verreault 1968), protogalaxies (Arons 1972), and dead galaxies (Peebles 1968), the intergalactic gas in clusters of galaxies (Bahcall and Salpeter 1965, 1966), and galactic halos (Bahcall and Spitzer 1969; Bahcall 1975). The observational data have been compared with the predictions of various cosmologies to determine the validity of the intervening hypothesis (Bahcall and Peebles 1969; Burbidge and Burbidge 1969; Bahcall 1971; Roeder 1972). The lack of a sufficiently large sample and unknown evolutionary effects have prevented any firm conclusions to be drawn.

A strong case can be made that a few of the absorption systems with low excitation and $z_{em} >> z_{abs}$ are cosmological. On the other hand, the large number of systems with $z_{em} \approx z_{abs}$ are almost certain intrinsic. This

has led Bahcall (1971) to suggest that possibly both intervening and intrinsic systems exist. Ignoring the few highest velocity systems thus seems legitimate, and eases somewhat the requirements of any proposed acceleration mechanism. This truncation of the velocity distribution in Figure 1 leaves a range of velocities reminiscent of those observed in emission. Furthermore, the bulk of the observations suggest that the absorbing and emitting gases are both in the form of clouds with similar physical conditions and that they are both photoionized by the central, continuum source. Therefore, an attractive idea is that a common acceleration mechanism is operating. It is natural to consider radiation pressure acceleration because of the large photon fluxes associated with QSOs and because of the possibility that it acts uniformly throughout the gas (if the optical depth is small), thereby producing the requisite highly coherent flows seen in absorption.

C. Previous Work on Radiation Pressure Acceleration

Ultraviolet observations of O and B stars in the late 1960's found that the resonance lines of many ions have P Cygni profiles (Morton 1967a,b; Morton et al. 1968; Stecher 1970). That is, a blue-shifted absorption component lies in the wing of an undisplaced emission line.

This confirmed other evidence (Morton 1967a) that the hot stars are losing mass and indicated terminal velocities for these flows near 2500 km/sec. Lucy and Solomon (1970) pointed out that radiation pressure due to resonance line scattering could account for these observations (see also Lucy (1971) and Cassinelli and Castor (1973)). At least two QSOs, PHL 5200 and RS 23, possess similar P Cygni line profiles. Scargle et al. (1970; see also Caroff et al. (1972) and Noerdlinger and Scargle (1972)) demonstrated that such profiles could be understood as the transfer of resonance line radiation through a differentially expanding atmosphere.

Mushotzky et al. (1972) estimated the strength of the radiative force due to individual lines and concluded that it was sufficient to produce gas flows of 10^4 km/sec. Detailed ionization equilibrium calculations for an optically thin gas by Tarter and McKee (1973), by Kippenhahn et al. (1974), and by Mathews (1974) found even larger accelerations. Although the results depend somewhat on the chosen shape of the ionizing spectrum, on the assumed elemental abundances, and on the details of the calculational procedure, it was generally concluded by these authors that the radiative acceleration is roughly proportional to the gas density. It does not depend on the distance to the ionizing source

because the $1/r^2$ dilution of the radiation is cancelled by an approximately r^2 growth in the fraction of recombined species. As pointed out by Mathews (1974), this dependence of the radiative acceleration on the gas density leads to a natural explanation of the observation that the velocity dispersion is considerably greater in the emitting region producing the permitted lines than in that producing the forbidden ones.

Williams (1972) was one of the first to point out a difficulty with acceleration by radiation pressure. He calculated the radiative force as a function of line optical depth in static, uniform slabs of gas assumed to be thin to continuum radiation but thick in the lines. He found that under the conditions believed to exist in QSOs, the outward diffusion of internally created photons is large enough to disrupt the clouds. Weymann (1973, 1976) employed a different approach to the same problem and reached a similar conclusion. However, he argued (Weymann 1976; see also Mathews (1976)) that at least for early times thermal pressure gradients within the clouds can counteract such differential forces providing the clouds are confined by an external pressure. McKee and Tarter (1975) considered the case where the continuum is optically thick. Here the internally created photons tend to blow off the portion of the cloud farthest from the QSO. This

occurs because at large optical depths the gas is essentially un-ionized and consequently it has the largest cross section per atom. They also found that a somewhat smaller disruptive force is exerted by the incident radiation on the gas in the ionization transition zones. Noerdlinger and Rybicki (1974) reported that qualitatively similar expansive forces occur in differentially expanding atmospheres. All of these calculations are one-dimensional and fail to include a proper treatment of the gasdynamics.

Mathews (1974) has computed trajectories for pure hydrogen clouds which are either thick or thin in the Lyman continuum. He showed that for a wide range of physical parameters such clouds have a characteristic expansion time which is much less than their acceleration time. Therefore terminal velocities are limited to about 1000 km/sec if the clouds are allowed to freely expand, but can reach $5\text{-}50 \times 10^3$ km/sec if the clouds are confined by some external pressure. While the latter model can account for the broad emission line wings, it falls short of the highest velocities seen in absorption. These conclusions are not significantly altered when the strength of the radiation pressure is increased by the inclusion of the heavy elements (see Chapter II, Kippenhahn et al. (1974) and McKee and Tarter (1975)). An alternative point of view is taken by Noerdlinger (1973, 1974), who argues that gas

pressure may be unimportant (but see Davidson (1972) and Weymann (1973)) and considers the relativistic ejection of single particles by radiation pressure (see also Nakada (1973) and Gordon (1975)).

As noted earlier, Blumenthal and Mathews (1975) have proposed a model for the emission line region which is able to reproduce the logarithmic line profiles observed for some QSOs. It depends on the continuous creation of large numbers of small, confined clouds accelerated by radiation pressure. Mathews (1976) has concluded that such clouds are stable to outward propagating sound waves.

Further support for the importance of radiation pressure comes from the idea that the line-locking mechanism (Scargle et al. 1970; Mushotzky et al. 1972; Scargle 1973; Weymann 1973) may be capable of trapping matter in velocity space and may thereby account for the sharpness of the absorption lines. A complete theory of line-locking has not been worked out, but there does appear to be observational evidence for its occurrence (Burbidge and Burbidge 1975; Williams et al. 1975). Another suggestive observation is the fact that the relative velocity of absorber and emitter appears to increase with increasing QSO luminosity (Kippenhahn et al. 1974).

It is possible that the discrete clouds are the result

of instabilities in a spherically symmetric wind or that they are swept out by such a flow. Various time-independent, galactic-wind models have been presented by Yahil and Ostriker (1973), Wolfe (1974), and Ipavich (1975). Mathews and Baker (1971) calculated nonsteady winds from normal elliptical galaxies. Kippenhahn, Mestel, and Perry (1975) dealt with steady-state, radiatively driven winds specifically applicable to QSOs. Weymann (1973) has reviewed some of the theoretical difficulties with such continuous flows. He points out that if the wind is at the temperature indicated by the forbidden lines ($\simeq 2 \times 10^4$ °K), then the radiative acceleration must remain relatively small until the flow becomes supersonic, at which point the opacity must increase drastically if the flow is to reach significantly greater velocities. This phenomenon, which does occur in the stellar solutions of Lucy and Solomon (1970) and has been called the "after-burner effect" by Cassinelli and Castor (1973), appears to be rather unlikely for the flat spectra of QSOs (Weymann 1973; McKee and Tarter 1975). Wind solutions can produce large velocities if the gas is very hot ($\gtrsim 10^8$ °K), but maintaining such temperatures throughout the flow is difficult. Possible heating mechanisms are bow shocks or collisions of discrete clouds (Osterbrock and Parker 1965; Oke and Sargent 1968; Daltabuit and Cox 1972). Such models may account for the P Cygni

profiles in objects like PHL 5200 (Scargle et al. 1970), but have not been reconciled with the narrow, detached absorption lines more representative of QSOs.

Variations of these wind models have also been considered. Rees (1970) has suggested that the absorption clouds may be condensations which form in and are trapped by the rapidly expanding remnants of radio clouds which have been ejected from the QSOs. Eilek (1975) has presented wind models driven by cosmic rays. She has treated the gasdynamics in some detail and has found velocities as large as 8000 km/sec. Velocities as large as 10^5 km/sec may be possible for discrete clouds accelerated by cosmic ray pressure (Eilek 1975; Eilek and Caroff 1976), but a more rigorous treatment of this problem is needed.

Many authors have dealt with the apparent failures and successes of radiation pressure, yet its role in accelerating QSO clouds is still unclear. One fact which seems fairly well established is that for radiation pressure to be important, the clouds must be confined by some external pressure (see Chapter II). The nature of this confining pressure is uncertain; suggestions include ram pressure, thermal gas pressure, magnetic fields, electromagnetic waves, and relativistic particles. Little attention has been paid to the dynamical effects of such pressures. A complete discussion is formidable, as it includes a

simultaneous treatment of the gasdynamics, the radiative transfer, and the ionization and thermal equilibrium.

Numerous studies of the radiative transfer and the ionization and thermal equilibrium exist (references given above). This thesis represents a preliminary investigation of the time-dependent evolution of gas clouds permitted to interact with an external medium. Confinement is either by ram pressure or by thermal gas pressure. For simplicity, the gas flow is assumed to be adiabatic and the radiative acceleration is approximated by the static, optically thin results of Tarter and McKee (1973). The validity of these approximations and the choices of initial conditions are discussed in Chapter III. Chapter IV gives some details of the two-dimensional, gasdynamic computer code. The results for the numerical models are presented in Chapter V. In Chapter VI the results are reexamined and summarized; the implications for radiation pressure acceleration are discussed.

II. FREELY EXPANDING CLOUDS

A. The Basic Equations

Mathews (1974) presented simple analytical models for the dynamical evolution of hydrogen clouds undergoing radiative acceleration. He concluded that the clouds must be confined by an external pressure if they are to reach velocities greater than 1000 km/sec. Because of the importance of this result, Mathews' work is critically re-examined and extended in this chapter. For the optically thin case Tarter and McKee's (1973) photoionization equilibrium cross sections are used in place of the hydrogen continuum cross section. This inclusion of the heavy elements increases the coupling of the radiation to the gas by an order of magnitude. For the optically thick case the general solution to the equation of motion is obtained numerically. It is shown that Mathews' limit of 1000 km/sec holds for both the optically thin and optically thick case for an arbitrary choice of cloud parameters. Furthermore, this result is shown to be rather independent of the details of the cloud expansion.

The clouds are assumed to be isothermal spheres of radius $a(t)$ and uniform density $\rho(t)$. Their masses are constant so $\rho(t) = \rho_o a_o^3/a^3(t)$, where subscripted zeros denote initial values. Under these idealized conditions

the dynamical form of the virial theorem (Spitzer 1968; Mathews 1974) is

$$a \frac{d^2a}{dt^2} = \frac{5P_c}{\rho} - \frac{5P_{ic}}{\rho} - \frac{4\pi}{3} \rho a^2 G, \tag{2.1}$$

provided that no magnetic fields are present. This equation can be solved for the cloud radius as a function of time once the pressure in the cloud, P_c, and the pressure in the intercloud medium, P_{ic}, are specified. For a freely expanding cloud ($P_{ic} = 0$) with negligible self-gravitation ($\rho a^2 < 10^{19}$ g/cm), Equation 2.1 reduces to

$$a \frac{d^2a}{dt^2} = 3c_c^2 , \tag{2.2}$$

where c_c is the adiabatic sound speed in the cloud. The gas is assumed to be highly ionized so that $\gamma = 5/3$.

For an isothermal expansion, c_c is constant and Equation 2.2 becomes

$$\frac{d^2a}{dt^2} = \frac{3c_o^2}{a} , \tag{2.3}$$

while for an adiabatic expansion it becomes

$$\frac{d^2a}{dt^2} = \frac{3c_o^2 a_o^2}{a^3} . \tag{2.4}$$

The former might be a more realistic approximation of the real situation, but the latter is more easily solved. Two integrations of Equation 2.4 yield

$$a(t) = a_o[(\frac{\dot{a}_o^2}{c_o^2} + 3)s^2 + 2(\frac{\dot{a}_o}{c_o})s + 1]^{1/2}, \qquad (2.5)$$

where $\dot{a}_o$ is the initial expansion rate of the cloud. The dimensionless variable $s = c_o t/a_o$ measures time in terms of the cloud's characteristic "expansion time". Equation 2.5 is plotted in Figure 2 for $\dot{a}_o = c_o$. Also plotted in Figure 2 are a numerical solution of Equation 2.3 with $\dot{a}_o = c_o$ and the linear expansion rule, $a(t) = a_o + c_o t$, used by Mathews (1974). The expansion is the greatest for the isothermal case because it is driven by the continuous input of thermal energy required to maintain the initial temperature.

The bulk motion of a cloud is in the radial direction, r, and is governed by the equation

$$\frac{d^2r}{dt^2} = G_{rad} - G_{grav} - G_{drag}\ , \qquad (2.6)$$

where G_{grav} represents the gravitational attraction of the QSO and G_{drag} represents the drag of the external medium. The remaining term, the radiation pressure acceleration, is

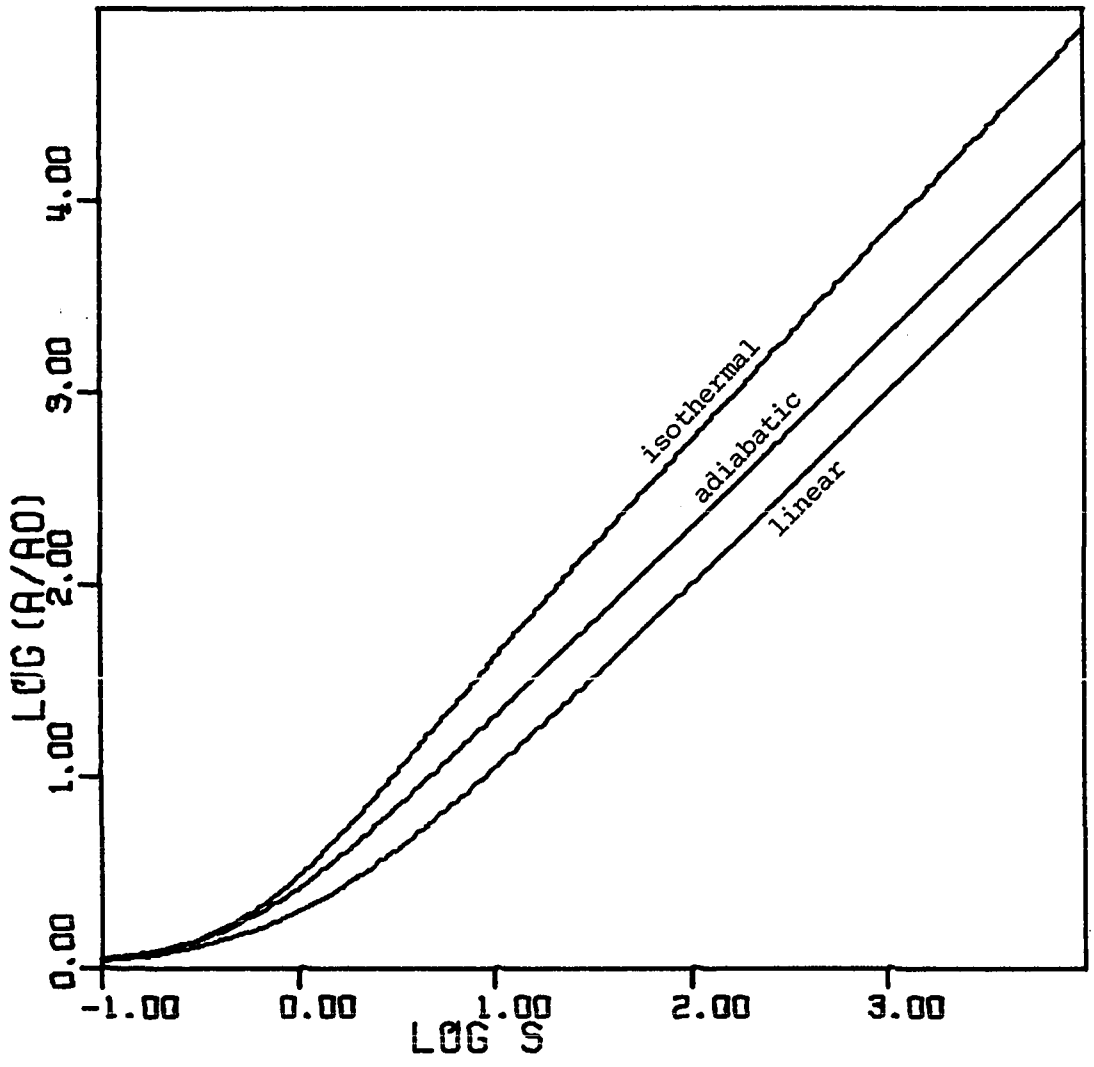

Figure 2. Normalized cloud radius a/a_o as a function of time s for three different expansion laws

$$G_{rad} = \int_0^\infty \frac{L(\nu)}{4\pi r^2 c} \frac{\pi a^2}{m_c} [1 - \exp(-\tau(\nu))]\, d\nu, \qquad (2.7)$$

where $L(\nu)$ is the QSO luminosity and $\tau(\nu)$ is the optical depth of the cloud, both functions of the frequency ν. Following Mathews (1974), geometrical factors of order unity are at times neglected. The cloud is regarded as spherical for dynamical purposes and as a slab for calculating the radiative transfer.

B. The Optically Thin Case

For the optically thin case, Equation 2.7 reduces to

$$G_{rad} = \frac{L_{ion}\sigma_{tot}}{4\pi r^2 c \mu_i m_o}, \qquad (2.8)$$

where $\sigma_{tot} = \langle\sigma_a\rangle + \sigma_{es}$ is the flux-averaged cross section. The electron scattering contribution is $\sigma_{es} = \sigma_T n_e/n$, where σ_T is the Thomson cross section (6.65×10^{-25} cm^2). The contribution of photoionization and line absorption is

$$\langle\sigma_a\rangle = \frac{1}{L_{ion}} \int_0^\infty L(\nu) [\Sigma_j \sigma_j(\nu)\, n_j/n] d\nu, \qquad (2.9)$$

where $\sigma_j(\nu)$ is the cross section for these processes for ion j at frequency ν. The value of this integral depends upon the ionization equilibrium in the gas through n_j,

the density of ion j.

The physical conditions in a low-density, optically thin gas in photoionization equilibrium depend upon the shape of the ionizing spectrum and on the parameter $\xi = L_{ion}/nr^2$ (Williams 1967; Tarter et al. 1969). Tarter and McKee (1973, hereafter referred to as TM) have evaluated the integral in Equation 2.9 as a function of ξ for a power-law spectrum with $\alpha = 1.5$. Their results (kindly supplied by Tarter (1975)) are displayed in Figures 3 through 6. Figure 3 shows the contributions of bound-bound absorption, bound-free absorption, and electron scattering to the total cross section. Notice that electron scattering is only important for highly ionized systems with $\xi > 2 \times 10^3$. It is probably not important in accelerating clouds, as it never exceeds gravity provided that $M_{QSO} > 7 \times 10^7 \, L_{46} M_\odot$ ($L_{46} = 10^{-46} \, L_{ion}$ erg/sec).

Using the sum of these cross sections in Equation 2.8 gives the total radiative acceleration. This is represented in Figure 4 by the curve labeled GCL. For gas optically thick in the lines, the radiative acceleration is approximated by the sum of the bound-free and electron scattering contributions and is shown in Figure 4 by the curve labeled GC. The cross section for bound-free absorption is roughly 1/4 that for bound-bound absorption over a wide range of ξ. The neutral hydrogen fraction is plotted in Figure 5 and the electron temperature is plotted in

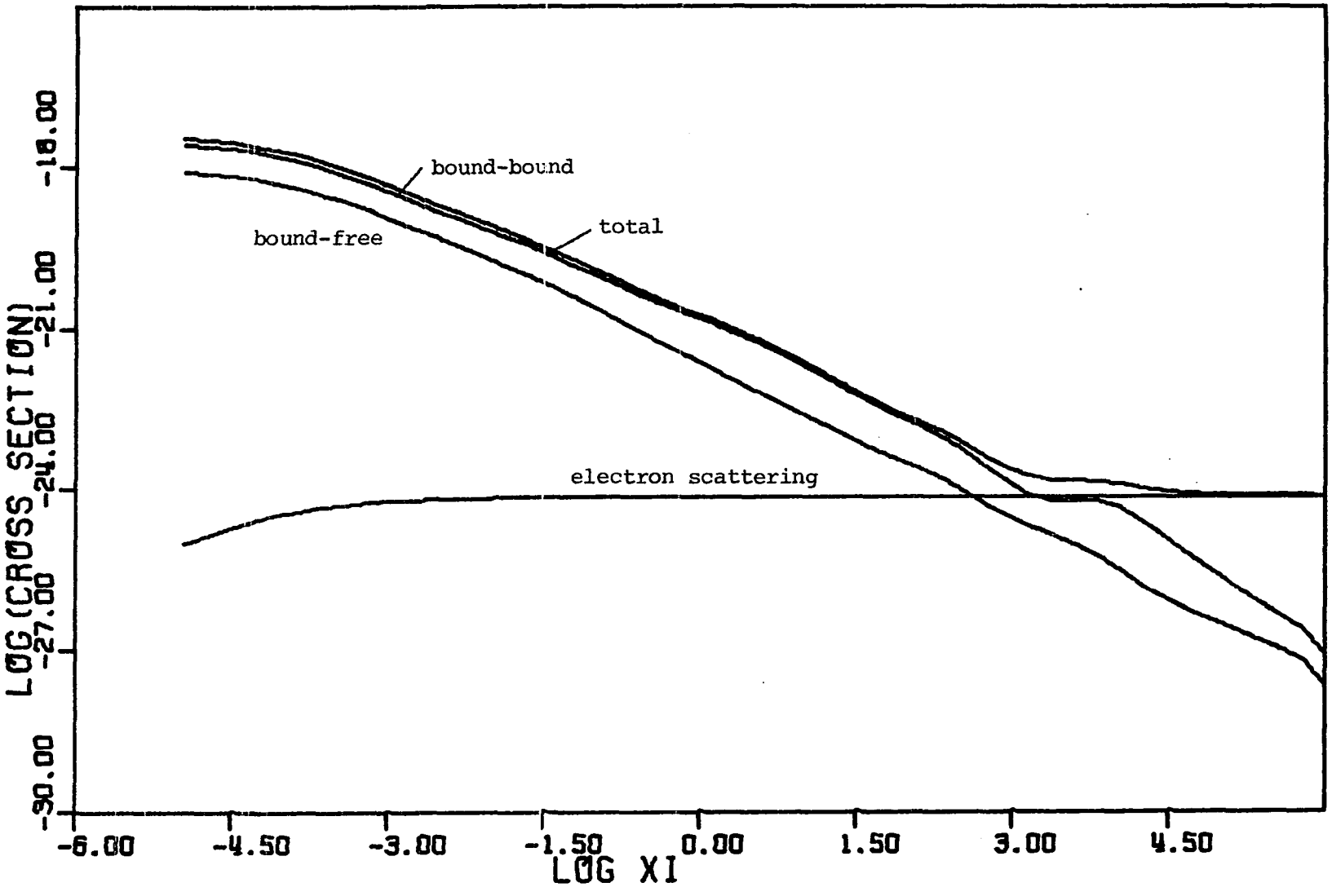

Figure 3. The cross section per atom as a function of ξ for an optically thin gas (TM)

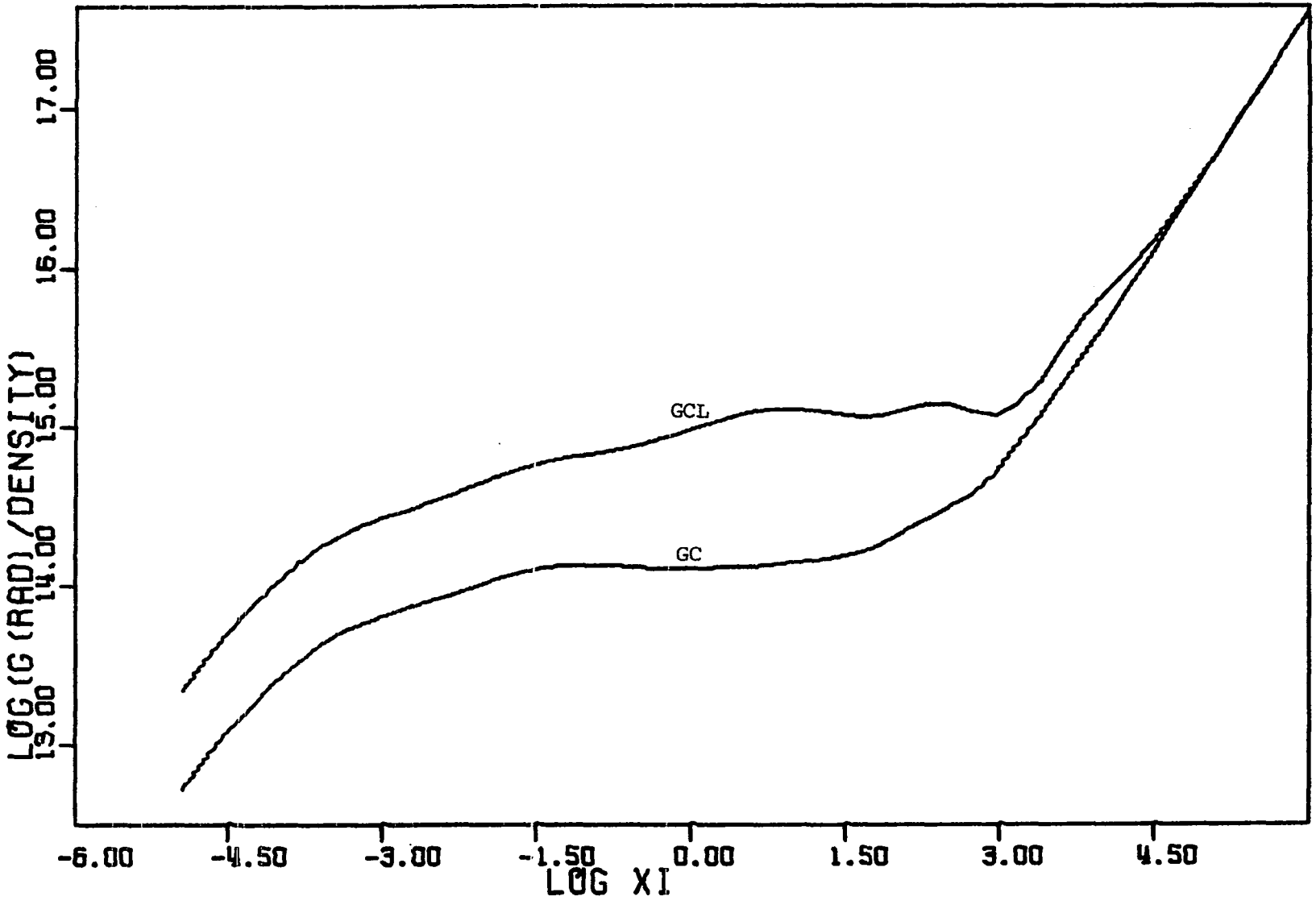

Figure 4. The radiative acceleration (divided by the gas density ρ) as a function of ξ for an optically thin gas (TM). GCL includes bound-bound absorption, GC does not

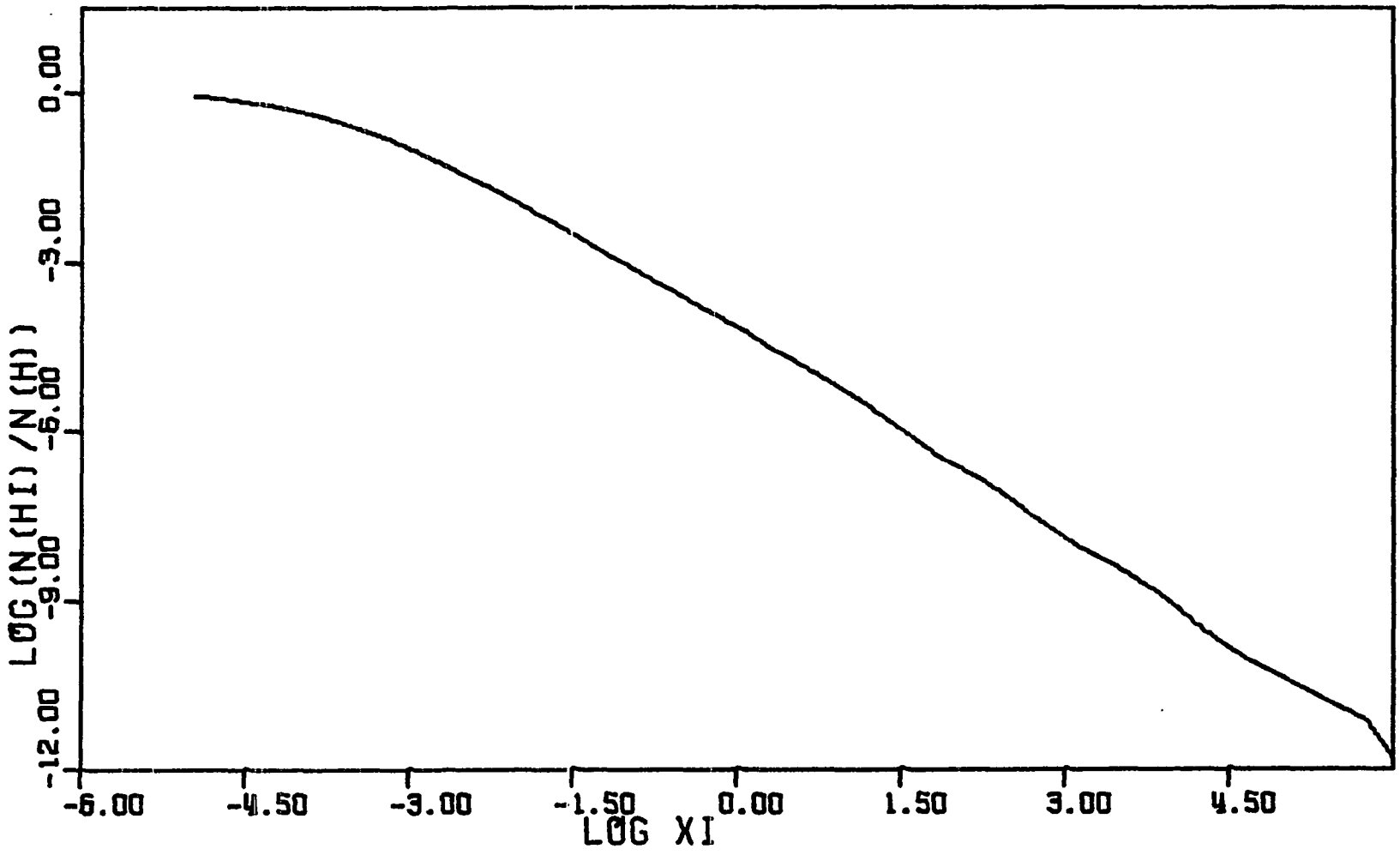

Figure 5. The neutral hydrogen fraction n(HI)/n(H) as a function of ξ for an optically thin gas (TM)

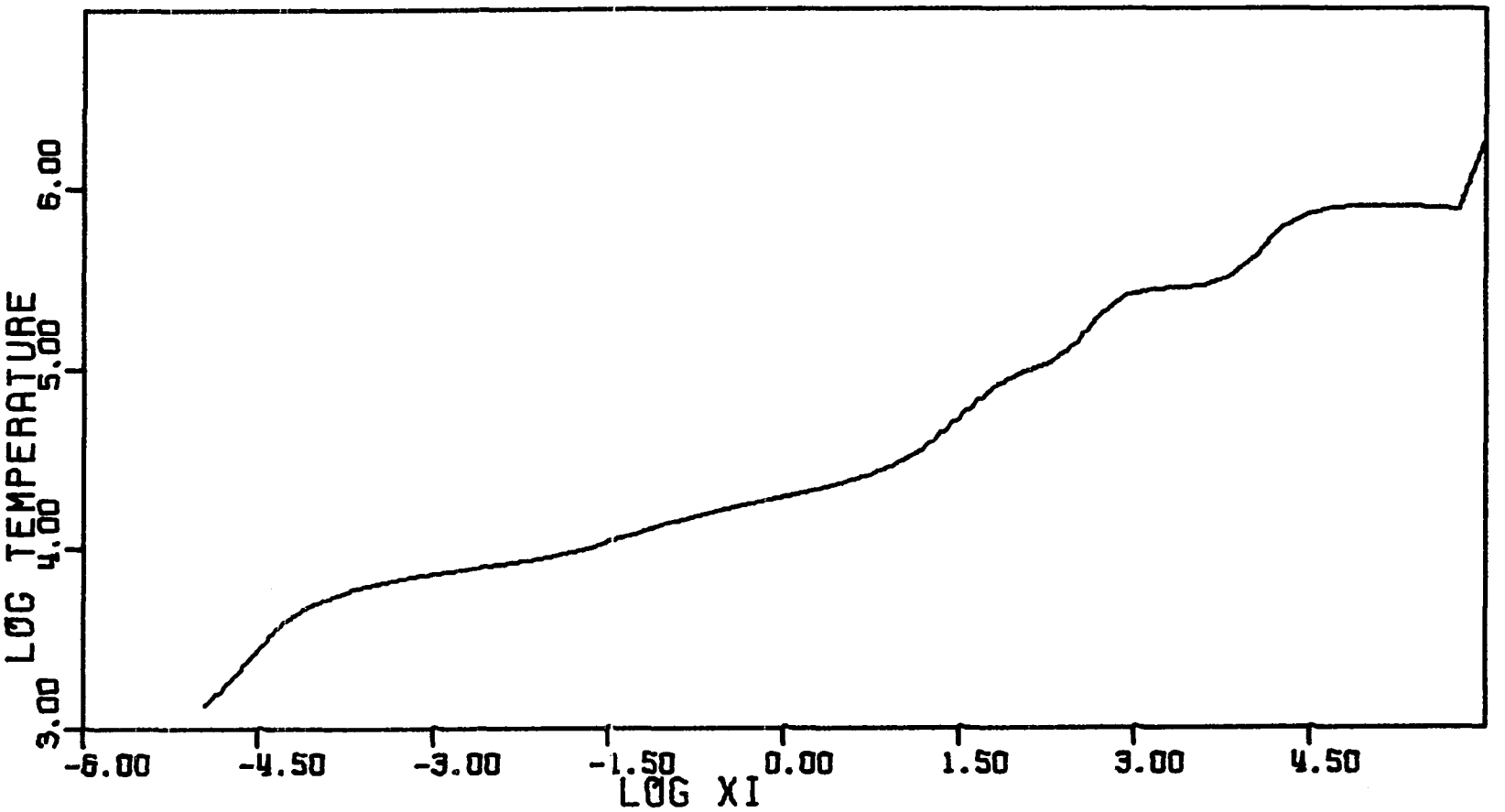

Figure 6. The electron temperature as a function of ξ for an optically thin gas (TM)

Figure 6. Kippenhahn et al. (1974) and Mathews (1974) obtain similar results.

For a wide range in ξ, a good approximation to Equation 2.9 is $\langle\sigma_a\rangle = 2 \times 10^3 \sigma_T/\xi$ (TM) (cgs units used throughout unless otherwise specified). Neglecting electron scattering, Equation 2.8 then becomes

$$G_{rad} = \frac{2 \times 10^3 \sigma_T n}{4\pi c \mu_i m_o} = \beta n, \tag{2.10}$$

where $\beta \simeq 1.6 \times 10^{-9}$. For a constant mass cloud, Equations 2.6 and 2.10 combine to give

$$\frac{d^2r}{dt^2} = \beta n_o (a_o/a)^3, \tag{2.11}$$

provided that the gravitational and drag forces are negligible. A simple integration of this equation with a(t) given by Equation 2.5 yields

$$v(s) = v_o + \frac{\beta n_o a_o}{3c_o} \left[\frac{4s+1}{(4s^2+2s+1)^{1/2}} - 1\right], \tag{2.12}$$

where again $\dot{a}_o = c_o$. Hence the cloud's terminal velocity is

$$v_\infty = v_o + B\beta n_o a_o/c_o \tag{2.13}$$

with $B = 1/3$. A similar calculation with $\dot{a}_o = 0$ gives $B = 1/\sqrt{3}$. The linear expansion rate, $a(t) = a_o + c_o t$, gives

B = 1/2 and an isothermal expansion with $\dot{a}_o = c_o$ gives B = 0.296. The constant B is relatively insensitive to the cloud expansion rate because most of the acceleration occurs at small s before the cloud has expanded appreciably.

If the clouds are accelerated from rest, $v_\infty \simeq 4 \times 10^{-16} n_o a_o$ for B = 1/2 and a cloud temperature of 2×10^4 °K. Hence the clouds with sufficient column density to receive large accelerations are most likely optically thick in the lines. Using only the continuum absorption gives

$$v_\infty \simeq 8 \times 10^{-17} n_o a_o \ . \qquad (2.14)$$

An upper limit is placed on $n_o a_o$ in the following way. The radiative acceleration must exceed gravity if the net acceleration is to be positive outward. This restriction is

$$nr^2 > GM_{QSO}/\beta_{continuum} = 4 \times 10^{43} M_8 \qquad (2.15)$$

(where M_8 is the QSO's mass in units of $10^8 M_\odot$) or $\xi < 240\ L_{46}/M_8$. TM's calculations (Figure 5) then show that $n(HI)/n(H) \gtrsim 10^{-7.1} M_8/L_{46}$, and consequently the cloud is thin at the Lyman continuum edge only if

$$an \lesssim 10^{24} L_{46}/M_8 \ . \qquad (2.16)$$

Taking this for the initial column density in Equation 2.14 limits the maximum terminal velocity to less than 1000

km/sec because the mass to light ratio is restricted to $M_8/L_{46} > 1$ by energy considerations (Chapter I.B). The effects of drag and gravity further reduce this limiting velocity.

Therefore, optically thin, freely expanding clouds which are driven by radiation pressure cannot achieve the high velocities observed. For comparison, an optically thin cloud of constant size ($P_c = P_{ic}$ in Equation 2.1) has

$$v - v_o = \beta n_o t = \frac{\beta n_o a_o}{c_o} s \ , \qquad (2.17)$$

implying that large velocities are achievable. However, terminal velocities are imposed on this solution because the gas recombines as it moves away from the QSO and eventually the cloud becomes optically thick. When this occurs, the amount of momentum absorbed per unit mass begins to decrease with increasing optical depth. Mathews (1974) finds terminal velocities of 5-50 x 10^3 km/sec for pure hydrogen clouds of constant size. Kippenhahn *et al.* (1974) find somewhat larger velocities because they include the contributions of the heavy elements and because they assume a low cutoff to the high energy tail of the QSO spectrum, thereby preventing complete ionization of the gas. Numerical models which include the effects of the

external medium on the cloud dynamics are the subject of the present investigation (Chapters III through VI).

C. The Optically Thick Case

For the optically thick case Equation 2.7 becomes

$$G_{rad} = \frac{L}{4\pi r^2 c} \frac{\pi a^2}{m_c} . \qquad (2.18)$$

Again neglecting the gravitational and drag terms, Equation 2.6 is now

$$\frac{d^2(r/r_o)}{ds^2} = A \frac{(a/a_o)^2}{(r/r_o)^2} , \qquad (2.19)$$

where $A = (t_{exp}/t_{acc})^2$. The characteristic acceleration time is $t_{acc} = [r_o/G_{rad}(0)]^{1/2}$, and the expansion time is $t_{exp} = a_o/c_o$. Equation 2.19 was solved numerically for a/a_o given by Equation 2.5 with $\dot{a}_o = c_o$. Plots of r/r_o and $d(r/r_o)/ds$ for representative values of A are displayed in Figures 7 and 8. The asymptotic solution for $s > A^{-0.25}$ is $d(r/r_o)/ds = 4(9As)^{1/3}/3$.

These solutions are only valid as long as the clouds remain optically thick. An approximate expression for the variation of optical depth at the Lyman continuum edge is

$$\tau_c = 2an(HI)\sigma_o \simeq \tau_o \frac{(r/r_o)^2}{(a/a_o)^5} . \qquad (2.20)$$

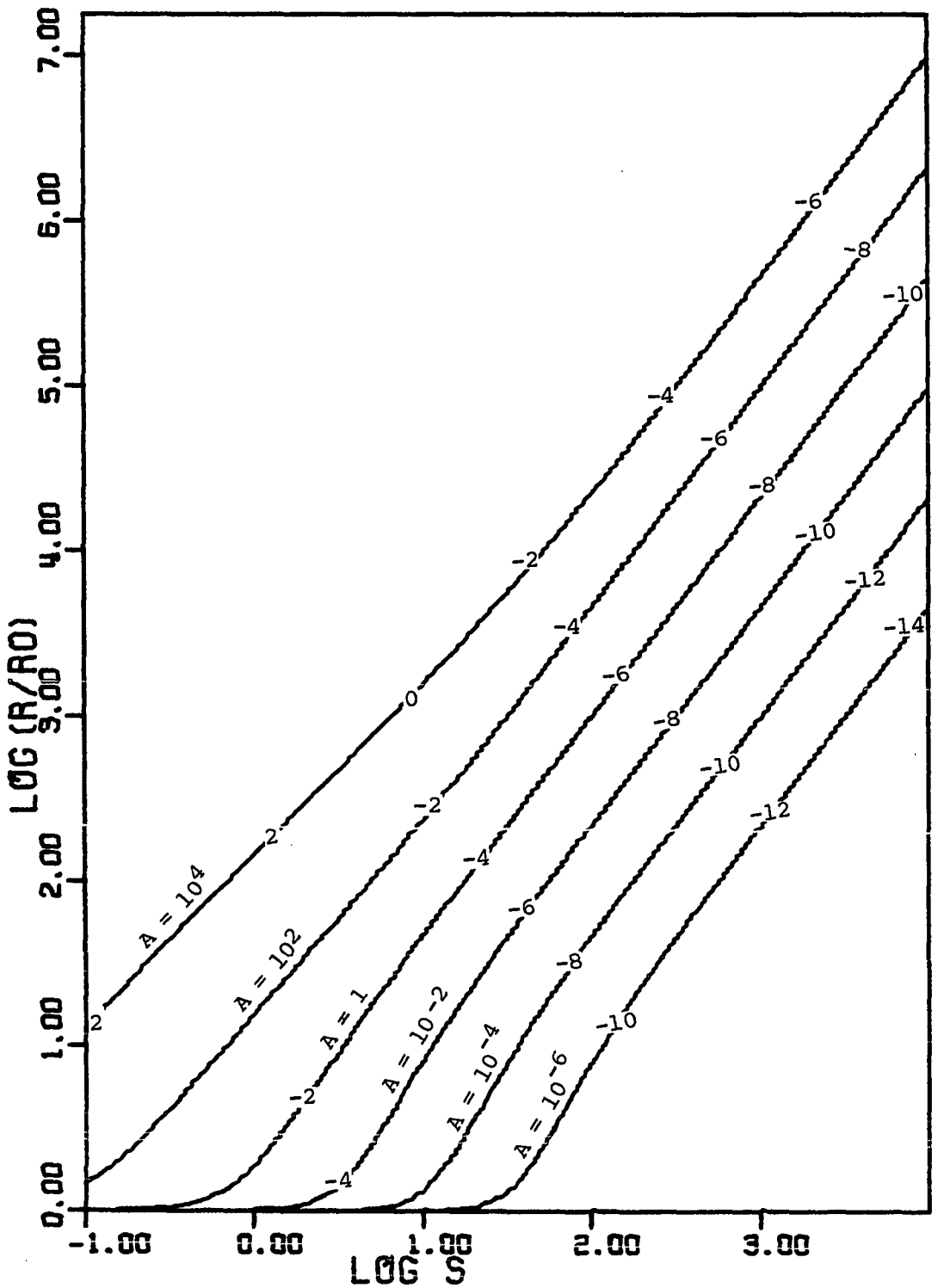

Figure 7. Cloud position r/r_o as a function of time s for various values of A. The numbers on the curves give $\log(\tau_c/\tau_o)$

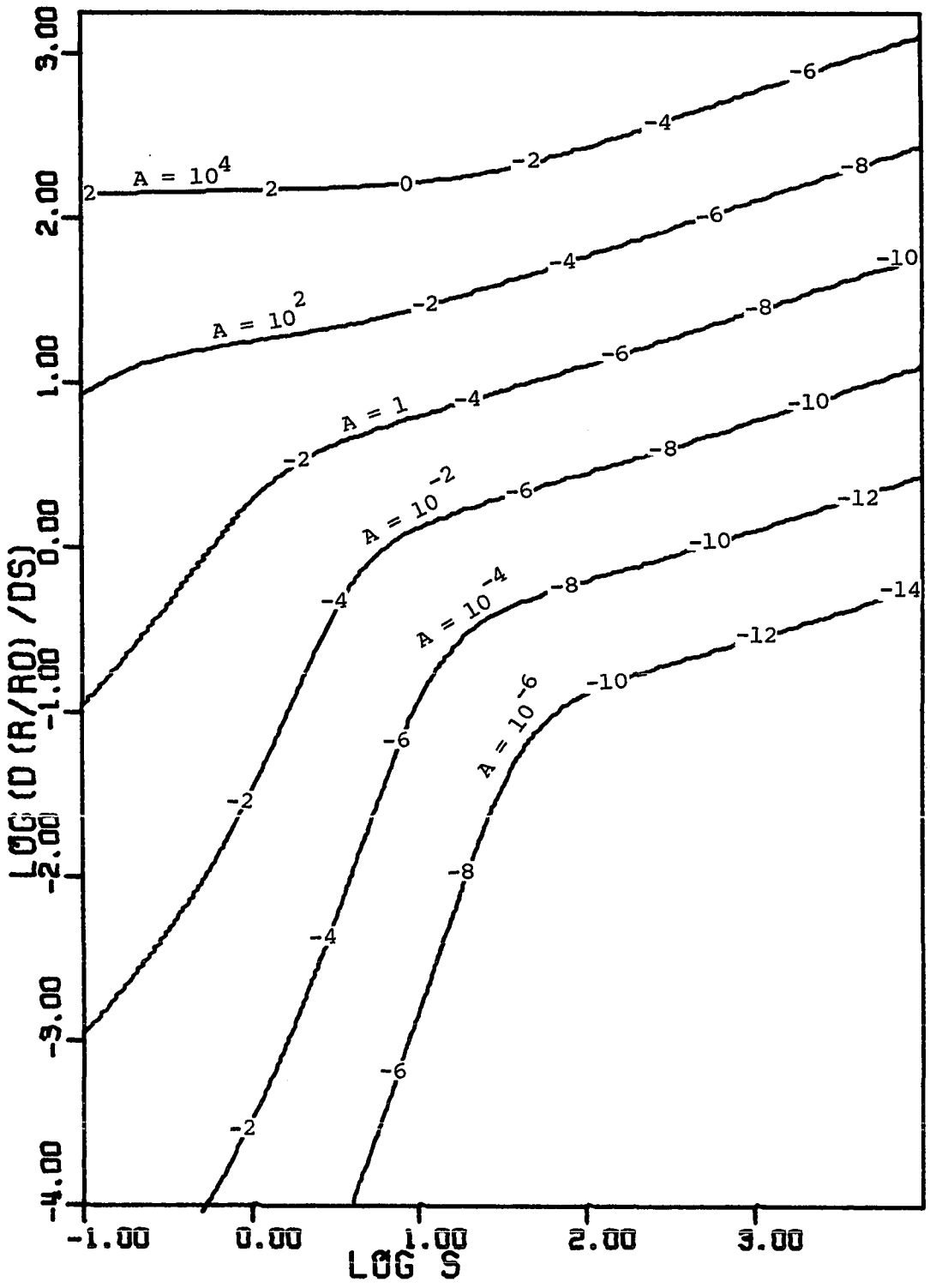

Figure 8. Cloud velocity $d(r/r_o)/ds$ as a function of time s for various values of A. The numbers on the curves give $\log(\tau_c/\tau_o)$

This relation depends on the fact that n(HI)/n(H) is roughly proportional to ξ^{-1} for $\xi > 10^{-4}$ (see Figure 5) and that na^3 is assumed constant (cf Mathews (1974)). The numbers on the curves in Figures 7 and 8 give log (τ_c/τ_o).

For certain combinations of A and τ_o very large velocities are obtainable, but these two parameters are not independent. Optically thick clouds experience a positive outward acceleration provided that $G_{rad} > G_{grav}$ or that

$$n_o a_o < \frac{3L}{16\pi cGM_{QSO}\mu_i m_o} = 7.0 \times 10^{23}\ L_{46}/M_8 \ . \qquad (2.21)$$

For convenience, $L_{46}/M_8 = 1$ in what follows. Such clouds are optically thick at the Lyman continuum edge if $n(HI)/n(H) > 1.2 \times 10^{-7}$. This implies that $\xi < 10^{2.3}$ (see Figure 5), and hence that $nr^2 > 5.0 \times 10^{43}$. This latter inequality demands that

$$A = \frac{3L}{16\pi c\mu_i m_o c_o^2} \frac{(a_o/r_o)}{n_o r_o^2} < 50(a_o/r_o), \qquad (2.22)$$

and therefore that

$$v = \frac{c_o r_o}{a_o} \frac{d(r/r_o)}{ds} < \frac{10^8}{A} \frac{d(r/r_o)}{ds} \ . \qquad (2.23)$$

These clouds started out with $\tau_o = 1$, and hence they remain optically thick only if $A >> 1$. But Equation 2.22 restricts $A < 50$ (as $a_o < r_o$) and Equation 2.23 shows that

large velocities are obtained only for small A. Thus there are no solutions for $\tau_o = 1$ with terminal velocities as large as 1000 km/sec.

Starting with thicker clouds to allow for future expansion only makes matters worse. Generalizing the above arguments gives the approximate relations

$$A \lesssim \frac{50}{\tau_o} (a_o/r_o), \tag{2.24}$$

and

$$v \lesssim \frac{10^8}{A\tau_o} \frac{d(r/r_o)}{ds} . \tag{2.25}$$

Figure 8 shows that $d(r/r_o)/ds$ at $\tau_c = 1$ is always less than $A\tau_o$, and in fact, the ratio $(A\tau_o)^{-1}\, d(r/r_o)/ds$ decreases with increasing τ_o.

If the clouds are confined by a constant external pressure, $P_{ic} = P_c$, then $a(t) = a_o$ and Equation 2.19 gives

$$\frac{d(r/r_o)}{ds} = (2A)^{1/2}(1-r_o/r)^{1/2} . \tag{2.26}$$

The restrictions on A derived above still apply but now the clouds remain optically thick (see Equation 2.20). Hence, terminal velocities of

$$v_\infty = \frac{r_o c_o}{a_o} (2A)^{1/2} \lesssim \frac{2\times10^7}{\tau_o^{1/2}} (r_o/a_o)^{1/2} \qquad (2.27)$$

are attainable, so clouds starting out with unit optical depth and $r_o >> a_o$ can easily reach high velocities. This situation is very similar to that of the optically thin case (Chapter II.B). That is, radiation pressure can produce considerably larger velocities if the clouds are confined, rather than freely expanding.

III. THE INPUT PHYSICS

A. Confinement Mechanisms

The simple theory outlined in Chapter II suggests that a confining medium must exist if radiation pressure is to accelerate clouds to velocities $\gtrsim$ 1000 km/sec. However, the presence of such a medium introduces new complications. For optically thin, constant-size clouds the equation of motion becomes

$$\frac{dv_c}{dt} = \beta n_c - v_c^2/\ell \qquad (3.1)$$

when drag is included (cf Equation 2.6). The quantity $\ell = 4an_c/3n_{ic}$ is a characteristic "stopping" length since the solution of Equation 3.1 for $\beta=0$ is simply

$$v_c = v_o e^{-r/\ell} . \qquad (3.2)$$

The solution for accelerating clouds is

$$\frac{v_c}{v_\infty} = \frac{v_\infty \tanh(v_\infty t/\ell) + v_o}{v_\infty + v_o \tanh(v_\infty t/\ell)} , \qquad (3.3)$$

where $v_\infty = (\beta n_c \ell)^{1/2}$ is the terminal velocity. TM find $\beta \simeq 1.6 \times 10^{-9}$, so

$$v_\infty \simeq 3.3 \times 10^{-5} (2an_c)^{1/2} (n_c/n_{ic})^{1/2} . \qquad (3.4)$$

In Chapter II.B large terminal velocities are associated

with large column densities. The above calculation demonstrates that the ratio of the cloud to intercloud density is an equally important parameter when an external medium is present.

Two types of confinement are now considered: ram pressure confinement and thermal gas pressure confinement. Unless the intercloud medium is extremely hot or is moving with the clouds, the clouds are moving supersonically. (For example, 10^9 °K corresponds to a sound speed of 5000 km/sec.) In this case ram pressure ($\simeq 0.9\ \rho_{ic} v_c^2$) (Landau and Lifshitz 1959; Spreiter et al. 1966) dominates thermal gas pressure ($0.6\ \rho_{ic} c_{ic}^2$).

The effectiveness of ram pressure confinement has been demonstrated; the solar wind confines the Earth's magnetosphere (Spreiter et al. 1966) and an intergalactic medium is capable of confining the compact, double radio sources (De Young 1971). Can it work here? The ratio of the radiation pressure acceleration to the drag deceleration for an optically thin, constant size cloud is

$$\frac{G_{rad}}{G_{drag}} = \frac{4\beta n_c a}{3v_c^2}(n_c/n_{ic}) = \frac{v_\infty^2}{v_c^2} . \qquad (3.5)$$

The velocity at which ram pressure (at the head of the cloud) balances the cloud's internal gas pressure is

approximately $v_b = (2n_c/3n_{ic})^{1/2} c_c$. Plugging this into Equation 3.5, gives

$$v_b = c_c(2\beta n_c a)^{-1/2}\ v_\infty \simeq v_\infty/(8 \times 10^{-22}\ n_c a)^{1/2} \qquad (3.6)$$

for $T = 2 \times 10^4$ °K. Thus, large column densities are required if ram pressure is to be important in confining clouds at velocities much below their terminal velocities. Compare the upper limit on the column density given by Equation 2.16! Such a narrow range of acceptable column densities is rather disconcerting.

Thermal gas pressure is an appealing confinement mechanism because it does not require large velocities and because it is isotropic, thereby producing uniform confinement on all faces of a cloud. However, the presence of the requisite hot ($\gtrsim 10^9$ °K) intercloud medium is uncertain, as such temperatures are difficult to maintain (cf Figure 6). Bow shocks and cloud collisions have been suggested as possible heating mechanisms (Osterbrock and Parker 1965; Oke and Sargent 1968; Daltabuit and Cox 1972), but the details have not been worked out.

Such a medium will cool by emitting thermal bremsstrahlung. The resulting X-ray flux at the Earth is

$$F_x = 6.84 \times 10^{-38}\ n_e n_p T^{-1/2}\ \frac{(4\pi R^3/3)}{4\pi d^2} I(\nu_1, \nu_2, T), \qquad (3.7)$$

where

$$I(\nu_1,\nu_2,T) = \int_{\nu_1}^{\nu_2} \exp(-h\nu/kT)\ g_{ff}(\nu,T)d\nu \qquad (3.8)$$

and g_{ff} is the free-free Gaunt factor (Spitzer 1968). Of course Equation 3.7 is for Euclidean geometry; in a more detailed calculation d is a luminosity distance which depends on the cosmological model assumed for the universe. Evaluating the integral (Equation 3.8) for the 2-6 keV band for $T = 10^9$ °K gives

$$F_x \simeq 10^{-10}\ n_4^{\ 2} R_{20}^{\ 3} d_{27}^{\ -2}\ \text{ergs cm}^{-2}\ \text{sec}^{-1}, \qquad (3.9)$$

where for example, $R_{20} = 10^{-20}$ R cm. For comparison, the limiting flux which is detectable in this band by the UHURU satellite is about 5×10^{-11} (Burbidge 1973b). The QSO 3C 273 and the Seyfert galaxy NGC 4151 have been detected by UHURU, but in most cases only upper limits can be set (Burbidge 1973b). Therefore, Equation 3.9 places an important constraint on a thermally confining medium.

The actual situation is most likely very complex. Both ram pressure and thermal gas pressure may be important in confining the clouds. In fact, if the density and temperature of the intercloud medium were to decrease in the proper way, thermal gas pressure could confine the clouds at low velocities near the QSO and ram pressure

could take over at high velocities and large distances. Such a model avoids the low-velocity confinement problems of ram pressure and yet keeps the X-ray emitting region associated with thermal confinement small enough to escape detection.

Are these simple ideas too simple? Yes, the assumptions of spherical symmetry, uniform density and temperature, and sharp cloud boundaries are unrealistic. More detailed calculations are required to determine whether confinement is actually possible and to fully assess its dynamical effects. This investigation presents multi-dimensional, gasdynamic calculations for both ram-pressure-confined clouds and thermal-gas-pressure-confined clouds. For simplicity the density and temperature of the undisturbed medium are assumed constant. It is found that under the best of conditions, neither pressure provides satisfactory confinement.

B. The Ionization and Thermal Structure

The present numerical calculations concentrate on the gasdynamics of the cloud-intercloud interaction. The gas is assumed optically thin to all radiation so that radiative transfer can be neglected. As the simultaneous solution of the two-dimensional gasdynamic equations and

the ionization equations in every cell at each time step requires excessive amounts of computer time, the detailed ionization structure of the gas is not calculated. Consequently, neither the heating and cooling functions which should serve as source and sink terms for the energy equation (see Equation 4.2), nor the integral for the radiation pressure acceleration (see Equation 2.9) can be explicitly evaluated. The gas flow is assumed to be adiabatic and the radiation pressure acceleration is approximated by the optically thin, equilibrium results of TM (specifically GCL as displayed in Figure 4). This means that detailed spectra cannot be predicted and phenomena such as line-locking (references in Chapter I.C) cannot be investigated. However, as discussed below (see also Chapter VI.B), the gross properties of the flow can still be determined.

The results of TM are presented in Figures 3 through 6 and are discussed briefly in Chapter II.B. TM assume that the elemental abundances are solar ($\mu_i = 1.30$), that the ionizing spectrum is a power-law, $\nu^{-\alpha}$, with $\alpha = 1.5$, and that the gas velocity relative to this source of radiation is zero. There is little evidence to support large departures from these abundances (Hartwick 1971; Williams 1971; Davidson 1972; MacAlpine 1972; Jura 1973;

Scargle et al. 1974; Chan and Burbidge 1975). The use of different compositions (Kippenhahn et al. 1974; Mathews 1974) or spectral indices (McKee and Tarter 1975) alters the results of TM, but the conclusions of the present investigation are relatively insensitive to such changes. For nonzero gas velocities, the ionizing radiation is Doppler-shifted with respect to the clouds, but the effect on GCL is small compared to uncertainties in the absorption cross sections (Kippenhahn et al. 1974).

TM find that an optically thin gas is more than 90% ionized for $\xi \gtrsim 10^{-3}$ (see Figure 5). Therefore, it is assumed that no ionization fronts occur in either the clouds or the intercloud medium and that the adiabatic index $\gamma = 5/3$ throughout. TM's results represent a self-consistent solution of the ionization and thermal equations for a static gas in which the heating by ultraviolet photons is exactly balanced by radiative cooling. In the present dynamic models, this ionization and thermal equilibrium may be altered in a number of ways which are now discussed.

1. Thermally confined clouds

First consider the case for thermally confined clouds. As long as the flow is subsonic, shock waves do not occur. The gas does suffer adiabatic compression (expansion), but

the effects are small. The density rarely changes by as much as a factor of 2, which means that the temperature changes by less than a factor of 1.6. If this compressed (expanding) gas were allowed to cool (warm) at constant pressure to the photoionization equilibrium temperature of TM (Figure 6), its density would increase (decrease) by an additional factor of 2.3 and its temperature would decrease (increase) by the same factor, making its final temperature 1.5 times lower (higher) than the original.[1] Such factors of 2 do not significantly alter the ionization and thermal structure of the gas.

The initial temperatures of the thermally confined clouds are chosen consistent with TM (Figure 6) and lie in the range 2-3 x 10^4 °K. The initial temperatures of the intercloud medium ($T_{ic}(0) = 10^2$-10^3 $T_c(\xi_c)$) are chosen so that its thermal pressure balances that in the clouds. (The initial conditions are discussed more fully in Chapter III.D.) These latter temperatures are ≃ 25-75 times higher than the equilibrium temperatures (Figure 6) calculated using ξ_{ic}. Whatever heating mechanism maintains these high temperatures probably also ionizes the gas, so TM underestimate the ionization. However,

[1] For this calculation, the temperatures of TM (Figure 6) have been approximated by the expression $T(\xi) = T(\xi=1)\xi^{1/4}$.

the momentum available per frequency interval is comparable (equal if $F_\nu \propto \nu^{-1}$), so any state of ionization short of complete ionization results in a similar value for the acceleration.[1] Therefore, it is reasonable to use GCL to represent the acceleration in the intercloud medium as well as in the clouds.

The hot intercloud medium may be responsible for additional cloud heating. It radiatively cools primarily by bremsstrahlung X-rays when $T \gtrsim 10^7$ °K and by line emission from highly ionized C, O, and other abundant elements for $T \lesssim 10^7$ °K (Cox and Tucker 1969; Cox and Daltabuit 1971). The bulk of this radiation is capable of ionizing hydrogen and some of it is energetic enough to also ionize the heavier elements. Neglecting optical depth effects the energy flux from this hot gas, which falls on an embedded cloud, is $F_{ic} \simeq \pi a^3 \, \varepsilon(T_e)(R/a)$, provided that $R/a \gg 1$ (where R is the size of the surrounding emitting region). This radiation is nearly isotropic and exerts a mildly compressive force on the cloud (cf Williams 1972; McKee and Tarter 1975; Weymann 1976). For comparison, the flux from the QSO which strikes the cloud is

[1] This is born out by the numerical calculations of TM, Mathews (1974), and Kippenhahn et al. (1974), which show that $G_{rad}/\rho \simeq$ constant for a wide range of ionization. The density dependence comes about because there is approximately one ionization per resonance scattering (unless there is a high energy cutoff (Kippenhahn et al. 1974)) and so the radiation pressure is dominated by the recombination rate.

$$F_{QSO} = \frac{L_{QSO} a^2}{4r^2} . \qquad (3.10)$$

Since the total luminosity of the intercloud region is $L_{ic} = 4\pi R^3 \varepsilon(T_e)/3$, the ratio of these two fluxes is

$$\frac{F_{ic}}{F_{QSO}} = 3(L_{ic}/L_{QSO}) \frac{r^2}{R^2} . \qquad (3.11)$$

The quantity $r/R \lesssim 1$ and unless there is some other energy source for heating the intercloud medium,[1] $L_{ic}/L_{QSO} << 1$. Therefore $F_{ic}/F_{QSO} << 1$, and radiative heating by the medium is safely ignored.

Finally, the presence of large temperature gradients suggests that heat conduction may be an important source of cloud heating and ionization (cf Chevalier 1975a,b; McKee and Cowie 1975). The rate of heat flow is $Q = -\kappa \nabla T$, where $\kappa \simeq 2 \times 10^{-14} T^{5/2}$ for an ionized gas (Spitzer 1962). Its importance relative to the mechanical energy

---

[1] Since the intercloud medium must be thin to the radiation from the QSO, if it is heated by this radiation, then $L_{ic}/L_{QSO} \simeq \tau_{ic} << 1$ (where τ_{ic} is the optical depth). If it is not heated by this photon flux, but by supersonic cloud motion or some other such mechanism, then it is still true that $L_{ic}/L_{QSO} << 1$ if a steady state prevails because L_{QSO} must ultimately supply the clouds' energy. The only cases in which this inequality does not hold are: (a) if the QSOs are very transient and L_{QSO} (present) $<< L_{QSO}$ (past) or (b) if significant energy is released from the QSO in some other form (e.g., cosmic rays).

transfer is of order

$$\frac{1}{Pe} = \frac{\kappa}{\rho c_p U D}, \tag{3.12}$$

where Pe is the Peclet number (Zel'dovich and Raizer 1966), U is the characteristic flow velocity, and D is the characteristic dimension of the flow region. Thus Pe >> 1 means that heat conduction is negligible. The adiabatic cloud models of Chapter V ignore heat conduction even though

$$Pe \simeq \frac{\rho_{ic} c_p c_{ic} a_o}{\kappa} \simeq \frac{4n_4}{T_7^2} \tag{3.13}$$

is of order unity. This is a reasonable assumption as the presence of even a weak (10^{-6} gauss) turbulent magnetic field substantially reduces the conductivity (Spitzer 1962), making Pe >> 1.

2. Ram-pressure-confined clouds

For the ram pressure models, the initial temperatures of both the cloud ($\simeq$ 2-3 x 10^4 °K) and the intercloud medium ($\simeq$ 1-4 x 10^5 °K) are taken from Figure 6. (The initial conditions are more fully discussed in Chapter III.D.) The intercloud gas is compressed ($\simeq 4\rho_{ic}(0)$), heated ($\simeq$ 5-50 $T_{ic}(0)$), and ionized as it passes through the bow shock. The equilibrium results of TM underestimate the level of ionization for this region. However,

as discussed above for the thermally confining medium, GCL probably remains an adequate representation of the radiative acceleration.

This shock-heated gas adiabatically cools as it flows past the clouds on a time scale of order $t_{flow} = a_o/v_c(0)$. Its temperature is greater than the equilibrium temperature, so normally it would radiatively cool on a time scale of order $t_{cool} = 3nkT/2\Lambda$ (Spitzer 1968). The cooling rate (Λ) depends primarily on the temperature of the gas for $n<10^8$ (Cox and Tucker 1969; Cox and Daltabuit 1971). For the present cloud models (Table 1) the time scales t_{flow} and t_{cool} are comparable ($\simeq 10^8$-10^9 sec). This means that the standard ram models, which do not radiatively cool (i.e., $t_{cool} = \infty$), overestimate the temperature in the gas surrounding the clouds. This becomes increasingly important as the evolutions progress because significant mixing of cloud and intercloud gas occurs. While this significantly raises the temperature in the clouds, its effect on the pressure (the important dynamical quantity) is probably smaller (cf Chapter VI.B).

It is the thermal pressure of this hot, shocked gas which actually confines the clouds.[1] To examine how the

[1]The directed kinetic energy of the intercloud gas is thermalized at the bow shock.

thermal structure of the gas affects the cloud dynamics, model RC221 was generated (see Chapter V.C). For it, the energy equation and the assumption of adiabatic flow are discarded, and the temperature of the gas is forced to agree with the equilibrium results of TM at each time step. This is tantamount to assuming that the radiative cooling is so efficient ($\Lambda \to \infty$) that the gas cools to its equilibrium temperature infinitely fast ($t_{cool} \to 0$). The idea was to bracket the "true" solution by the two limiting cases ($t_{cool} = \infty$ and $t_{cool} = 0$), similar to the concept of "nonradiating" and "isothermal" shocks (cf Spitzer 1968). It turns out that the cooling in RC221 is far too efficient to be realistic. It lowers the pressure in the shocked intercloud gas so drastically that the confinement is extremely poor (see Chapter V.C for details). The actual radiative cooling most likely occurs at nearly constant pressure, making the standard adiabatic models (Chapter V.B) a reasonable approximation.

The radiation from the hot, shocked plasma in front of the supersonically moving clouds is not unlike that from the thermally confining medium discussed earlier (cf Daltabuit and Cox 1972). The ratio of this flux to that of the QSO is approximately

$$\frac{F_{shock}}{F_{QSO}} = \frac{\frac{1}{2}\rho_{ic}v_c^3}{(L_{ion}/4\pi r^2)} = 2\pi\mu_i m_o v_c^3 \xi_{ic}^{-1} \quad . \qquad (3.14)$$

This ratio is initially $\simeq 5 \times 10^{-4}$ for all of the standard ram-pressure-confined clouds of Table 1. Furthermore, only a fraction of this energy is actually radiated because adiabatic expansion quickly lowers the postshock temperature. Of that which is radiated, less than half strikes the cloud, and it is not strongly absorbed as long as the cloud's optical depth remains small (cf Daltabuit and Cox 1972). Therefore, this secondary radiation has a minimal effect on cloud dynamics and is safely ignored.

In summary, the intercloud medium probably does not significantly heat the clouds either radiatively or by conduction. However, the assumption of adiabatic flow is still not correct because radiative cooling is expected to occur. Fortunately it is not the thermal structure, but the pressure structure, which is important dynamically. The latter is reasonably approximated because cooling is expected to occur at nearly constant pressure. Secondly, the equilibrium results of TM for the radiation pressure are a good approximation, even though their ionization structure is not, since the former does not depend strongly on the latter for the optically thin case.

C. Gasdynamic Approximations

The use of the gasdynamic equations (see Chapter IV.A) to describe the physical conditions in the gas is valid provided that the mean free path is small compared to the characteristic dimensions of the flow. The mean free path is given by

$$\lambda = \bar{v} t_c, \tag{3.15}$$

where

$$\bar{v} = \left(\frac{8kT}{\pi m_p}\right)^{1/2} \tag{3.16}$$

is the mean thermal speed, and

$$t_c = \frac{11.7\ T^{3/2}}{n \ln \Lambda_c} \text{ sec} \tag{3.17}$$

is the self-collision time for protons in an ionized gas (Spitzer 1962, 1968). The quantity

$$\Lambda_c = 1.24 \times 10^4 T^{3/2} n^{-1/2} \tag{3.18}$$

is a "cutoff" factor resulting from the ineffectiveness of particle encounters beyond some critical distance. The mean free path for electrons is the same as for protons because t_c is a factor of $(m_p/m_e)^{1/2}$ smaller and $\bar{v}$ is larger by the same factor.

The mean free path within the model clouds ($\lambda \simeq 10^6$-10^7 cm) is small compared to the size of the clouds ($a \simeq 10^{15}$-10^{16} cm). However, the mean free path in the

hot gas behind the shock fronts and in the thermally confining medium is $\simeq 10^{15} T_{7.5}^{2} n_4^{-1}$ and is comparable to a. Therefore, magnetic field effects are invoked to keep the mean free path sufficiently small in these regions. The gyroradius of a proton is

$$r_g = \frac{m_p c}{eB} v_\perp \simeq 10^{-4} \frac{v_\perp}{B} , \qquad (3.19)$$

so a field of only 10^{-6} gauss is more than sufficient, as then $r_g = 10^{10}$ cm for $v_\perp = 10^8$ cm/sec. This field is comparable to those observed in our own galaxy. Since the QSO continuum radiation is believed to be largely synchrotron emission, even larger fields are probably associated with QSOs. The dynamical effects of such a field are completely negligible, as the magnetic pressure, $B^2/8\pi$, is still small compared to the thermal gas pressure. Hence it is entirely consistent to use the gasdynamic equations (Chapter IV.A) with B=0.

A considerable portion of the kinetic energy of the gas entering a shock wave is irreversibly converted into heat by ion viscous forces. The time required for the electrons to reach temperature equilibrium with the positive ions is

$$t_{eq} = \frac{250\ T_e^{3/2}}{n_e \ln \Lambda_c} \simeq 10^5 \frac{T_{5.3}^{3/2}}{n_4} \text{ sec} \qquad (3.20)$$

(Spitzer 1962, 1968; Zel'dovich and Raizer 1966). The dynamics is affected very little by this transition since the total pressure is unchanged. Hence, the equations for

one-fluid flow are used throughout (see Equations 4.1 to 4.4).

In the absence of a magnetic field, the coefficient of viscosity for an ionized gas is

$$\mu = 2.21 \times 10^{-15} \frac{T^{5/2}}{\ln \Lambda_c} \quad \frac{gm}{cm\text{-}sec} \tag{3.21}$$

(Spitzer 1962). The importance of viscous effects can be estimated from the Reynolds number

$$Re = \frac{\rho U D}{\mu} \tag{3.22}$$

(Zel'dovich and Raizer 1966), which compares the inertial forces in the equation of motion to the viscous forces. Since

$$Re \simeq \frac{150\ n_4}{T_7^2} \gg 1 \tag{3.23}$$

for the present cloud models, the gas flow is assumed inviscid. This leads to problems at shock fronts, as there is no dissipative mechanism to thermalize the ordered kinetic energy of the entering gas (Roache 1972; Potter 1973). Artificial viscous pressures are introduced into the numerical code to circumvent this difficulty (see Chapter IV.E). This procedure is possible because the Rankine-Hugoniot relations (i.e., the "jump conditions") are valid across the shock no matter what the dissipative processes inside the shock (Roache 1972).

D. Initial Conditions

The present investigation is concerned with the acceleration of clouds once they are formed. A possible scenario for the condensation of clouds out of the intercloud medium is given, for example, by Weymann (1973, 1976). The physical conditions in the absorbing and emitting gas are not well known. Observations are difficult as the QSOs are extremely faint, the vast majority having visual magnitudes greater than 16 (De Veny et al. 1971). The observations which have been made suggest that the physical conditions differ substantially from object to object. It is tempting to argue that this implies that the acceleration mechanism is insensitive to the clouds' physical make-up. It must be remembered, however, that the majority of QSOs possess no absorption lines at all, and the related class of objects typified by BL Lacertae (Oke and Gunn 1974; Stein et al. 1976) have no emission or absorption lines. This may be due to a simple deficiency of gas in these objects.

A number of factors enter into the selection of initial conditions for the present gasdynamic models. First of all, they must be consistent with the observations. This still allows considerable freedom since the physical conditions in the newly formed clouds may differ from those

in clouds already accelerated to high velocities. Secondly, the results of the simple calculations outlined above are used as guidelines. They imply that significant radiation pressure acceleration is difficult under the best of conditions, so optimum values of the various parameters are chosen whenever possible. Finally, it is important to keep in mind the limitations of the numerical code and work within them.

In this spirit, the clouds are assumed to be optically thin to all radiation. Observations of the absorption and emission regions suggest that such clouds probably exist, but clouds optically thick in the Lyman continuum probably also exist (Bahcall and Oke 1971; Williams 1971; Morton and Morton 1972; Baldwin et al. 1974; Scargle et al. 1974; Carswell et al. 1975; Chan and Burbidge 1975; McKee and Tarter 1975). Static photoionization models for the emission regions are able to reproduce the observed line intensities reasonably well whether the gas is assumed thick or thin (Davidson 1972, 1973; MacAlpine 1972; Scargle et al. 1974; Chan and Burbidge 1975; Shields and Oke 1975). However, the calculations are greatly simplified if the clouds are optically thin, as then radiative transfer can be ignored. Presumably such clouds are more stable than thick ones because the differential

radiative forces due to internally created line photons are smaller (Williams 1972; McKee and Tarter 1975; Weymann 1976). In addition, clouds with optical depths less than unity are more efficiently accelerated because they absorb more momentum per unit mass from the radiation field.

As individual emission clouds are not observed, the number of them and their sizes are essentially unknown. The HI column densities of absorption clouds range from $\simeq 10^{14}$ to 10^{21} (Chan and Burbidge 1971; Morton and Morton 1972; Baldwin et al. 1974; Carswell et al. 1975; Wingert 1975). Accurate determinations are difficult as the individual lines are hard to resolve and many of them are saturated, making them insensitive indicators of the amount of absorbing material. To convert the HI column densities to total column densities requires knowledge of the ionization state of the gas. Since many of the clouds are observed to be highly ionized, their total column densities may be very large (i.e., $>> 10^{21}$).

Total column densities of 10^{22} to 10^{23} are assumed so that ram pressure can confine the clouds at relatively low velocities where drag has not yet become important (see Equation 3.6). For larger column densities the clouds' motion is probably dominated by gravity (see Equations 2.16 and 2.21). (In these calculations, for simplicity, the mass of the QSO has been taken as zero.) Lower column

densities could be used for the thermally confined clouds, but they give lower terminal velocities (see Equation 3.4) and prevent intercomparison of the model results. These column densities correspond to cloud masses of 5-50 x 10^{-4} $M_\odot$ (see Equation 3.27), smaller than those considered by Kippenhahn et al. (1974), but larger than those favored by Mathews (1974, 1976) and Blumenthal and Mathews (1975). Substantially larger (10^2 to 10^7 $M_\odot$) clouds have been observed in the emission regions of Seyfert galaxies (Walker 1968a,b; Osterbrock 1971).

A cloud's optical depth at the Lyman continuum edge is

$$\tau_c = 2an\sigma_o \frac{n(HI)}{n(H)} \frac{n(H)}{n}, \qquad (3.24)$$

where $\sigma_o = 6.3 \times 10^{-18}$ and $n(H)/n = 0.91$. As already discussed in Chapter III.B, the ionization structure of the gas is approximated by the equilibrium results of TM. The quantity n(HI)/n(H) is plotted as a function of ξ in Figure 5. Thick (Davidson 1972) and thin (Scargle et al. 1974) photoionization models suggest that $\xi \simeq 10^{-1}$ for the emission region of a "composite" QSO. Similar calculations by McKee, Tarter, and Weisheit (1973) find $\xi \simeq 10^{-2}$ to 10^{0} for the various absorption systems of 4C 05.34. However, larger values of ξ are required if clouds with the above column densities are to be optically thin. The

value of ξ_c is chosen so that $\tau_c \simeq 2.5$ and thus it lies in the range $1 \lesssim \xi_c \lesssim 10$.

If thermal broadening is assumed, then these clouds have an optical depth in Lyman-α of

$$\tau_\ell = \frac{\sqrt{\pi}\, e^2}{m_e c} \frac{f\lambda_o}{v_D}\, 2n(HI)a \simeq 10^4, \qquad (3.25)$$

where $v_D = (2kT/m_o)^{1/2}$ (Spitzer 1968). Their optical depth in the other lines which significantly contribute to the radiation pressure is similar (cf Mathews 1974). The clouds are actually thinner than this because they are found to differentially expand (see Chapter V). The high velocity material is Doppler-shifted more than the low velocity material and no longer lies in its shadow. The factor by which the optical depth is reduced is roughly $\delta = (v_D/r)(dv/dr)^{-1}$ (Lucy 1971). Typical values are $\delta \simeq 10^2$, making $\tau_\ell \simeq 10^2$.

Despite the fact that these clouds are probably thick in the lines, the fully optically thin results of TM (i.e., GCL of Figure 4) are used. This neglect of radiative transfer effects leads to an overestimate of the bulk acceleration for the cloud by a factor of $\simeq 5$ (cf GC in Figure 4) and an underestimate of the dispersive forces within the cloud, perhaps by an even larger factor (again because of the internal creation of line photons

(Williams 1972; McKee and Tarter 1975; Weymann 1976)). This approximation is discussed again in Chapter VI.

Now consider the gas densities. It is the quantity $n_c(0)/n_{ic}(0)$ which is important in determining the terminal velocity of the clouds (see Equation 3.4). Values of 10^2 and 10^3 are used; larger values are difficult to treat numerically.[1] The intercloud density $n_{ic}(0)$ is arbitrarily fixed at 10^4 cm^{-3}, so the clouds have densities of $n_c(0) = 10^6$ and 10^7. These values of n_c are an order of magnitude or two less than those often quoted for the dense gas believed responsible for producing the broad emission line wings (see Chapter I.B). That is, densities of $\simeq 10^8$ are required to collisionally suppress the forbidden lines in this region (Adams 1973). However, collisional de-excitation may not be necessary (Scargle et al. 1974). The densities for absorption clouds are often estimated to be $\lesssim 10^3$ (Bahcall and Feldman 1970; Bahcall and Goldsmith 1971; Williams et al. 1975). Williams et al. (1975) have discussed the possibility that the absorption and emission both originate in the same low-density clouds! In any event, the specific value chosen for $n_c(0)$

[1] In the case of ram pressure confinement large n_c/n_{ic} leads to large Mach numbers and small time steps. For thermally confined clouds large n_c/n_{ic} corresponds to highly subsonic flows which are better handled by an incompressible gasdynamic code.

is relatively unimportant as the numerical results can be scaled to other values of this parameter for constant $n_c(0)/n_{ic}(0)$ (see Chapter III.E).

The clouds are initially assumed to be isothermal and in photoionization equilibrium with the QSO. For ξ_c in the range 1 to 10, TM (Figure 6) give temperatures[1] of 2-3 x 10^4 °K. The initial intercloud medium is also taken to be isothermal. Its temperature for the ram pressure models is obtained from Figure 6 using the value of ξ_{ic} calculated for the base of the initial grid (Y = 0 in Figure 10). The intercloud temperature for the thermally confined models is chosen so that pressure balance is achieved. These latter temperatures exceed the corresponding photoionization equilibrium temperatures by a factor of ≈ 25-75. As already discussed, some unspecified heating mechanism is assumed to maintain these high T_{ic}. Approximate pressure balance is achieved at the front of the ram-pressure-confined clouds by giving them an initial Mach number of

$$M_o = \frac{v_c}{c_{ic}} = \left[\frac{2}{3}\left(\frac{n_c}{n_{ic}} \frac{c_c^2}{c_{ic}^2} - 1\right)\right]^{1/2} . \qquad (3.26)$$

The thermally confined clouds are started out at Mach 0.05

[1] It is really e, the specific internal energy, which is used in the numerical code. However, $\mu \approx 0.62$ for $\xi \gtrsim 10^{-2}$ (gas nearly 100% ionized), so e is simply proportional to T and the two can be used interchangeably.

to 0.20 for computational convenience.

The ionizing luminosity is assumed to be 10^{47} ergs/sec. Little generality is lost because the numerical results only depend on L_{ion}/r^2, provided that $r >> a$. Initially the clouds are approximately spherical and their mass is

$$m_c = \frac{45}{32} \pi a^3 \mu_i m_o n_c \tag{3.27}$$

(see Chapter IV.B). The present clouds have masses of 5-50 x 10^{-4} $M_\odot$. The actual values of the parameters used in the gas-dynamic models can be found in Table 1 of Chapter V.

E. A Scaling Law

One big disadvantage of numerical modeling is that specific parameters must be chosen. This makes it difficult to develop general arguments such as those in Chapter II. This is unfortunate as the actual physical conditions in the QSO clouds are poorly known. However, a simple scaling law has been found which helps to reduce the number of free parameters which must be considered.

Within the approximations used in the present work, the results scale with $n_c(0)$, the initial cloud density. Assume that $n_c(0)a(0)$, $n_c(0)/n_{ic}(0)$, and L_{ion} remain constant[1] and that the density varies as $n_c'(0) = \Omega n_c(0)$,

[1] The assumption that $L_{ion} = 10^{47}$ can easily be relaxed provided that $r_o >> a_o$, since only L_{ion}/r^2 enters the calculations.

then $a'(0) = \Omega^{-1}a(0)$ and $m_c'(0) = \Omega^{-2}m_c(0)$. Since $\xi_c(0)$ has been fixed by the value of $n_c(0)a(0)$, it remains constant. This means that $r_o' = \Omega^{-1/2}r_o$ and $T_c'(0) = T_c(0)$. The terminal velocities for optically thin, freely expanding clouds (Equation 2.13) and for constant size, drag-limited clouds (Equation 3.4) are independent of Ω. The same is true for all velocities, since the accelerations G_{rad}, G_{drag}, and G_{grav} all vary as Ω and the time varies as Ω^{-1} ($c_o t/a_o$ and $v_\infty t/\ell$ are both proportional to t/a which goes as Ω^0). Hence, the adiabatic and shock heating (which depend on the gas velocity) are also invariant with respect to Ω. This scaling also remains valid when line cooling is included as long as collisional de-excitation can be ignored because then $\Lambda t \propto \Omega^0$.

One must be careful in applying this scaling law because the cloud radius a and the region in the immediate vicinity of the cloud scale as Ω^{-1}, while the initial cloud-QSO separation r_o scales as $\Omega^{-1/2}$. Since the present models already have $r_o >> a_o$, there is no problem in scaling to larger densities ($\Omega>1$). However, the scaling to very low densities runs into trouble because for sufficiently small Ω ($\simeq 10^{-3}$) it gives $r_o' \simeq a_o'$. In this case the incoming radiation is no longer parallel and there is a significant transverse component to the radiation pressure. Furthermore, the variation of ξ with time is no

longer dominated by the variation in n_c. Other effects also occur, let it suffice to say that the scaling breaks down for these small Ω. In summary, the present conclusions concerning terminal velocities and cloud confinement depend on the values of $n_c(0)a(0)$ and $n_c(0)/n_{ic}(0)$, but are rather independent of the values of L_{ion} and $n_c(0)$.

F. Physical Stability

A number of instabilities may play an important role in the dynamical evolution of these gas clouds. For instance, when a heavy layer of fluid is supported against gravity by a light, less dense fluid, the interface is susceptible to the Rayleigh-Taylor instability (Chandrasekhar 1961). This instability has been mentioned as being important in radiatively driven clouds in at least two connections. The first is the cloud-intercloud boundary at the leading edge of the flow. Blake (1972) has shown that radio clouds which are confined by ram pressure are Rayleigh-Taylor unstable because the deceleration due to drag leads to an inertial force in the clouds' reference frame from the dense gas to the less dense gas. This suggests that the heads of the accelerating clouds are Rayleigh-Taylor stable since the net acceleration (in the same frame) is now in the direction of the heavy fluid. In this case, however, a light fluid (photons) still supports a

heavy fluid (the clouds). Krolik (1976) has analyzed this problem for the case of an incompressible, constant density, one-dimensional cloud. He finds that the sign of the derivative of the local radiative acceleration with respect to optical depth determines the stability of the system and that the nature of the instability is qualitatively different from that in the standard gravitational case. Whether or not this instability can grow in amplitude to the point where it results in cloud disruption remains to be seen.

The Kelvin-Helmholtz instability is a second fluid dynamic instability which may well be important here. It occurs as a result of shearing motions at the cloud-intercloud boundary (Chandrasekhar 1961). Kelvin-Helmholtz waves develop along the front of the clouds and grow in amplitude as they propagate towards the rear (Blake 1972). They increase the surface area of the cloud-intercloud boundary, thereby increasing the rate at which mixing occurs and energy is exchanged (by conduction).

The role of the Rayleigh-Taylor and Kelvin-Helmholtz instabilities can be investigated numerically. For example, Woodward (1975) has followed their development and subsequent growth in interstellar gas clouds struck by shock waves. The fact that these instabilities do not manifest themselves in the present numerical models can probably be attributed to the poor resolution employed, since it is the smallest

wavelengths which grow the most rapidly.

Scargle (1973) has discussed the importance of the Milne instability in radiation-pressure-driven gas flows. This instability occurs when an atom (or a parcel of gas) at large optical depth is perturbed to a slightly higher velocity than the average velocity. At this point it is exposed to a stronger radiation field than previously (because it has been Doppler-shifted out of line center) and is accelerated. This situation is unstable because the acceleration increases the Doppler shift and moves the atom (or gas parcel) further from line center. Thus, the incident flux and the resulting acceleration continue to increase, at least until the atom (or gas) is Doppler-shifted completely out of the line. Of course, this instability cannot occur here because the clouds are assumed optically thin and radiative transfer is neglected.

Mathews (1976) has considered the stability of thermally confined clouds with respect to internally propagating sound waves. He concludes that only the clouds with $G_{rad} \gtrsim 2c_T^2/\lambda$ (c_T is the isothermal sound speed and λ is the wavelength of the instability) are unstable. For $\lambda < a$, this inequality becomes $\beta n_c a/2c_T^2 > 1$. The clouds which satisfy this latter inequality (i.e., are unstable) are also the ones which receive large radiative accelerations (cf

Equations 2.17 and 3.5), and consequently, have large radial expansion rates (cf Chapter VI.B, especially Equation 6.5). This rapid expansion is the only instability which appears in the present models (Chapter V). In this sense, the cloud confinement which is obtained is an overestimate since any other instabilities which may occur will tend to further disrupt the clouds.

IV. THE NUMERICAL CODE

A. Basic Concepts

The basic numerical code uses a variation of the two-dimensional, mixed Eulerian-Lagrangian differencing scheme developed by Sappenfield (1969). The original code was written in spherical coordinates; the present version employs cylindrical coordinates. To maintain internal consistency with the Fortran listing and the computer-drawn graphs, the symmetry axis is referred to as the y-axis and the perpendicular distance from this axis is measured by x. The y-coordinate is Lagrangian (moves with the fluid), the x-coordinate is Eulerian (stationary), and azimuthal symmetry is assumed. This is a convenient choice of coordinates for the present problem because the shocks occur primarily in the y-direction and are best handled by a Lagrangian treatment, whereas the subsonic flows in the x-direction can be adequately described by an Eulerian coordinate. Such a scheme avoids the severe grid distortions suffered by purely Lagrangian methods.

In these coordinates, a continuous flow is governed by four partial differential equations representing conservation of mass, conservation of energy, and momentum conservation in the x- and y-directions. For an inviscid, compressible, nonrelativistic, adiabatic, one-fluid flow

these equations are, respectively,

$$\frac{D\rho}{Dt} + u\frac{\partial\rho}{\partial x} + \frac{\rho}{x}\frac{\partial(xu)}{\partial x} + \rho\frac{\partial v}{\partial y} = 0, \tag{4.1}$$

$$\rho\frac{DE}{Dt} + \rho u\frac{\partial E}{\partial x} + \frac{1}{x}\frac{\partial(x\,Pu)}{\partial x} + \frac{\partial(Pv)}{\partial y} - \rho(g_x u + g_y v) = 0, \tag{4.2}$$

$$\rho\frac{Du}{Dt} + \rho u\frac{\partial u}{\partial x} + \frac{\partial P}{\partial x} - \rho g_x = 0, \tag{4.3}$$

and

$$\rho\frac{Dv}{Dt} + \rho u\frac{\partial v}{\partial x} + \frac{\partial P}{\partial y} - \rho g_y = 0, \tag{4.4}$$

where $D/Dt = \partial/\partial t + v\partial/\partial y$ is the Lagrangian time derivative. Here ρ is the density, u is the x-component of velocity, v is the y-component of velocity, and P is the gas pressure. The total energy per unit mass is represented by $E = e + \frac{1}{2}(u^2 + v^2)$, where e is the specific internal energy. The external accelerations, such as gravity and radiation pressure, are collectively symbolized by $\vec{g}$. This system of equations is closed by choosing an appropriate equation of state. Here the ideal gas equation,

$$P = (\gamma-1)\rho e, \tag{4.5}$$

is used with $\gamma=5/3$ throughout.

Magnetic field effects are not included in Equations 4.1 through 4.5. Also, the gas flow is assumed to be

adiabatic, so no source or sink terms are included in the energy equation (Equation 4.2). That is, heat conduction and radiative heating and cooling are neglected. An external gravitational field is used in at least one of the test solutions (Appendix A), but none is used for the QSO cloud models (i.e., $M_{QSO} = 0$). The radiative acceleration is approximated by $GCL(\xi)\cdot\rho$ (see Figure 4). The value of $GCL(\xi)$ is determined by calculating ξ for each grid point and then linearly interpolating in a table of 51 values in the range $-5 < \log \xi < 6$. These assumptions and their dynamical effects are discussed in Chapters III and VI.

Some numerical schemes rely on rather straightforward conversions of the above differential equations into finite difference equations, but the present scheme employs a more geometrical approach. The form of the difference equations in spherical coordinates is derived by Sappenfield (1969). The details for cylindrical coordinates can be found in the Fortran IV listing of the code presented in Appendix C.

It is worthwhile to sketch the basic program layout. All the scalar quantities, such as pressure and density, are defined at cell centers. The vector quantities, velocity and acceleration, are defined at cell centers for the Eulerian coordinate and at cell boundaries for the Lagrangian coordinate. Two passes through the grid are

required at each time step. During the first one, artificial Lagrangian cell boundaries are constructed because the cells in adjoining Eulerian zones do not remain aligned (see for example, Figure 9). The rates of change of mass, momentum, and internal energy are then computed for these artificial cells and summed for each real cell. The second pass through the grid advances all the physical variables in time, computes the new artificial viscous pressures (Chapter IV.E), and checks the size of the time step (see Equation 4.8 below).

Various other aspects of the code are discussed in the remaining sections of this chapter. Particular attention is paid to areas not covered by Sappenfield (1969) or which differ from his treatment. Rigorous testing of the code was performed to insure its accuracy. These tests are described in Appendix A.

B. Grid Geometry

The standard cloud models are computed on a grid of 2403 cells. There are 89 cells in the Lagrangian (y) direction and 27 cells in the Eulerian (x) direction. The clouds are axially symmetric because the external medium is assumed uniform and the QSO is located on the symmetry axis, but off the grid at large negative y. Initially the clouds occupy 26 cells whose outline approximates that of

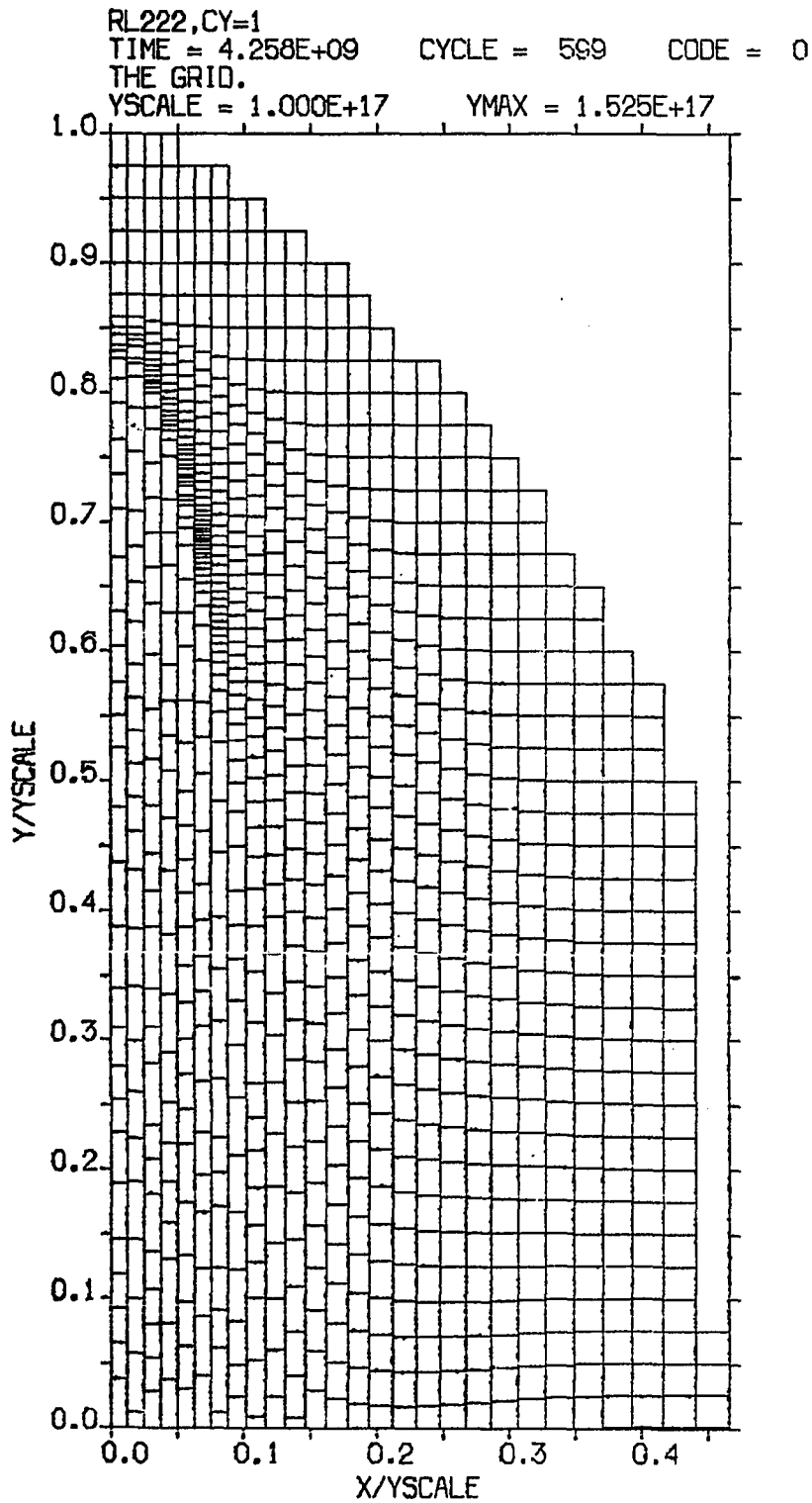

Figure 9. A portion of the grid in the vicinity of the cloud RL222 after an evolution of 4.258×10^9 sec

a sphere. To increase the resolution in areas of interest, a nonuniform cell size has been introduced. The Eulerian zones are fixed in size within the cloud, but increase exponentially thereafter in such a way that the outermost zone is twice as wide as the innermost one. In the Lagrangian direction the cells exterior to the cloud are initially twice as large as the interior cells. This resolution was found to be adequate by comparing the results with those obtained with a somewhat finer grid and with a uniform grid. A cross section of the lower portion of the undistorted grid is shown in Figure 10. Initially, the cloud occupies the cells marked by cross-hatching and lies 4 cloud diameters from the rear of the grid. For an example of how the grid is distorted during the course of an evolution, see Figure 9.

C. Boundary Conditions

The outer (right hand) Eulerian boundary is a "hard wall" through which no matter can pass. In the thermally confined models it reflects low-amplitude sound waves back into the vicinity of the clouds. Boundary conditions which allow matter to flow off the grid were also tried, but in the present differencing scheme they were difficult to handle computationally and did not completely eliminate these reflection problems. (This code is not really

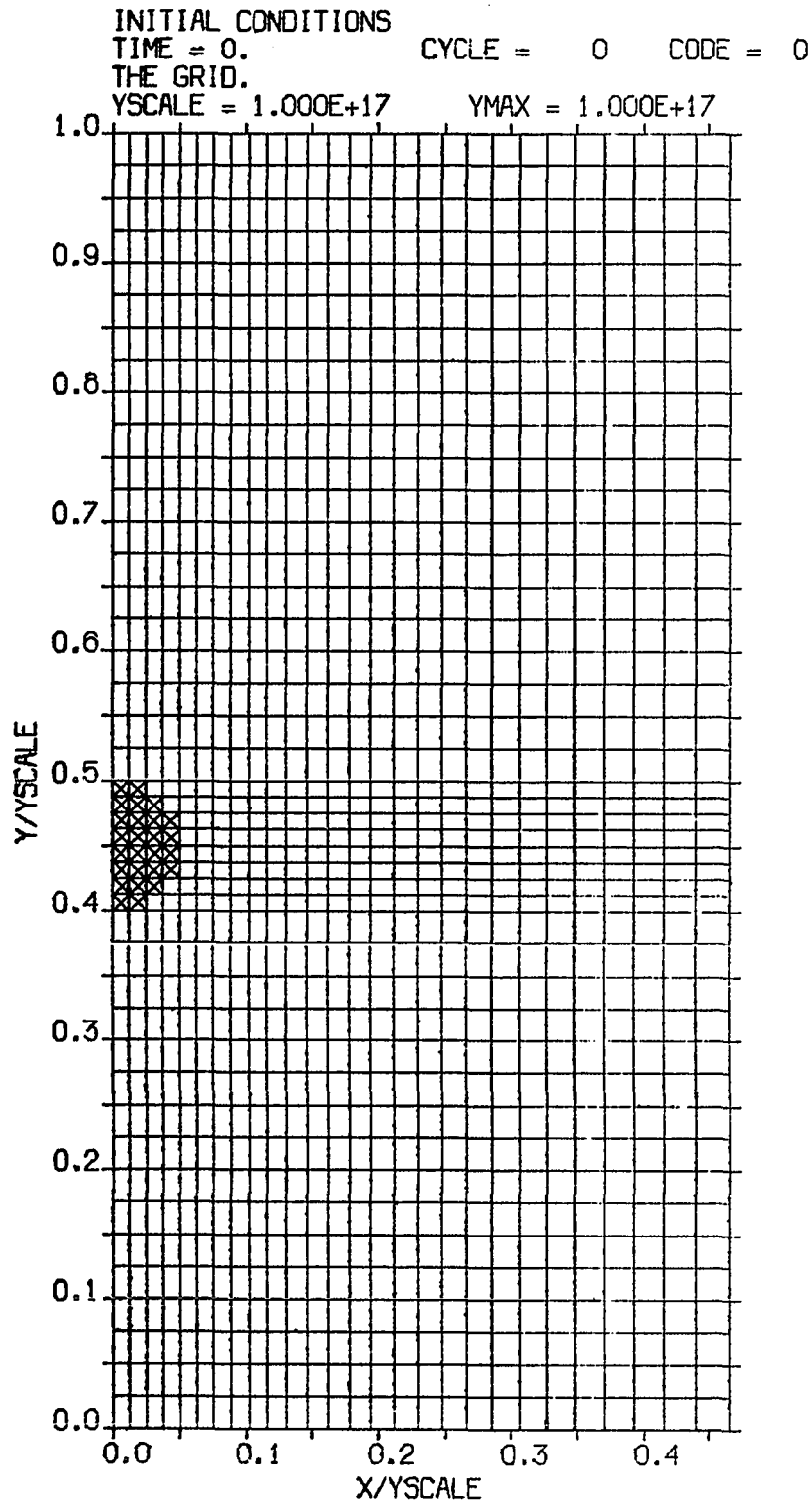

Figure 10. The lower portion of the undistorted grid at t=0 with the position of the cloud indicated by cross-hatching

intended for use in modeling subsonic flows.) Such reflected waves are expected to have a minimal effect on the large scale dynamics. This boundary is sufficiently distant that the bow shocks generated in the ram pressure models strike it far behind the clouds.

The velocity and position of the lower Lagrangian surfaces of the first row of cells in the x-direction are not advanced in time. This keeps the lower Lagrangian boundary of the grid confined to a plane. When this first row of cells is treated normally in all respects except the above, this is referred to as the case 1a boundary condition. The case 1b treatment of these cells is very similar. The only difference is that instead of the normal practice of dividing the y-momentum transferred across Eulerian boundaries equally between the upper and lower cell surfaces, it is all given to the upper cell surface. This is reasonable for many problems as the lower surface is not time-advanced and hence it "wastes" any momentum given to it. Case 1b was initially the standard boundary condition, and case 1a was used only for the spherically symmetric blast wave test (see Appendix A). This proved entirely satisfactory until sufficiently long cloud evolutions were run and chopping (see Chapter IV.D) became necessary. Under these circumstances the top surface of

the new boundary cells often had a large velocity while the lower surface was again held fixed. This caused these cells to expand by an abnormal amount while their masses remained nearly constant. Hence a nonphysical rarefaction[1] developed along the boundary. To prevent this, the case 2 boundary condition was introduced. It divides the momentum as in case 1b, but holds the density and internal energy of the first row of cells fixed, rather than calculating values as usual. In retrospect, the flow pattern near the clouds is not very sensitive to the choice of this boundary condition. Therefore, models using both case 1b and case 2 are included here.

The code monitors the gas flow in the positive y-direction in each Eulerian zone, and advances the upper Lagrangian boundary to stay ahead of it. Thus the gas-dynamics is only done in the cells where something is happening. When a shock front lies at the leading edge of the flow, it is particularly easy to find criteria which advance this boundary in a uniform manner. This is illustrated in Figure 9 and in Figure 41c of Appendix A, where only the cells below the present boundary are plotted. This procedure requires modification for subsonic flows because

[1]This rarefaction should not be confused with the physically real one that occurs behind the clouds as a result of their forward motion through the medium.

of the aforementioned low-amplitude sound waves. These waves trigger the boundary to move upwards in a very irregular fashion. In this case the boundary is advanced in all the Eulerian zones at the maximum rate required by any zone. Of course, the evolution is stopped whenever this boundary reaches the top of the grid (except in the first test solution of Appendix A).

The intercloud medium is initially stationary, but it is accelerated by radiation pressure as are the clouds. Since the magnitude of the acceleration is proportional to the gas density (Figure 4), the medium never achieves a significant velocity. The clouds continue to move into stationary gas because the cells above the upper Lagrangian boundary (where the gasdynamics is not done) retain their initial conditions until they are included in the calculation.

D. Grid Manipulation

After every four time steps each Eulerian zone is searched for cells which have been compressed in the Lagrangian direction. Any cell whose y-dimension is smaller than some specified value (usually 0.05 to 0.20 of the original y-dimension) is combined with the cell ahead of it. The principal reason for doing this so-called

fine rezoning is that the largest permissible time step is generally determined by the cell with the smallest y-dimension (see Chapter IV.E). Therefore, vast amounts of computation time can be saved by the elimination of cells which are significantly smaller than average. Fine rezoning is particularly useful in the vicinity of strong shocks as they are capable of compressing the cells containing intercloud gas to very small sizes, thereby reducing the allowable time step to nearly zero.

On the other hand, extremely large cells are obtained in regions of the grid where rapid expansion is occurring (e.g., behind a fast moving cloud). This leads to insufficient resolution for accurate calculations to be performed, so cells which become abnormally large are split in half. Usually cells are split when their Lagrangian height is twice that of the initial cells exterior to the cloud. Numerical tests show that the exact point at which fine rezoning or cell division is triggered has little effect on the resulting dynamics.

Initially the grid only spans about 20 cloud diameters in the Lagrangian direction. As a model is evolved this usually increases slightly because of fine rezoning. That is, if there are more cells combined than split, array elements are freed and used to add cells to the top of the

grid. Nevertheless, it is clear that as a cloud moves away from the QSO at high velocity, it will soon reach the top of such a grid and the evolution must then be halted. Increasing the dimensions of the 24 doubly-subscripted arrays used by the code permits additional cells to be added. However, this becomes prohibitively expensive because it increases both the computation time and the core allocation requirements. Thus, the grid is fixed at a size such that the 17 most commonly referenced arrays just fit in the small core memory,[1] and an alternate method is used to add new cells to the top of the grid.

This method involves procedures referred to as course rezoning and chopping. These are only required for the latter phases of the cloud evolutions, as the models can be evolved on the original grid (as extended by fine rezoning) for several cloud expansion times. Course rezoning is initiated first. It is exactly like the fine rezoning already discussed, except that considerably larger cells are combined, usually in pairs, but sometimes in quadruples. This can free many additional array elements for adding new cells to the top of the grid. When course rezoning can no longer be effective without seriously impairing

[1]The NASA/Ames CDC 7600 computer has 160,000 octal words of usable small core memory and 1.4 million words of usable large core memory. The latter has a significantly longer access time.

resolution, chopping is begun. It consists of discarding cells at the rear of the grid and adding an equivalent number of new ones at the top. This makes the lower Lagrangian boundary difficult to treat (see Chapter IV.C) and inaccuracies are certainly introduced. These are minimized by only chopping off the trailing 15% of the grid at any one time. The evolution of a model is terminated whenever chopping is required to continue and the rear of the cloud already lies in the lower 30% of the grid.

Course rezoning and/or chopping are performed only a small number of times (never more than ten) during a cloud evolution. The fact that the cloud's velocity, size, and column depth continue to vary reasonably smoothly suggests that the induced errors are tolerable. Especially for the ram pressure models, the effects of chopping are expected to be small because the resulting disturbances travel at the sound speed and should not be able to overtake the supersonic clouds. These techniques do not permit as long evolutions to be run as initially envisioned because of the large radial expansions which occur (Chapter V).

E. Numerical Stability

Artificial viscosities stabilize the gas flow behind shock fronts by providing a dissipative mechanism which converts the ordered kinetic energy into internal energy. The resulting shocks are spread out over several cells, but propagate at the correct speed. The idea of artificial viscosities was first introduced in the open literature by von Neumann and Richtmyer (1950). Recent discussions can be found in Roache (1972) and in Potter (1973).

The present code introduces artificial viscous pressures by replacing the actual pressure gradients, $\partial P/\partial x$ and $\partial P/\partial y$, with $\partial (P+Q_E)/\partial x$ and $\partial (P+Q_L)/\partial y$. The Eulerian artificial viscous pressure is

$$Q_E = \max \{0,\ C_Q\ c_L\ \frac{\Delta m}{\Delta t}\ \bar{A}_E^{-1}\}, \tag{4.6}$$

and the Lagrangian artificial viscous pressure is

$$Q_L = \max \{0,\ C_Q\ c_L\ \rho \Delta v\}. \tag{4.7}$$

In these equations, c_L is the local sound speed, $\Delta m/\Delta t$ is the time rate of change of cell mass, A_E is the area of the outer Eulerian cell surface, and Δv is the velocity of the lower Lagrangian cell surface minus the velocity of the upper one. C_Q is an arbitrary constant near unity. Numerical experimentation found that larger time steps are

permitted and slightly improved results are obtained for $C_Q = 2$ than for somewhat smaller values.

As in all explicit methods, a restriction on the allowable time step size is necessary to insure stability (Roache 1972; Potter 1973). Here the time step is limited so that the inequality

$$\Delta t^2 < \frac{0.6}{c_L^2} \left[\min \{\Delta x^2, \Delta y^2\} + 4\left|\frac{\Delta V}{V}\right| + 4\left|\frac{\Delta m}{m}\right|\right] \qquad (4.8)$$

is valid for all cells. The first term in the brackets represents the Courant-Friedrichs-Lewy condition (1928). Simply stated, it insures that a sound wave cannot travel more than one cell length in one time increment. The latter two terms in Equation 4.8 restrict the fractional changes of volume and mass so that the artificial viscous pressures do not become excessively large.

V. THE NUMERICAL CLOUD MODELS

A. Model Identification and Parameters

Each numerical model has a five character name. The first character identifies the major confinement mechanism: R is for ram pressure and T is for thermal gas pressure. The second character designates some special feature of the model; the standard models with $L_{ion} = 10^{47}$ have an L in this place. Other possibilities are a 0 to signify that the radiation pressure has been turned off, a C for cooling (the nonadiabatic model RC221 in Chapter V.C), and a P for planar (the one-dimensional model RP221 in Chapter V.D). The third place in the model name specifies the value of $\log(2n_c(0)a_o)-20$ and is either a "2" or a "3". The value of $\log(n_c(0)/n_{ic}(0))$ is given by the numeral in the fourth place; it is also a "2" or a "3". The fifth and last character distinguishes various models which have the same first four characters. Such models differ in resolution, the type or amount of rezoning performed (Chapter IV.D), or some other computational or physical detail.

A complete list of the cloud models to be discussed is presented in Table 1. Columns 2 through 10 of this table give the initial conditions. The motivation and method for choosing these particular values is discussed in Chapter III. Column 11 gives $M_\infty = v_\infty/c_{ic}(0)$ where v_∞ =

Table 1. Model parameters

Model name	$2n_c a$	$\frac{n_c}{n_{ic}}$	$n_c(0)$	$\xi_c(0)$	$T_c(0)$	$T_{ic}(0)$	$c_c(0)$	$c_{ic}(0)$	M_o	M_∞	$a_o/c_c(0)$
RL331	10^{23}	10^3	10^7	11.08	3.16×10^4	4.30×10^5	2.66×10^6	9.81×10^6	7.37[a]	43.9	1.88×10^9
RL222	10^{22}	10^2	10^6	1.50	2.06×10^4	1.01×10^5	2.15×10^6	4.76×10^6	3.59	8.21	2.33×10^9
R0334	The same as RL331 except that there is no radiation pressure acceleration.										
R0221	The same as RL222 except that there is no radiation pressure acceleration.										
RC221	The same as RL222 except that it is not adiabatic, the temperatures of TM are used throughout.										
RP221	The same as RL222 except that it is one-dimensional.										
TL335	10^{23}	10^3	10^7	11.08	3.16×10^4	3.16×10^7	2.66×10^6	8.42×10^7	0.20	5.12	1.88×10^9
TL221	10^{22}	10^2	10^6	1.50	2.06×10^4	2.06×10^6	2.15×10^6	2.15×10^7	0.20	1.82	2.33×10^9
TL231	10^{22}	10^3	10^7	11.08[b]	3.16×10^4	3.16×10^7	2.66×10^6	8.42×10^7	0.20	1.62	1.88×10^9
TL337	The same as TL335 except that the radiation pressure is turned on linearly for $s < 1.5$.										
TL338	The same as TL335 except that $M_o = 0.05$.										

[a] Equation 3.26 gives 6.95.

[b] This ξ_c gives an optical depth at the Lyman continuum edge of 0.25, a factor of 10 less than for the other models.

$(GCL(\xi_c)\rho_c(0)\ell)^{1/2}$ is the terminal velocity for the corresponding constant-size, drag-decelerated cloud (cf Equation 3.3). Column 12 gives $a_o/c_{ic}(0)$, the characteristic time for the cloud to freely expand (Chapter II.A).

The next four sections of this chapter present the numerical results for the standard, ram-pressure-confined clouds, a nonadiabatic, ram-pressure-confined cloud, a one-dimensional, ram-pressure-confined cloud, and the thermal-gas-pressure-confined clouds. The behavior of one model of each type is described in detail using a variety of computer-generated plots. A physical explanation is given for their behavior, sometimes immediately and sometimes only after it becomes clear due to the intercomparison of the models. Additional plots accompany the discussion of the other models in each section if they are useful in explaining differences between the models or qualitatively new features which appear. The final section of this chapter is devoted to a discussion of the transients which occur as a result of the crude initial conditions employed.

B. Ram-Pressure-Confined Clouds

1. RL331

Model RL331, with an initial column density of 10^{23}, $n_c(0)/n_{ic}(0) = 10^3$, and $L_{ion} = 10^{47}$, has been evolved for 2.15 cloud expansion times. Contour plots of the velocity, density, internal energy,[1] and pressure at s = 0.95 (t = 1.79×10^9 sec) are displayed in Figures 11a-d; a plot of the grid has already been given in Figure 9. As usual, $s = c_c(0)t/a_o$ measures time in units of cloud expansion times. The scaling factor for both the x- and y-axes (YSCALE) is given in centimeters at the tops of the plots. (In later plots the x-scaling differs from YSCALE by an integer multiple as noted.) The initial size of the cloud is indicated to scale by the cross-hatched semicircles. Selected contours are labelled on each plot, the units appear in the individual figure captions. Notice that it is actually the logarithm of the various quantities which is contoured. The values of the unlabelled contours can usually be inferred from the labelled ones and the contour interval (CONINT) which is given at the top of each plot. Plots of the velocity, density, internal energy, and

---

[1] Since $\mu \simeq 0.62$ for $\xi \gtrsim 10^{-2}$ (gas nearly 100% ionized), the temperature and the specific internal energy are related by a constant and the two are used interchangeably.

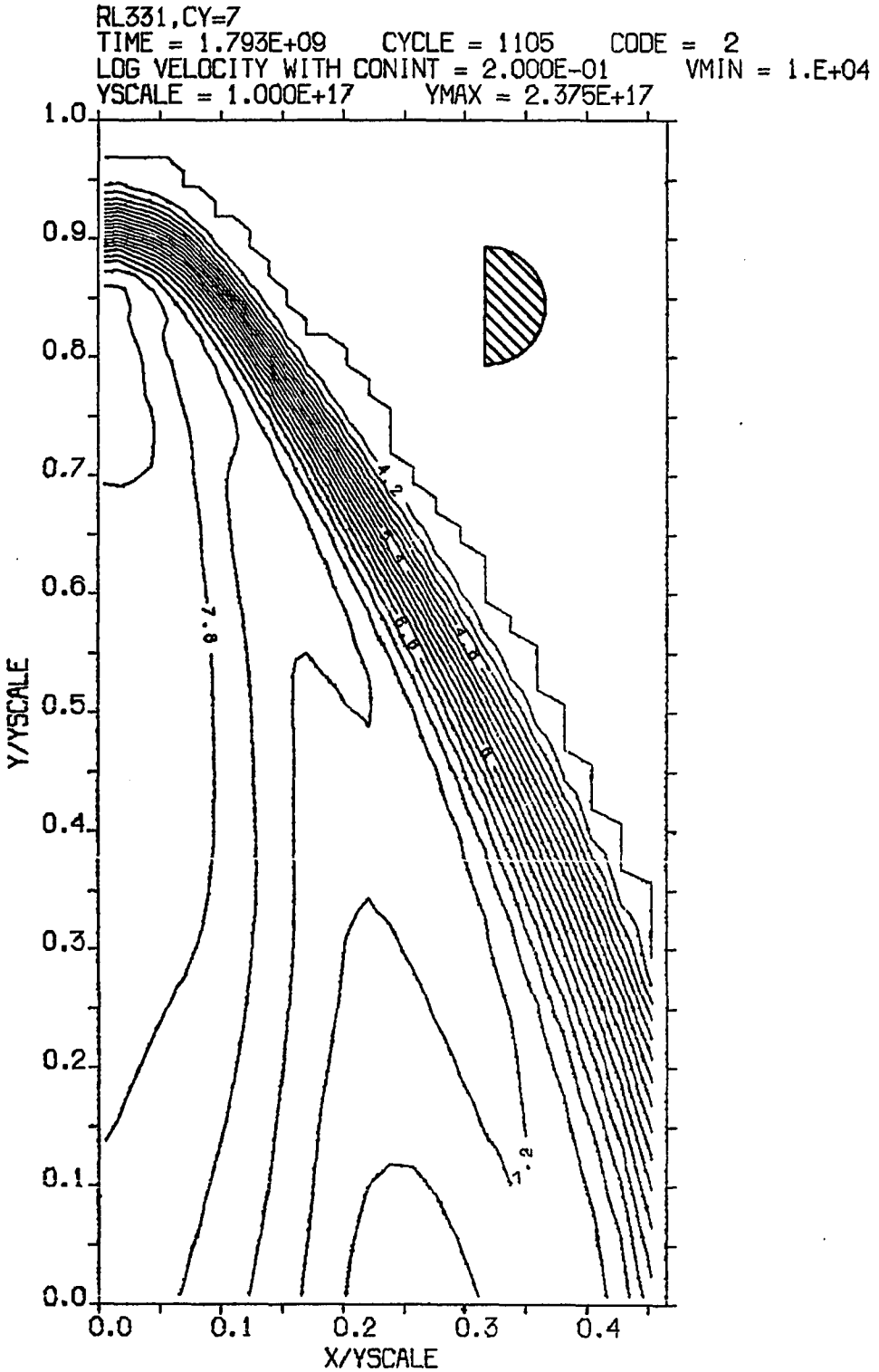

Figure 11a. Contours of the logarithm of velocity (in cm/sec) at s = 0.95 for model RL331

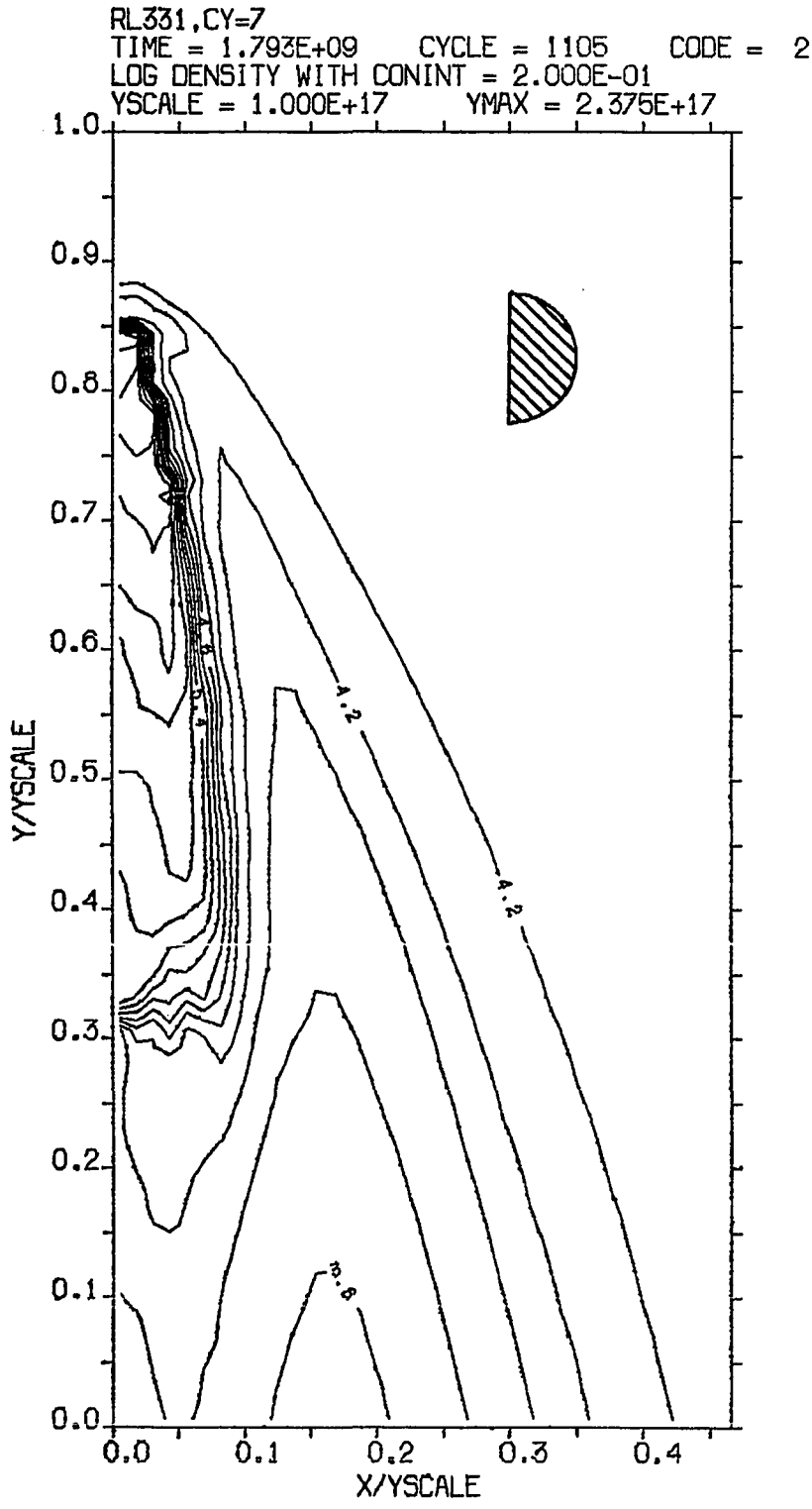

Figure 11b. Contours of the logarithm of density (in nucleons/cm^3) at s = 0.95 for model RL331

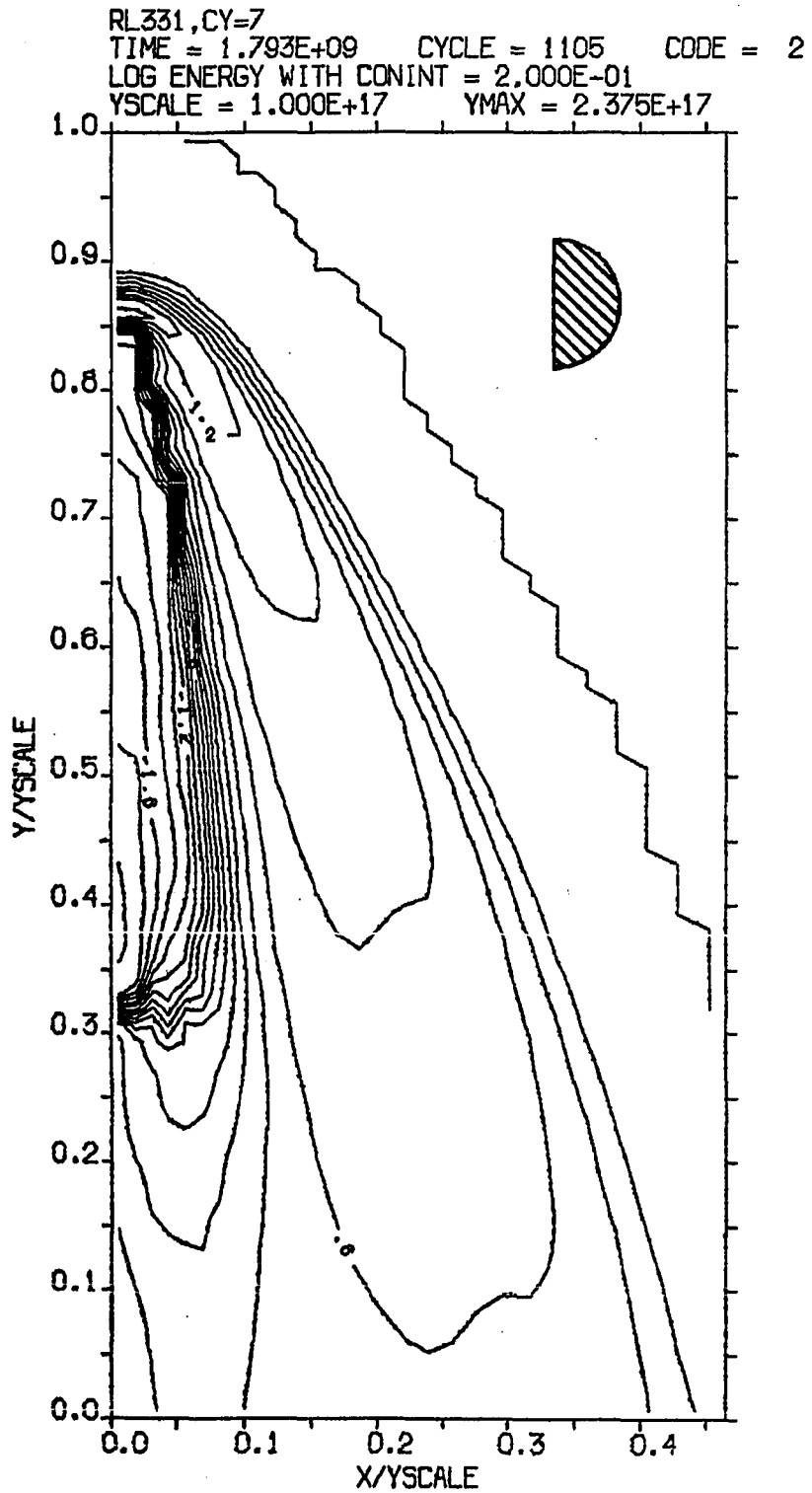

Figure 11c. Contours of the logarithm of specific internal energy (in units where $e_{ic}(0) = 1.0$) at $s = 0.95$ for model RL331

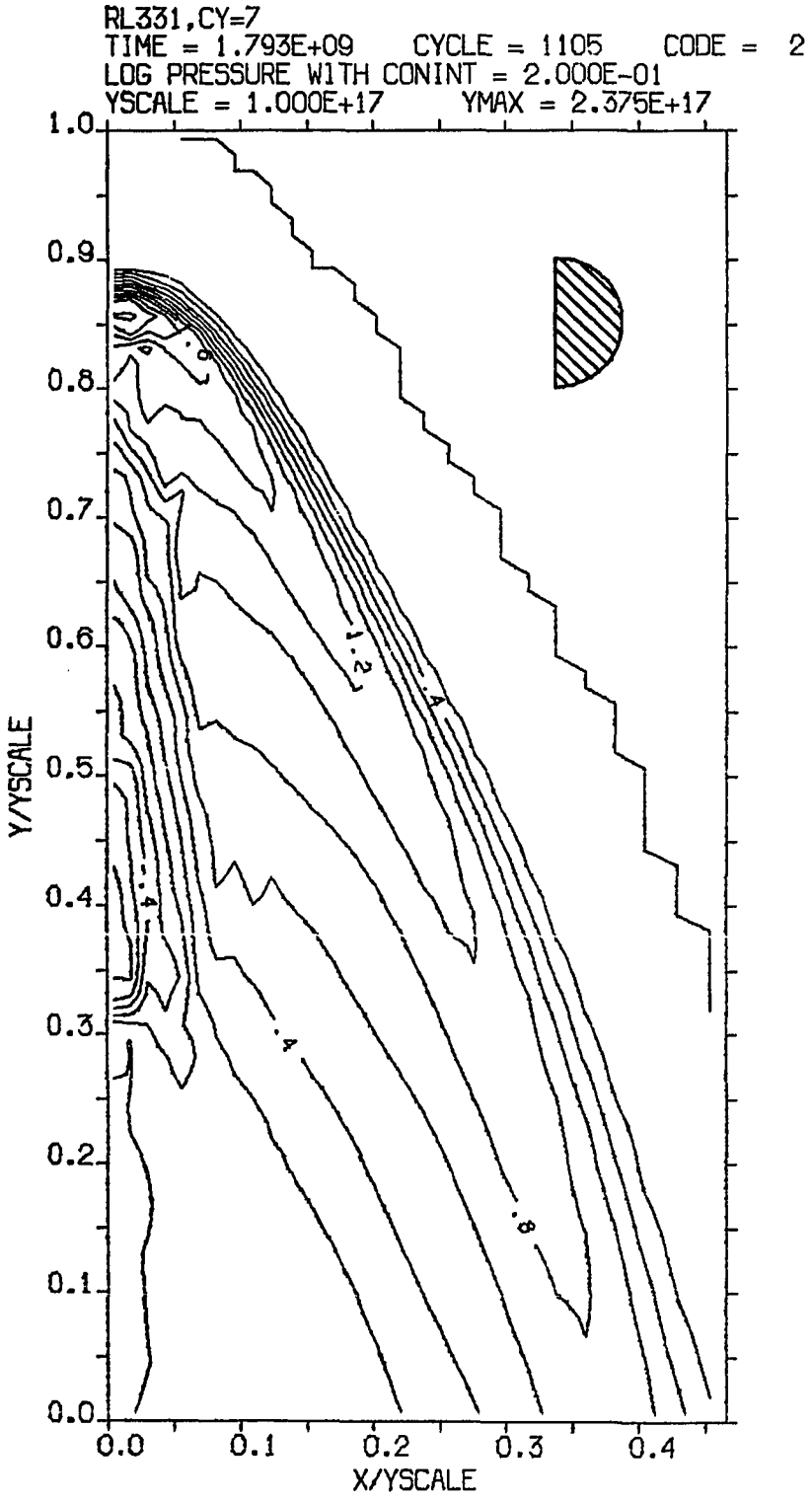

Figure 11d. Contours of the logarithm of pressure (in units where $P_{ic}(0) = 1.0$) at s = 0.95 for model RL331

pressure along the symmetry (y) axis are presented in Figures 12a-d. The profiles at s=0 are indicated to scale, but the cloud's starting position is off the graphs. The plotting conventions for both these types of plots (Figures 11 and 12) are discussed more fully in Appendix B.

As the cloud is moving supersonically (initial Mach number, M_o = 7.37) through the intercloud medium, a shock wave quickly develops at the leading edge of the flow. The position of the bow shock is clearly visible on the contour plot of velocity (Figure 11a). The shock-heated gas directly ahead of the cloud has a density of 3.5 $\rho_{ic}(0)$ (Figure 12b) and a temperature of 58 $T_{ic}(0)$ (Figure 12c). For comparison, the stagnation density at the nose of a blunt obstacle in a supersonic flow with a free stream Mach number of M_∞ is

$$\frac{\rho_s}{\rho_{ic}(0)} = \frac{256}{75}\left(\frac{5}{3}\right)^{0.5} \frac{M_\infty^2}{M_\infty^2+3}\left(\frac{M_\infty^2}{M_\infty^2-0.2}\right)^{1.5} \simeq \frac{4.41\ M_\infty^2}{M_\infty^2+3}, \tag{5.1}$$

and the stagnation temperature is

$$T_s/T_{ic}(0) = 1 + M_\infty^2/3 \tag{5.2}$$

for $\gamma = 5/3$ (Landau and Lifshitz 1959). Using the Mach number for the leading edge of the flow (M=11.9) gives ρ_s = 4.3 $\rho_{ic}(0)$ and T_s = 48 $T_{ic}(0)$. This is rather typical

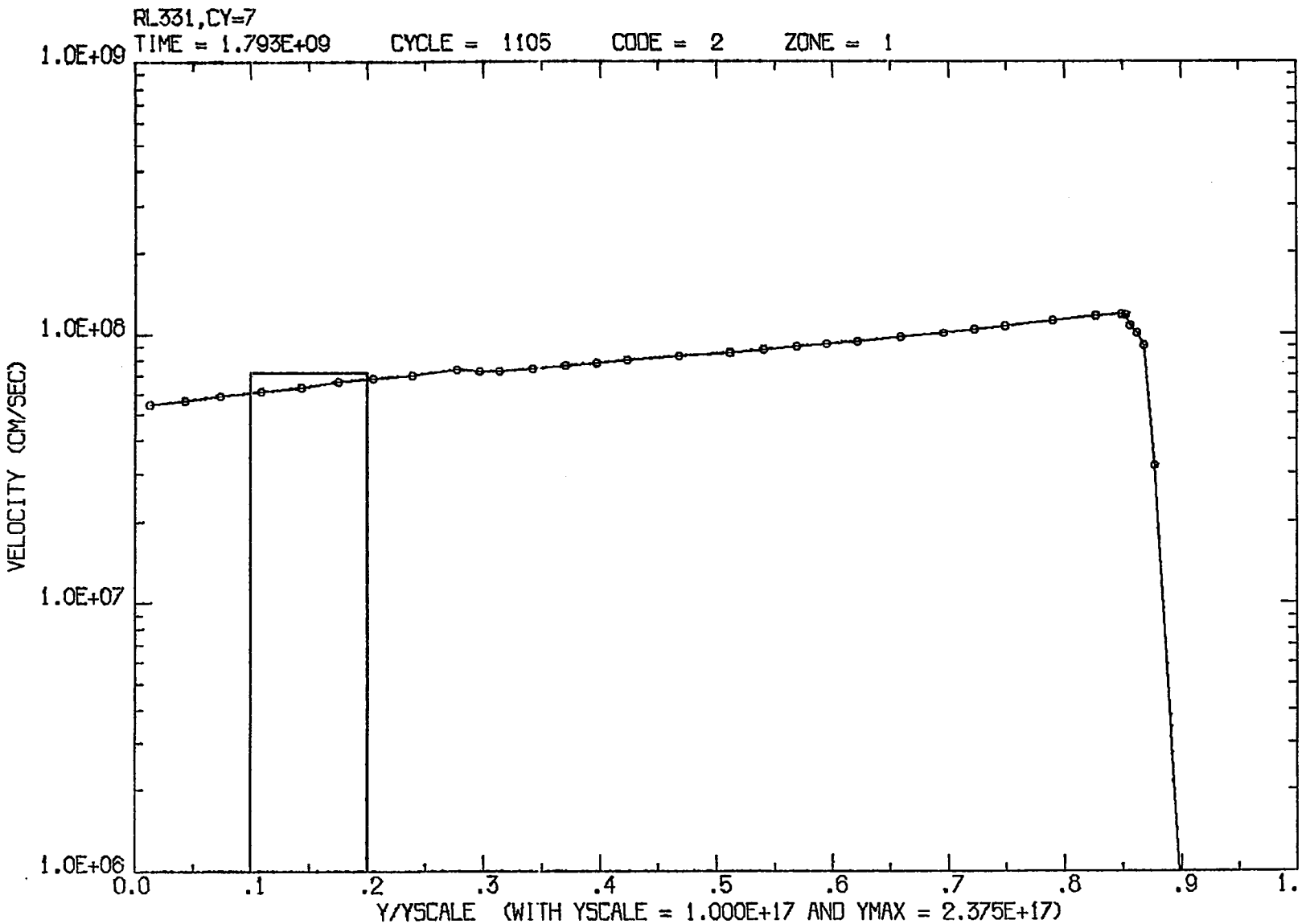

Figure 12a. The velocity (in cm/sec) along the symmetry (y) axis at s = 0.95 for model RL331

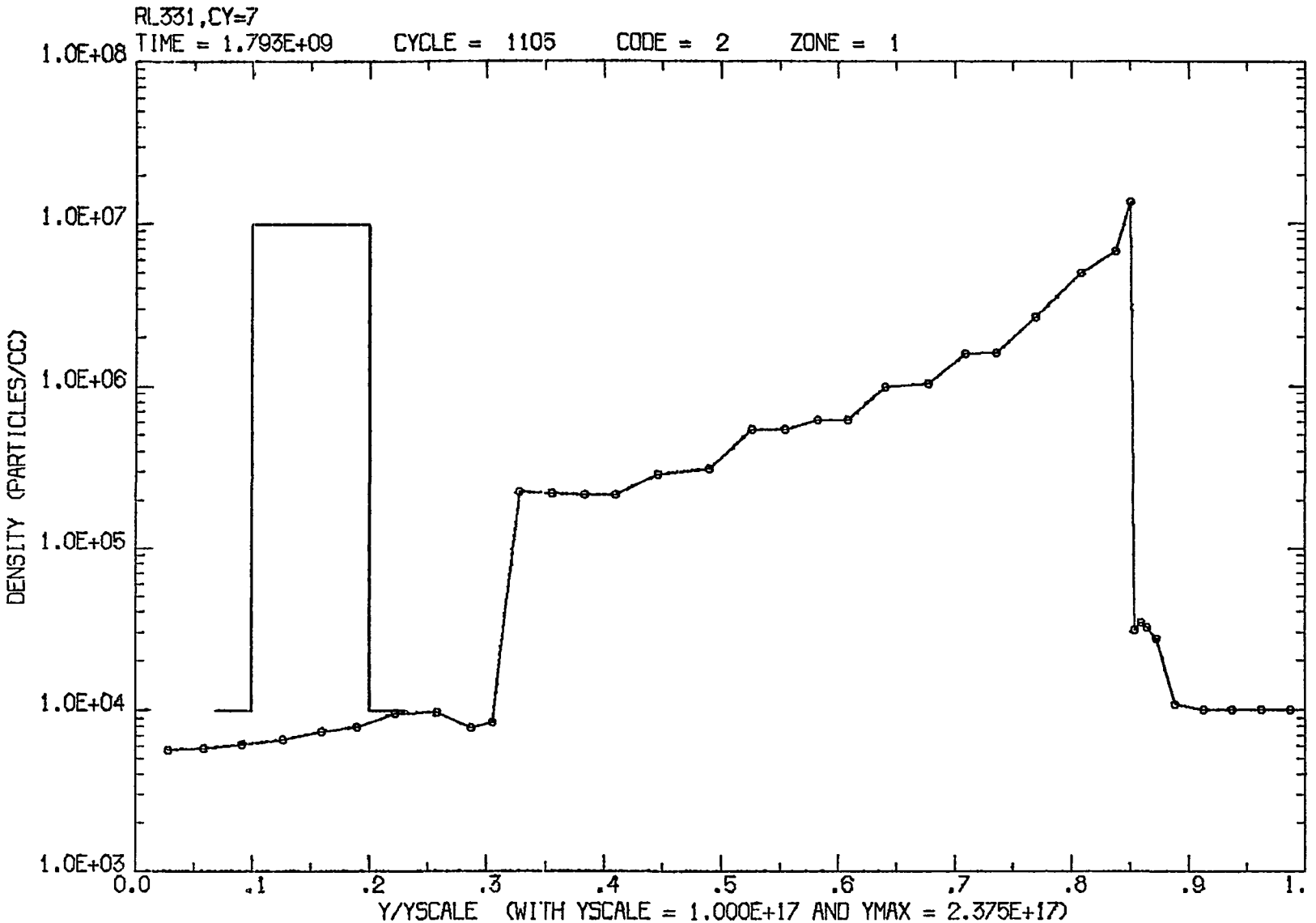

Figure 12b. The density (in nucleons/cm^3) along the symmetry (y) axis at s = 0.95 for model RL331

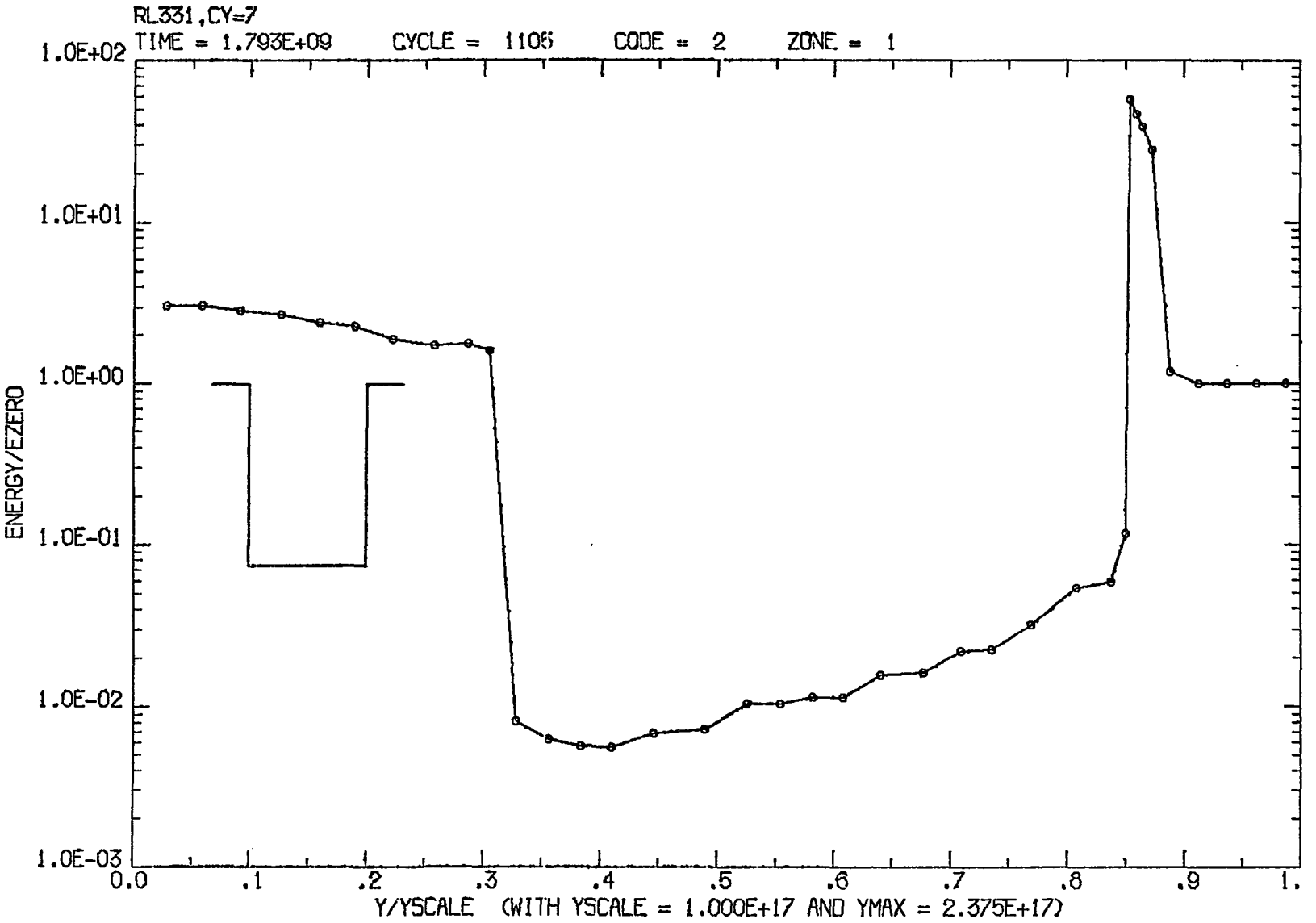

Figure 12c. The specific internal energy (in units where $e_{ic}(0) = 1.0$) along the symmetry (y) axis at s = 0.95 for model RL331

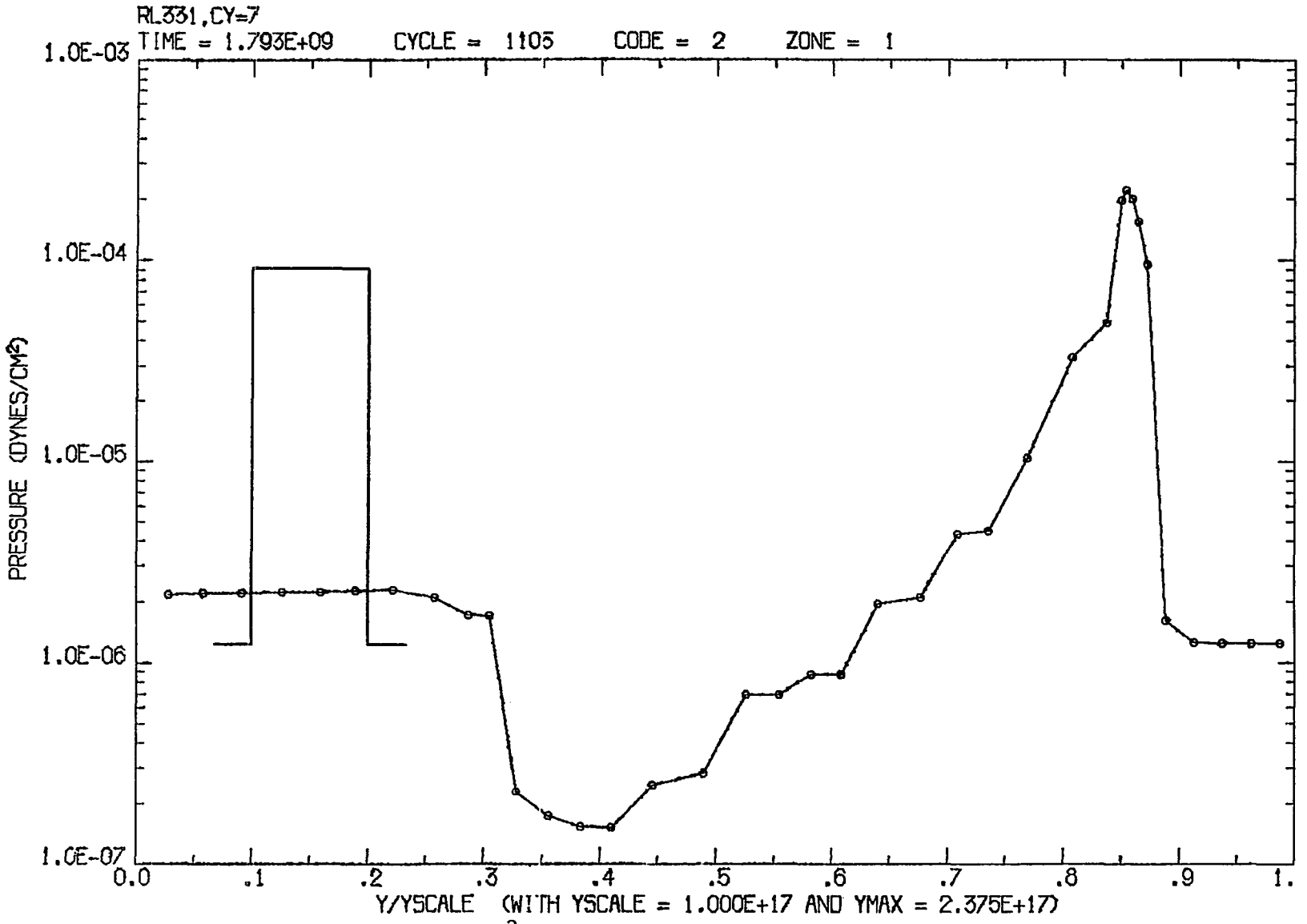

Figure 12d. The pressure (in dynes/cm^2) along the symmetry (y) axis at s = 0.95 for model RL331

agreement; the results of the ram-pressure-confined cloud models generally agree with the predictions of Equations 5.1 and 5.2 to within 30%. The stagnation density and pressure are usually too low and the temperature too high. These errors are comparable to those quoted for the test solutions of Appendix A. Considering the course resolution which is used, these results are entirely reasonable.

The shape of the cloud is well illustrated by the density and internal energy contour plots (Figures 11b and 11c). Initially the gas pressure within the cloud is 74 times the external gas pressure, but it is approximately balanced at the forward face by ram pressure (see Equation 3.26). The resulting confinement at the head of the cloud is reasonably good; the initial density is maintained (Figure 12b). However, adiabatic expansion occurs at the rear, causing density, temperature, and pressure gradients to develop within the cloud (Figures 12b-d). Since the radiation pressure is proportional to the gas density, the leading portion of the cloud is now accelerated more strongly than the rear. This increases the rate of radial expansion above that for free expansion (cf R0334 below); at s = 0.95 the cloud is already 5.5 times longer than its original diameter. Since rarefaction shocks cannot occur in normal gases (Thompson 1972), no shock waves develop within the cloud even though its expansion is

supersonic.

The internal gas pressure in the rear of the cloud has dropped far below the external pressure (Figures 11d and 12d). This is a transient effect due to the use of non-equilibrium initial conditions. The gas pressure within the cloud is initially much greater than the external gas pressure so the cloud expands; it overshoots pressure equilibrium because of the finite response time of the gas. This is primarily a transverse effect; it occurs whether or not there is radiative acceleration and radial expansion (see R0334 and R0221 below), but does not occur if transverse motion is forbidden (see RP221 in Chapter V.D). It is restricted to the rear of the cloud because ram pressure provides transverse compression in the forward portion.

Contour plots of the velocity, density, internal energy, and pressure for RL331 at s = 2.15 (t = 4.05 x 10^9) are displayed in Figures 13a-d. (Note the difference in scaling factors for the x- and y-axes.) Figures 14a-d show the run of these quantities along the symmetry axis at this time. The size of the cloud at s=0 is indicated to scale; its initial position lies off these plots. The transverse gas flow has reversed directions and refilled the pressure cavity at the rear of the cloud and $P_c > P_{ic}$ once again (Figures 13d and 14d). Presumably the gas will

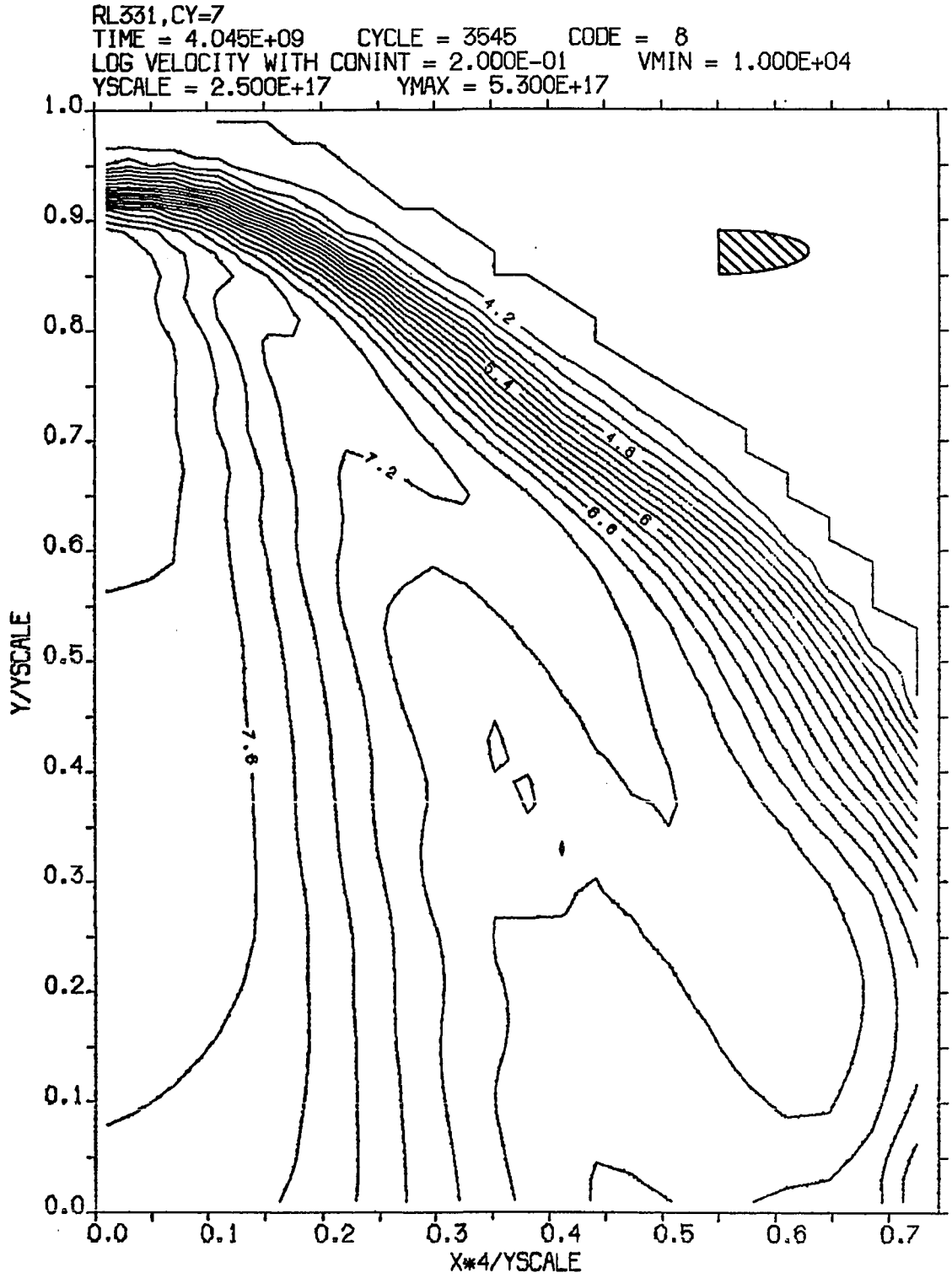

Figure 13a. Contours of the logarithm of velocity (in cm/sec) at s = 2.15 for model RL331

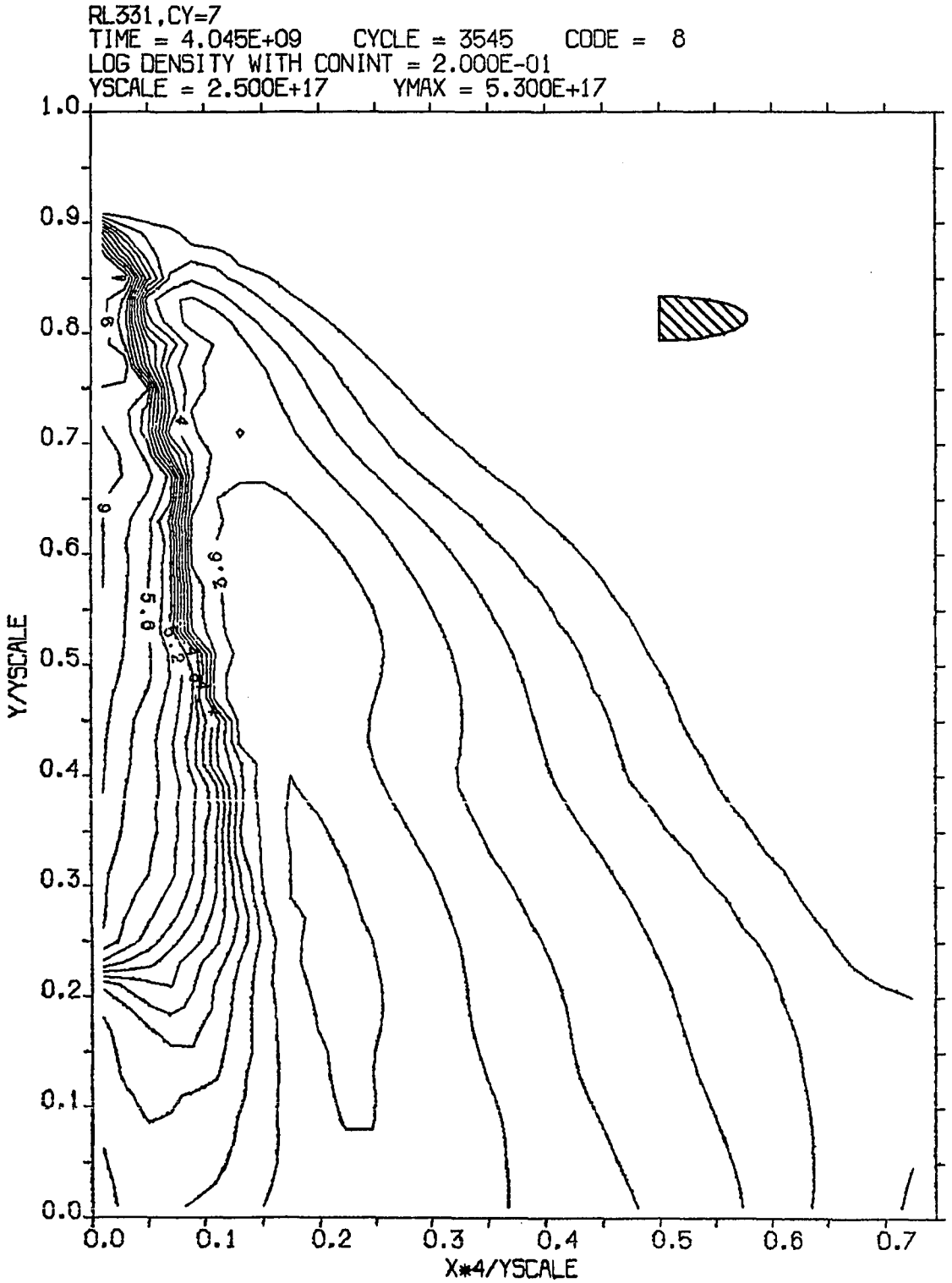

Figure 13b. Contours of the logarithm of density (in nucleons/cm^3) at s = 2.15 for model RL331

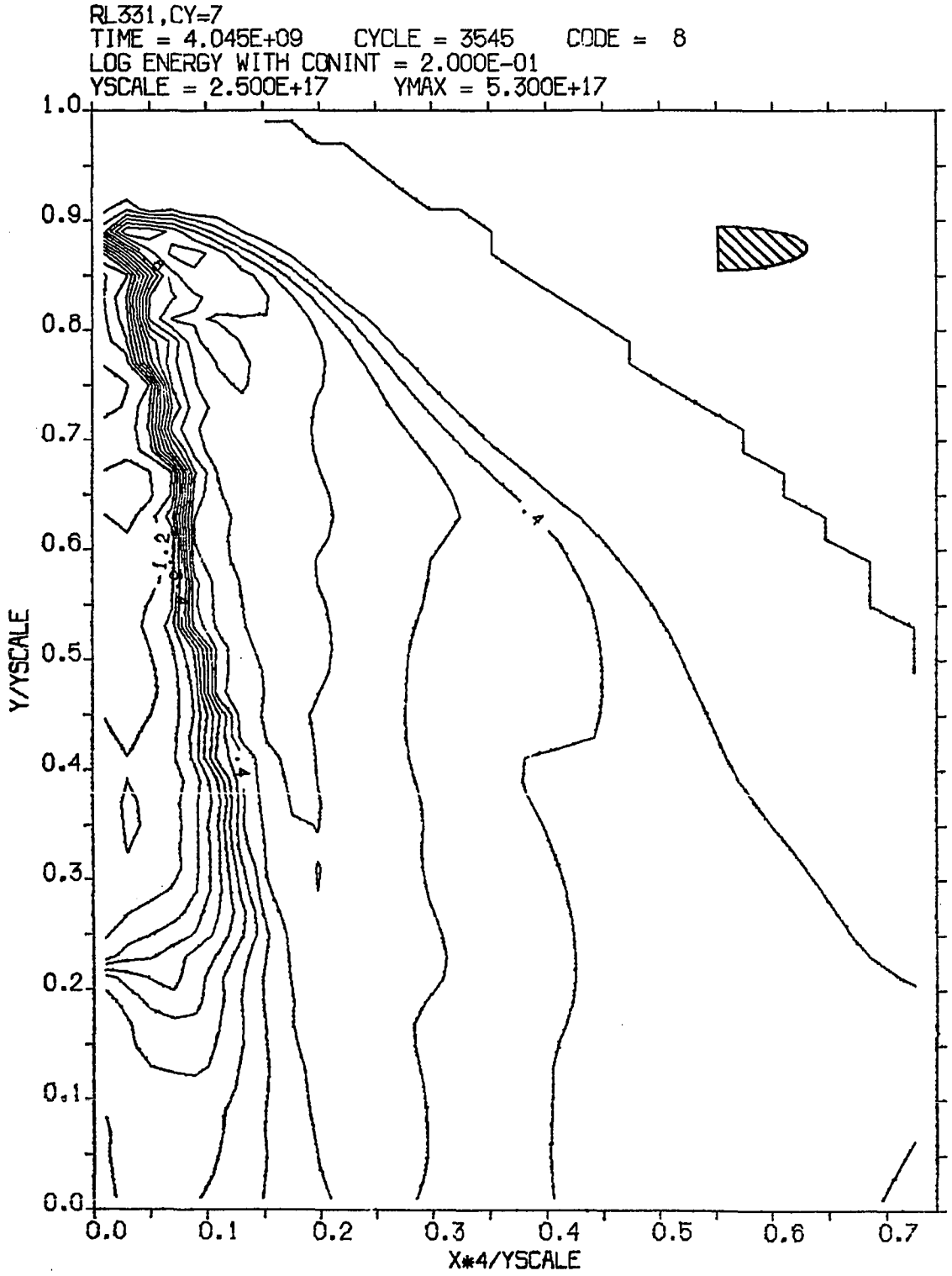

Figure 13c. Contours of the logarithm of specific internal energy (in units where $e_{ic}(0) = 1.0$) at s = 2.15 for model RL331

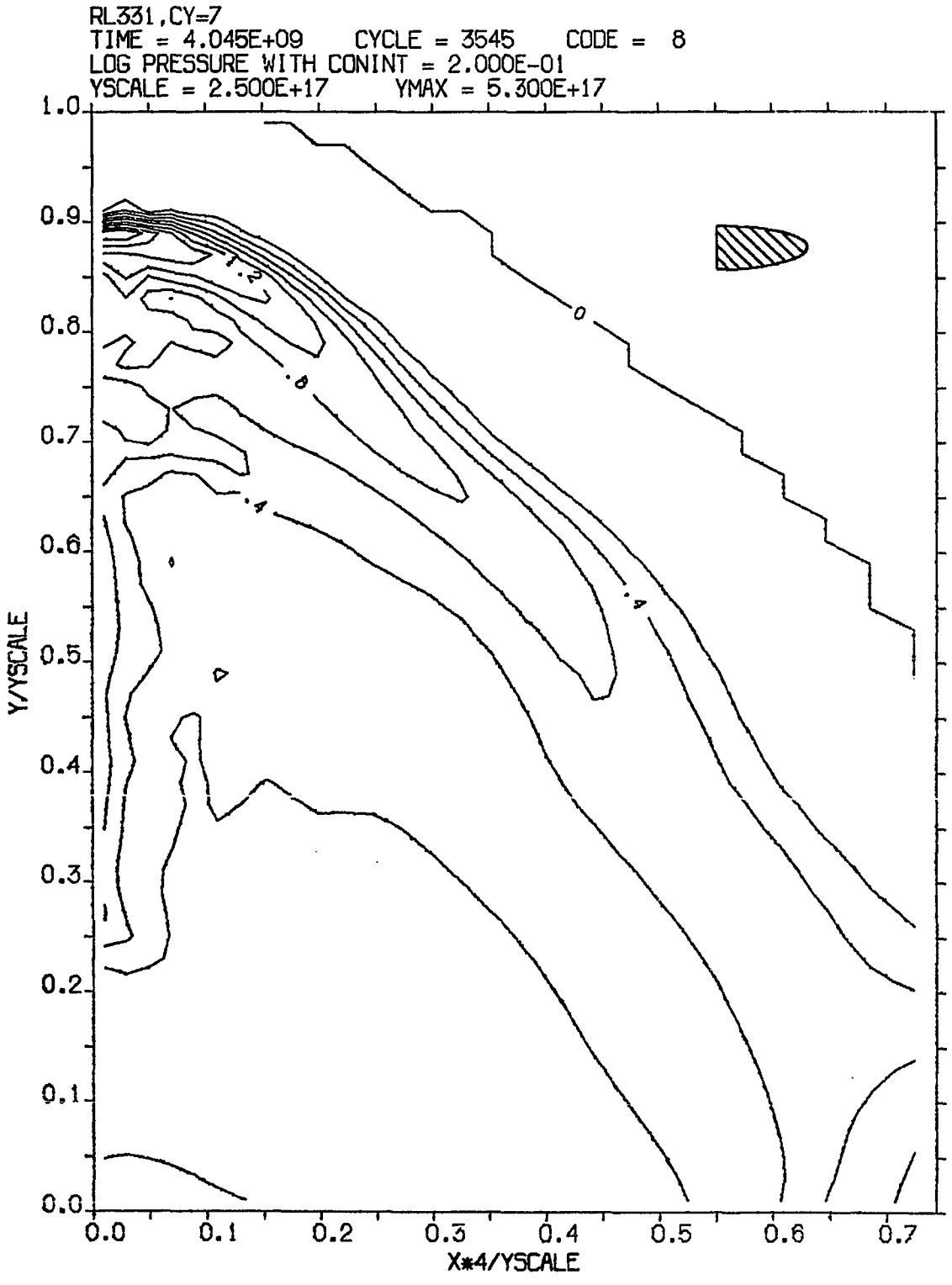

Figure 13d. Contours of the logarithm of pressure (in units where $P_{ic}(0) = 1.0$) at s = 2.15 for model RL331

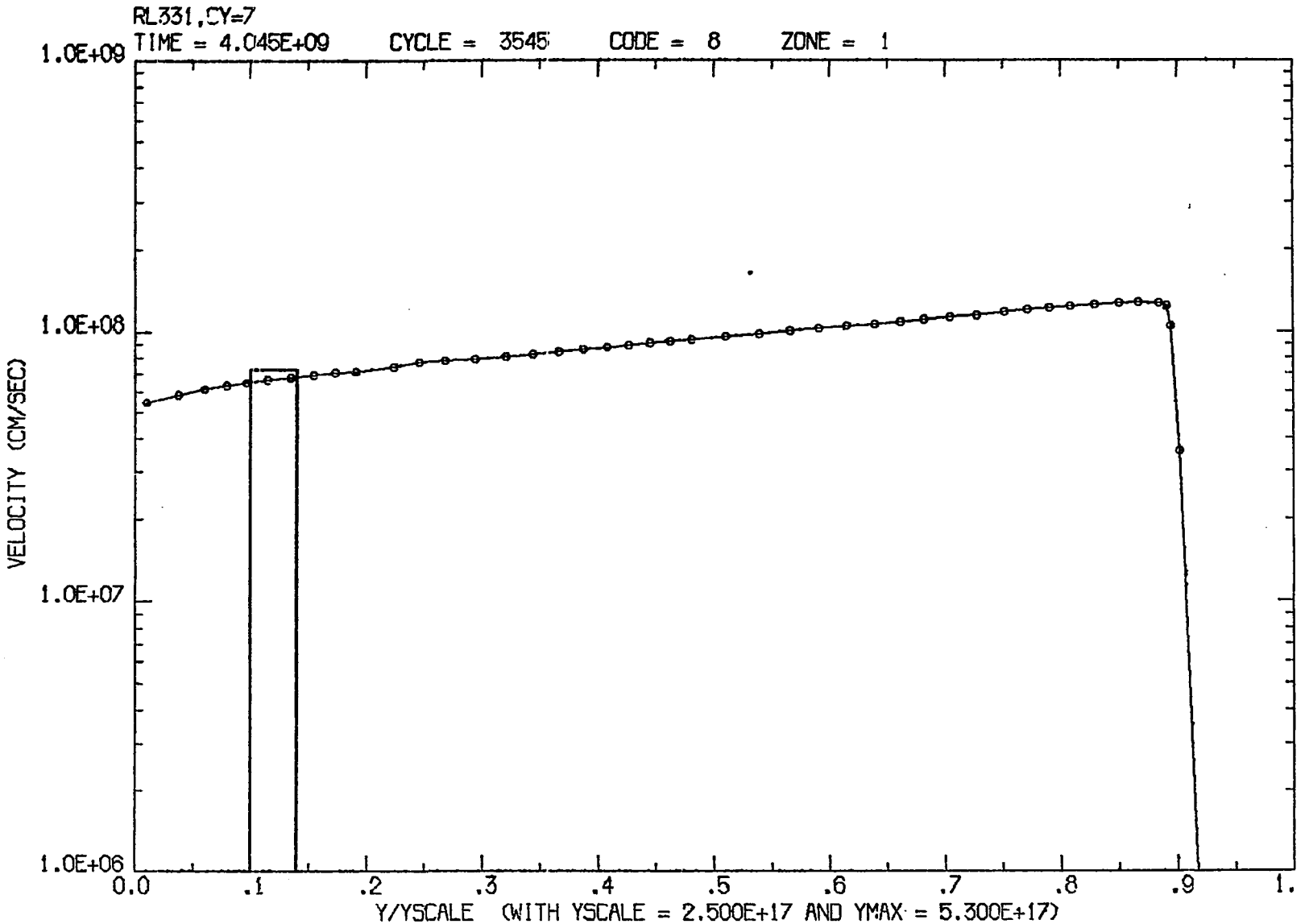

Figure 14a. The velocity (in cm/sec) along the symmetry (y) axis at s = 2.15 for model RL331

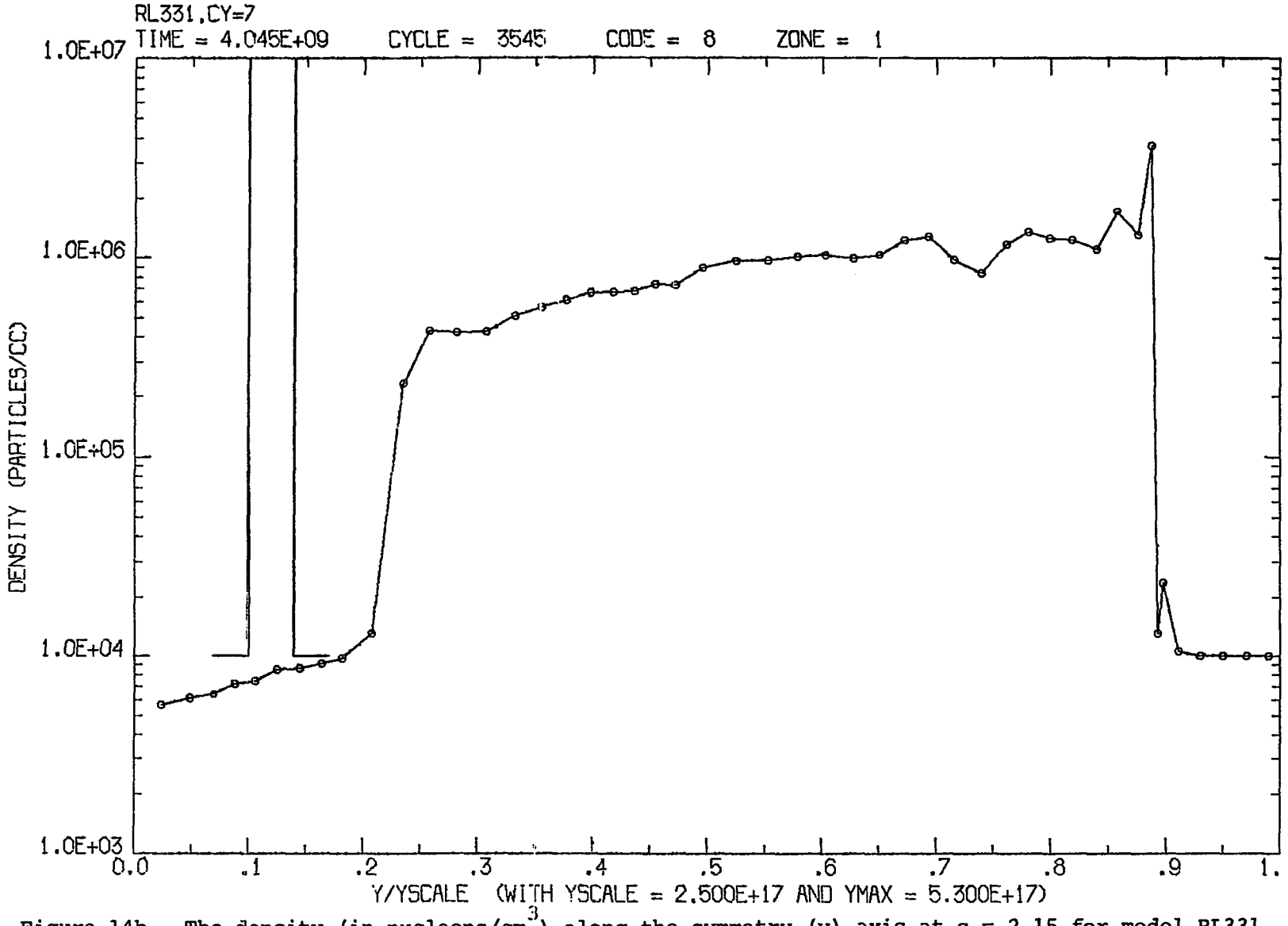

Figure 14b. The density (in nucleons/cm^3) along the symmetry (y) axis at s = 2.15 for model RL331

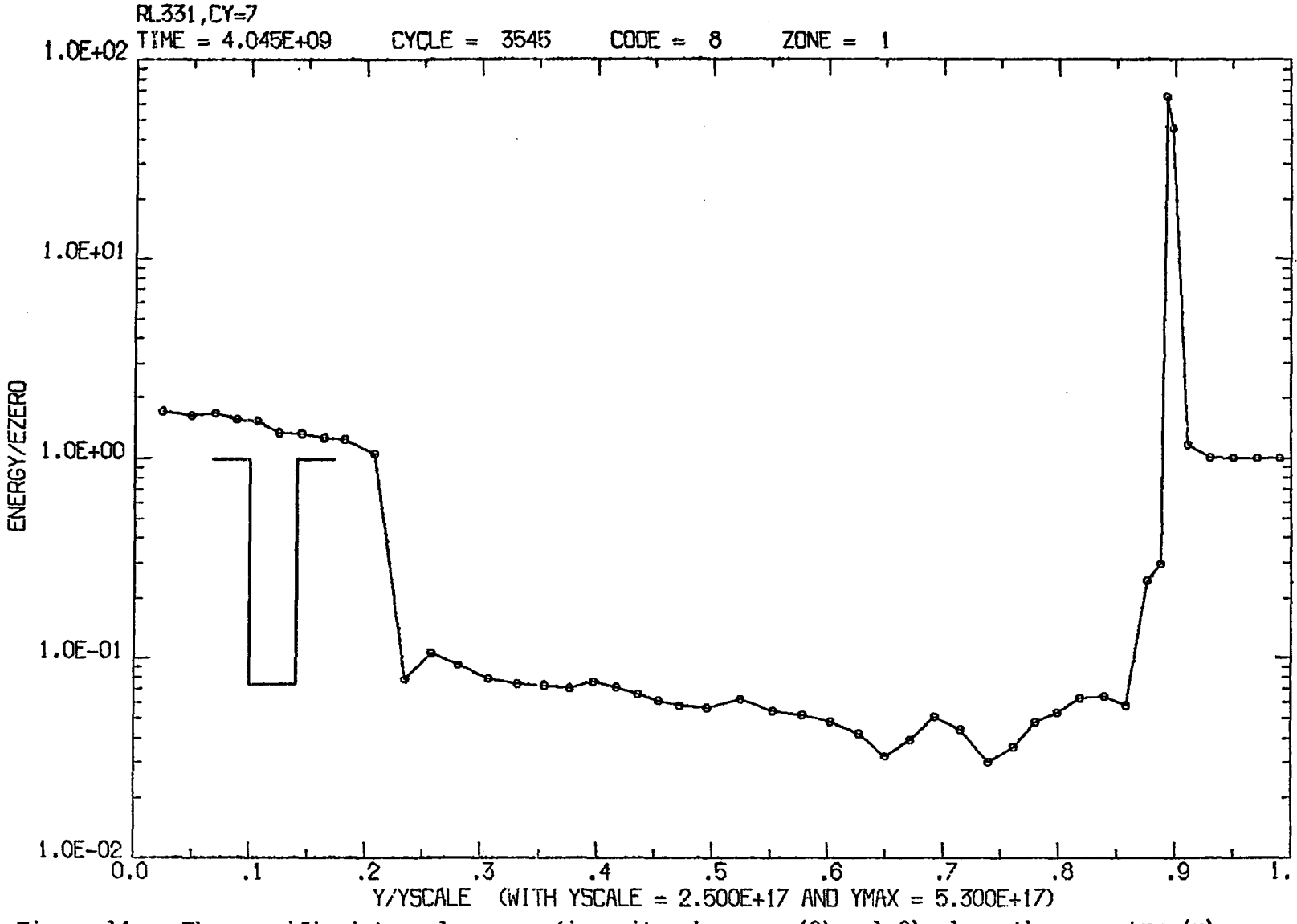

Figure 14c. The specific internal energy (in units where $e_{ic}(0) = 1.0$) along the symmetry (y) axis at s = 2.15 for model RL331

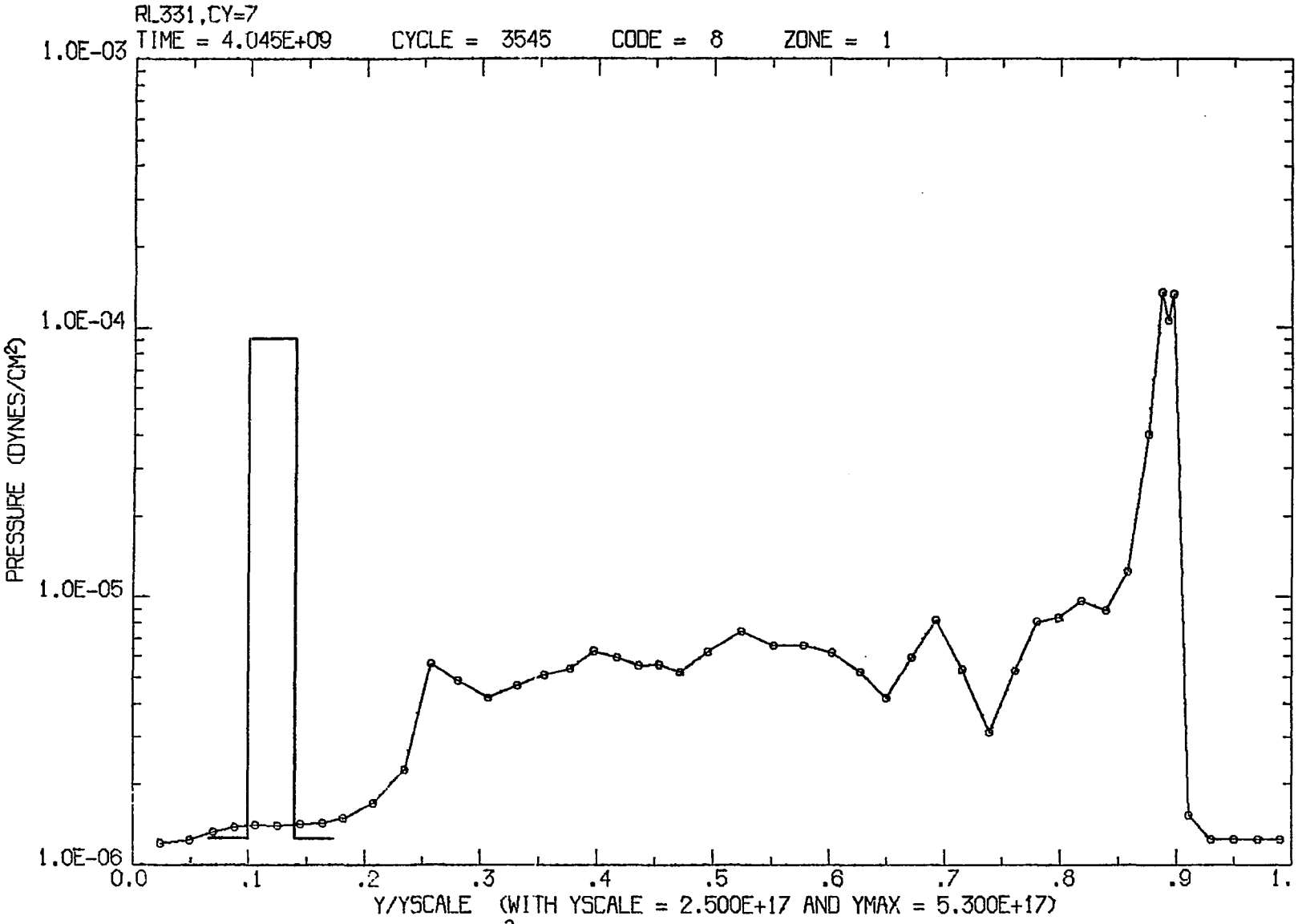

Figure 14d. The pressure (in dynes/cm^2) along the symmetry (y) axis at s = 2.15 for model RL331

flow outwards a second time (at least in the rear) so that pressure equilibrium is ultimately achieved. This second pressure oscillation is probably much smaller than the first one because the pressure did not return to $P_c(0)$ and the gradients are considerably smaller than at s=0. The oscillations have been damped out by the mixing of the cloud and intercloud gas and, to a lesser extent, by the transverse artificial viscous pressure (Equation 4.6). Intercomparison of the various models which have been run suggests that the dynamical effects of this transient phenomenon are small. Discussion of this point is deferred until after the presentation of all the model results (see Chapter V.F).

The column density of the cloud reflects this transient behavior. Figure 15 shows the column density as a function of time for the first eight Eulerian zones of the grid.[1]

[1]These are the column densities between the current, upper Lagrangian boundary and the original, lower Lagrangian boundary (i.e., corrections for chopping (Chapter IV.D) have been included). Thus these curves include the contribution of the external medium as well as that of the cloud. At s=0 the upper boundary is at $y = 6 \times 10^{16}$ cm, so the medium only contributes 0.5%. The grid is extended as the evolution progresses so by s = 2.15 the column density of the undisturbed medium is 5.3×10^{21} (indicated by the arrow in Figure 15). Thus, the column density of the cloud is only slightly smaller than given by the curves in Figure 15, but cannot be obtained by a simple subtraction. The contribution of the external medium is more important for the models with $n_c(0)/n_{ic}(0) = 10^2$ (see below).

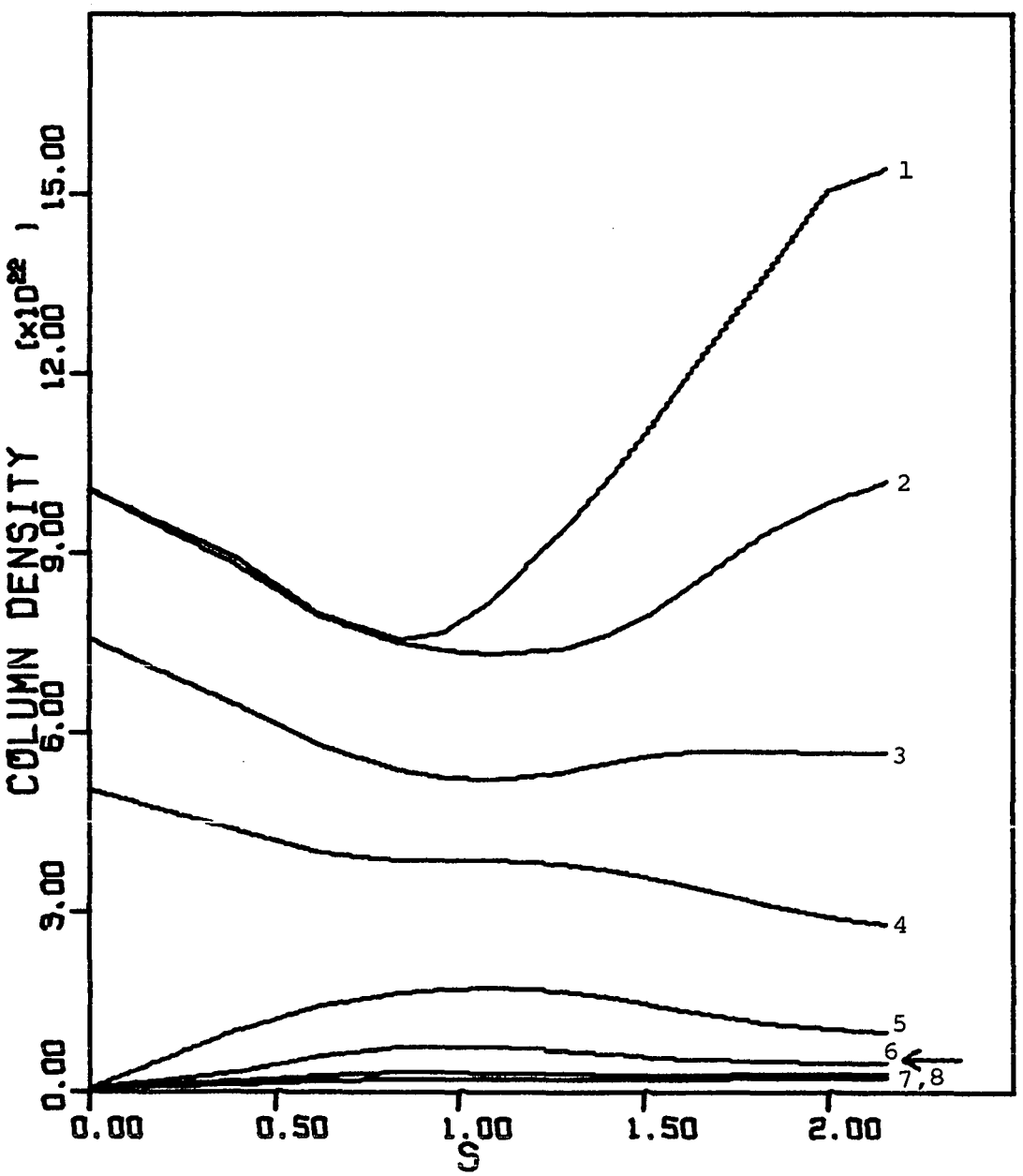

Figure 15. The column density as a function of time for the first eight Eulerian zones of model RL331

The cloud is initially contained in the first four zones (Figure 10). For $s \lesssim 0.8$ transverse expansion occurs and the column densities of zones 1 through 4 decrease, while those of zones 5 and 6 increase.[1] When $s \simeq 0.8$ the flow reverses directions and the column density of the cloud begins to increase again. Actually, the true situation is slightly more complicated than this. Ram pressure compresses the head of the cloud while the rear is still expanding. By $s \simeq 0.8$ the compression at the head exceeds the expansion at the rear so the column density in the inner zones begins to increase, but the cloud is not compressed over its entire length until $s \simeq 1.3$. The column densities of zones 7 and 8 fall below that of the undisturbed medium because of the large, shallow rarefaction which develops behind the cloud (Figure 13b).

The column density (Figure 15) in the first two Eulerian zones has begun to bend over by $s = 2.15$ (also see Figure 18 below, a plot of the column density for RL222). Transverse expansion in the rear of the cloud (the second pressure oscillation mentioned above) is not the sole reason for this behavior. The cloud has reached a terminal velocity (see Figure 17 and the discussion below), so the

---

[1] If it appears that mass is not conserved, remember that these curves must be multiplied by the cross-sectional area of the zone (which goes as $\simeq x^2$ in cylindrical coordinates) to obtain the mass. As discussed in Appendix A, the total mass is conserved to a fraction of a percent.

ram pressure is no longer increasing and therefore the rate of transverse compression at the head of the cloud decreases. In addition, the rate at which mass is being forced out of the cloud along the bow shock is continuing unabated (see discussion below). This also leads to an eventual decline in the column density for the inner few Eulerian zones.

There are other features of interest in Figures 13 and 14. The pressure contours now cross the cloud boundary smoothly, rendering the cloud nearly invisible (Figure 13d). The pressure gradients which remain are primarily in the vicinity of the bow shock (Figure 14d). The shocked intercloud gas adiabatically cools as it moves downstream; by the time it reaches the rear of the cloud its pressure is once again nearly $P_{ic}(0)$. Its density is now somewhat less than $n_{ic}(0)$ and its temperature is slightly higher than $T_{ic}(0)$.

The transverse inflow of matter has raised both the density and the temperature in the rear of the cloud so that its profile (Figures 14b and c) is flatter than at $s = 0.95$. The shape of the cloud is still easily discernible on the contour plots of density and internal energy (Figures 13b and c). The cloud has been compressed in the transverse direction, but by just how much is

difficult to say because of the poor resolution. The cloud has continued to expand in the radial direction and is now 17 times its original length. The length of RL331 as a function of time is plotted in Figure 16; the expansion shows no sign of slowing down.

It is difficult and expensive to evolve this model further because of the large Mach numbers ($\simeq$ 13) and the extreme length of the cloud. The original grid only spanned 21 cloud diameters in the y-direction! This grid was extended by the methods outlined in Chapter IV.D, but the cloud still reached the top by s = 1.63. At this time the resolution in the y-direction was reduced by a factor of 2 (every two cells were combined) so that the model could be evolved further to s = 2.15.

How much has the cloud been accelerated? This is not an easy question to answer because the cloud is no longer moving coherently and because its boundaries are no longer sharply defined. A useful approach is to define the densest material in the grid as the cloud and then determine its acceleration. To this end, the grid cells are ordered according to their density (at a few selected times) with the subscript i denoting the i-th densest cell. Then the quantities $j_n(s)$ are determined by forming the 20 sums

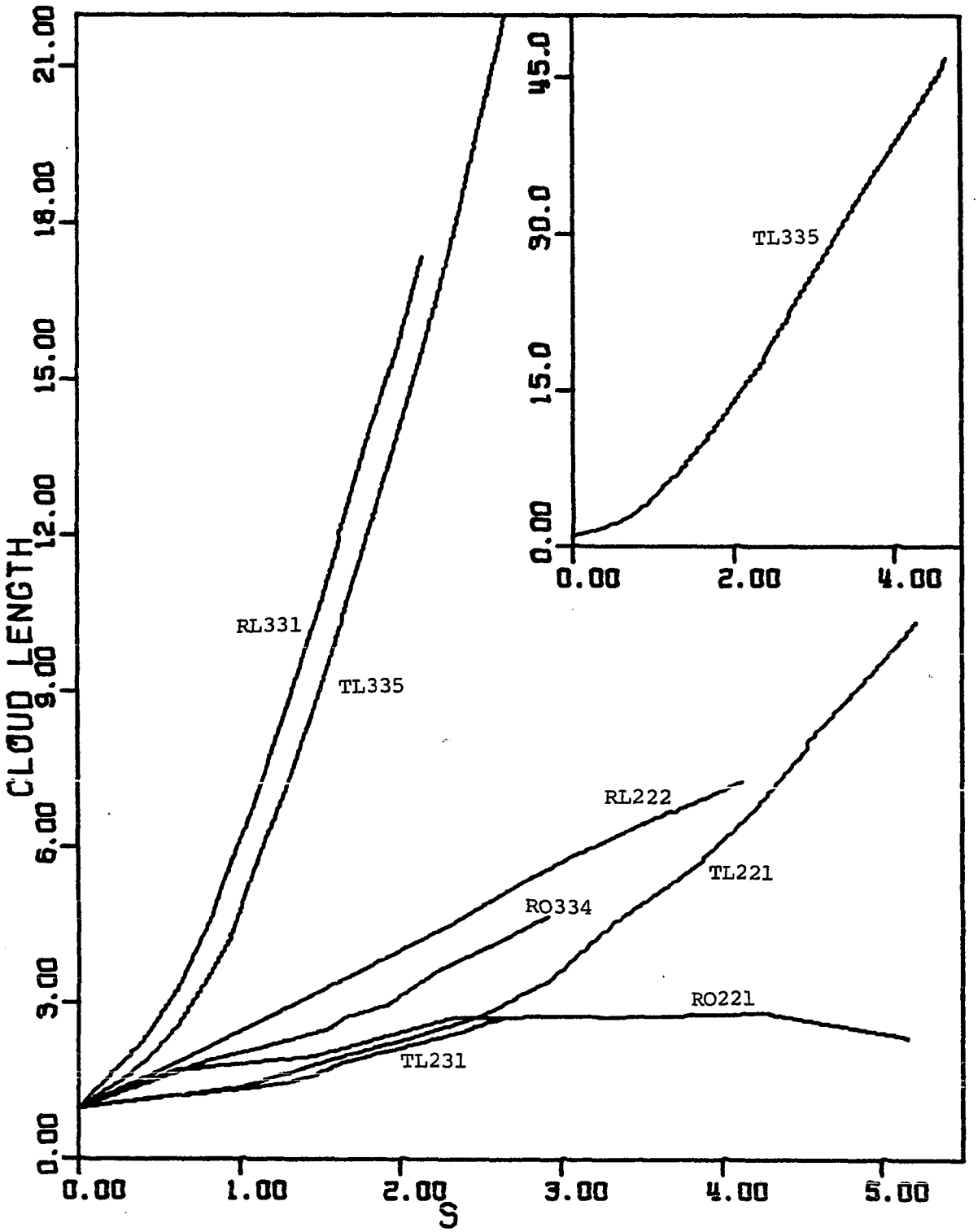

Figure 16. Normalized cloud length L/L_o as a function of time s. Insert shows entire curve for TL335 on a reduced scale

$$\sum_{i=j_{n-1}}^{j_n} m_i(s) = 0.05\ m_c(0), \qquad (5.3)$$

where m_i is the mass of the i-th densest grid cell. The subscript n runs from 1 to 20 and denotes the n-th densest group of grid cells with a mass of 5% of the original cloud. Each sum starts where the previous one ended and the j_n are noninteger so that Equation 5.3 is satisfied exactly. By definition, $j_0 = 1$ and j_{20} is the total number of cells contained in the cloud. Now, the average Mach number for each 5% of $m_c(0)$ is defined by the simple momentum average

$$\bar{M}_n(s) = \sum_{i=j_{n-1}}^{j_n} m_i(s)v_i(s)/0.05\ m_c(0)c_{ic}(0)\ . \qquad (5.4)$$

Thus, $\bar{M}_1(s)$ is the average Mach number for the grid cells with the highest density and a mass of $0.05\ m_c(0)$. The number of whole cells averaged in an $\bar{M}_n$ ranges from 0 to 10 for $n \lesssim 10$, but may be a hundred for $n > 10$. The $\bar{M}_n$ are computed every few hundred time steps; the jumps at constant s are due to grid rezoning (Chapter IV.D).

Figure 17 displays $\bar{M}_n(s)$ for RL331; the curves are labelled by n. In general, the densest material has been accelerated the most. However, even $\bar{M}_1(s)$ is quickly approaching a rather low terminal velocity. For comparison, the curve labelled CS gives the acceleration for an optically thin cloud of constant size (Equation 2.17). For the

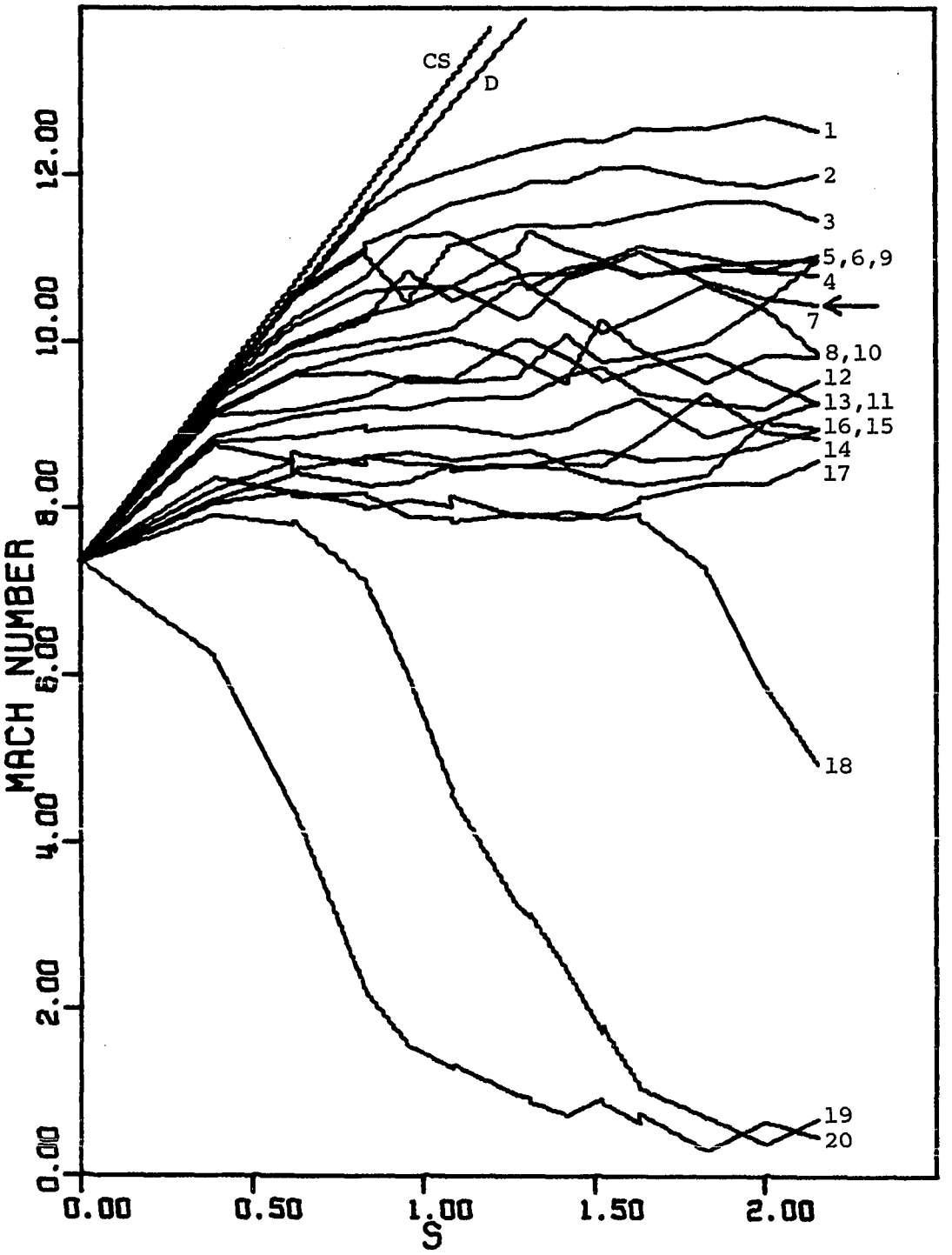

Figure 17. The Mach number for each 5% of the cloud RL331 as a function of time

parameters of RL331, the simple drag theory of Chapter III.A gives $M_\infty = 43.9$ and the trajectory labelled D in Figure 17 (Equation 3.3). The arrow at $s = 2.5$ indicates the terminal velocity obtained from the theory of optically thin, freely expanding clouds given in Chapter II.B (Equation 2.13) with $B = 1/\sqrt{3}$). It is clear that the terminal velocity attained by RL331 is far below that expected were the cloud to remain of constant size (with or without drag). In fact, the cloud's center of mass has a terminal Mach number of only 9.0, less than that of its freely expanding counterpart. The primary reason for this low terminal velocity is the fact that the one-dimensional, radiation-pressure-driven expansion of RL331 is as effective in lowering the average cloud density as is the three-dimensional, free expansion of the simple clouds in Chapter II. Discussion of the apparent mass shedding (see $\bar{M}_n(s)$ for $n \geq 18$) is deferred momentarily.

2. RL222

Model RL222 has an initial column density of 10^{22} and $n_c(0)/n_{ic}(0) = 10^2$, both a factor of ten less than for RL331. A complete list of the parameters is given in Table 1. RL222 has been evolved twice as long as RL331; the results are qualitatively similar. A plot of the column density as a function of time for the first eight

Eulerian zones is given in Figure 18. The actual variation is smoother than depicted by this small number of linearly connected data points. The dotted line indicates the growth of the column density for the undisturbed medium due to the extension of the grid. As in RL331, the outer zones (6-8) fall below this curve because of the rarefaction behind the cloud. Qualitatively, the column density behaves very similarly to that of RL331 (Figure 15). As discussed there, the oscillations are primarily a transient response to the use of nonequilibrium initial conditions. RL222 has a deeper minimum ($s \simeq 1.2$) and a lower maximum ($s \simeq 2.8$) than RL331. This is probably a result of the larger rate at which matter flows out along the bow shock (see below). Also, RL222 receives less acceleration, so the ram-pressure compression at the head of the cloud is smaller.

The run of density, internal energy, and pressure along the symmetry axis at the end of the evolution ($s = 4.13$, $t = 9.62 \times 10^9$) are displayed in Figures 19a-c. For comparison, the initial profiles are given to scale. The rear of the cloud is in pressure equilibrium with the ambient medium, essentially at $P_{ic}(0)$ (Figure 19c). From the pressure profiles at earlier times and the column density as a function of time, it appears that this is true equilibrium. That is, the pressure oscillations have been damped out.

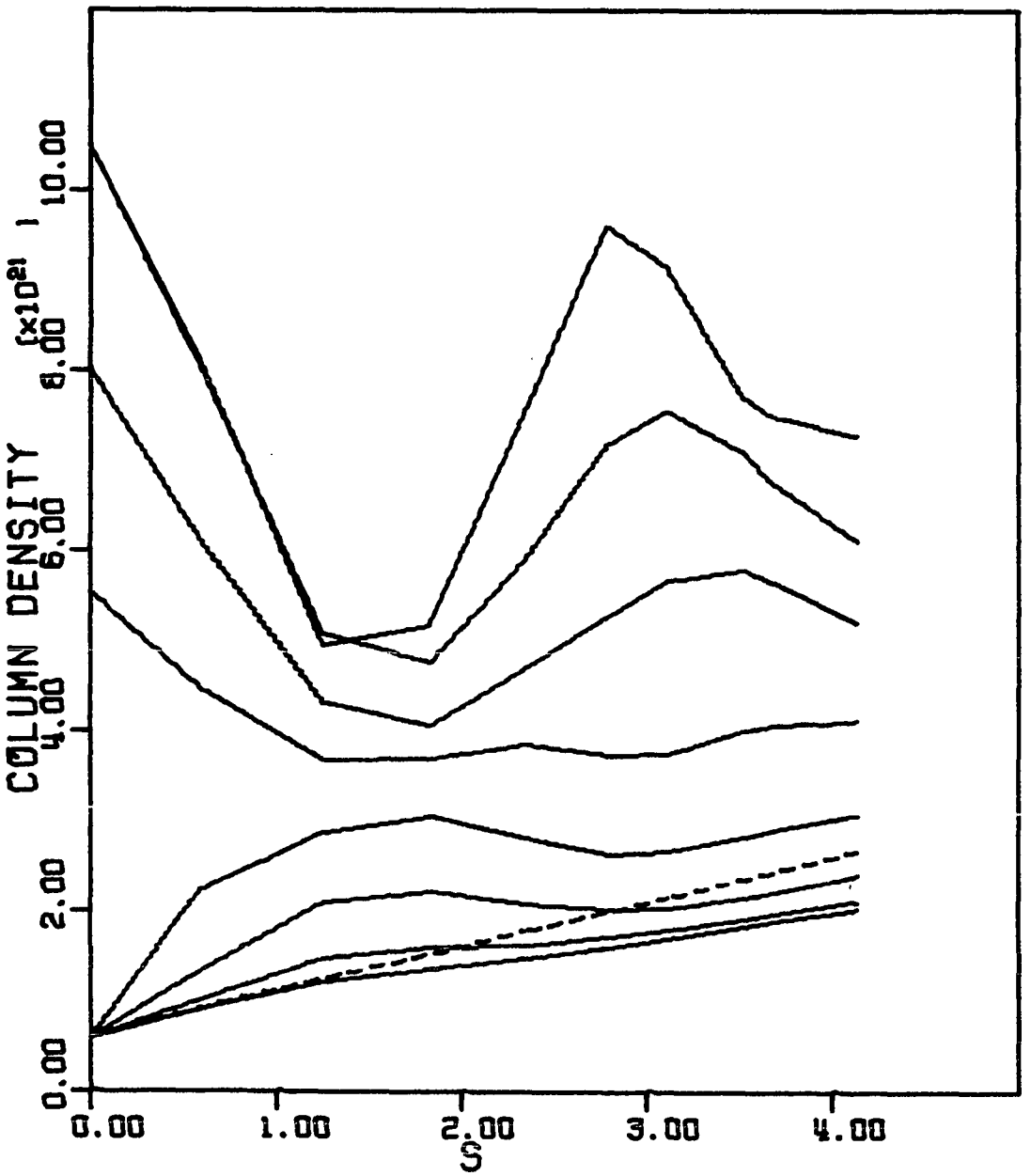

Figure 18. The column density as a function of time for the first eight Eulerian zones of model RL222

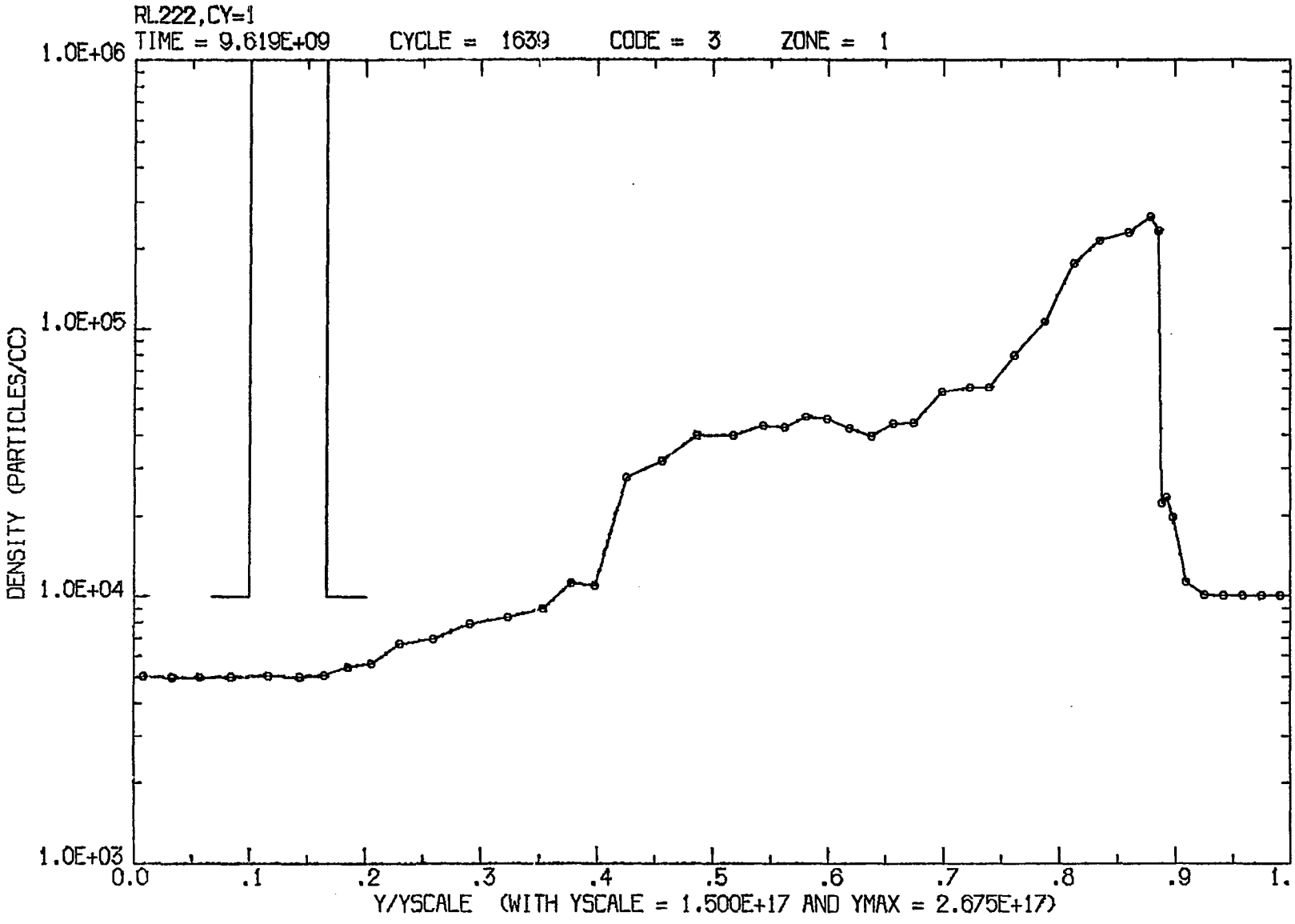

Figure 19a. The density (in nucleons/cm^3) along the symmetry (y) axis at s = 4.13 for model RL222

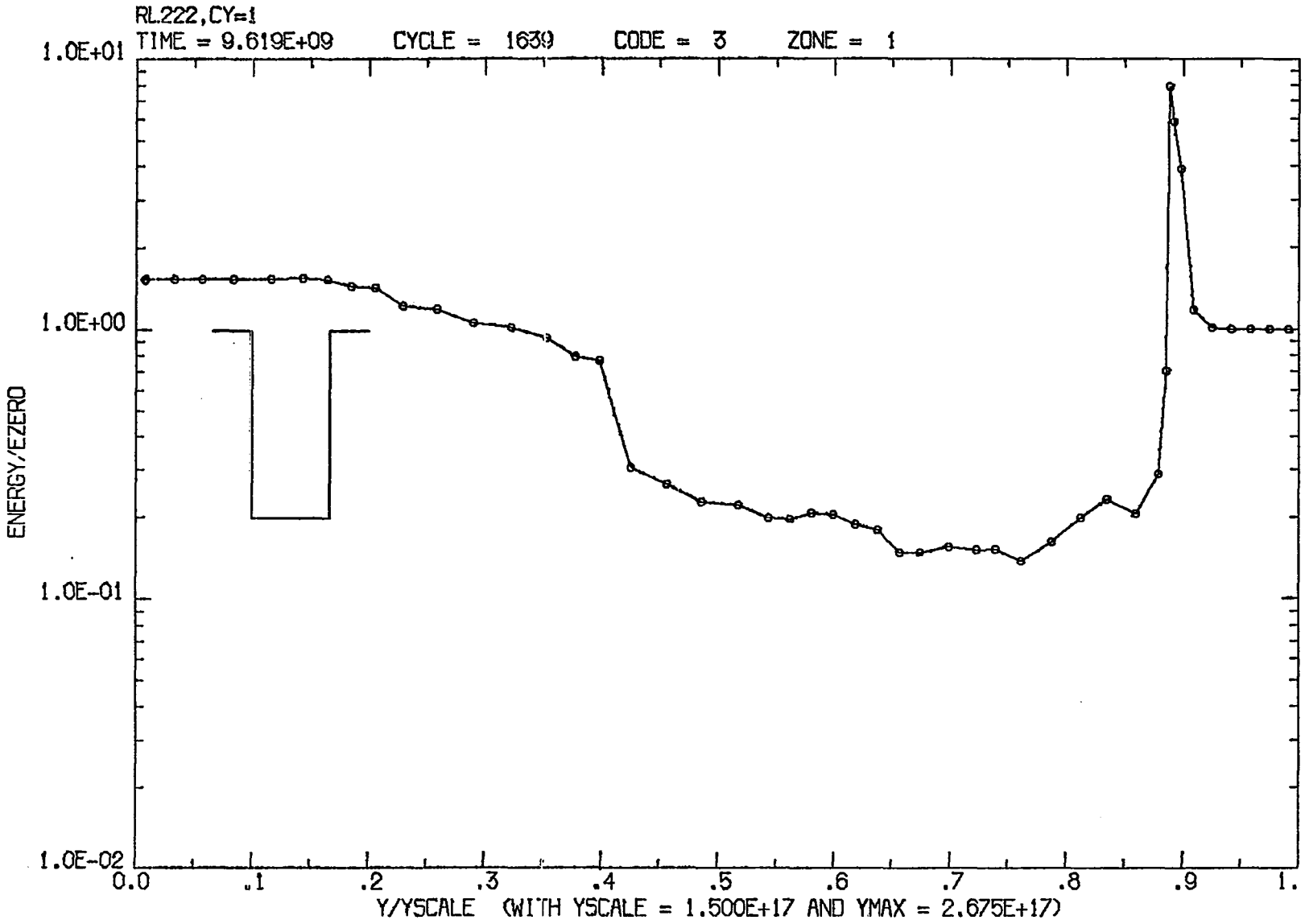

Figure 19b. The specific internal energy (in units where $e_{ic}(0) = 1.0$) along the symmetry (y) axis at s = 4.13 for model RL222

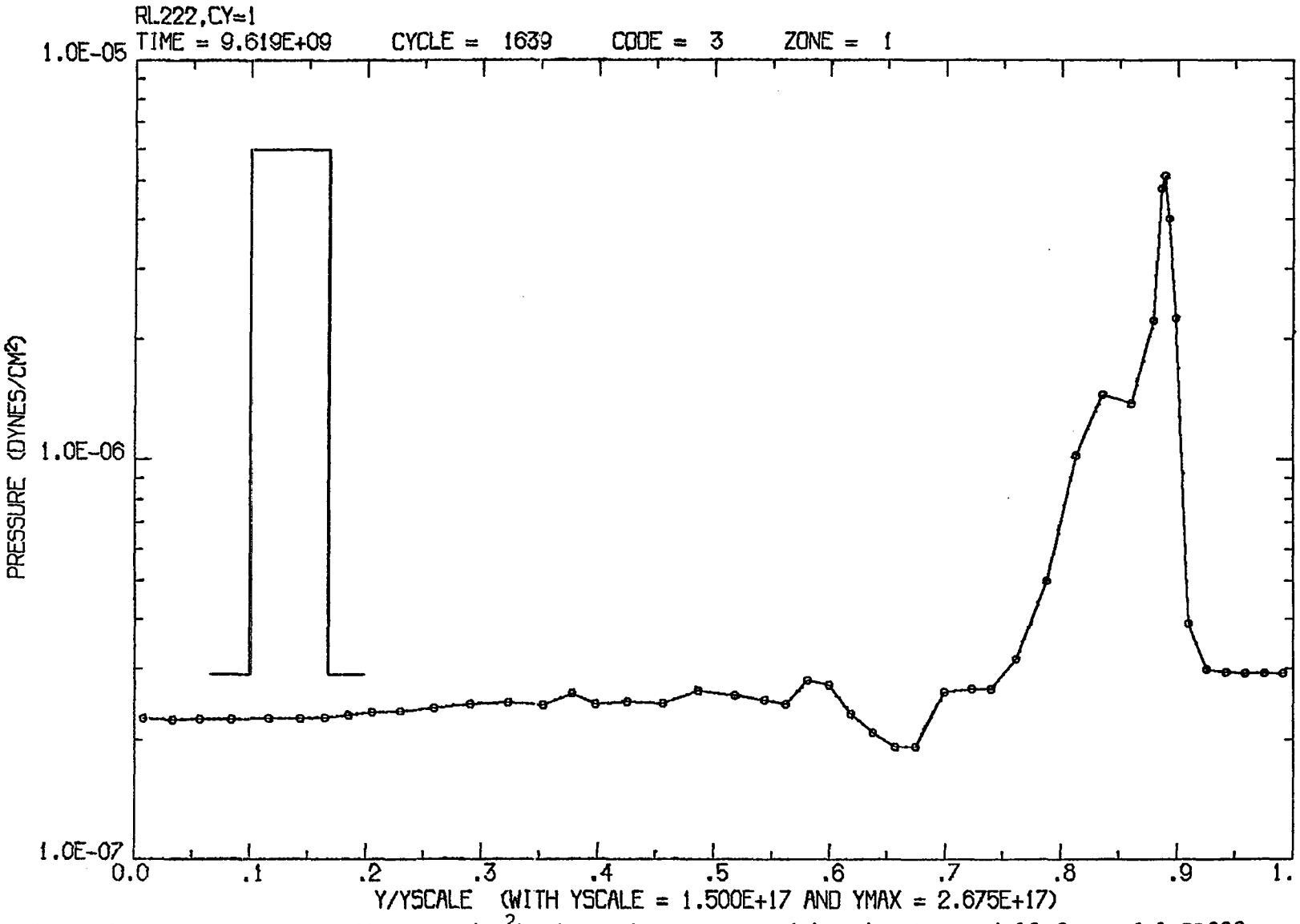

Figure 19c. The pressure (in dynes/cm^2) along the symmetry (y) axis at s = 4.13 for model RL222

RL222 has not expanded in the radial direction as rapidly as did RL331 (Figure 16). This is a direct result of the column density, and consequently the radiation pressure, being an order of magnitude smaller.

However, the decrease in radiation pressure also means a decrease in the acceleration. Figure 20 displays $\bar{M}_n(s)$ with n=1 to 20 for RL222 (see Equation 5.4). The behavior of $\bar{M}_n(s)$ for large n is even more striking than in RL331 (Figure 17). Nearly 50% of the initial cloud's mass has suffered a large deceleration and is essentially at rest. How does this happen? Figure 21a presents the velocity contours for RL222 at s = 4.13 and Figure 21b presents the corresponding density contours. The size of the original cloud is shown to scale. Ranking the cells according to density (as for Equation 5.3) results in the contours plotted in Figure 21c. The contour labels refer to the mass enclosed by the respective contours; the contour interval is 10% of $m_c(0)$. This figure shows that the confinement at the head of the cloud is not nearly as good as it might have appeared in Figure 21b. The pressure gradients along the bow shock (cf Figures 11d and 13d for RL331) force mass out of the cloud; it is then mixed with shocked intercloud gas and decelerated. This effect is more pronounced in RL222 than in RL331 because the bow shock is

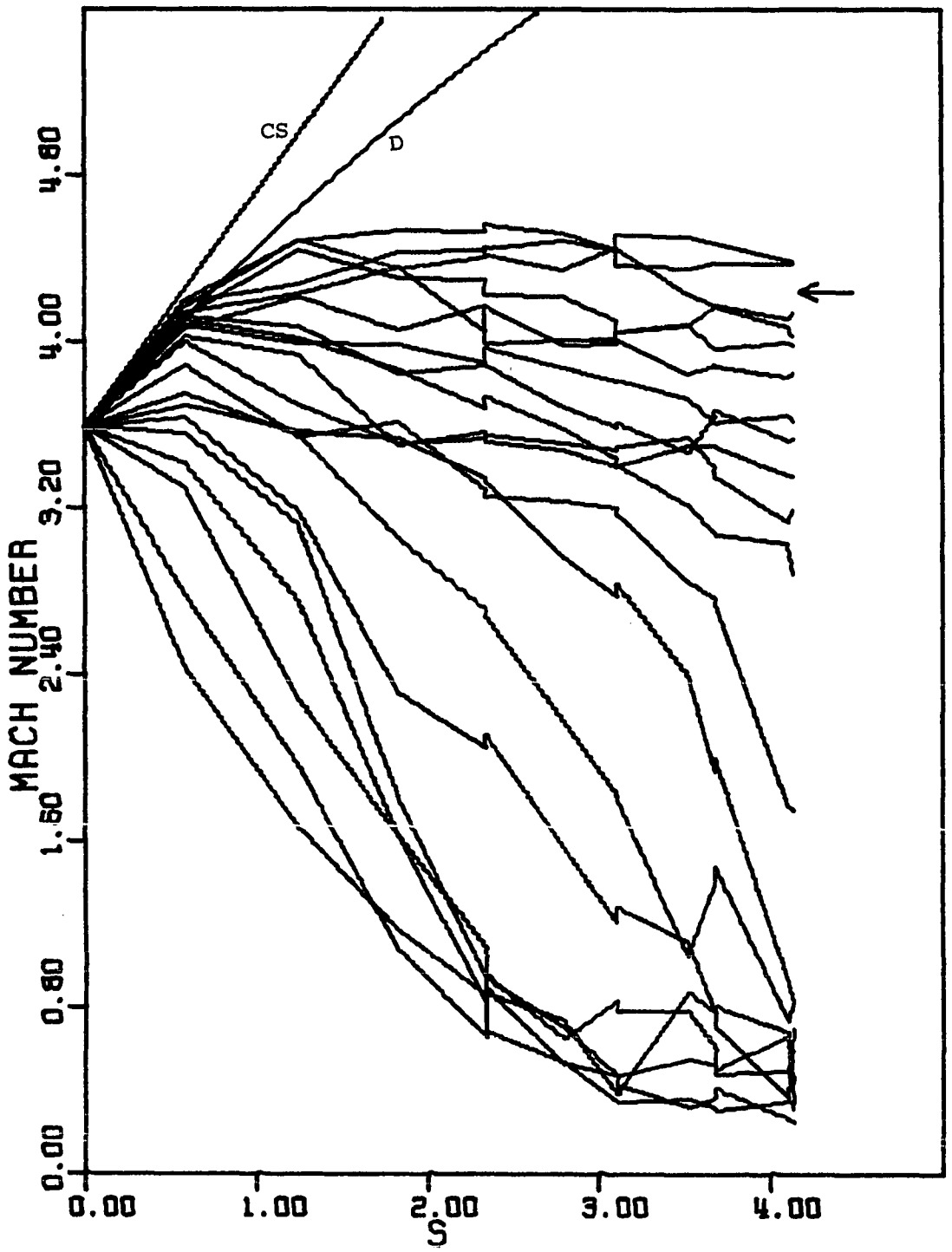

Figure 20. The Mach number for each 5% of the cloud RL222 as a function of time

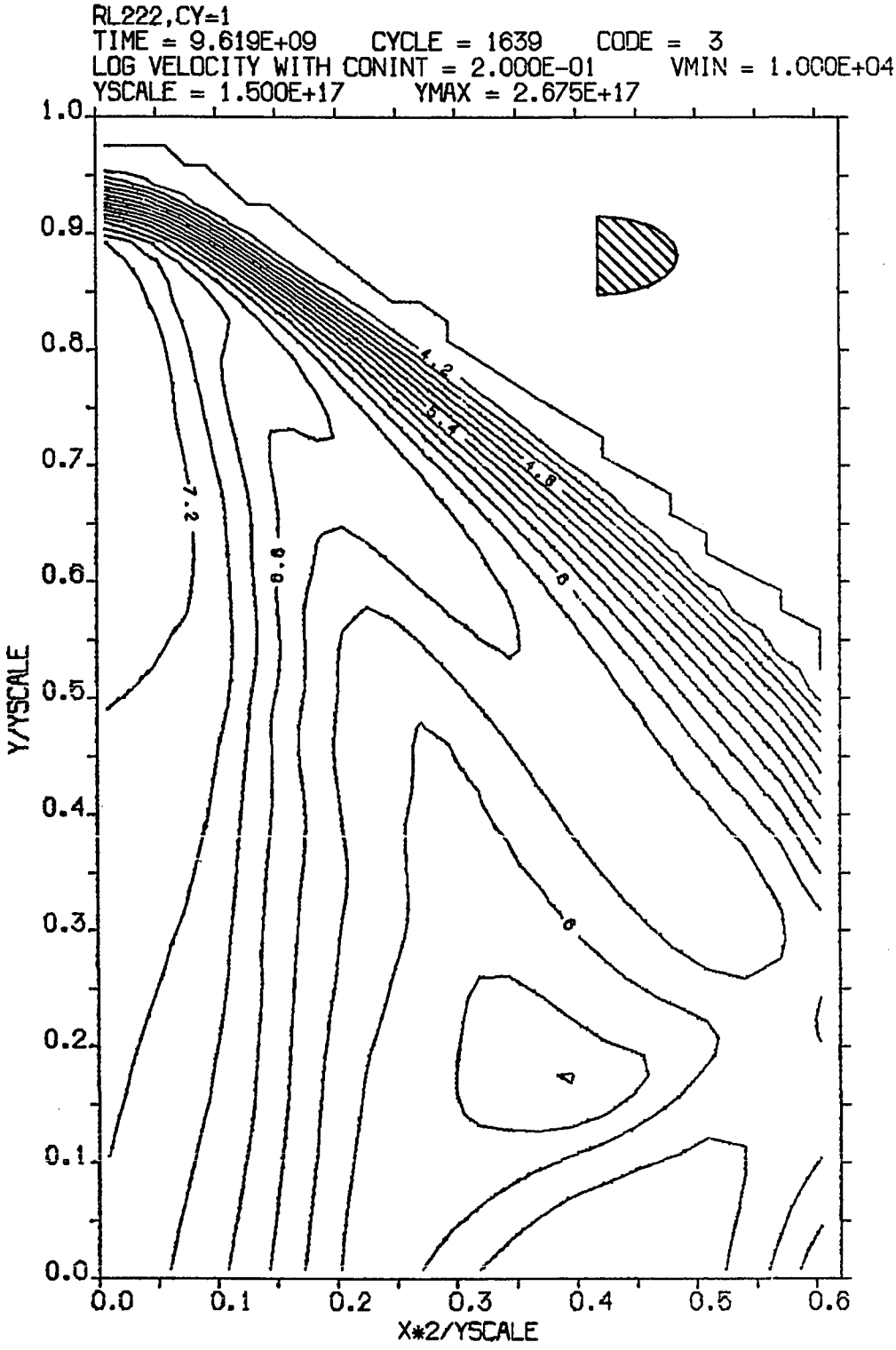

Figure 21a. Contours of the logarithm of velocity (in cm/sec) at s = 4.13 for model RL222

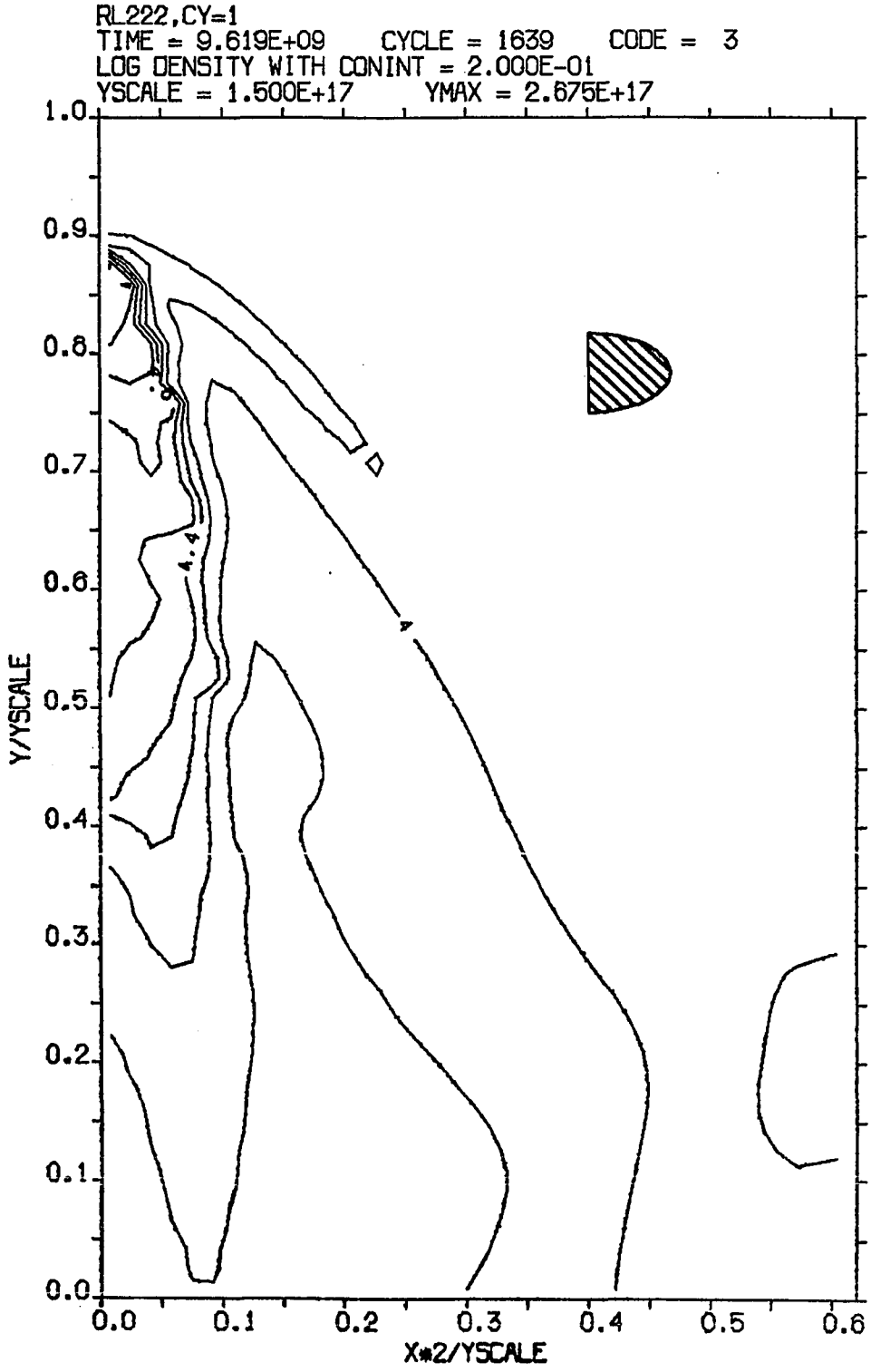

Figure 21b. Contours of the logarithm of density (in nucleons/cm^3) at s = 4.13 for model RL222

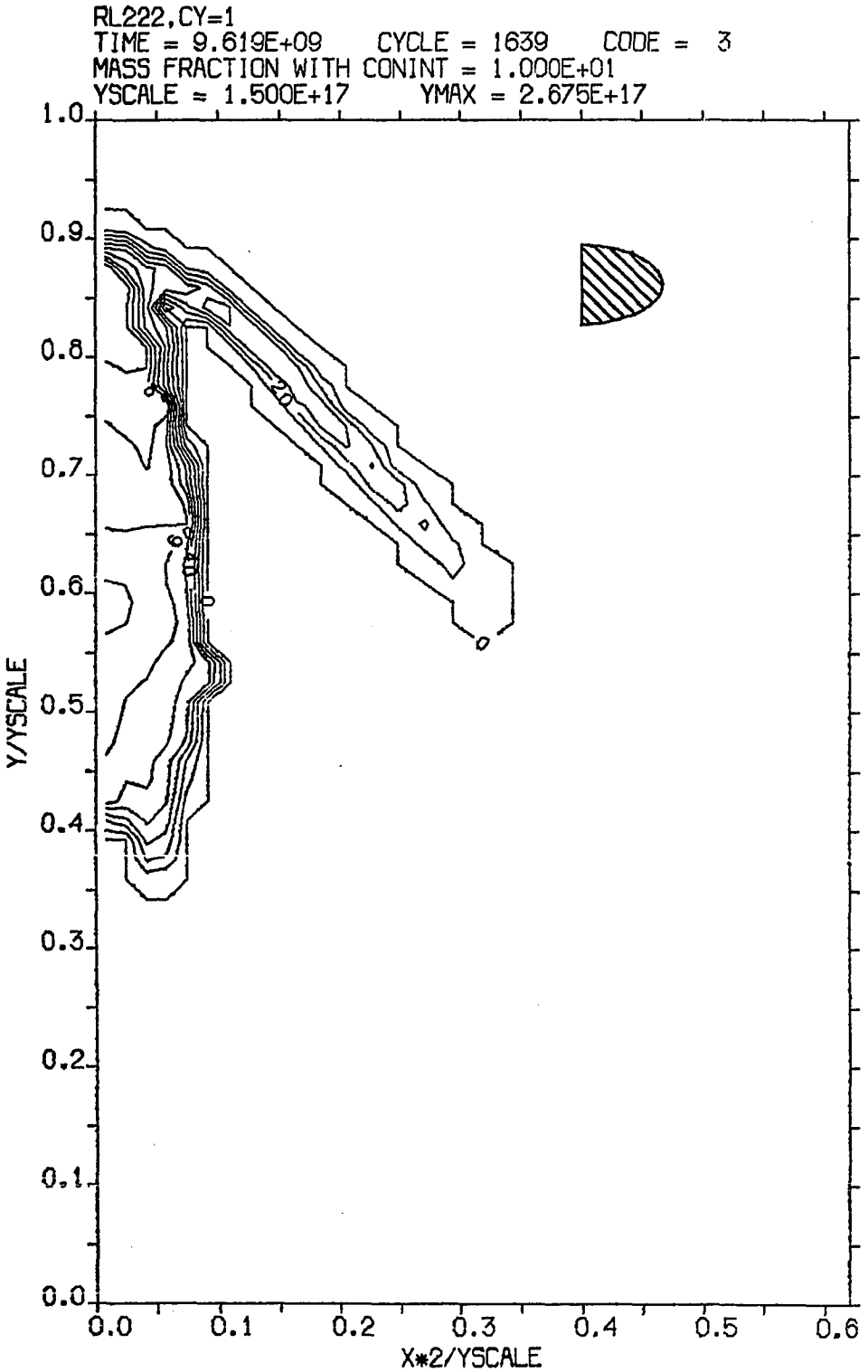

Figure 21c. Contours indicating the location of the cloud mass (in percent) at s = 4.13 for model RL222

significantly weaker and is therefore not swept back as sharply, thereby allowing more transverse expansion to obtain.

In Figure 20, as in Figure 17, CS labels the trajectory for a cloud of constant size, curve D includes the effects of drag, and the arrow marks the terminal velocity for a freely expanding cloud. Only 10 or 15% of the cloud's mass has reached a terminal velocity larger than expected for the case of free expansion. This is even worse than RL331, which has a larger radial expansion rate (Figure 16), because of the increased rate of mass loss along the bow shock. The clouds can experience large accelerations only if their density remains high. Ram pressure alone does not appear capable of providing the necessary confinement.

3. R0334

Cloud model R0334 is the drag-decelerated counterpart of RL331 (i.e., the radiation pressure is turned off, compare Equation 3.2). The ionization and thermal structure depend on $\xi = L_{ion}/nr^2$ (Chapters II.B and III.B), so they change drastically if L_{ion} is set to zero. Therefore, one might envision that the cloud is isotropically bathed in radiation, such that ξ is unchanged from RL331, yet there is no directed momentum to be absorbed. The results of such

a model are useful in understanding RL331.

The column density as a function of time for the first eight Eulerian zones is plotted in Figure 22. The arrow again indicates the column density for the undisturbed medium at the end of the evolution. The behavior of the column densities in the various zones is qualitatively similar to that of RL331 (Figure 15). However, the primary minima is deeper and occurs at a later time; the secondary maxima at $s \simeq 3$ is not as large. These are reflections of the decreased compression at the head of the cloud due to the relatively weaker bow shock (RL331 is accelerated while R0334 is not). The gas pressure drops below $P_{ic}(0)$ in the rear of the cloud R0334, just as in RL331. The fact that these two models show such qualitatively similar behavior supports the idea that these oscillations are a transient effect associated with the use of nonequilibrium initial conditions rather than an effect of the radial stretching by radiation pressure.

The length of R0334 as a function of time is plotted in Figure 16. Comparing its rate of expansion with that of RL331 clearly illustrates the importance of radiation pressure in elongating the clouds. The quantities $\bar{M}_n(s)$ (see Equation 5.4) are plotted in Figure 23. They show that the rate at which mass leaks out of the cloud, mixes with

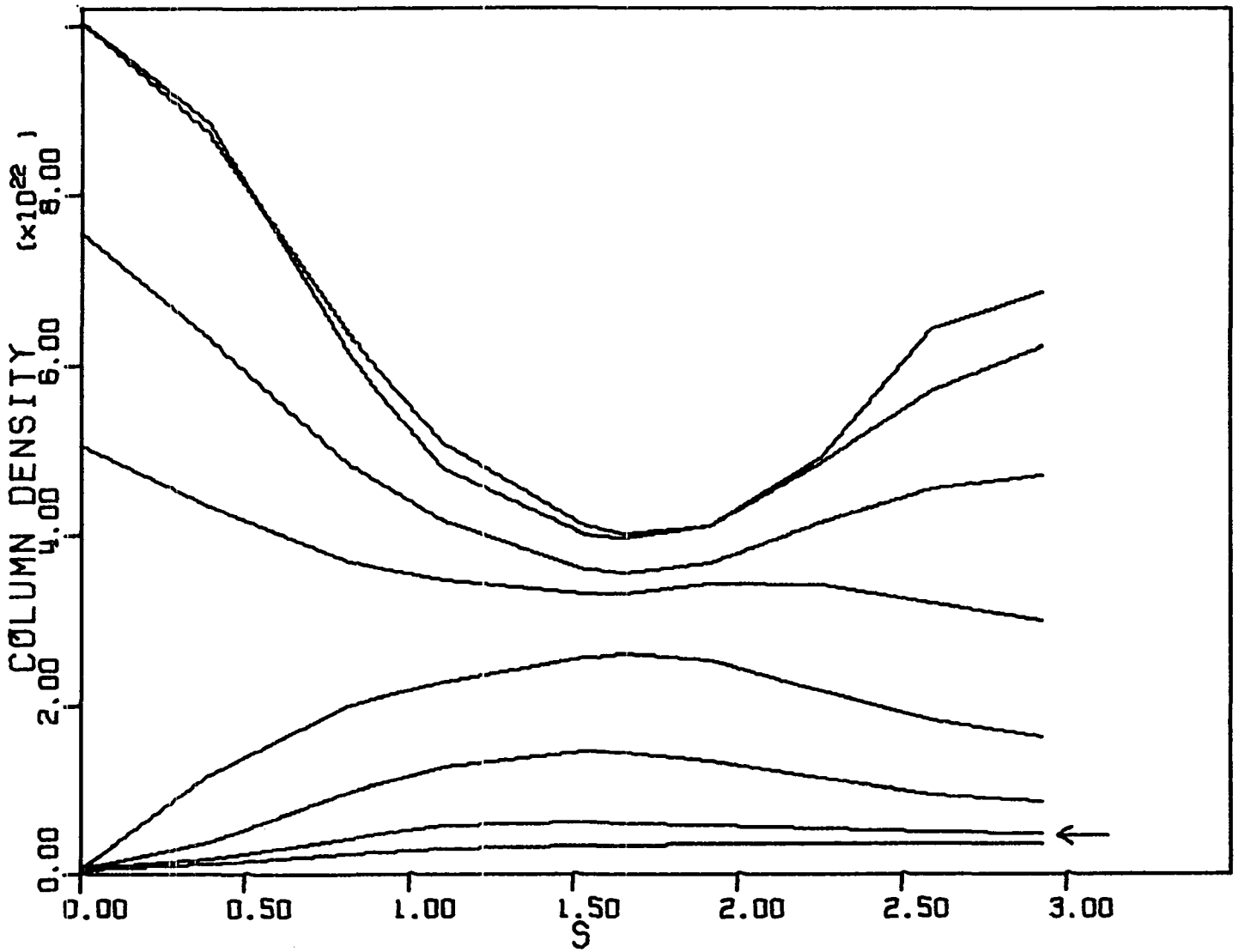

Figure 22. The column density as a function of time for the first eight Eulerian zones of model RO334

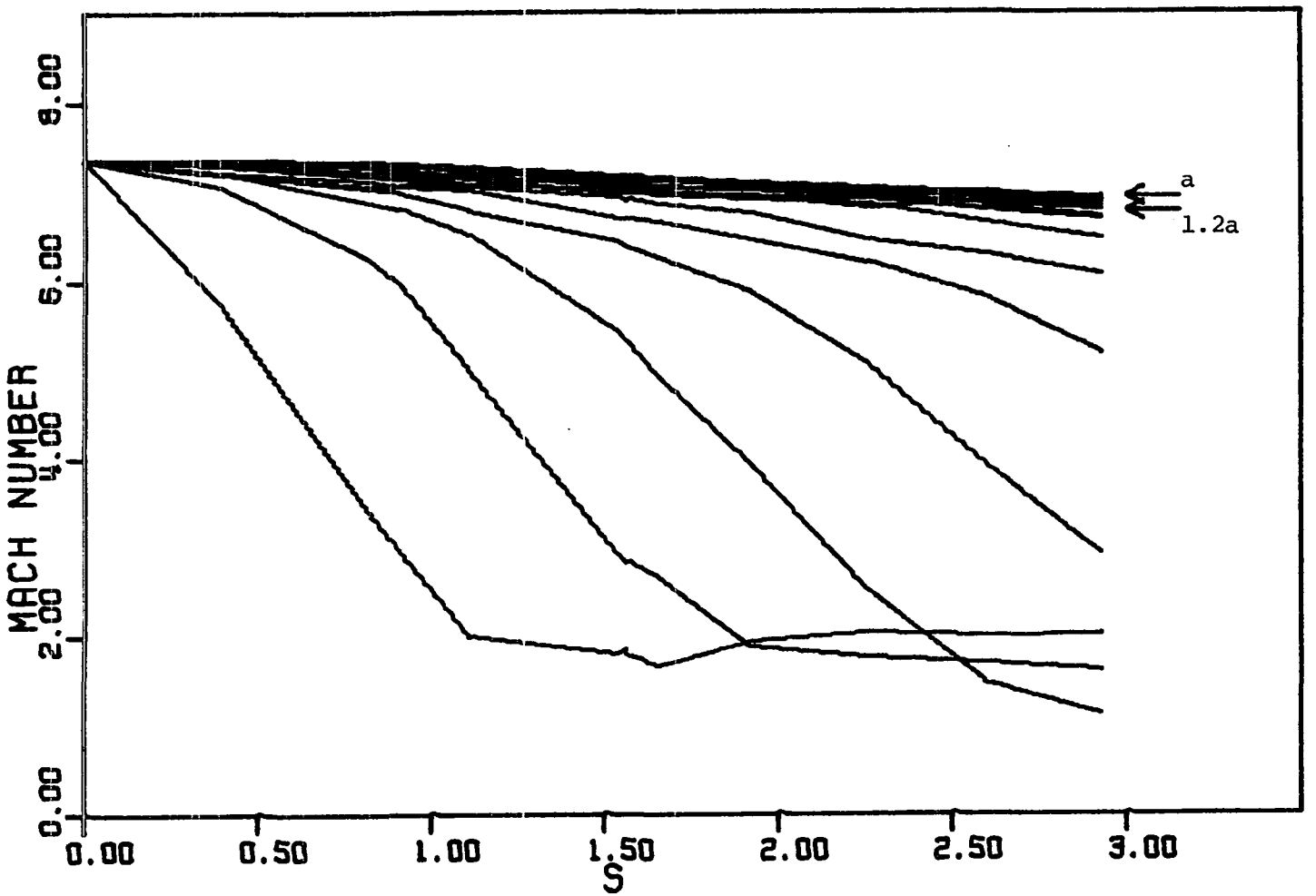

Figure 23. The Mach number for each 5% of the cloud RO334 as a function of time

the shocked intercloud gas, and decelerates is roughly twice as large as for RL331 (Figure 17). This is again due to the fact that the bow shock is relatively weaker. The part of the cloud which has not spread out along the bow shock is moving fairly coherently, much in contrast to RL331.

It is clear from Figure 23 that R0334 is decelerating, this is due to the drag of the intercloud medium. The simple theory of Chapter III.A gives the trajectory for a constant-size, drag-decelerated cloud as

$$v_c(t) = \frac{v_o \ell}{v_o t + \ell} \qquad (5.5)$$

(cf Equation 3.2). The velocity predicted by this equation at s = 3 is indicated in Figure 23 by the arrow labelled a. Taking the effective cross-sectional area of the cloud as $\pi(1.2a)^2$ (cf Hayes and Probstein 1959) gives the velocity at s = 3 indicated by the arrow labelled 1.2a. The former appears to be a better approximation to $\bar{M}_1(3)$, but the latter matches the slope of $\bar{M}_1(s)$ more closely. This is probably due to some initial relaxation of the model at small s (cf R0221 below).

4. R0221

For completeness, a brief summary of the results for R0221 is given. It is the unaccelerated counterpart of RL222. All the remarks concerning the relation between

R0334 and RL331 apply equally to the pair R0221 and RL222. The column densities for the first eight zones of R0221 are plotted in Figure 24. The dotted line shows the increase in the column density of the undisturbed medium due to the extension of the grid. The length of R0221 is given in Figure 16 and the $\bar{M}_n(s)$ are displayed in Figure 25. R0221 loses about 45 to 50% of its initial mass by s = 4. This is only slightly higher than the loss rate for RL222 because their Mach numbers are comparable (RL222 receives little acceleration). The dotted line in Figure 25 gives the solution of Equation 5.5 if the effective cross-sectional area of the cloud is πa^2. The arrow at s = 5 indicates the result for $\pi(1.2a)^2$. Away from s = 0, the latter is again a better approximation of the numerical results.

C. A Nonadiabatic, Ram-Pressure-Confined Cloud

Model RC221 is the nonadiabatic counterpart of RL222. The standard energy equation (Equation 4.2) is discarded and the temperature in each cell at each time step is obtained by using the local value of ξ to interpolate in a table of TM's equilibrium temperatures (Figure 6). This model provides insight into the effects of radiative cooling on cloud dynamics (see Chapter III.B for a further

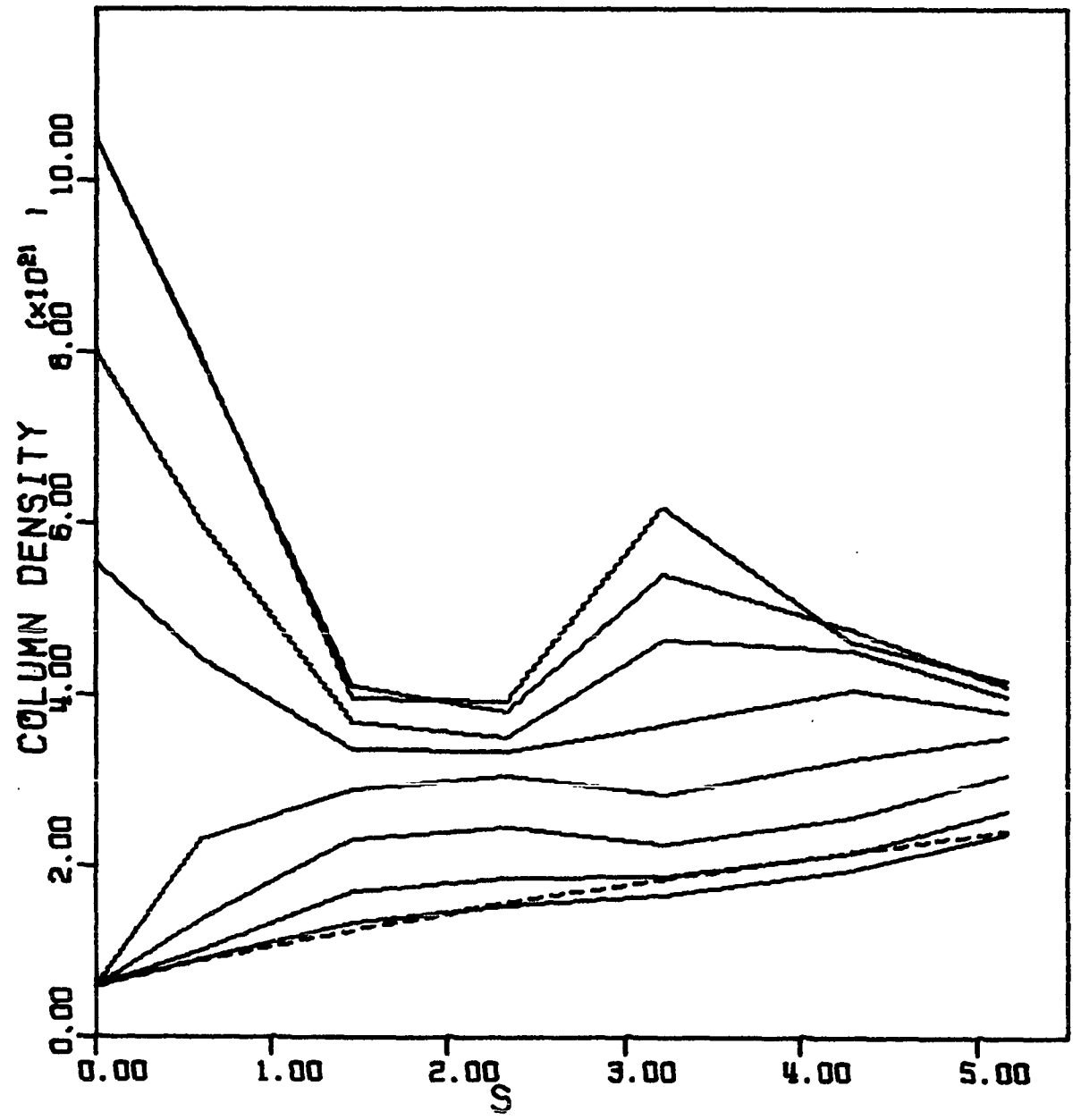

Figure 24. The column density as a function of time for the first eight Eulerian zones of model RO221

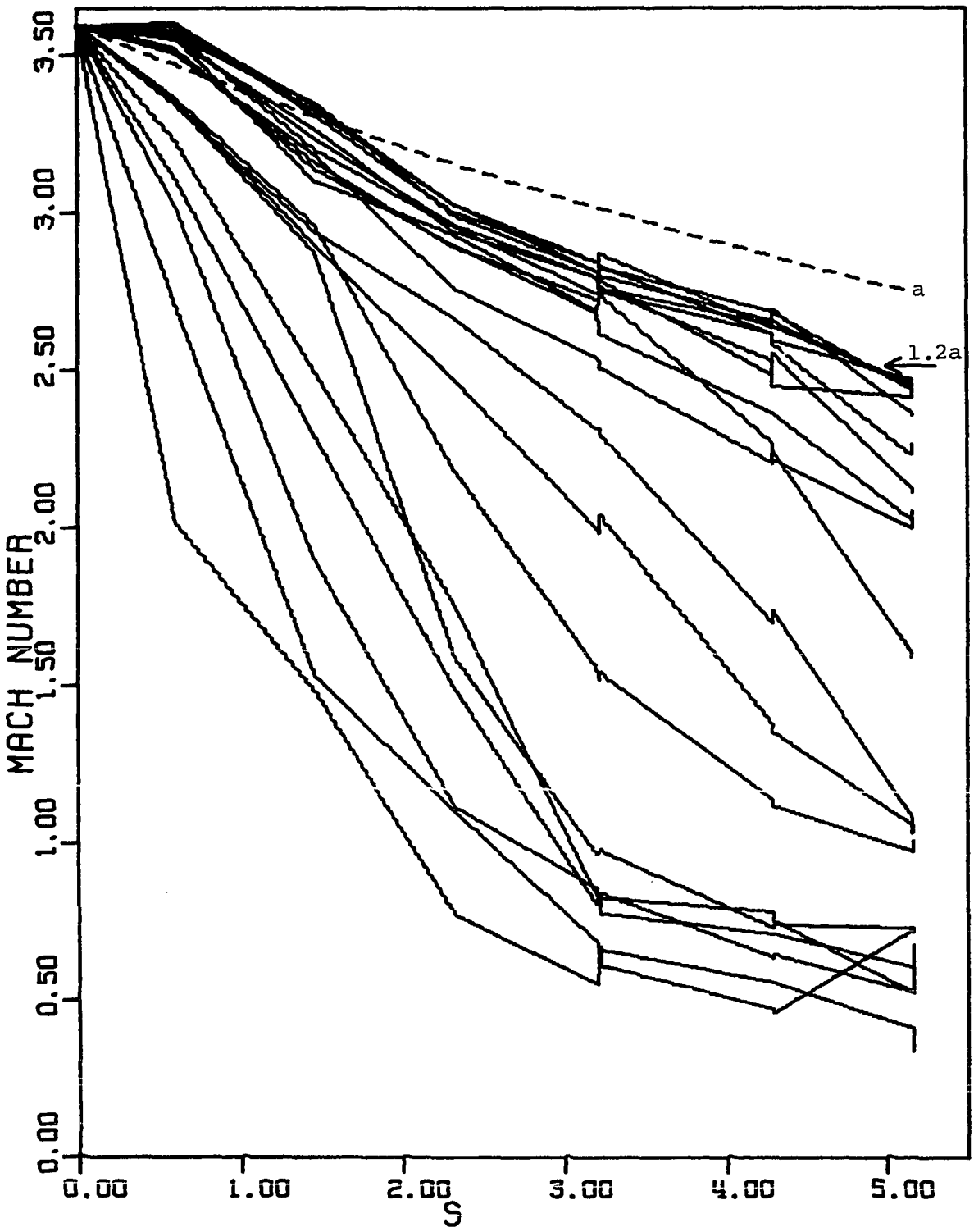

Figure 25. The Mach number for each 5% of the cloud RO221 as a function of time

discussion).

Contour plots of the velocity and density appear in Figures 26a and 26b for RC221 at the end of the evolution ($s = 3.76$, $t = 8.75 \times 10^9$). For comparison, the initial cloud is shown to scale by the cross-hatched semicircles. A shock wave forms in front of the cloud as usual because it is moving supersonically through the external medium. However, no shock heating occurs; it is assumed that the radiative cooling is so effective that the temperature never strays from the equilibrium temperatures of TM. This model is unrealistic because the gas is forced to cool at constant density. (Cooling at constant pressure is probably more realistic.) Thus, the pressure in the shocked intercloud gas between the cloud and the bow shock is abnormally low and the transverse pressure gradients are abnormally large. This results in huge amounts of cloud material flowing out to a large x and decelerating. The location of the dense material (i.e., the cloud) at the end of the evolution is given by the contour plot in Figure 26c (cf Figure 21c for RL222). The cloud has not stretched out in the radial direction as have the standard models of Chapter V.B (see Figure 16).

Figure 27 shows the column density as a function of time for the first eight Eulerian zones. As before, the

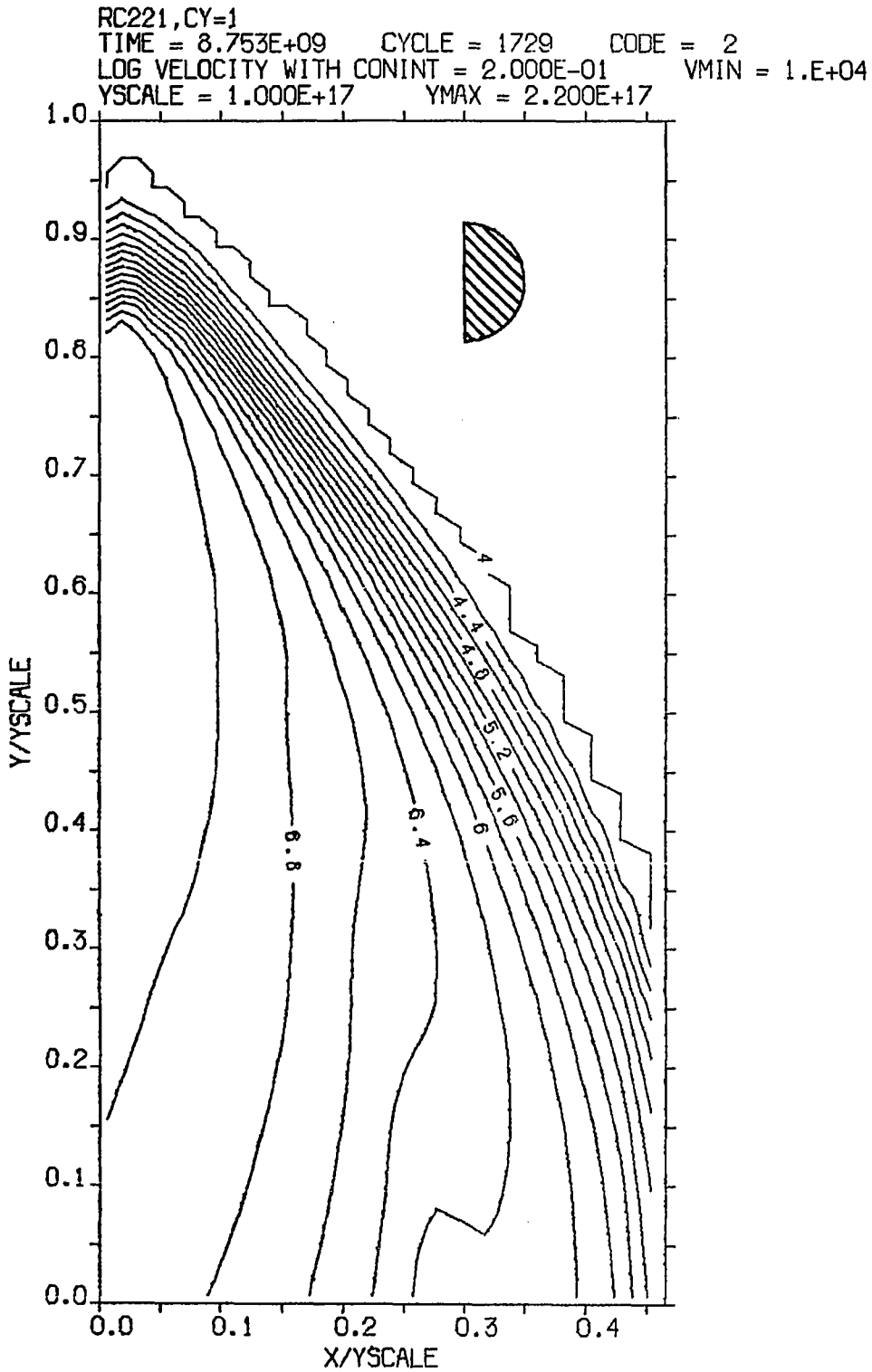

Figure 26a. Contours of the logarithm of velocity (in cm/sec) at s = 3.76 for model RC221

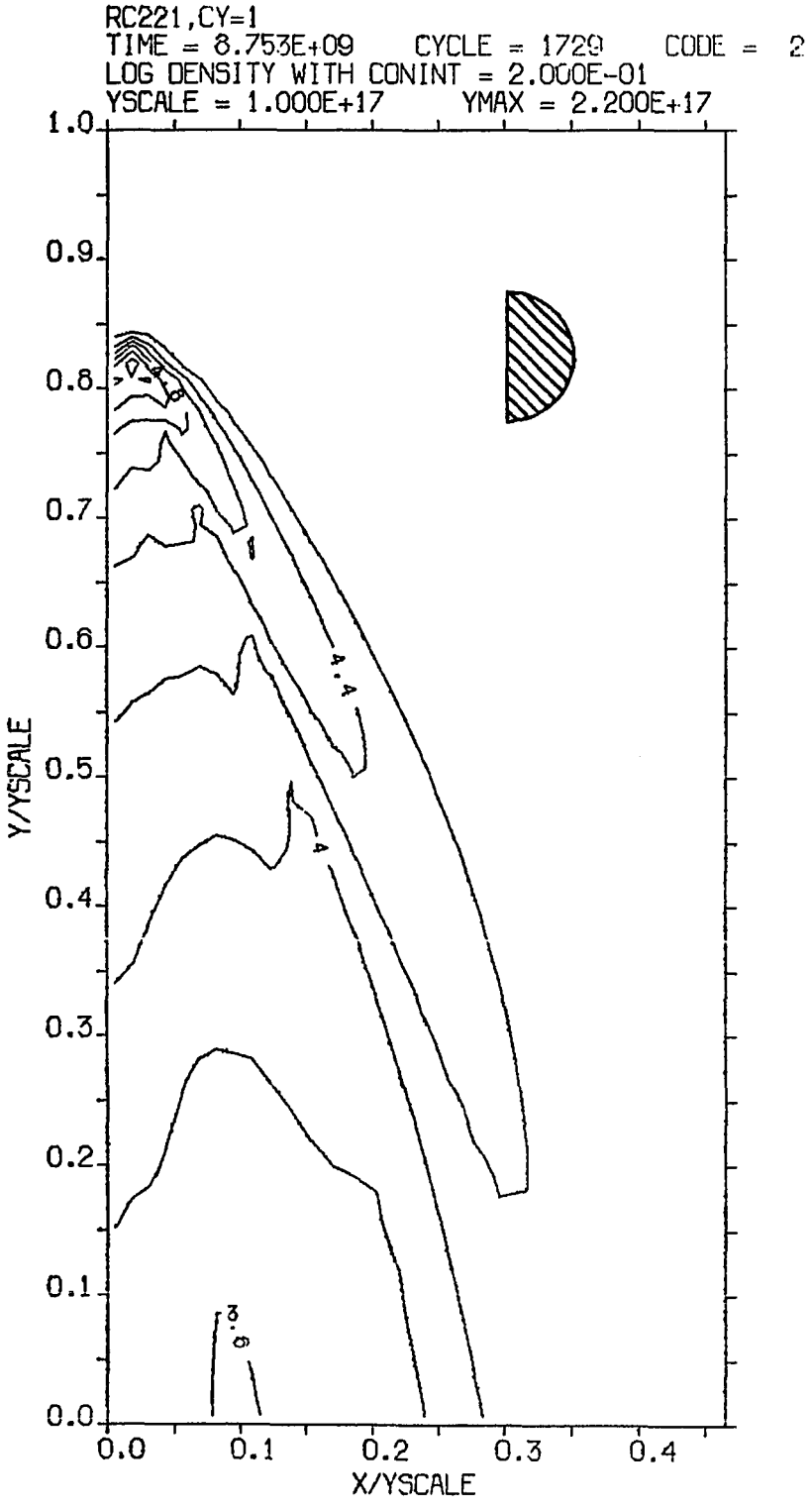

Figure 26b. Contours of the logarithm of density (in nucleons/cm^3) at s = 3.76 for model RC221

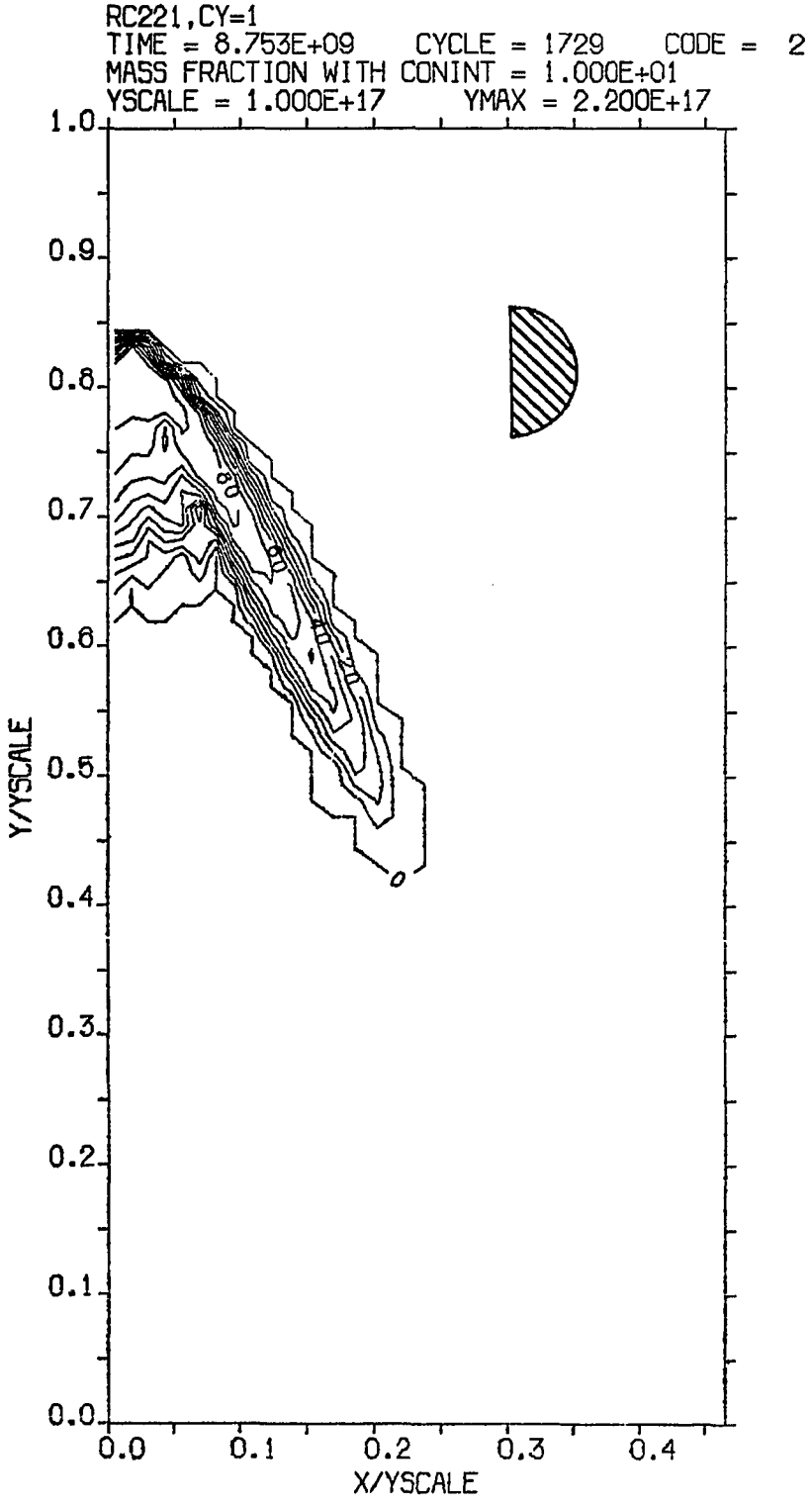

Figure 26c. Contours indicating the location of the cloud mass (in percent) at s = 3.76 for model RC221

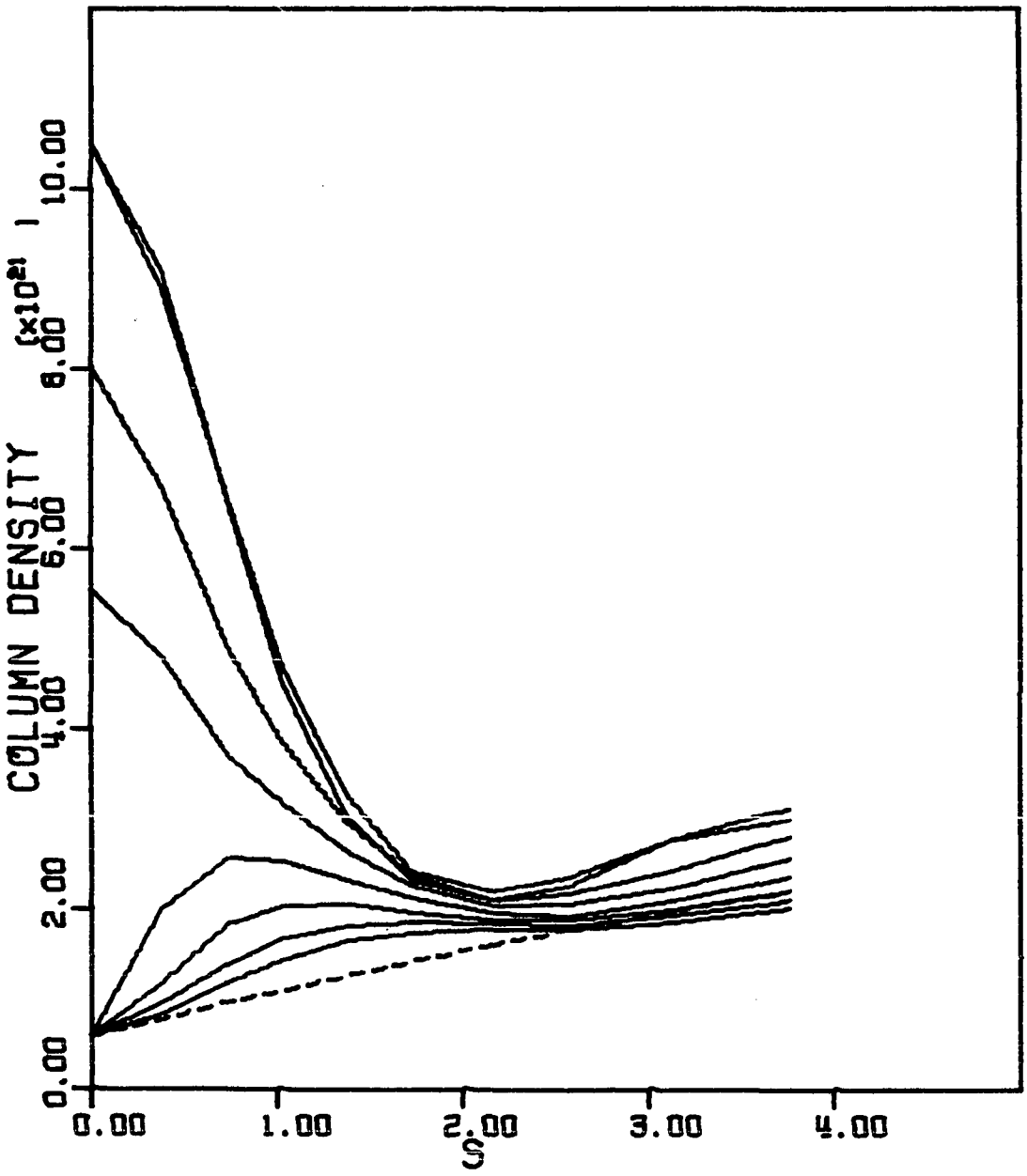

Figure 27. The column density as a function of time for the first eight Eulerian zones of model RC221

dotted line indicates the effect of extending the grid as the evolution progresses. The sharp decrease in the cloud's column density is caused by the rapid outflow of material along the bow shock (Figure 26c). The rate of outflow slows down as the cloud's internal pressure approaches $P_{ic}(0)$. The small rise in the column density for $s > 2.2$ is partially due to the increasing size of the grid and partially due to a transverse pressure oscillation as discussed above for the standard models. The pressure oscillation is significantly smaller for RC221 because of the nonadiabatic nature of this model. For an adiabatic expansion the pressure decreases as $\rho^{5/3}$, whereas for RC221 it only drops as $\rho^{3/4}$ since the temperature now varies roughly as $\rho^{-1/4}$ (see Figure 6).

The quantities $\bar{M}_n(s)$ are plotted in Figure 28 for RC221 (see Equation 5.4). The transverse expansion quickly reduces the density and increases the cross-sectional area of the cloud. Therefore, the radiation pressure is already overcome by drag effects at $s \simeq 1$.

The behavior of RC221 is quite different from that of RL222. This emphasizes the importance of including a proper treatment of the energy equation. Ram pressure does not confine the clouds directly via the directed momentum of the intercloud particles. Rather, the directed kinetic

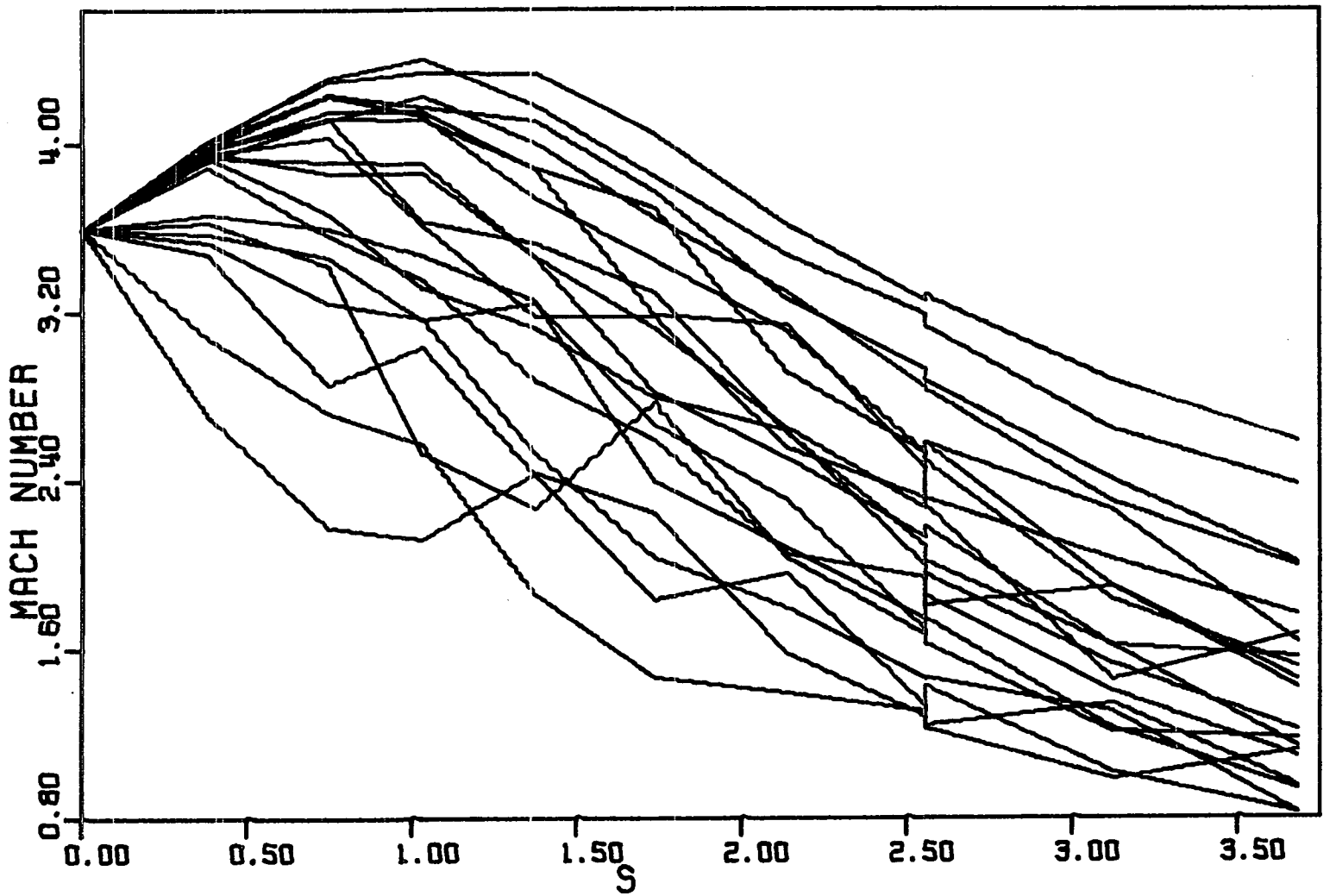

Figure 28. The Mach number for each 5% of the cloud RC221 as a function of time

energy of the inflowing particles is thermalized at the bow shock and it is the resulting thermal gas pressure which confines the clouds. In RC221 this thermal energy is assumed to be instantaneously radiated away and consequently the cloud is not confined.

Now it is true that the cooling time for the shocked gas in the standard, ram pressure models (Chapter V.B) is comparable to the time required for the gas to flow around the clouds (cf Chapter III.B). However these models, which neglect radiative cooling and assume that the gas flow is adiabatic, are still closer to the real physical situation than is RC221. This is because, in actual fact, shock heating does occur. The gas then radiatively cools, not at constant density, but more nearly at constant pressure (cf Spitzer 1968; Daltabuit and Cox 1972). Hence the standard models overestimate the temperature in the post-shock region, but they do not overestimate the pressure by the same large factor. Thus, the amount of confinement found there is expected to be a reasonably good approximation of the truth.

D. A One-Dimensional, Ram-Pressure-Confined Cloud

Model RP221 has only two Eulerian zones; they have the same initial conditions as in RL222. Since these two zones are in pressure balance at s=0 and there is no transverse flow, none develops and the model is one-dimensional. Such a model helps isolate the truly two-dimensional aspects of the flow.

RP221 was evolved for 3.76 cloud expansion times. The run of velocity, density, internal energy, and pressure along the y-axis at s=2.15 are shown in Figures 29a-d. The profiles of the original cloud are indicated as usual; for this case their location is also correct. One of the most striking features is the large pile-up of shock-heated gas; it can not flow around the cloud as in the two-dimensional case. This is an example of the classic "piston" problem (Hayes and Probstein 1959; Landau and Lifshitz 1959). The free stream Mach number is related to the piston velocity ($v_p = M_p c_{ic}(0)$) by

$$M_\infty = 2M_p/3 + [(2M_p/3)^2 + 1]^{1/2} \qquad (5.6)$$

if $\gamma = 5/3$. The Rankine-Hugoniot relations then give the postshock density as

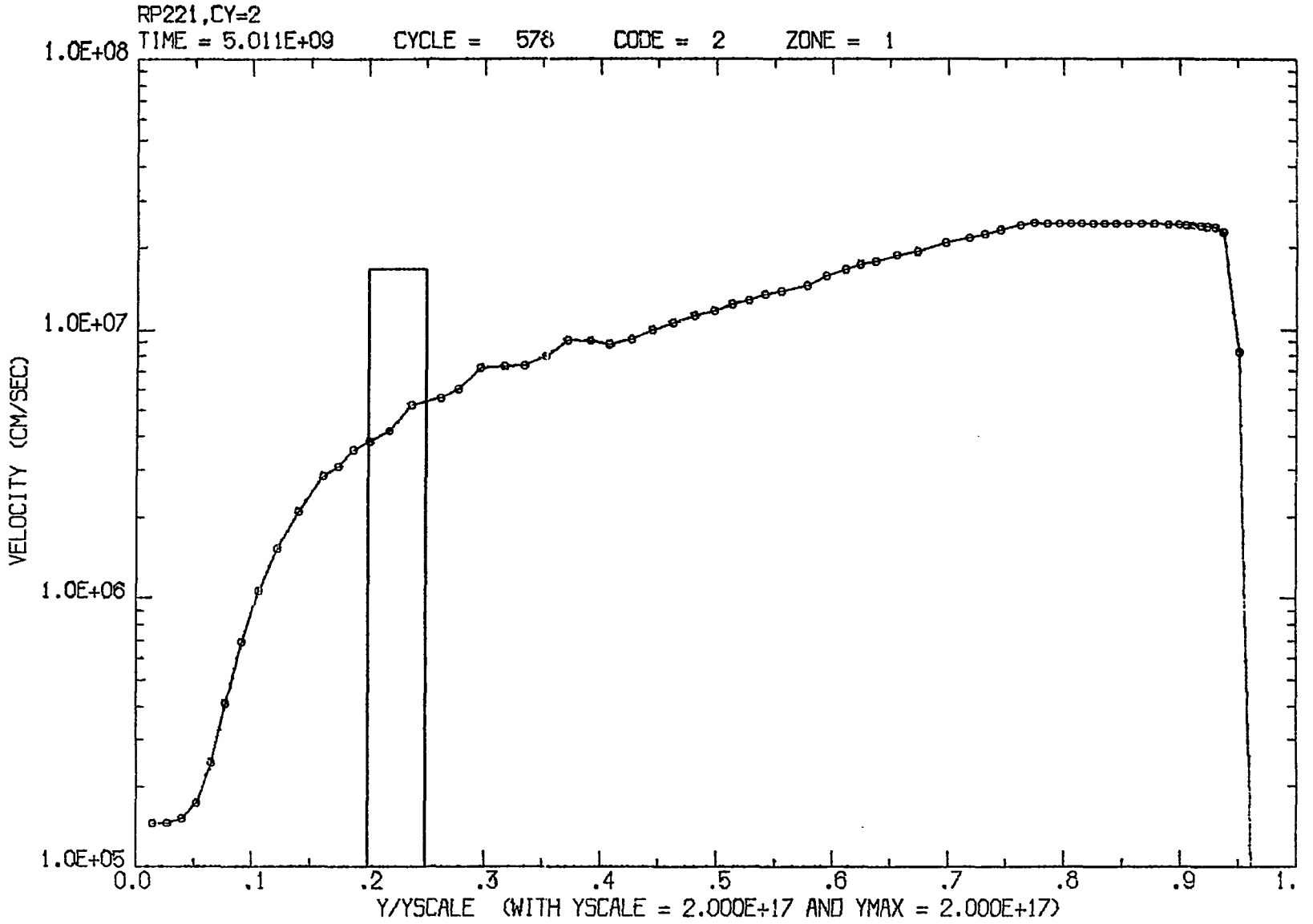

Figure 29a. The velocity (in cm/sec) along the symmetry (y) axis at s = 2.15 for model RP221

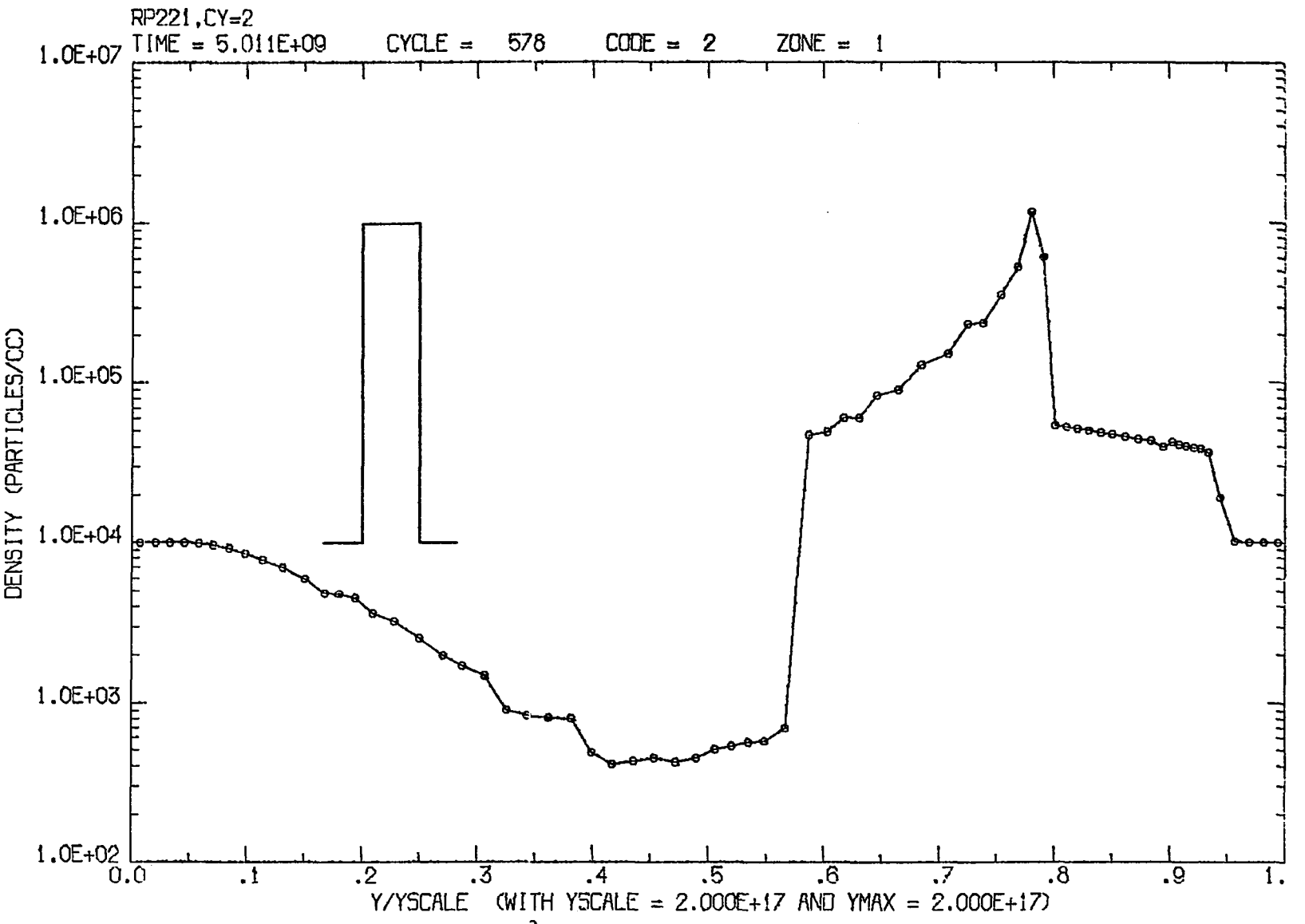

Figure 29b. The density (in nucleons/cm^3) along the symmetry (y) axis at s = 2.15 for model RP221

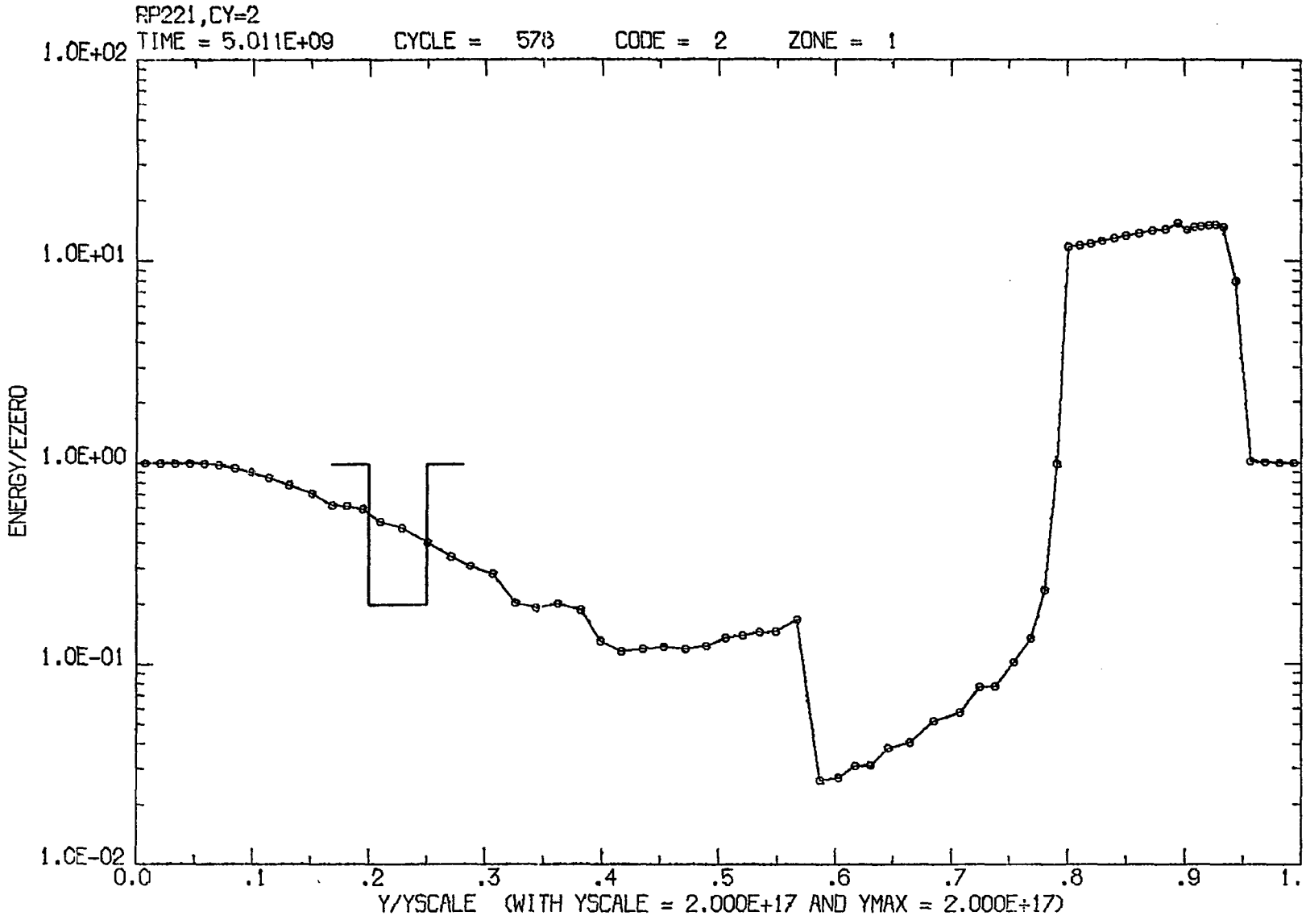

Figure 29c. The specific internal energy (in units where $e_{ic}(0) = 1.0$) along the symmetry (y) axis at s = 2.15 for model RP221

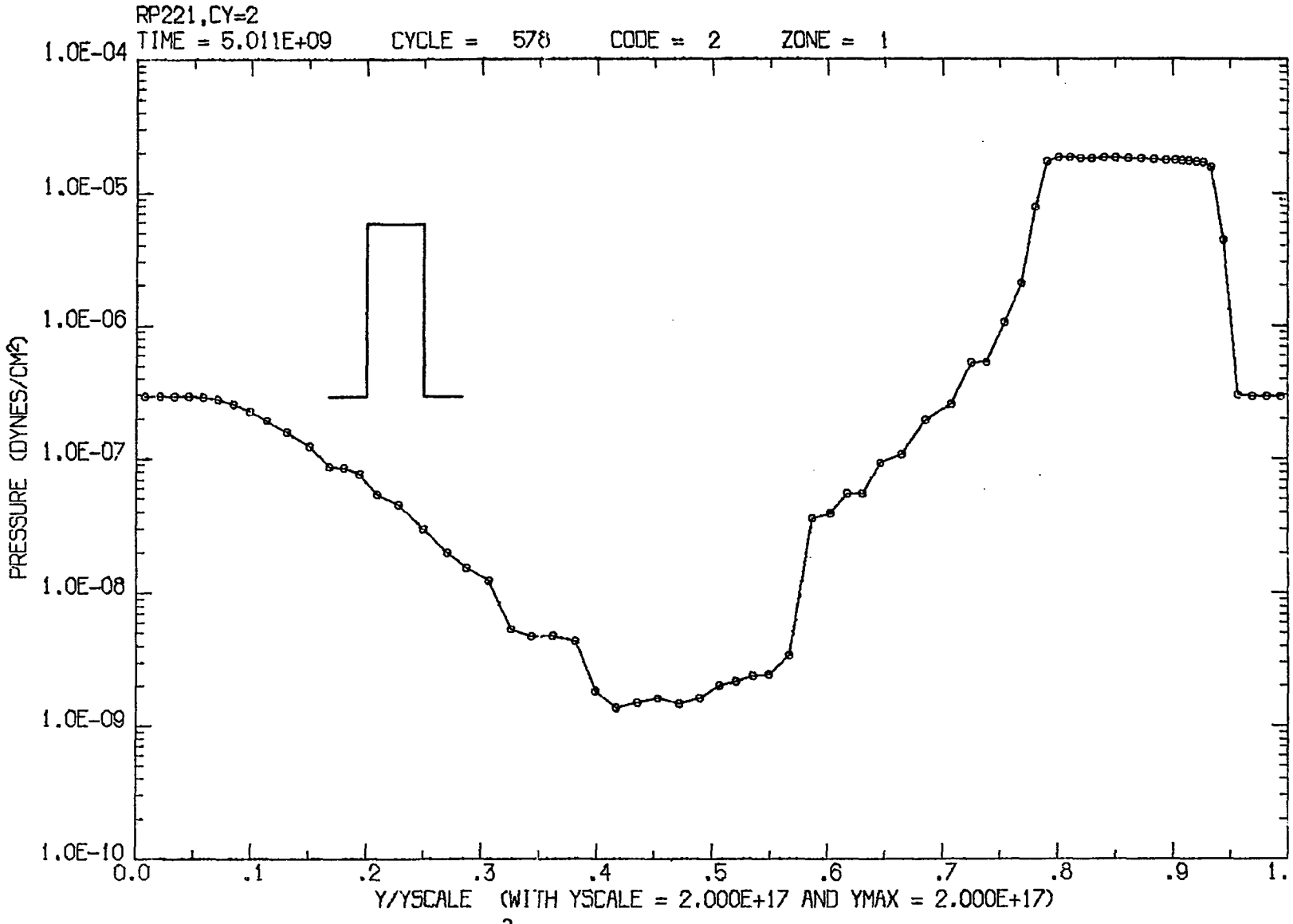

Figure 29d. The pressure (in dynes/cm^2) along the symmetry (y) axis at s = 2.15 for model RP221

$$\frac{\rho_s}{\rho_{ic}(0)} = \frac{4M_\infty^2}{M_\infty^2+3} \tag{5.7}$$

and the temperature as

$$\frac{T_s}{T_{ic}(0)} = 1 + \frac{5(M_\infty^2+0.6)(M_\infty^2-1)}{M_\infty^2} . \tag{5.8}$$

At s = 2.15 the leading edge of the cloud is travelling at 2.45×10^7 cm/sec, so $M_\infty = 7.0$, $\rho_s/\rho_{ic}(0) = 3.8$, and $T_s/T_{ic}(0) = 16.2$. These values agree with the numerical results (Figures 29b and 29c) to within 10% at s = 2.15 and throughout the evolution.

The absence of transverse flow in RP221 produces other differences from RL222. The rarefaction behind the cloud is considerably wider and deeper; gas cannot flow radially into this region as fast as it is evacuated by the supersonically moving cloud. The temperature is lower in the rear of the cloud because no transverse inflow of hot intercloud gas is permitted. A large pressure cavity does not appear in the rear portion of the cloud as in RL222, even for small s (cf Chapter V.B). This fact strengthens the contention that when such behavior does occur, it is a result of transverse expansion associated with the use of nonequilibrium initial conditions. If it were due to the stretching of the cloud by radiation pressure, it would

appear in RP221 just as well as in RL222 because the radial expansion is the same to within 10% (RP221 is slightly longer at any given time).

RP221 is accelerated to higher velocities than is RL222; $\bar{M}_1 = 5.3$ (Equation 5.4) at $s = 3.76$ compared to $\bar{M}_1 = 4.1$ for RL222 (Figure 20). Nevertheless, it appears to reach a terminal velocity ($\lesssim$ Mach 5.6) considerably less than produced by drag effects alone ($\simeq$ Mach 8.2, see Equation 3.3). This is a result of the cloud's lower density in its stretched condition. The difference in the acceleration of RP221 and RL222 results from the absence of transverse flow in the former. Recall that the density of RL222 is lowered not only by stretching, but also by the outflow of matter along the bow shock. In summary, it is safe to say that the response of RP221 to radiation pressure acceleration is qualitatively very similar to that of RL222; the differences which do exist are easily understood as two-dimensional effects.

E. Thermal-Gas-Pressure-Confined Clouds

1. TL221

Model TL221 has an initial column density of 10^{22} and $n_c(0)/n_{ic}(0) = 10^2$, its other properties can be found in Table 1. The initial conditions differ from those of RL222

in that the intercloud medium is considerably hotter and the cloud's initial velocity is somewhat lower. Thus, thermal gas pressure confines the cloud rather than ram pressure.

Contours of velocity, density, and internal energy for TL221 at s = 2.53 ($t = 5.89 \times 10^9$) are displayed in Figures 30a-c. The pressure is not contoured because it is nearly constant throughout the grid and thus yields a very uninteresting plot. The velocity, density, internal energy, and pressure along the y-axis are given in Figures 31a-d. In the contour plot of velocity many low-velocity waves are visible (Figure 30a). Some of these are real, for example, the subsonic flow ahead of the cloud (Figure 31a). These waves reflect off the grid boundaries and the cloud, leading to the propagation of unphysical waves. These latter waves serve as a reminder that the present numerical code is not really intended for use in modeling subsonic (incompressible) flows. The effect on the cloud dynamics is minimal, as these waves carry little energy.

The shape of the cloud is illustrated by the density (Figure 30b) and temperature (Figure 30c) contour plots. Its length in the radial direction is 2.6 times its original diameter; it has been slightly compressed in the transverse direction. The explanation of this behavior is fairly straightforward. Even though ram pressure does not

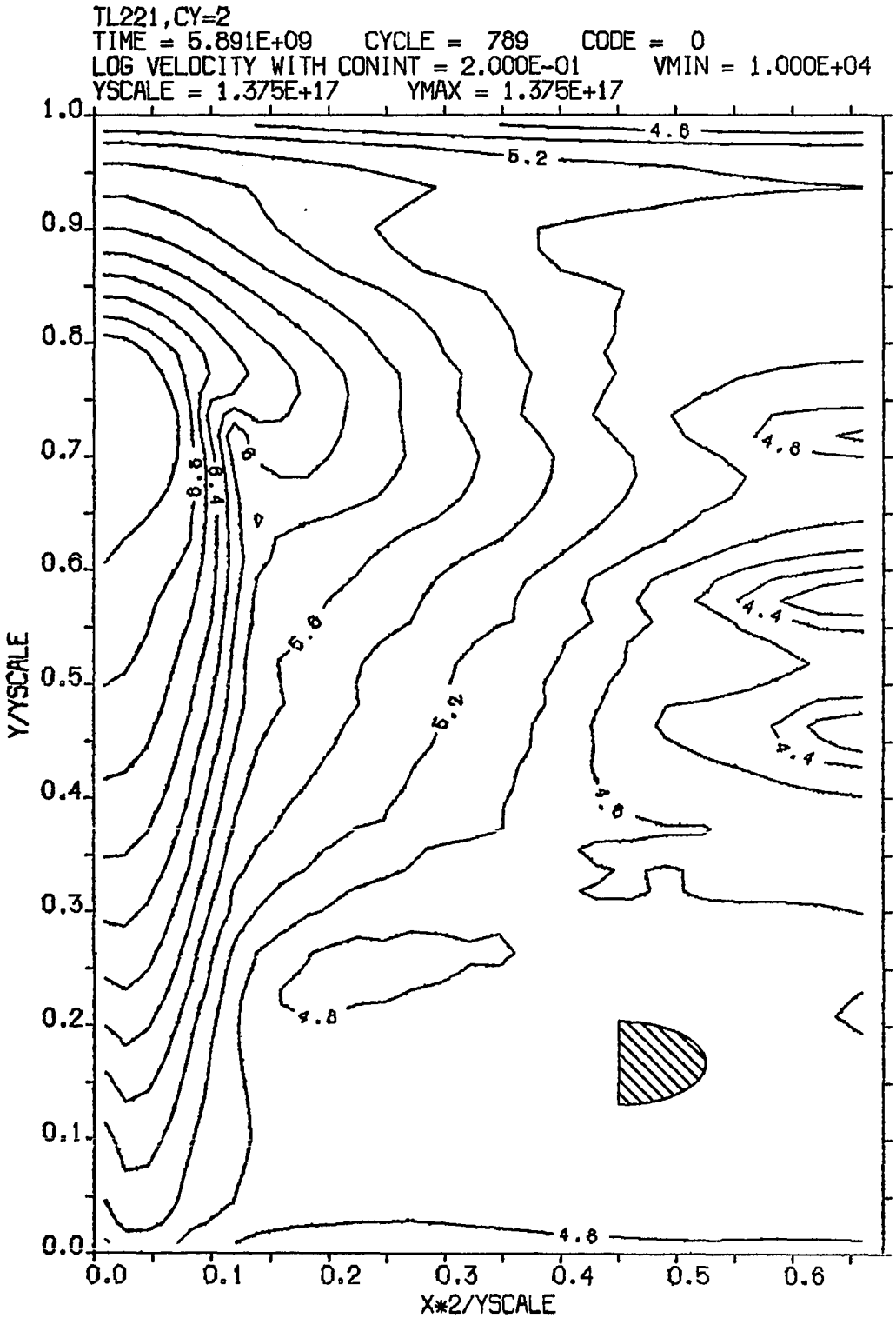

Figure 30a. Contours of the logarithm of velocity (in cm/sec) at s = 2.53 for model TL221

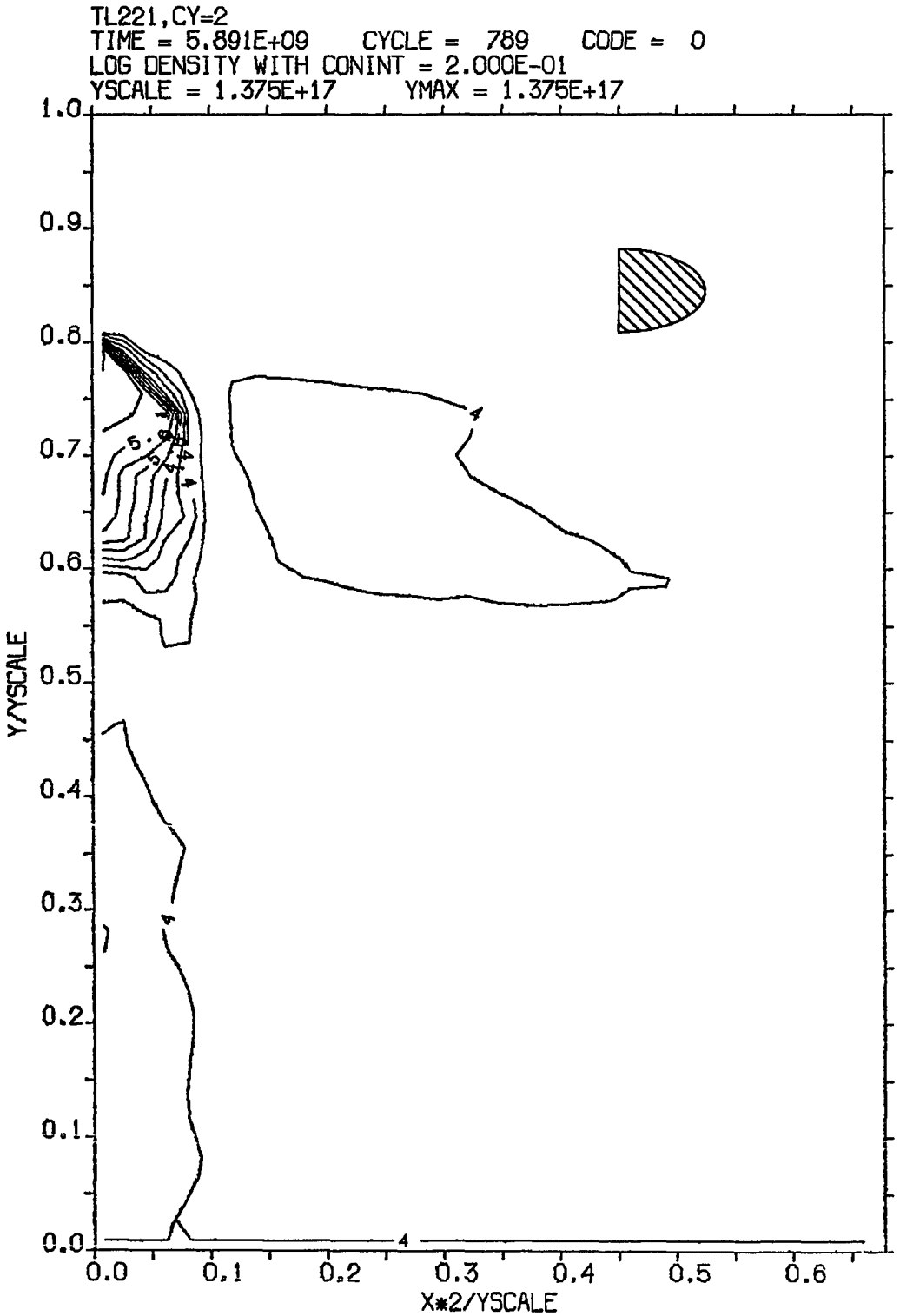

Figure 30b. Contours of the logarithm of density (in nucleons/cm^3) at s = 2.53 for model TL221

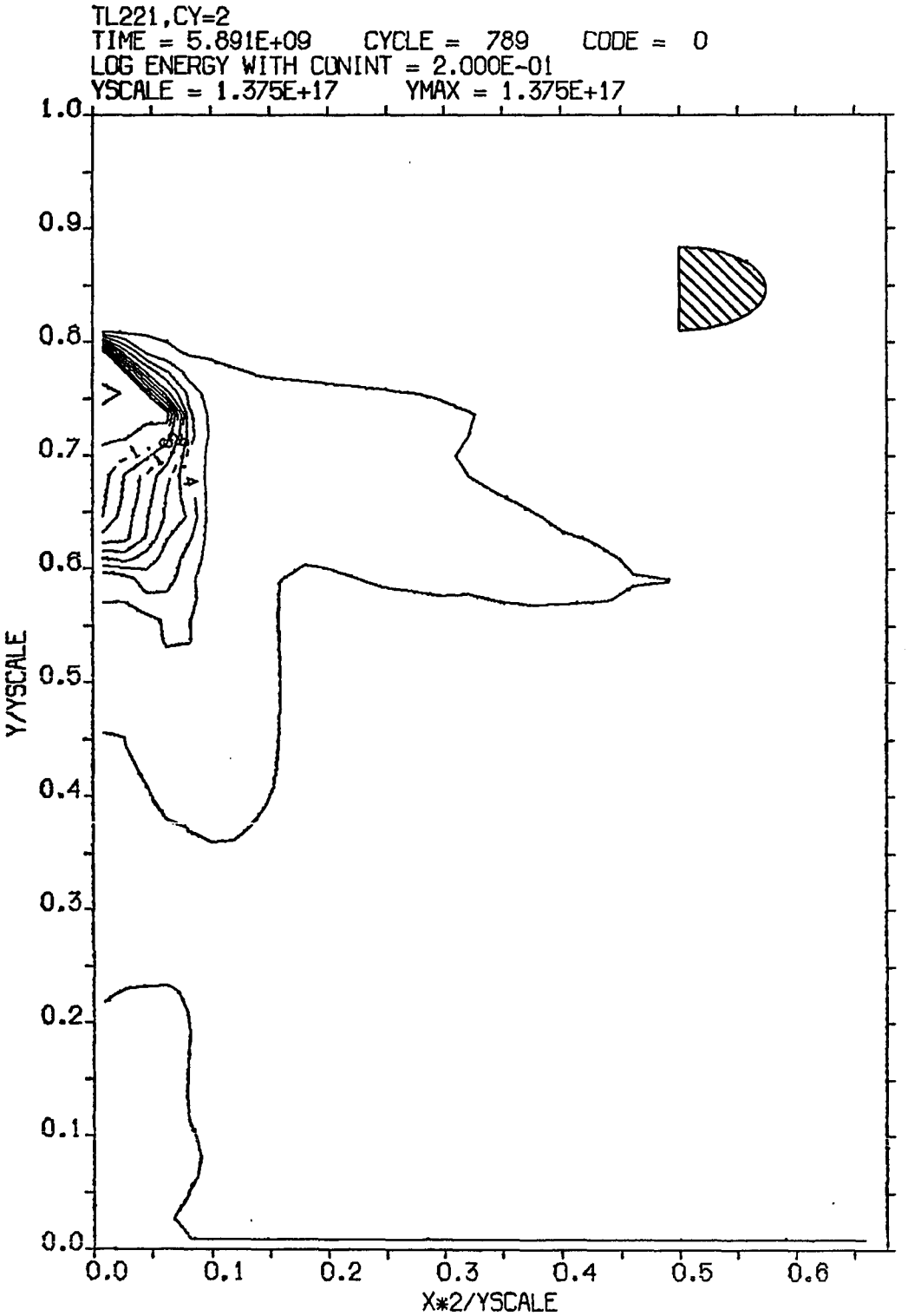

Figure 30c. Contours of the logarithm of specific internal energy (in units where $e_{ic}(0) = 1.0$) at s = 2.53 for model TL221

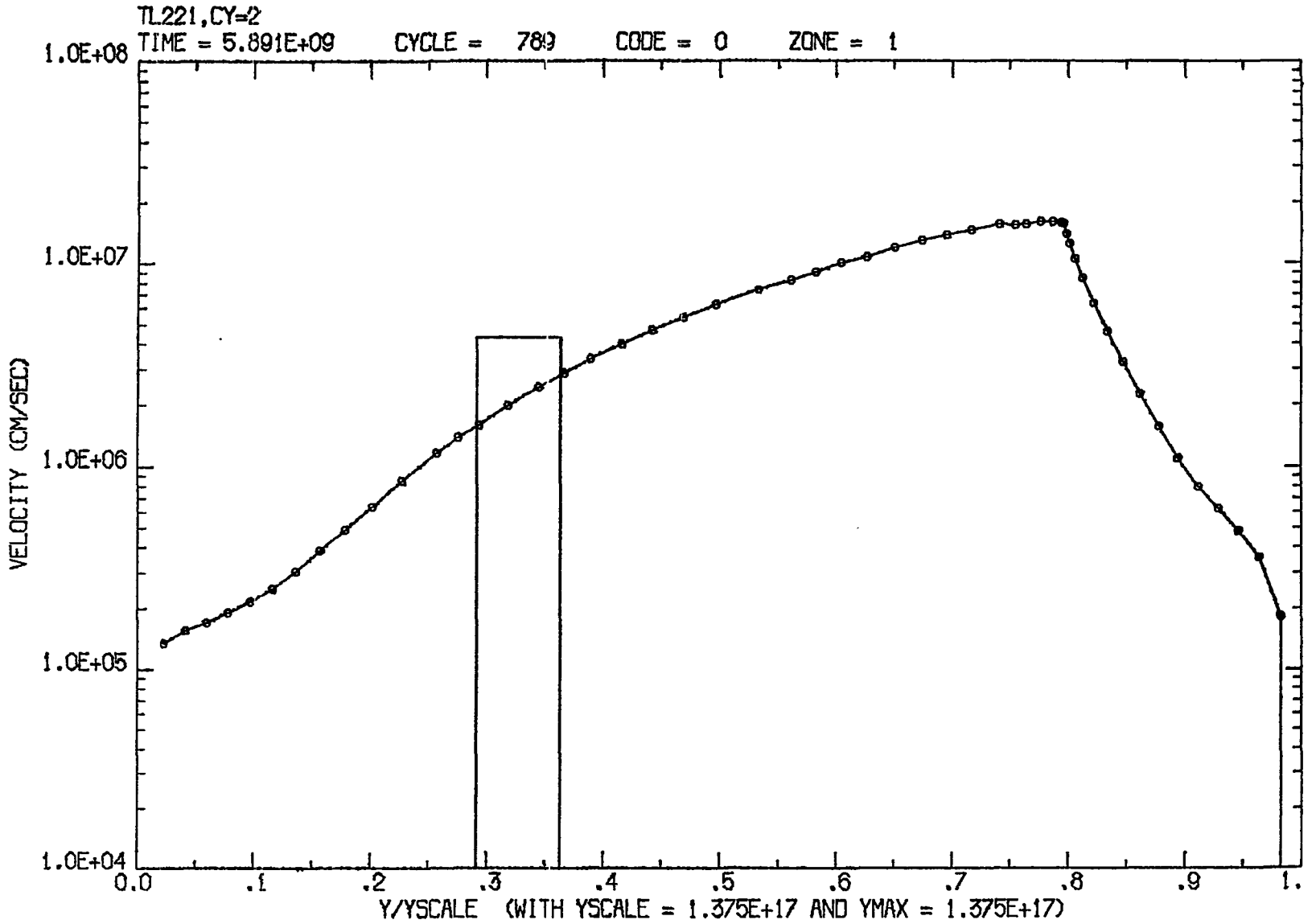

Figure 31a. The velocity (in cm/sec) along the symmetry (y) axis at s = 2.53 for model TL221

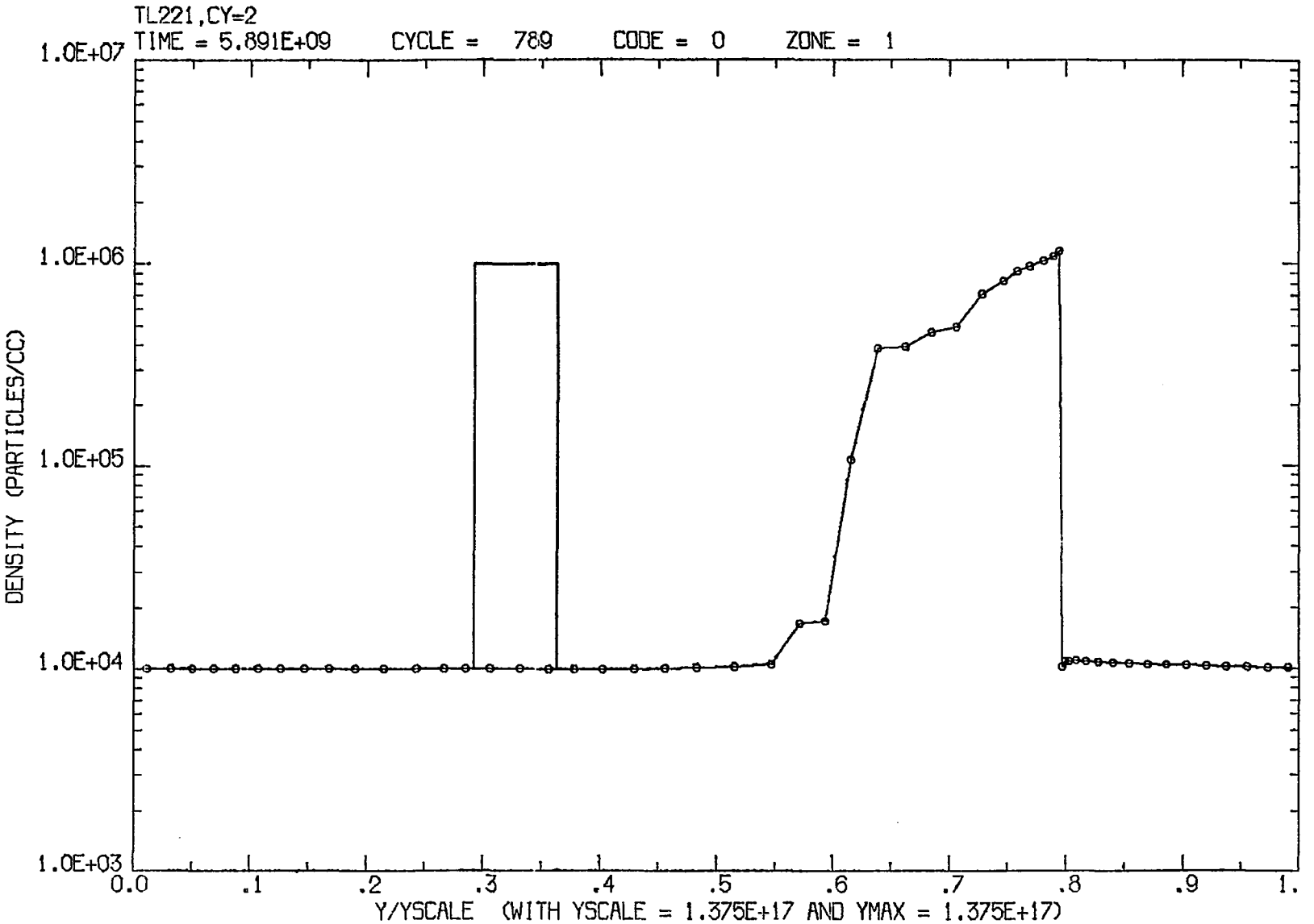

Figure 31b. The density (in nucleons/cm^3) along the symmetry (y) axis at s = 2.53 for model TL221

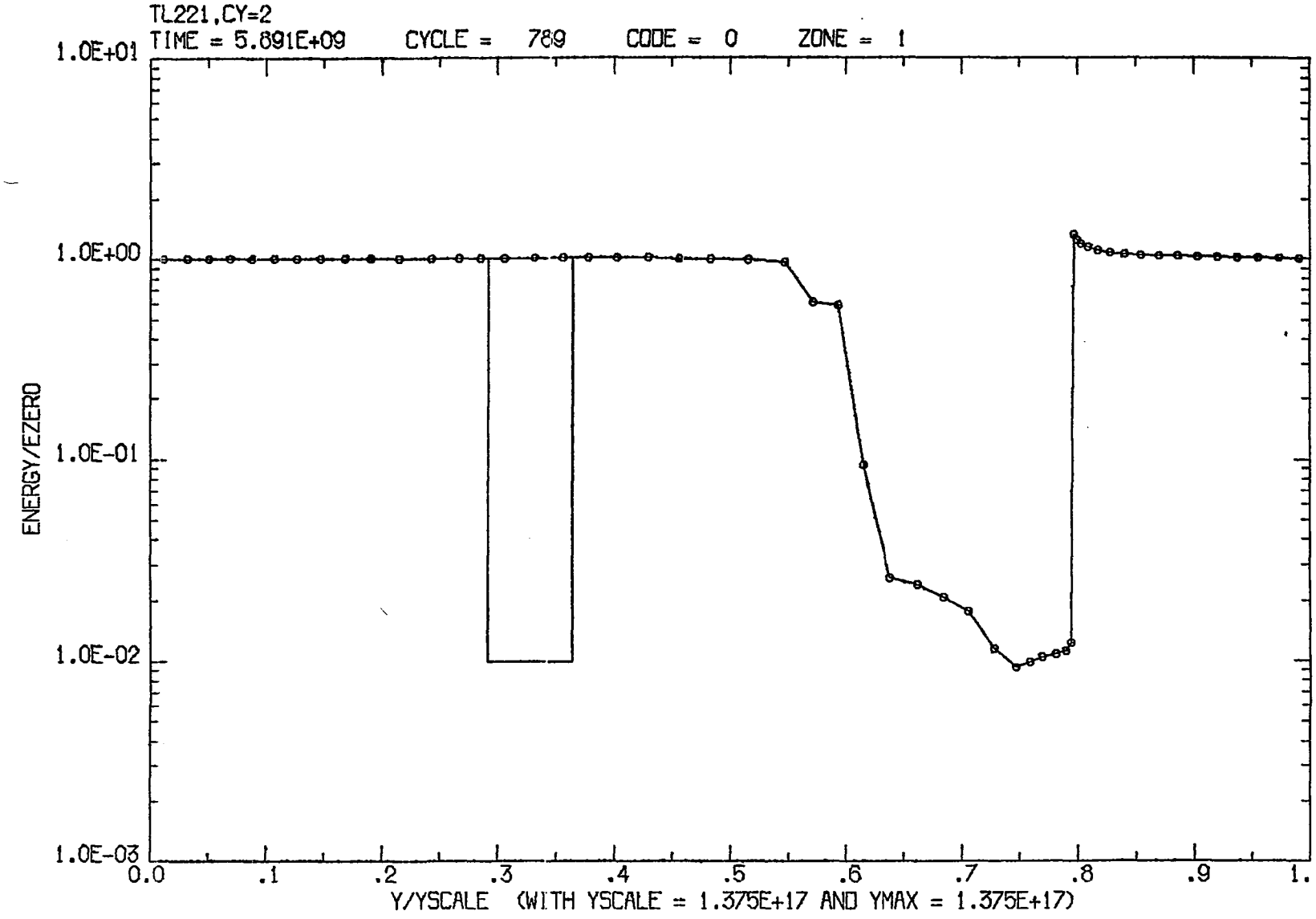

Figure 31c. The specific internal energy (in units where $e_{ic}(0) = 1.0$) along the symmetry (y) axis at s = 2.53 for model TL221

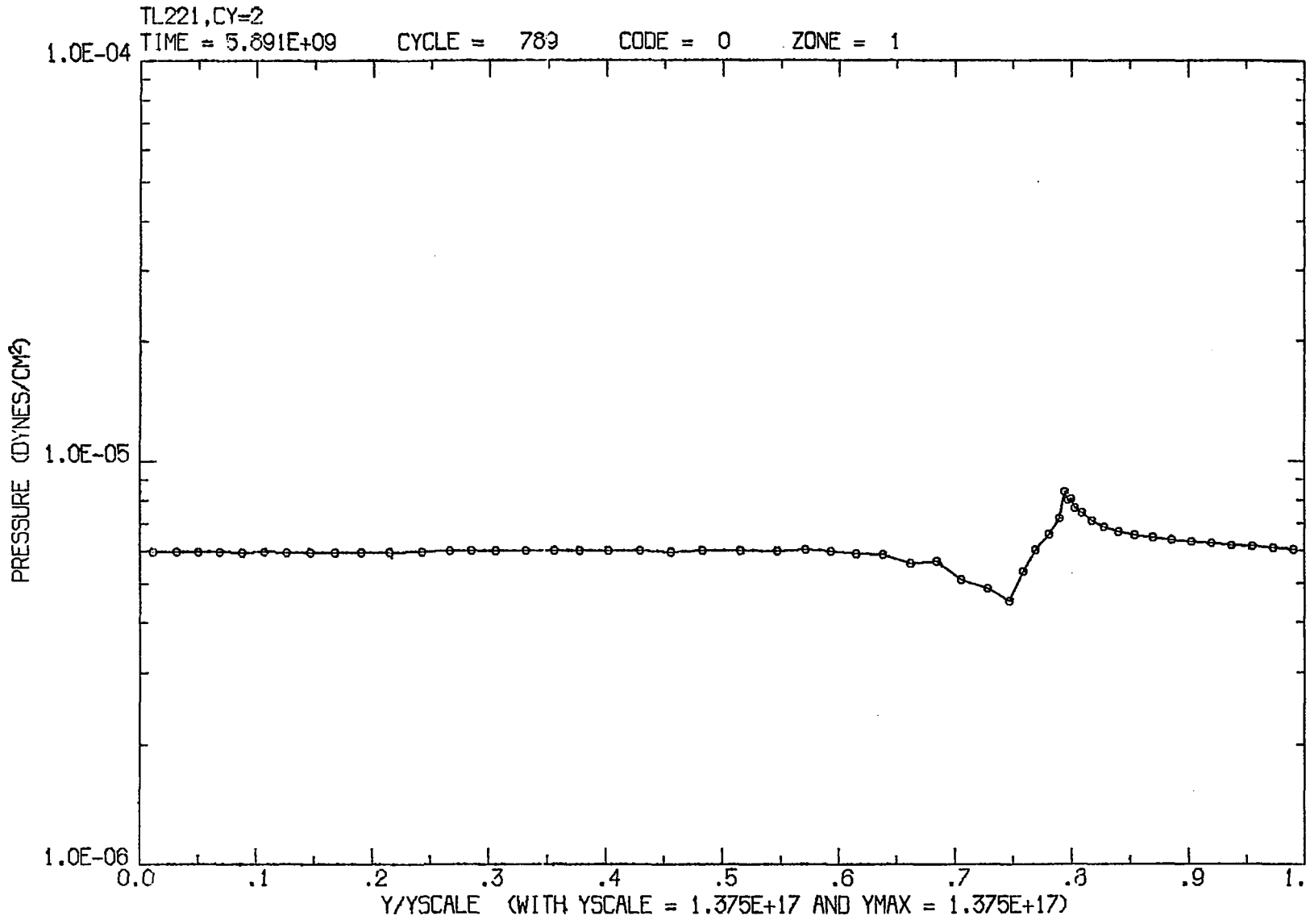

Figure 31d. The pressure (in dynes/cm^2) along the symmetry (y) axis at s = 2.53 for model TL221

dominate thermal gas pressure, it becomes increasingly important as the cloud is accelerated. The subsequent increase in pressure on the front face of the cloud results in a mild compression. Since the radiation pressure is proportional to density, this in turn leads to differential acceleration and expansion in the radial direction. Because the expansion is adiabatic, the internal gas pressure drops as the cloud is stretched. The resulting pressure gradients set up a transverse flow of intercloud gas which compresses the cloud, maintaining its pressure at $\simeq P_c(0)$. Some of this hot, tenuous gas mixes with the colder, denser cloud gas, especially in the rear of the cloud where the radial expansion is the largest. Thus, the density is lowered and the temperature is raised (Figures 31b and 31c).

Figure 32 shows the time variation of the column density for the first eight Eulerian zones of TL221. The smooth rise in the cloud's column density right from s = 0 shows that the transverse compression begins as soon as the model is turned on. The increase in the column density for zone 8 is almost entirely due to the grid extension. The large pressure oscillations which occurred in the ram pressure models at early times never develop here. This is because the cloud is initially in pressure equilibrium with the intercloud medium, so large outward expansions do

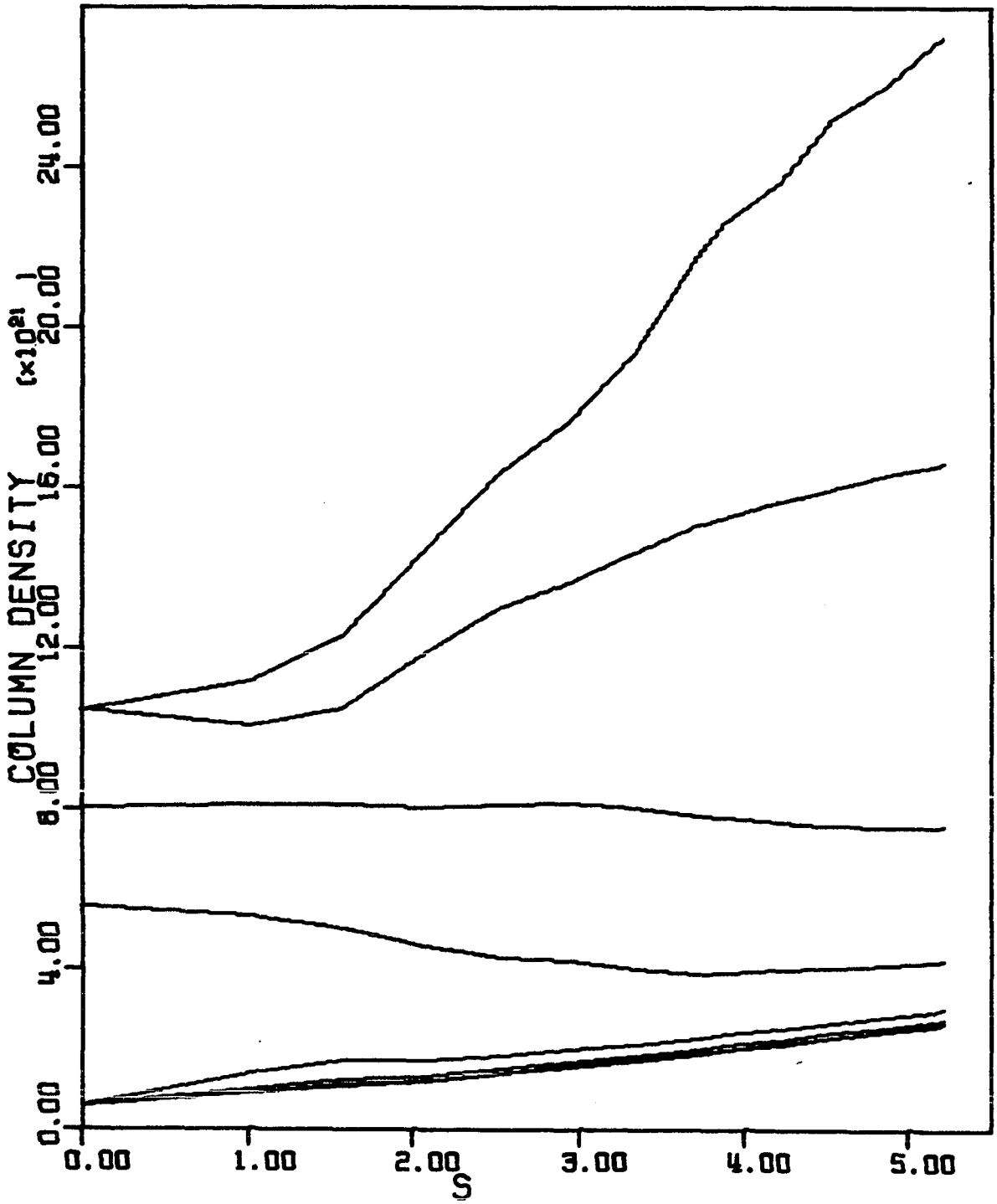

Figure 32. The column density as a function of time for the first eight Eulerian zones of TL221

not occur. Also the flow is subsonic, so the hot intercloud gas has time to respond to changes in the cloud's internal pressure.

The contours of velocity, pressure, and internal energy at the end of the evolution (s = 5.21, t = 1.21 x 10^{10}) are plotted in Figures 33a-c. The run of these variables, as well as the pressure, along the y-axis are shown in Figures 34a-d. Basically, these plots are similar to those at s = 2.53, but a few interesting features deserve special mention. Note the near discontinuity in the velocity at the head of the cloud (Figure 34a). A shock is beginning to form because the front of the cloud has a Mach number of 1.1. Compare the smooth trail off in velocity in Figure 31a at s = 2.53 when the flow is subsonic (Mach 0.7) and the sharp drop off for the highly supersonic flow (Mach 11.9) of RL331 (Figure 12a).

The cloud has continued to stretch out in the radial direction (Figure 16) and to be compressed in the transverse direction. More mixing of cloud and intercloud gas has occurred, considerably raising the temperature in the rear of the cloud (Figure 34c). Confinement at the head of the cloud remains excellent; the temperature and density have changed little from the initial conditions (Figures 34b and 34c). Because approximate pressure balance is maintained

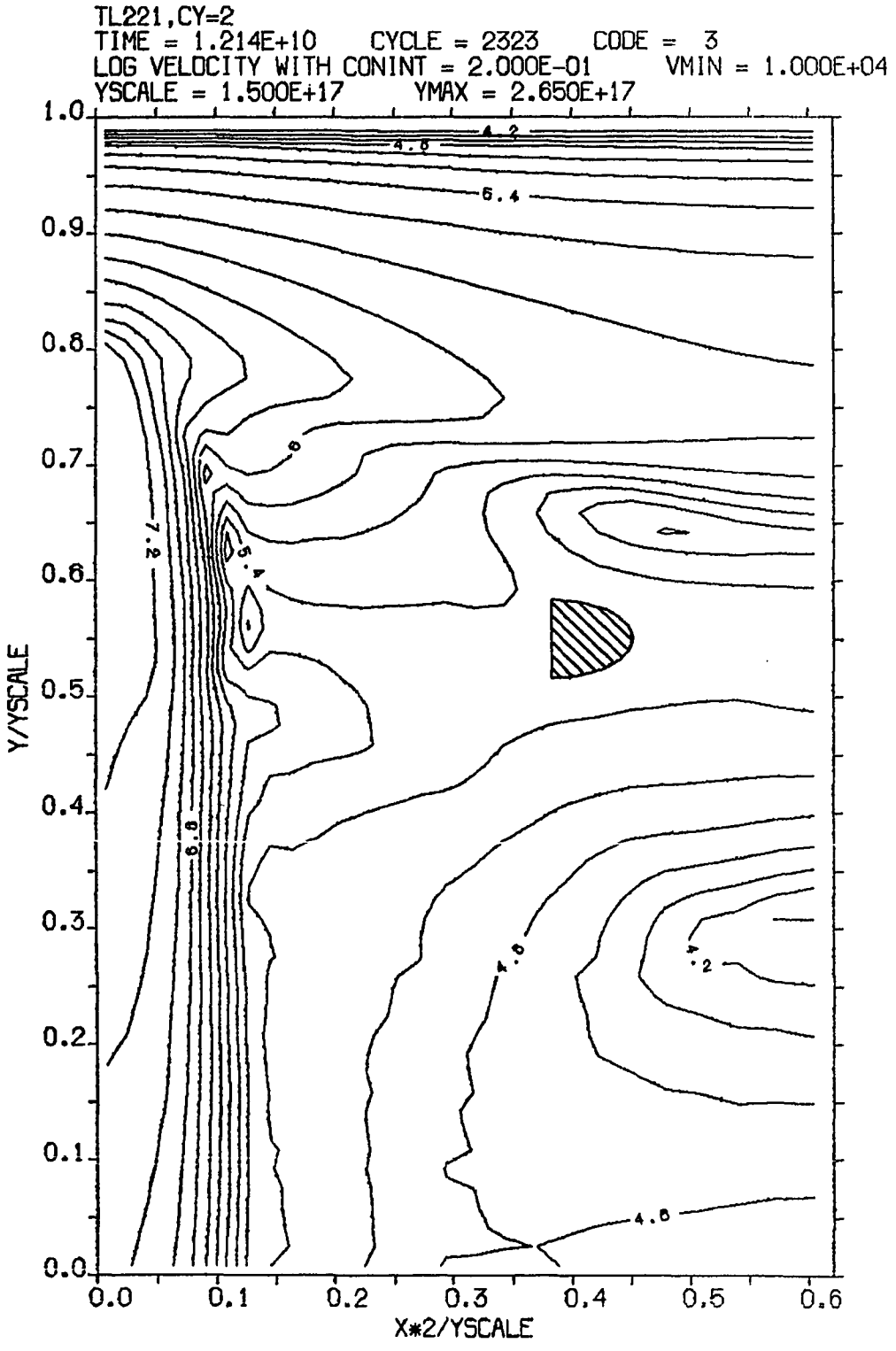

Figure 33a. Contours of the logarithm of velocity (in cm/sec) at s = 5.21 for model TL221

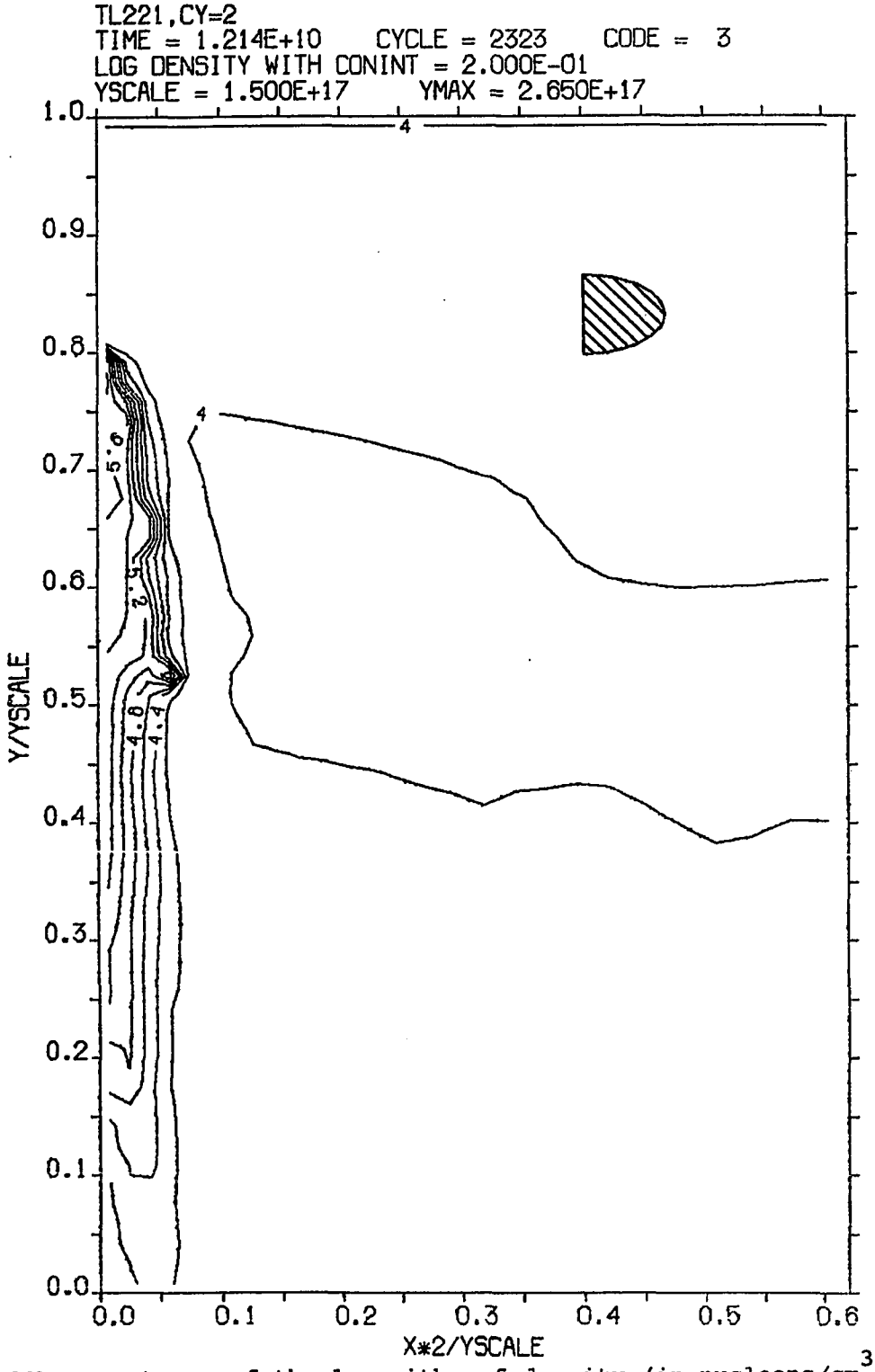

Figure 33b. Contours of the logarithm of density (in nucleons/cm^3) at s = 5.21 for model TL221

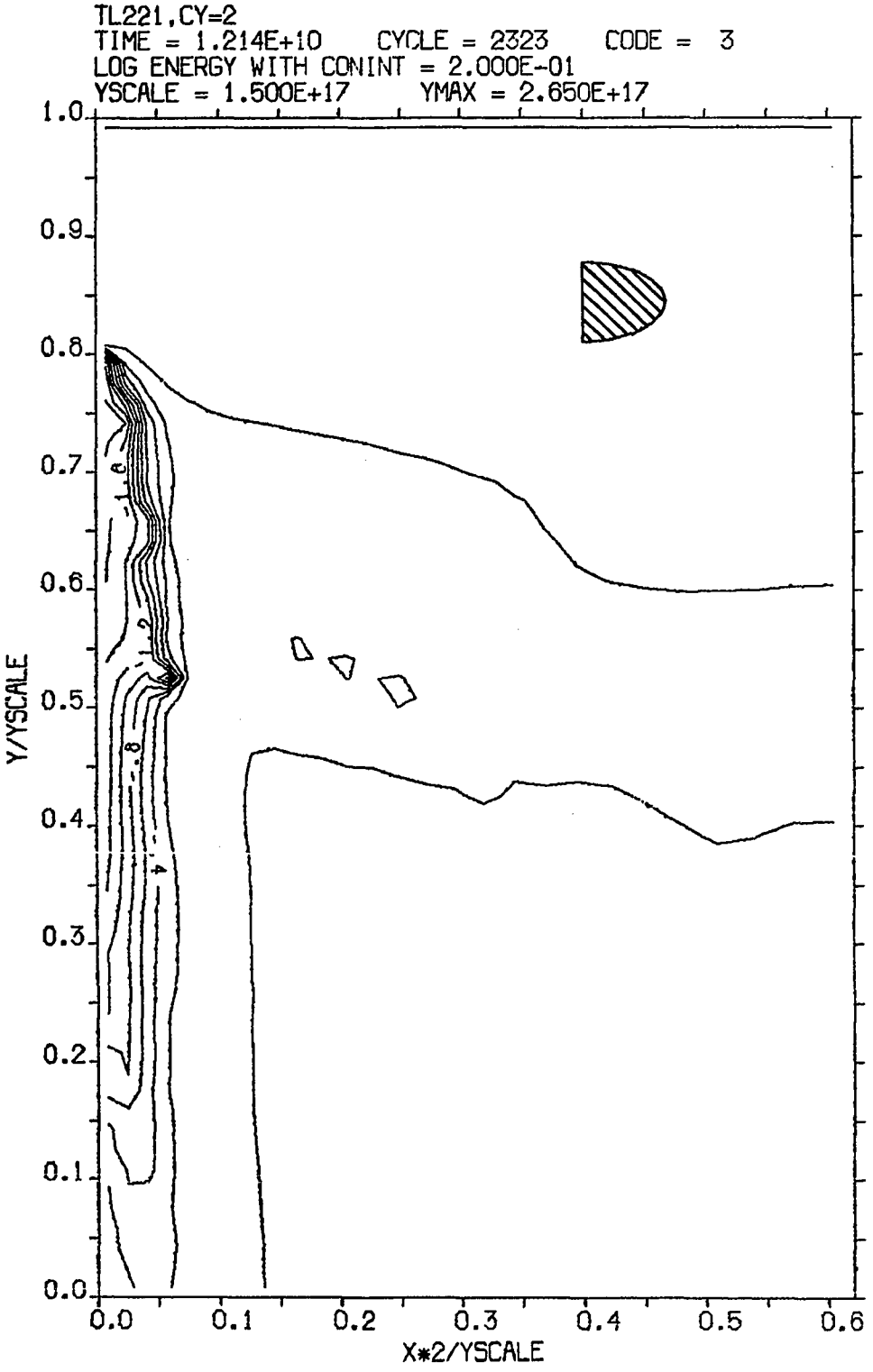

Figure 33c. Contours of the logarithm of specific internal energy (in units where $e_{ic}(0) = 1.0$) at s = 5.21 for model TL221

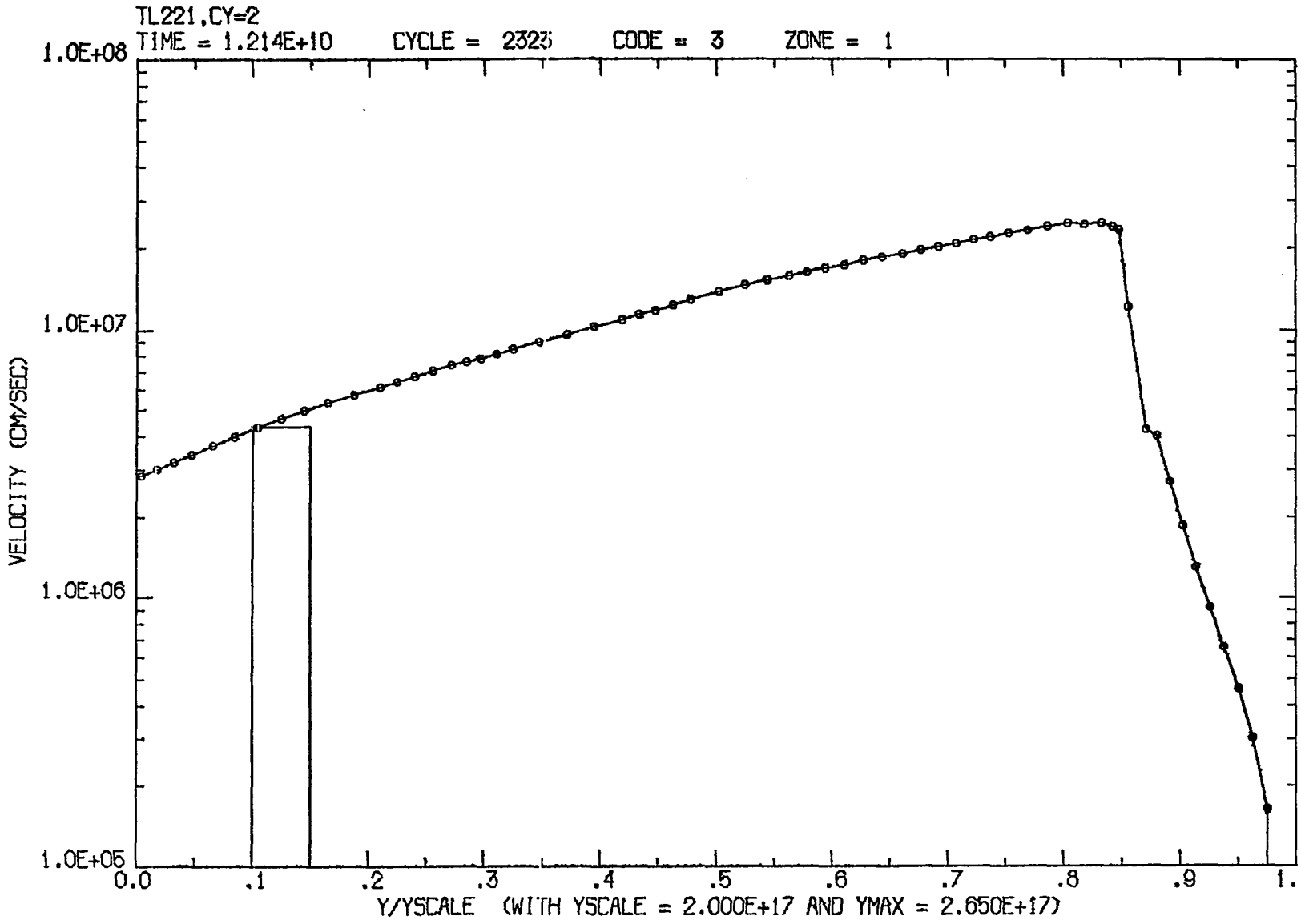

Figure 34a. The velocity (in cm/sec) along the symmetry (y) axis at s = 5.21 for model TL221

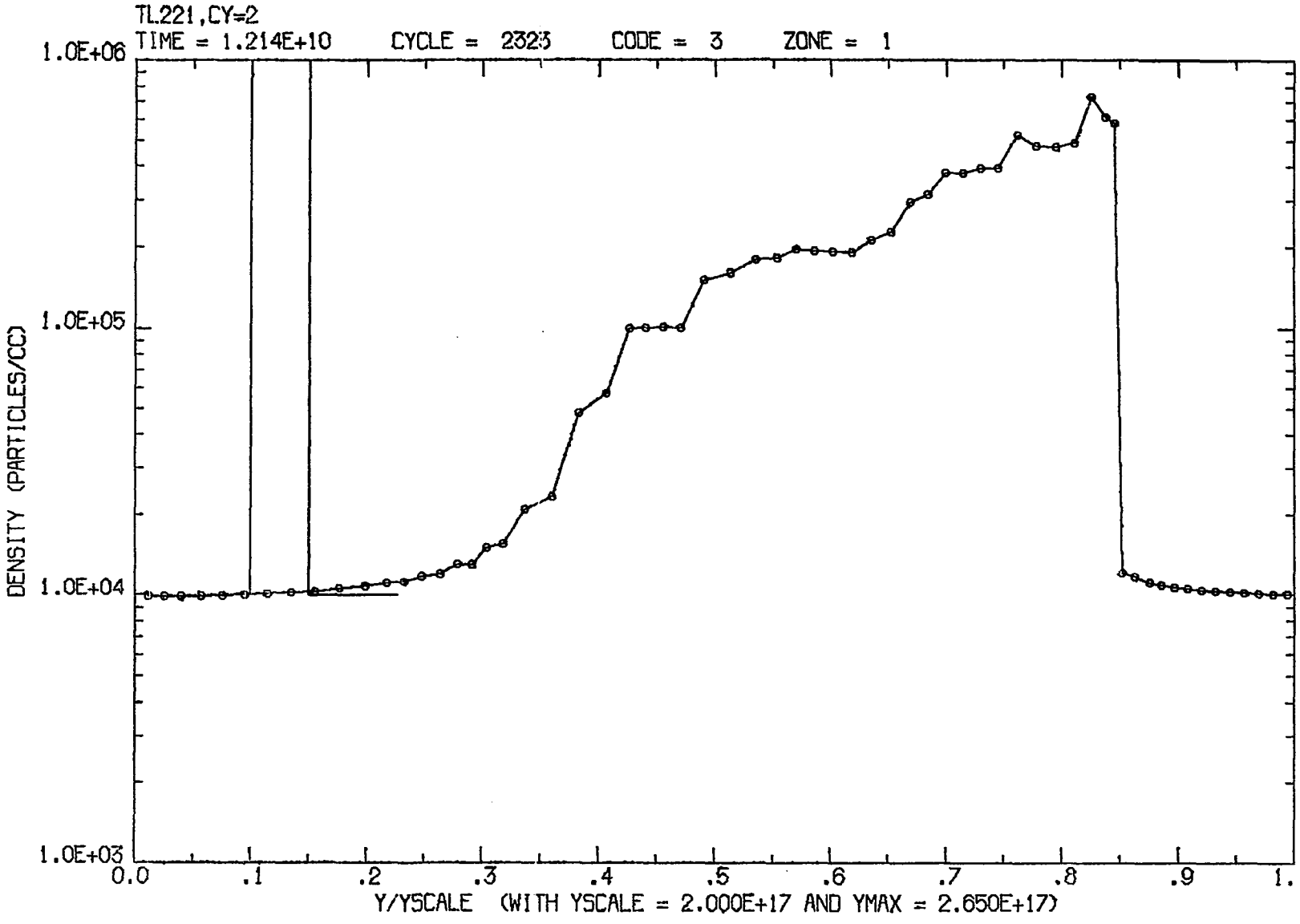

Figure 34b. The density (in nucleons/cm^3) along the symmetry (y) axis at s = 5.21 for model TL221

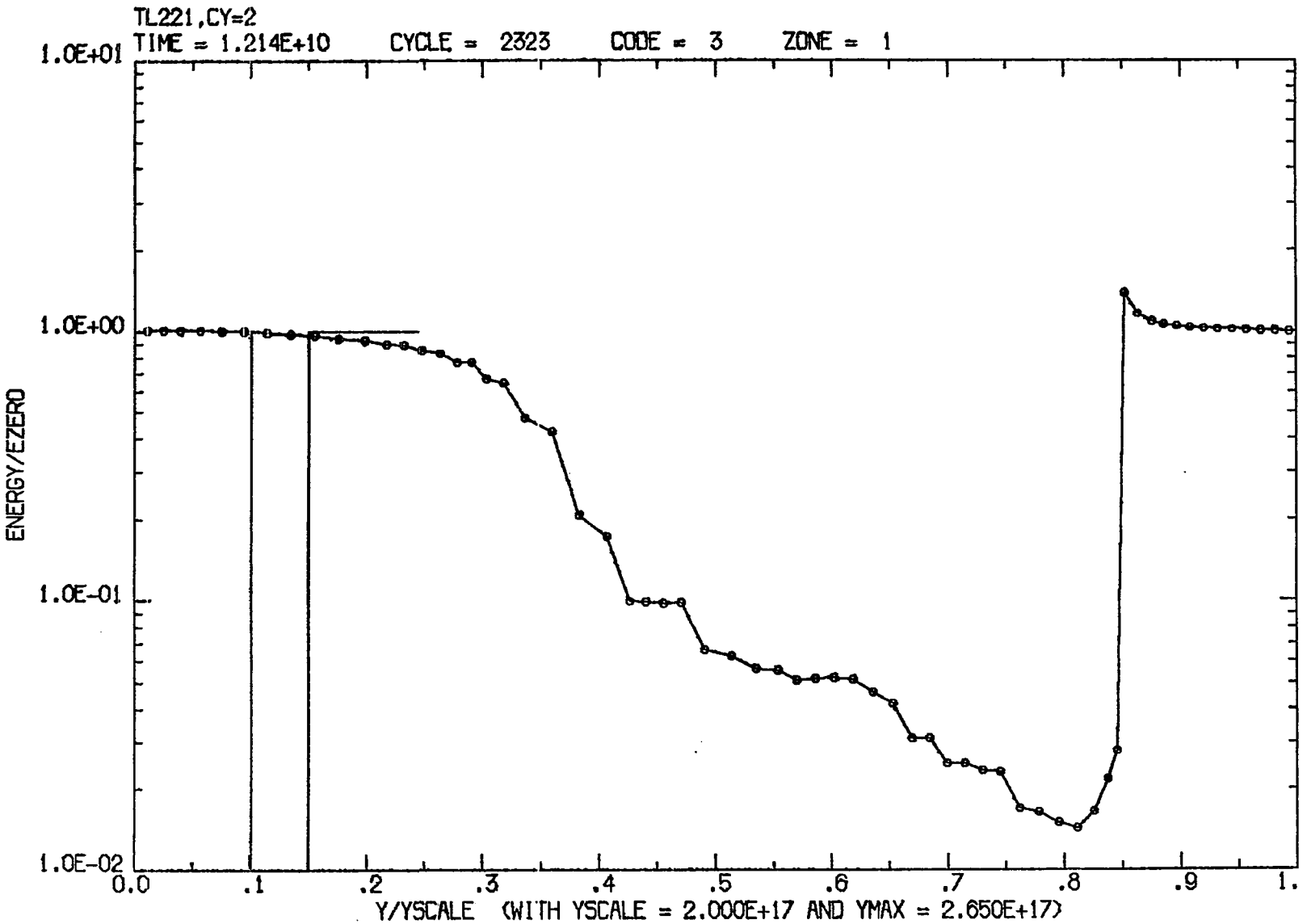

Figure 34c. The specific internal energy (in units where $e_{ic}(0) = 1.0$) along the symmetry (y) axis at s = 5.21 for model TL221

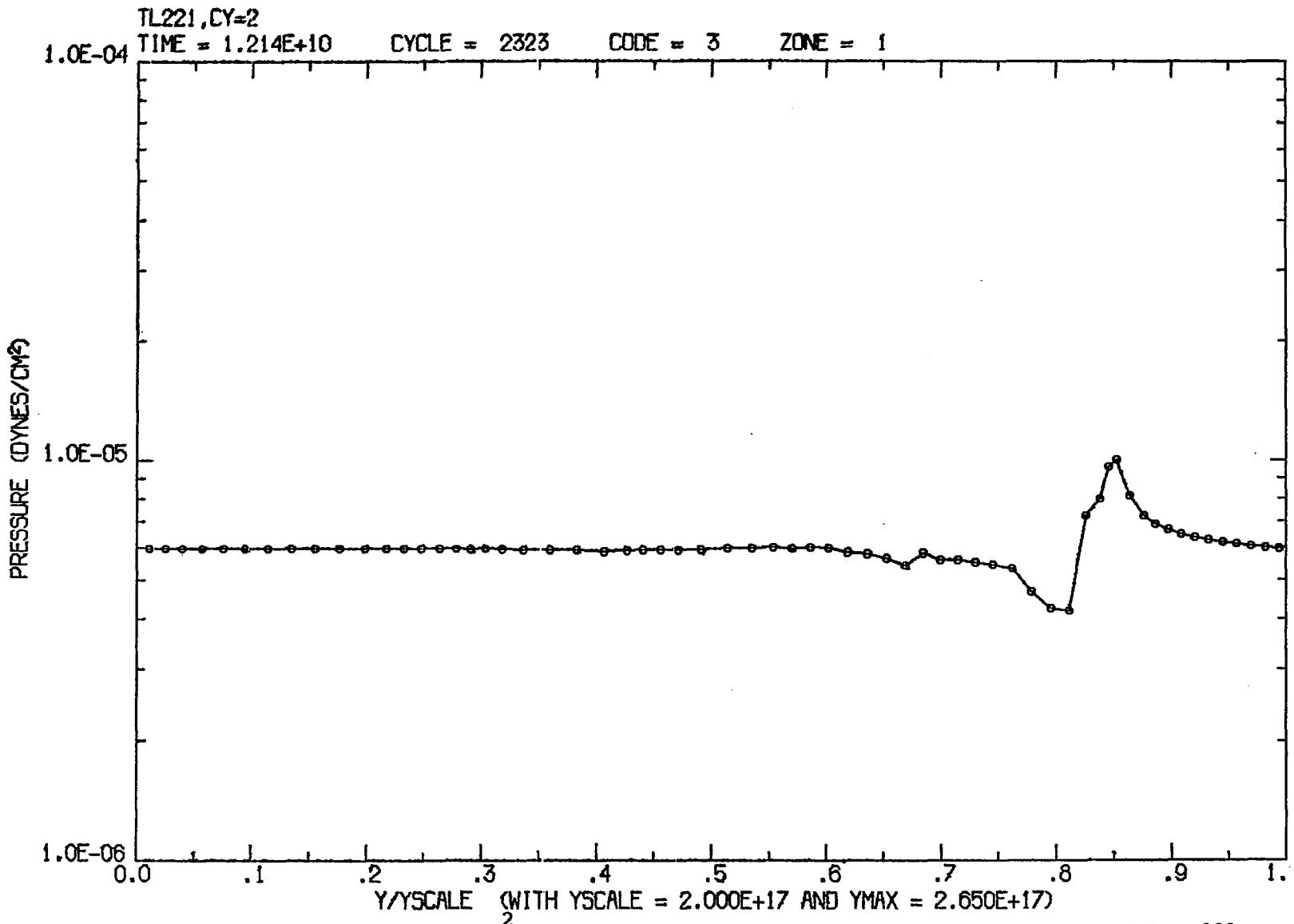

Figure 34d. The pressure (in dynes/cm^2) along the symmetry (y) axis at s = 5.21 for model TL221

(Figure 34d), there is little outflow of cloud material in the transverse direction as occurred along the bow shock in the ram pressure models (see Chapter V.B and V.C).

The average Mach number for each 5% of the cloud's mass ($\bar{M}_n(s)$ in Equation 5.4) is plotted in Figure 35. In general, the densest material has received the most acceleration, however the curves are very noisy. This is a result of the course grid used for these models. Initially the cloud occupies only 26 cells spanning four Eulerian zones (Figure 10), so as much as 0.078 $m_c(0)$ is contained in a single cell. The thermally confined clouds do not spill out into the neighboring grid cells as do the ram-pressure-confined clouds. At s = 2.53, twelve of the 20 $\bar{M}_n$ are still calculated from one or two cells, while in RL222 at a similar time, only one of the $\bar{M}_n$ depends on so few cells. Thus even fine rezoning (see Chapter IV.D) disturbs the density ranking of cells in TL221 enough to drastically change the individual $\bar{M}_n$. Add to this the fact that $\bar{M}_n$ is only calculated every few hundred time steps (in order to save computer time) and it is clear why the curves are not smooth. Course rezoning and/or chopping (Chapter IV.D) at s = 3.88, 4.54, and 5.21 are responsible for some of the largest jumps in $\bar{M}_n(s)$.

Although the $\bar{M}_n(s)$ in Figure 35 are noisy, they contain useful information concerning the amount of

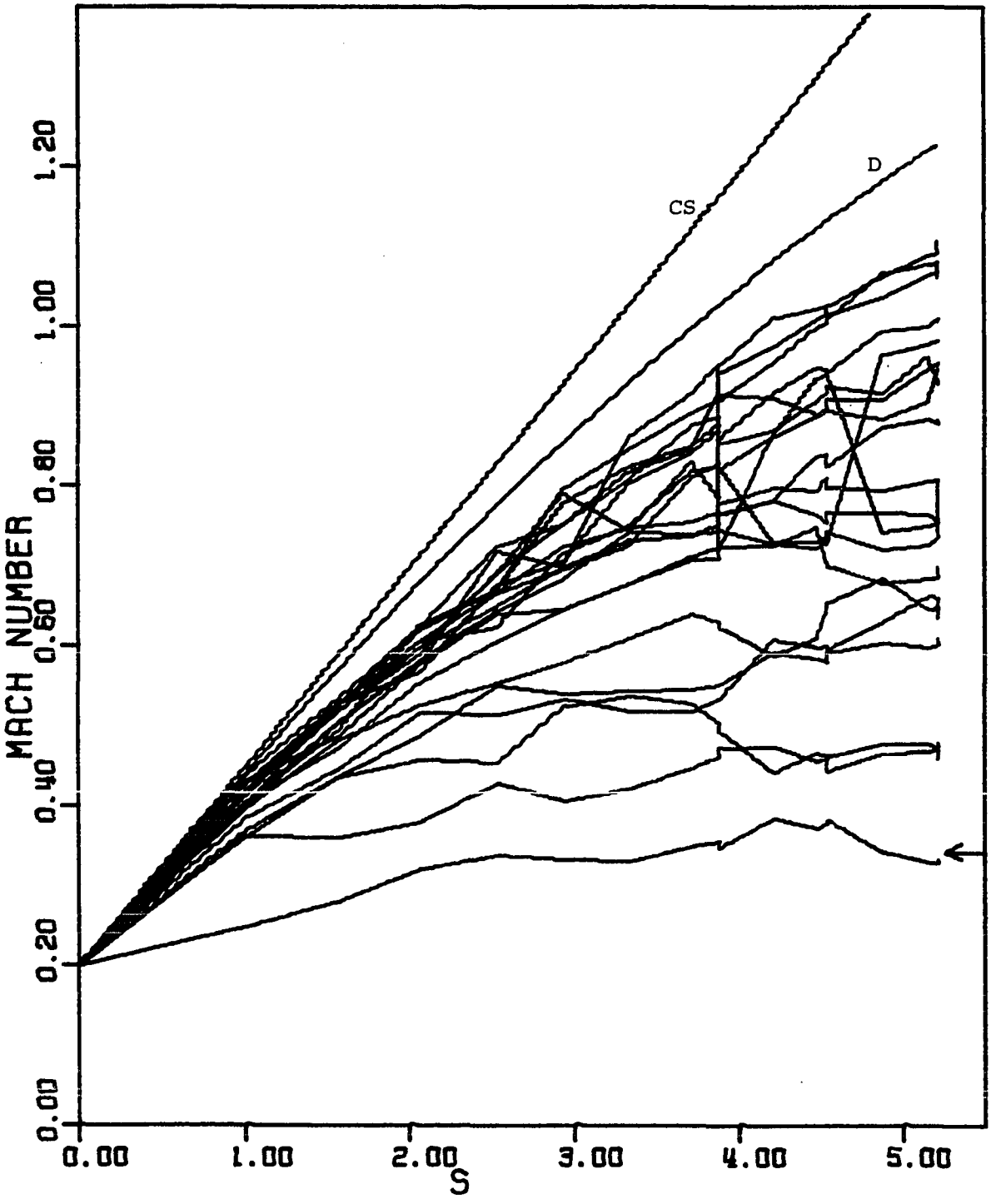

Figure 35. The Mach number for each 5% of the cloud TL221 as a function of time

acceleration which has occurred. The curve labelled CS shows the acceleration for an optically thin, constant-size cloud (Equation 2.17); the curve labelled D includes the effects of drag (Equation 3.3). The arrow at s = 5 indicates the terminal velocity for a freely expanding cloud (Equation 2.13). Notice that the entire cloud TL221 has been accelerated to velocities above this terminal velocity, in contrast to the case for RL222 (Figure 20). The cloud has not yet reached a terminal velocity, but the $\overline{M}_n$ are bending over, away from curve D. Thermal gas pressure is more effective in confining the clouds in the transverse direction than is ram pressure, making somewhat larger accelerations possible. However, in both cases radiation pressure causes differential expansion in the radial direction, thereby seriously impairing further acceleration.

2. TL335

The results for TL335 are qualitatively similar to those for TL221, so only a brief discussion is necessary. TL335 is the thermal counterpart of the ram pressure model RL331 and thus it has an initial column density of 10^{23} and $n_c(0)/n_{ic}(0) = 10^3$. Its other properties are listed in Table 1.

TL335 very rapidly increases in length (Figure 16) just as RL331 does. In order to continue the evolution

after the cloud has reached the top of the grid as extended by the methods outlined in Chapter IV.D, the resolution was halved at s = 1.65 and again at s = 2.68. Hence the latter phases of the evolution have cells with y-dimensions as large as 2×10^{16} cm, although most are somewhat smaller. This is twice the diameter of the original cloud! The length of the cloud discontinuously changes by only 3% due to this rezoning. The effect on the cloud's velocity is given in Figure 36, where $\overline{M}_n(s)$ is plotted (Equation 5.4). Since the essential features of the flow are well established by s = 1.63, it is doubtful that these subsequent, rather gross, cell manipulations lead to serious error.

The initial column density is an order of magnitude greater for TL335 than for TL221. Therefore it is not surprising that it reaches higher velocities (see Equation 3.3). However, TL335 departs more strongly from the trajectory for a constant-size cloud (cf Figures 35 and 36). It approaches a terminal velocity rather quickly, yet its radial expansion (Figure 16) shows no sign of slowing down.

The density and temperature profiles along the y-axis flatten out more rapidly in TL335 than in TL221 because of the larger rate of radial expansion. A large oscillation develops in the pressure profile as soon as the evolu-

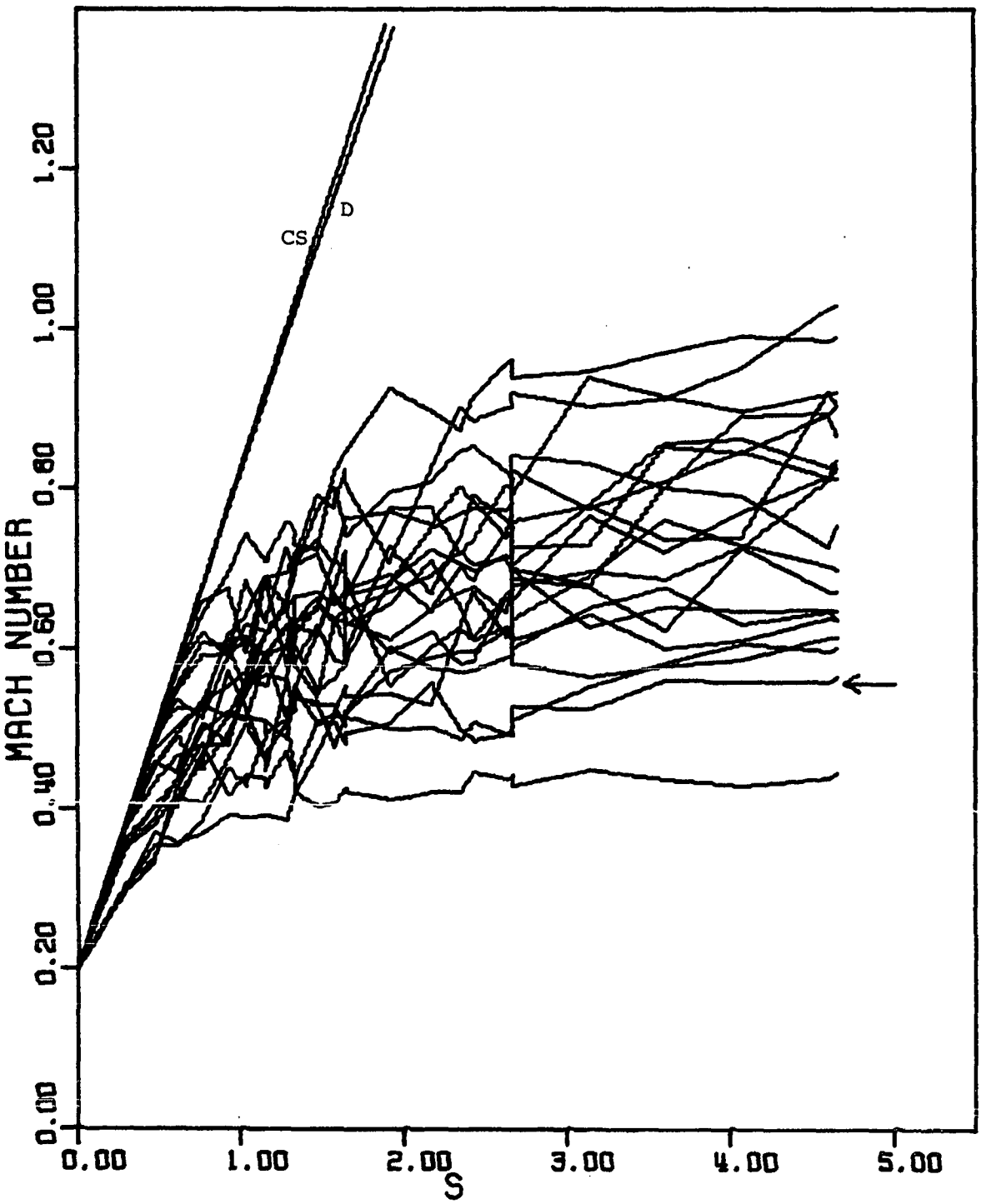

Figure 36. The Mach number for each 5% of the cloud TL335 as a function of time

tion begins. It starts out very similarly to those described for the ram pressure models (see Chapter V.B), with a minima at the rear of the cloud and a maxima at the front. As the evolution progresses, the minima grows and moves forward in the cloud. By s = 1 the minima is $\simeq 1/13\ P_{ic}(0)$ and lies at the front of the cloud; a maxima of $\simeq 2P_{ic}(0)$ lies at the rear. From this time onward, the amplitude of the oscillation slowly decreases until at s = 2 it has almost completely disappeared and the cloud's internal pressure is again nearly uniform and $\simeq P_{ic}(0)$. Much smaller oscillations (minima $\gtrsim \frac{1}{2} P_{ic}(0)$) occur in TL221 and TL231, which have smaller column densities. Hence it is presumed that the oscillations are a transient response to the sudden turn-on of the radiation pressure at t = 0. This is born out by the results for models TL337 and TL338 (Chapter V.F).

3. TL231

This section is closed by giving the results for TL231. As its name implies, it has an initial column density of 10^{22} and $n_c(0)/n_{ic}(0) = 10^3$. The initial diameter of the cloud is 10^{15} and its optical depth at the Lyman continuum edge is $\simeq 0.25$; both are a factor of ten less than for the other models (see Table 1 for more details).

The length of TL231 as a function of time is nearly

identical to that of TL221 (Figure 16). This demonstrates that the rate of radial expansion depends strongly on the column density and is essentially independent of the ratio $n_c(0)/n_{ic}(0)$. (Note that both of these are increased for TL335 and RL331 compared to TL221 and RL222.) The Mach number for each 5% of $m_c(0)$ (Equation 5.4) is plotted in Figure 37. Their departure from the trajectory for a constant-size cloud is less than for any of the other models. The reason for this is unclear; more models (with different initial conditions) need to be run in order to understand why. Nevertheless, the velocity dispersion is rapidly increasing and the cloud appears to be reaching a rather low terminal velocity. Thus, the results are in qualitative agreement with those of the earlier models.

F. Transient Phenomena

The ram-pressure-confined, radiatively accelerated clouds (RL331 and RL222) initially expand because their internal pressure is much larger than the external gas pressure. These clouds subsequently overshoot pressure equilibrium and large, low pressure regions develop in their rear sections (Chapter V.B). The models with no radiative acceleration (R0334 and R0221) develop similar pressure cavities, yet they do not experience the same

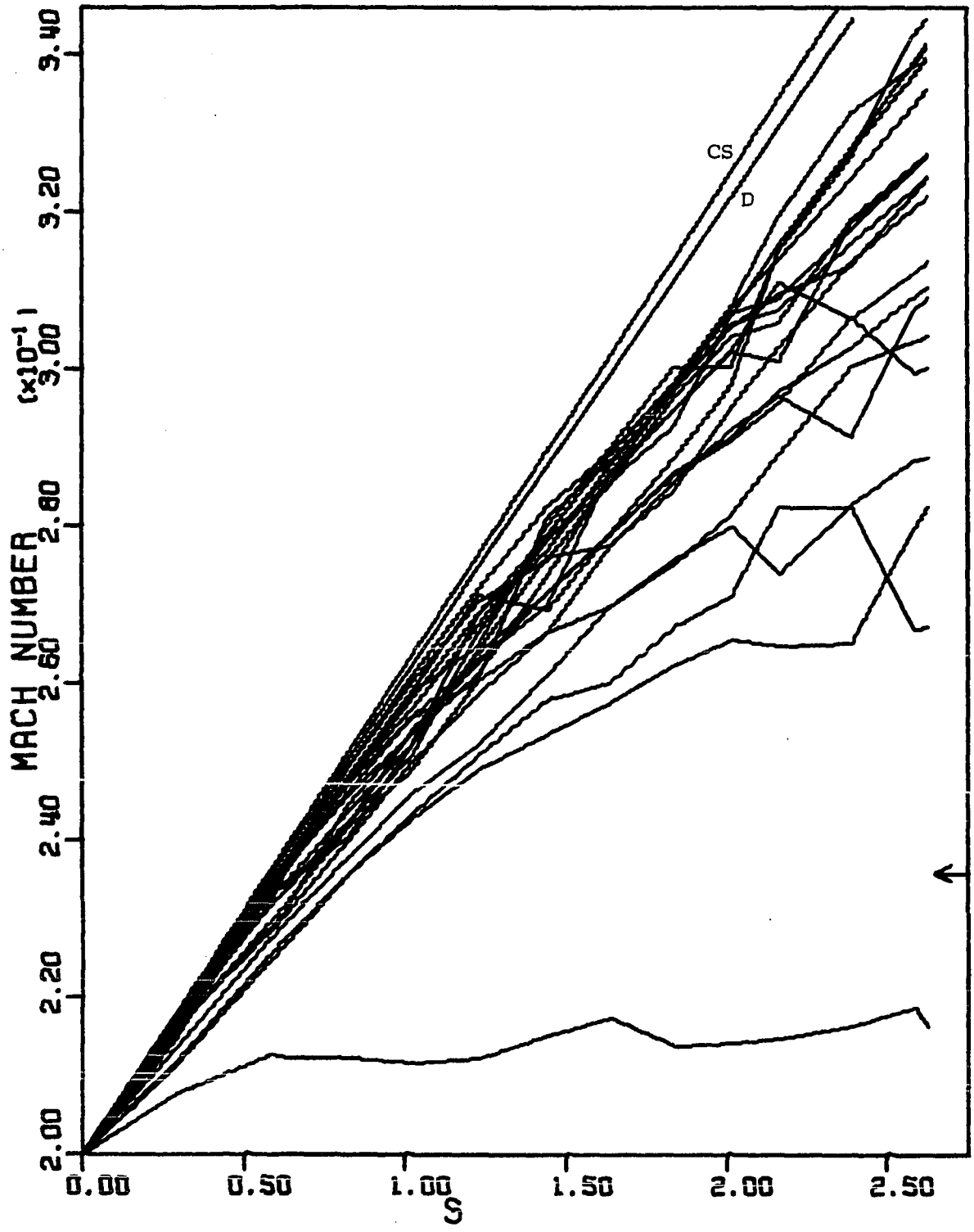

Figure 37. The Mach number for each 5% of the cloud TL231 as a function of time

large radial expansions (Figure 16). This suggests that only the latter behavior is a response to the radiation pressure acceleration.

The pressure cavities are believed to be a transient response to the use of nonequilibrium initial conditions. Their presence is unfortunate, at best, because they complicate the interpretation of the model results. They are difficult to eliminate because better initial conditions are hard to come by; the gas in the region between the bow shock and the cloud would have to be modeled in detail. In any event, these pressure cavities are refilled by a transverse inflow of gas within a few cloud expansion times. A second, smaller oscillation may then occur (Chapter V.B). By this time the clouds are greatly distended in the radial direction and consequently they have already reached rather low terminal velocities (Figures 17 and 20). The evolutions are terminated because the nature of the gas flow seems well established and because it becomes increasingly expensive to continue them. (These stretched out clouds require very large grids.)

Now one might argue that the cloud dynamics is so strongly affected by the presence of these transient phenomena that the results are meaningless. That is to say, the cloud stretching and the corresponding reduction in the acceleration occur because of, not in spite of,

these transients. The results for RP221 (Chapter V.D) and the thermally confined clouds (Chapter V.E) suggest that this is not the case. RP221 has no transverse gas flow and no pressure cavity develops, yet its response to radiation pressure is very similar to that of RL222, the corresponding two-dimensional model. The radial expansion of the thermally confined clouds, TL221 and TL335, is comparable to that of their respective ram pressure counterparts, RL222 and RL331 (Figure 16). Since TL221 is relatively free of transients, the physical reality of the cloud stretching seems well established, at least within the confines of the present assumptions (Chapter III).

A physical explanation for the radial expansion is proposed in Chapter V.B and E. It is considered again in Chapter VI.B. This latter discussion reveals why the transients are not important dynamically. To summarize, it is the pressure gradients, not the pressure, which is important to the dynamics. Since the pressure gradients remain small relative to the radiative acceleration, their effect is minimal.

As already mentioned, the thermally confined clouds do not develop large pressure cavities in their rear sections as do the ram-pressure-confined clouds. This is because the initial models are in pressure equilibrium.

However, this equilibrium is not a dynamical equilibrium because the advective terms in Equations 4.1 through 4.4 have discontinuities at the cloud boundaries and the radiation pressure is turned on discontinuously at t=0. Thus, transients still occur, particularly in TL335 (see description in Chapter V.E). These transients differ in character from those in the ram-pressure-confined clouds; they grow more slowly and move about within the clouds. The explanation as to why they are unimportant to the cloud dynamics is the same as for those in the ram pressure models. That is, the pressure gradients remain small compared to the radiative acceleration (Chapter VI.B, especially Figure 39).

It is still of interest to determine the cause of these pressure waves. The fact that they are much smaller in TL221 and TL231 than in TL335 provides a clue as to their origin. They are probably related to the sudden turn-on of the radiation pressure since the model which receives the largest acceleration at t=0 develops the largest transients. They are probably <u>not</u> related to the advective term discontinuities at t=0 since all three models start out at Mach 0.2.

These conclusions are supported by the results of model TL338, which is identical to TL335 except that

$M_o = 0.05$. By $s = 0.23$ when $\bar{M}_1$ (Equation 5.4) has reached 0.2, $\bar{M}_1 - \bar{M}_{20} = 0.02$ and the cloud's length is $\simeq 1.5$ times its original length. Thus the confinement is relatively good for such small Mach numbers, but radial expansion occurs nevertheless. Now the transients in TL338 at a given s are virtually identical (in magnitude) to those in TL335 at the same s. This implies that they may be associated with the sudden turn-on of the acceleration at t=0, but are not a result of discontinuities associated with M_o.

To further investigate the nature of the TL335 transients, model TL337 is evolved with the radiation pressure turned on slowly so that

$$G_{rad}(s) = \min\{2s/3,\ 1\} \cdot GCL(\xi). \qquad (5.9)$$

The starting model and the other numerical details for TL337 are identical to those of TL335. The magnitude of the maximum pressure oscillation is not significantly reduced compared to that in TL335, however this maximum occurs at a later time ($s \simeq 2$ instead of $s \simeq 1$). For the early, relatively transient-free times ($s \lesssim 1$), the proportionately smaller accelerations and rates of radial expansion are well understood on the basis of the reduced radiation pressure. This is additional evidence that the

transients are associated with the sudden turn-on of the radiation pressure and that they do not dominate the dynamics.

VI. DISCUSSION

A. Summary of the Numerical Results

Both the ram-pressure-confined and the thermal-gas-pressure-confined clouds rapidly expand in the radial direction (Figure 16). This expansion is driven by the radiation pressure (Chapter VI.B). Thus, the rate is essentially independent of which confinement mechanism is operating, but does depend on the strength of the radiation pressure. In contrast, some compression occurs in the direction transverse to the cloud motion for both the ram-pressure-confined and the thermally confined clouds. Just how much is difficult to determine because of the poor resolution employed (Figure 10), but it probably does not exceed a factor of 2 or so for any of the present models (at least for $s \lesssim 5$). In the ram models this compression is primarily at the heads of the clouds and is due to the transverse component of the ram pressure (Chapter V.B). In the thermal models it is a result of the transverse inflow of gas which is required to maintain pressure balance in the face of the radial expansion (Chapter V.E).

The rate of radial expansion greatly exceeds the rate of transverse compression so the densities of the clouds rapidly decrease. This leads to decreased radiative acceleration and, consequently, to low terminal velocities.

The thermally confined clouds (Chapter V.E) reach terminal velocities larger than those of the corresponding freely expanding clouds (Chapter II), but not by factors large enough to account for the observations (Chapter I). The ram-pressure-confined clouds do not even do this well. For them, transverse pressure gradients near the bow shock force gas out of the clouds; it then mixes with shocked intercloud gas and decelerates (Chapter V.B). This mass loss causes the density and, therefore, the acceleration to decrease even faster than for the corresponding thermally confined clouds. The resulting terminal velocities are lower than those for the case of free expansion.

The rate at which mass is lost from the front of the ram-pressure-confined clouds appears to vary as the inverse of the Mach number for the flow. However, this proportionality is quite uncertain because it is based on the results of only four models (i.e., RL331, R0334, RL222 and R0221), which span a limited range of Mach number. Furthermore, $n_c(0)/n_{ic}(0)$ varies among them and two of the models see no radiation pressure. It is, however, a reasonable result because the lower Mach number clouds have relatively weaker bow shocks. This means that the shock is not swept back as sharply, thereby allowing more transverse expansion to occur.

The mixing of cloud and intercloud gas (and its subsequent deceleration) leads to the rapid dissipation of the ram-pressure-confined clouds. There is also a considerable amount of mixing of cloud and intercloud gas in the case of thermal confinement because of the transverse inflow of gas (Chapter V.E). In both cases then, mixing significantly alters the thermal and ionization structure of the clouds (Chapters III and V). In these models the flow is assumed to be adiabatic; the heating mechanism for the hot, thermally confining medium is not specified and radiative cooling is ignored. Therefore, the detailed structure of these clouds can not be taken too seriously. Nevertheless, it is argued (Chapters III.B and VI.B) that the general dynamical behavior described here is essentially correct.

The radial expansion results not only in low terminal velocities, but also in large velocity dispersions. A feel for the size of these dispersions can be obtained from the plots of velocity as a function of distance along the symmetry axis (Figures 12a, 14a, 31a, and 34a). To obtain more quantitative results, histograms displaying the column density as a function of its velocity were prepared. The velocity dispersion was then defined as the full velocity width at half the maximum column density. These

dispersions were typically found to be $\gtrsim 0.1\ v_{head}$ (where v_{head} is the velocity for the head of the cloud, i.e., the maximum velocity in the flow). The results are necessarily crude because of the poor resolution employed for these models.

B. Radial Expansion

The clouds rapidly expand in the radial direction and the rate is essentially independent of whether the clouds are confined by ram pressure or by thermal gas pressure (Figure 16). By intercomparing the results of the various models (Chapter V.F), it is argued that this expansion is a real physical effect, not a transient response to the use of crude initial conditions. An explanation for this expansion (for the case of ram pressure confinement) was proposed in Chapter V.B. To review, the front face of a cloud is compressed by ram pressure while its rear is free to expand, so a density gradient quickly develops across the cloud. Then, since the radiation pressure is proportional to the gas density (Figure 4), differential acceleration results. That is, the dense, forward portion of the cloud is accelerated more strongly than is the relatively low-density rear. This further increases the density gradient and, consequently,

leads to still more differential expansion.

This explanation is supported by the results for the decelerating clouds R0334 and R0221. That is, when the radiation pressure is turned off, the same type of density profile occurs (ρ decreases from front to rear), but the cloud expansion rate drops by an order of magnitude (Figure 16). It is also consistent with the fact that the rate of expansion increases with increasing radiation pressure. To see this, compare the lengths of RL331 and TL335 with those of RL222 and TL221 respectively. The fact that TL231 expands at the same rate as does TL221, not TL335, shows that the expansion rate does not depend strongly on the ratio $n_c(0)/n_{ic}(0)$.

Can this theory also account for the radial expansion of the thermally confined clouds? Yes, because the ram pressure, although substantially smaller than the external gas pressure, is not negligible. Once it establishes a small density gradient, radiation pressure latches on and magnifies it just as in the ram-pressure-confined clouds. This scenario is supported by the cloud lengths displayed in Figure 16 (cf RL331 to TL335 and RL222 to TL221). The thermally confined clouds expand more slowly at first because the density gradients produced by ram pressure are smaller. However, once the differential expansion begins,

radiation pressure produces its own density gradient and the rate of expansion becomes comparable to that for the ram pressure case.

This behavior warrants further discussion. Coherent acceleration would obtain if the gas pressure gradients within the clouds could adjust themselves so that they exactly balanced the differential radiation pressure. Such a situation can occur in the static case. Requiring that the effective acceleration,

$$g(r) = -\frac{1}{\rho}\frac{dP}{dr} + \beta n, \tag{6.1}$$

is a constant through a one-dimensional, isothermal cloud results in the density profile

$$n(r) = \frac{gn_o}{\beta n_o - (\beta n_o - g)\exp(g\mu r/k\bar{T})} . \tag{6.2}$$

The density at the rear boundary of the cloud (r=0) has been denoted by n_o. Once the column density of the cloud is specified and the boundary conditions $P_c(r=0) = P_{ic}(0)$ and $P_c(r=L) = P_{ic}(0) + 0.9\ \rho_{ic} v_c^2$ are imposed, the cloud's length (L) and its effective acceleration (g) are uniquely determined.

Provided that this cloud remains isothermal (in time and in space), the second boundary condition becomes

$$n(L)/n_o = 1 + 1.5\ M_c^2 \tag{6.3}$$

with $M_c = v_c/c_{ic}(0)$. This relationship shows that the density distribution is essentially flat at subsonic speeds, but is sharply peaked for supersonic motion. Therefore, as the cloud is accelerated, the density at its head must increase. Since the column density is a constant, independent of velocity (in the one-dimensional case), this means that the length of the cloud must decrease. But if the cloud is to contract as it is accelerated, then g(r) can not be a constant across it at each time. This is in direct contradiction with the original assumption that g(r) be independent of r.

Moreover, such contraction is in marked contrast to the rapid expansion found for the numerical models.[1] It is instructive, therefore, to examine the behavior of the effective acceleration,

$$g(r) = -\frac{1}{\rho}\frac{dP}{dr} + GCL(\xi)\rho, \qquad (6.4)$$

as a function of time for some of these models. This quantity is plotted on the right hand side of Figure 38 for the one-dimensional model RP221 (Chapter V.D). The left hand side of the figure gives the radiative accelera-

[1] It is worth noting that the assumed thermal structure is quite different in the two cases.

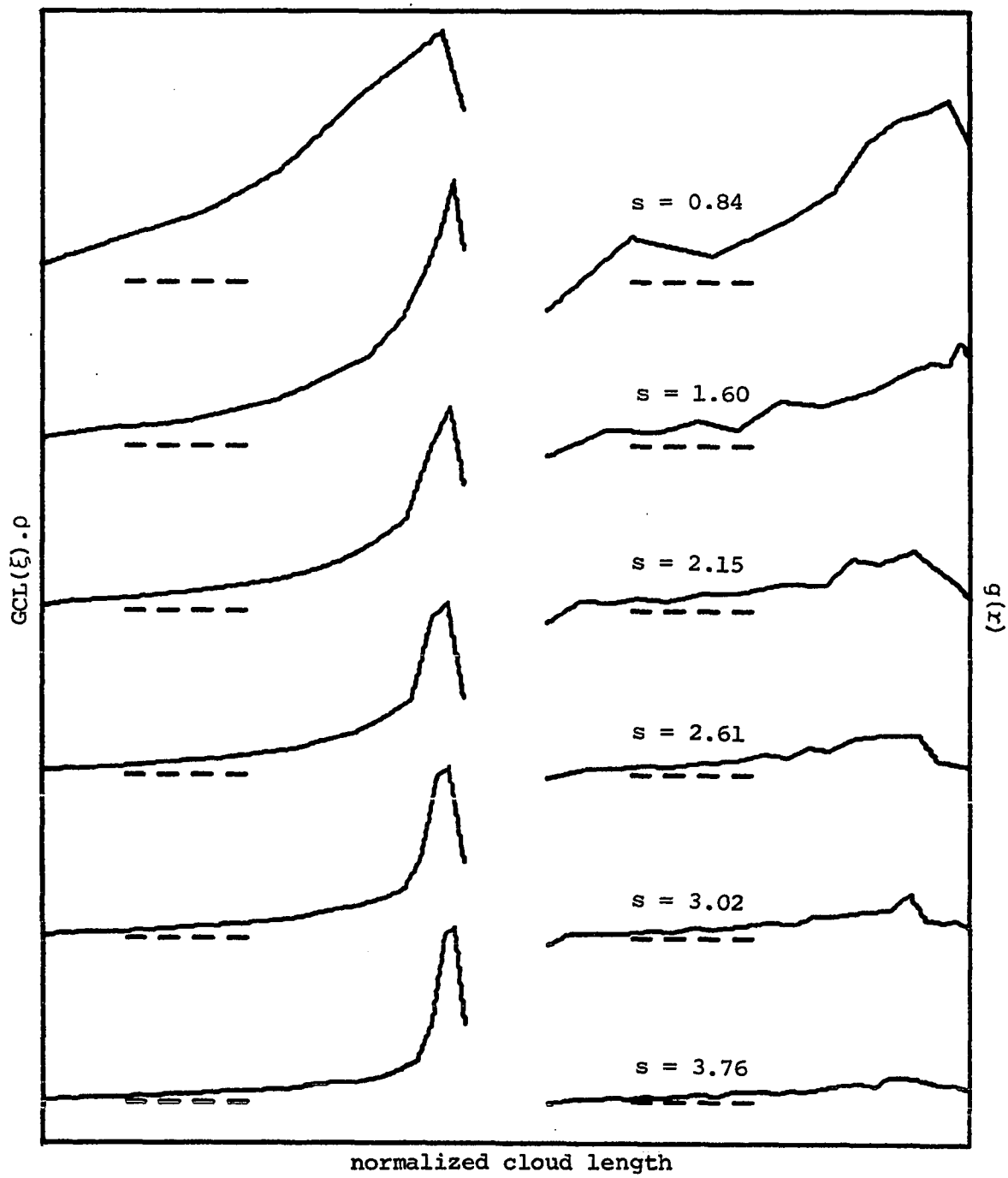

Figure 38. The radiative acceleration and the effective acceleration as a function of distance along the symmetry (y) axis for model RP221 at several different times

tion, $GCL(\xi)\rho$, at the same times. All these profiles are in terms of the same arbitrary units; zero is indicated by the dotted lines. The cloud's length has been normalized to unity in each case so that the profiles may be more easily compared. As usual, time is measured in terms of cloud expansion times.

At early times the effective acceleration is sharply peaked, but it flattens out as the evolution progresses. This is not so much a case of the pressure gradients readjusting themselves as it is a case of the radiation pressure decreasing due to cloud expansion. The density profile for the cloud at each time is practically identical to that for the radiative acceleration (Figure 38) because $GCL(\xi)$ is essentially constant (Figure 4). Note that the expansion begins in the rear of the cloud and proceeds towards the front. Only for the high density-high temperature region at the head of the cloud (Figure 29) is the pressure gradient term a significant fraction of $g(r)$.

The effective acceleration ($g(r)$) for the two-dimensional, radiatively driven models is complicated by the pressure transients associated with transverse expansion (Chapter V.B). At early times the density profiles are similar to those of RP221, but the mass loss at

the front of these clouds (Chapter V.B) causes the density to drop faster than in RP221. The resulting decrease in acceleration explains why RL222 does not expand quite as rapidly as does RP221.

More generally, the cloud expansion rates can be understood on the basis of g(r) as a function of time. At early times when g(L)>>g(0), the cloud expansion rate rapidly increases. At later times when g(L) has decreased in magnitude and g(L) ≈ g(0), the clouds enter a coasting phase and their lengths increase roughly linearly with time (Figure 16). This behavior is also evident in the plots of Mach number as a function of time (Figures 17 and 20). The clouds are no longer being accelerated, and in fact, RL222 has begun to decelerate due to the drag of the external medium (Figure 20, even $\bar{M}_1$ is slowly decreasing).

Again consider the case for thermal confinement. For a variety of reasons, the possibility of coherent acceleration initially seems more promising here. First, the large gas pressure differentials present in the ram pressure models at t=0 are absent; the clouds start out in pressure equilibrium. Secondly, the flow is subsonic so the external pressure is able to respond quickly to any changes in cloud pressure which may occur. Lastly, the ram pressure is extremely small compared to the gas pressure.

(The ratio of the former to the latter goes as the Mach number squared.) Despite these differences, the radial expansion for the thermally confined clouds is comparable to that of the ram-pressure-confined clouds.

The radiative acceleration, $GCL(\xi)\rho$, and the effective acceleration, $g(r)$ (Equation 6.4), along the symmetry axis are plotted in Figure 39 for TL221 at several different times. The scaling is identical to that in Figure 38. The gas pressure oscillations described in Chapter V.E show up in $g(r)$ at early times, but are quickly damped out. As in RP221, the radiative acceleration (left hand column of Figure 39) is the dominant contributor to $g(r)$. Any attempt by the gas pressure gradients to balance the differential radiation pressure is extremely weak and the behavior of $g(r)$ as a function of time directly reflects what the cloud's density distribution is doing. At early times, $g(r)$ is less sharply peaked for TL221 than for RP221 because of the increased ram pressure in the latter. But $g(r)$ flattens out more gradually in TL221 because the transverse inflow of matter (Chapter V.E) and the slightly smaller rate of radial expansion (Figure 16) mean that higher densities occur at comparable times.

The inability of the gas pressure gradients to balance the differential radiation pressure may seem surprising

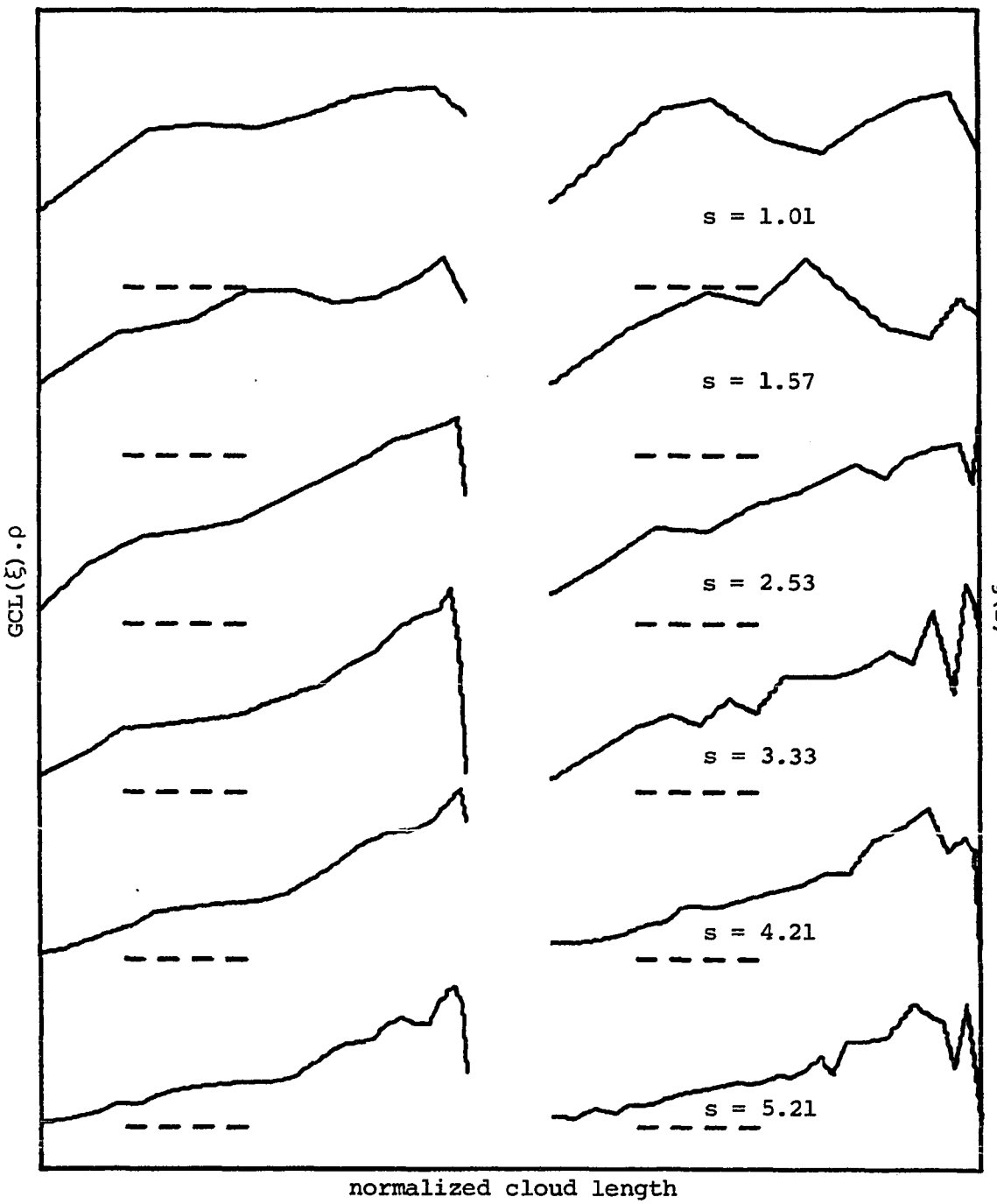

Figure 39. The radiative acceleration and the effective acceleration as a function of distance along the symmetry (y) axis for model TL221 at several different times

since the ratio of the radiation pressure to the gas pressure,

$$\frac{P_r}{P_g} \simeq 0.3\ \xi^{3/4} \tag{6.5}$$

(TM), starts out near unity ($\simeq$ 0.4 to 2) for all of these clouds. Two important points need to be made here. Firstly, despite the attention that this ratio has received in the literature (Davidson 1972; Weymann 1973; TM; McKee and Tarter 1975), it is actually the gradients $\partial P_r/\partial r$ and $\partial P_g/\partial r$ which are important for cloud acceleration. Of course, their ratio is not obtainable from Equation 6.5. Secondly, this ratio (Equation 6.5) has been calculated assuming that the thermal structure of the gas is that of TM. The present numerical models are adiabatic (except for RC221 in Chapter V.C) and have a considerably different thermal structure. It is not clear as to what extent the assumed thermal structure determines the sizes of the gas pressure gradients relative to the sizes of the radiation pressure gradients. It is interesting to point out however, that for a given density change (i.e., $\partial P_r/\partial r$ change), adiabatic expansion produces a larger change in the associated gas pressure gradient than does, say, isothermal expansion.

The following argument suggests that the inability of

the gas pressure gradients to balance the differential radiative acceleration, thereby preventing radial expansion, is a fairly general result. Assume that at one particular time a density gradient exists within a cloud such that an imbalance in the radiative acceleration ($\beta\Delta n$ with $\Delta n = n(L) - n_o$) occurs which is not cancelled by gas pressure gradients. Further assume that the gas pressure gradients attempt to readjust themselves to remove this imbalance (i.e., make $g(r)$ constant, see Equation 6.4). Now a gas flowing at speed c_c for a characteristic time of order L/c_c can overtake the differential radiative acceleration only if $\beta\Delta n << c_c^2/L$. Introducing the average density $\langle n \rangle = \int_0^L n dr/L$ and rearranging gives the inequality

$$\frac{\beta \langle n \rangle L}{c_c^2} << \frac{\langle n \rangle}{\Delta n} . \qquad (6.6)$$

First consider the case for ram-pressure-confined clouds. Unless the thermal structure is very unusual, the density gradient across the cloud is large enough that $\Delta n = n(L) - n_o \simeq n(L)$ and therefore, $\Delta n / \langle n \rangle \gtrsim 1$. It then follows from Equation 6.6 that $\beta \langle n \rangle L / c_c^2 << 1$ is a necessary (but certainly <u>not</u> a sufficient) condition for significant pressure gradients to develop. On the other hand, ram-pressure-confined clouds must have $\beta n_c L / c_c^2 > 1$ if the radiative acceleration is to exceed drag (cf Equation 3.5).

These two inequalities are mutually exclusive. Thus, it appears that no ram-pressure-confined cloud can be coherently accelerated.

The case for thermally confined clouds is not quite so definitive. Since ram pressure is relatively unimportant, a cloud's density profile may be relatively flat. Equation 6.3 suggests that $\Delta n/\langle n\rangle \simeq M^2$ (i.e., $\Delta n/n_o \simeq M^2$ and $\langle n\rangle/n_o \simeq 1$ for $M < 1$ where M is the Mach number for the head of the cloud). Under these conditions, Equation 6.6 becomes

$$\frac{\beta\langle n\rangle L}{c_c^2} << \frac{1}{M^2} . \qquad (6.7)$$

For thermal confinement, the requirement that the radiative acceleration exceed drag becomes $\beta n_c L/c_c^2 >> M^2$ (cf Equation 3.5; approximate pressure balance has been assumed). These last two inequalities can be simultaneously satisfied if $\beta n_c L/c_c^2 \simeq 1$ and M is sufficiently small. However, this does not imply that the gas pressure gradients will readjust themselves to balance the differential radiative acceleration, but only that they may be able to do so.

For the present cloud models (Table 1), $\beta n_c L/c_c^2$ lies in the range 5 to 40 at t=0. Thus the observed expansion is not unexpected, at least for the ram-pressure-confined clouds. Among the thermally confined clouds,

TL221 (with $1/M^2 = 25$ and $\beta n_c L/c_c^2 = 5$ at t=0) and TL338 (with $1/M^2 = 400$ and $\beta n_c L/c_c^2 = 40$ at t=0) do the best job of satisfying the inequality in Equation 6.7. Both of these clouds begin to expand as soon as the radiation pressure is turned on at t=0. This implies that if the gas pressure gradients can ever balance the differential radiative acceleration, it will probably be at extremely low Mach numbers. At least for $M \gtrsim 0.1$, it appears that if the radiation pressure is large enough to accelerate the clouds, then it is large enough to tear them apart at speeds greater than their internal sound speeds. The internal pressure gradients which result are unable to halt the expansions since they can not respond quickly enough.

C. Concluding Remarks

As discussed in Chapter I, velocities of at least 5000 km/sec are required to account for the widths of the emission lines. Still larger velocities, up to one-half the speed of light, are needed to explain the highest displaced absorption lines (Figure 1). Chapter II presented arguments which show that cloud confinement is required if velocities above 1000 km/sec are to be produced by radiation pressure acceleration. This investigation then proceeded to examine two confinement mechanisms (i.e., ram

pressure and thermal gas pressure) in detail using a two-dimensional, gasdynamic computer code. It was found that adequate cloud confinement is not easily obtained because radiation-pressure-driven, radial expansion occurs. This one-dimensional expansion is sufficient to limit the terminal velocities to values comparable to those obtained for the freely expanding clouds.

Even though the amount of acceleration received increases with increasing column density, the solution does not appear to lie with clouds of larger column density. Such clouds have difficulty overcoming the gravitational attraction of the QSOs (Equations 2.16 and 2.21). In addition, the rate of radial expansion and the velocity dispersion increase with increasing column density. This is a problem for the emission systems simply because expansion lowers the density, thereby preventing large radiative accelerations to obtain. In the case of the absorption regions, the large velocity dispersions found here ($v/\Delta v \lesssim 10$) are in direct contradiction with those observed ($v/\Delta v \simeq 10^3$, see Chapter I).

A more detailed comparison of these cloud models with the observations seems unnecessary, as it is already clear that there is serious disagreement. Other choices of the initial cloud parameters (Table 1) will probably not

resolve this discrepancy. For example, clouds with smaller column densities than those assumed here encounter large drag forces unless their motion is highly subsonic (cf Equation 3.5 and see discussion below). The problems with clouds of larger column density are mentioned above. The similarity in the behavior of the two thermally confined clouds, TL231 and TL221, suggests that the parameter $n_c(0)/n_{ic}(0)$ is relatively unimportant. And finally, the scaling law (Chapter III.E) can be used to argue that the present results are independent of $n_c(0)$ and L_{ion}.

What next? It has already been argued (Chapters III.B and VI.B) that the simplifying assumptions which were made concerning the ionization and thermal structure of the gas do not lead to serious error. If this is true, more fundamental changes are required if good cloud confinement is to be obtained in the face of radiation pressure acceleration. Some ideas for accomplishing this are now briefly discussed.

Reducing the effects of ram pressure by choosing an external medium so hot that the flow remains highly subsonic may result in better confinement, however the present results bode ill for such a model (cf Chapter VI.B). For example, model TL338 starts out at Mach 0.05 and yet begins to expand immediately. It is twice its original length by s = 0.45 when $\bar{M}_1 = 0.35$. To restrict a cloud

with a velocity of 5000 km/sec to Mach numbers below 0.05 requires temperatures in the external medium of order 5×10^{11} °K! Maintaining such high temperatures is difficult to say the least. The lack of a detectable X-ray flux from the QSOs also imposes severe size restrictions on such a medium (Chapter III.A). A second method of reducing the ram pressure is to assume that the external medium flows out with the clouds. Some of the problems encountered by such winds are discussed in Chapter I.C.

Detailed radiative transfer calculations should be done in conjunction with the gasdynamic calculations. The use of TM's optically thin results for the radiation pressure overestimates the acceleration in the front of the present clouds by roughly a factor of five (Figure 4), since their optical depths in Lyman-α are about 10^2 (Chapter III.D). However, it is not at all clear that a decrease in the radiative acceleration (at large line optical depths) by such a factor will alleviate the radial expansion problems (cf Figures 38 and 39). A large reduction in the incident continuum flux at the heads of the clouds can be achieved by making them optically thick at all frequencies, but the results of McKee and Tarter (1975) suggest that this does <u>not</u> result in less radial expansion. In fact, they find that the flux of internally

created line photons in such clouds produces even larger differential accelerations than those found here. Their largest accelerations are also at the heads of the clouds, where the gas is essentially un-ionized and therefore possesses the largest cross section per atom.

Radiation pressure is able to magnify density gradients within the clouds and drive their radial expansion because of its proportionality to gas density (Chapter VI.B). Three ways of eliminating this density dependence and the resulting expansion come readily to mind. The first one is for electron scattering to dominate the cross section; this occurs for $\xi \gtrsim 10^3$. Figures 3 and 4 show that in this range it is independent of density. However, electron scattering is exceeded by gravity unless the QSO's mass is $\lesssim 7 \times 10^7 \, L_{46} M_\odot$, a rather unlikely situation. The second possibility is for dust to dominate the ionic cross sections. Two serious difficulties with dust acceleration have been pointed out by Blumenthal and Mathews (1975). Namely, there is no evidence to suggest that this occurs and if it occurs, then the dust would be selectively accelerated and pushed through the clouds unless the grains experience unusually large collisional or Coulomb drag forces. Finally, a third possibility has been proposed by Kippenhahn et al. (1974). They assume a high energy cutoff in the QSO spectrum

which prevents the complete ionization of the heavier elements. In this case, the radiation pressure no longer depends upon the recombination rate (for $\xi \gtrsim 10$) and it becomes independent of density. Such a model cannot be ruled out since only the QSO 3C 273 has been detected in the X-ray. It does restrict the QSO mass to $\lesssim 7 \times 10^9 \, L_{46} M_\odot$ and predicts that some transitions with high ionization energies will not be observed.

VII. BIBLIOGRAPHY

M. Aaronson, J. H. Black, and C. F. McKee, 1974, Ap. J. (Letters), 191, L53.

M. Aaronson, C. F. McKee, and J. C. Weisheit, 1975, Ap. J., 198, 13.

T. F. Adams, 1972, Ap. J. (Letters), 176, L1.

T. F. Adams and D. W. Weedman, 1972, Ap. J. (Letters), 173, L109.

W. M. Adams, 1973, Ph.D. thesis, Stanford Institute for Plasma Research Report No. 553, Stanford University.

K. S. Anderson, 1970, Ap. J., 162, 743.

K. S. Anderson and R. P. Kraft, 1969, Ap. J., 158, 859.

R. J. Angione and H. J. Smith, 1972, Proc. IAU Symposium No. 44, External Galaxies and Quasi-Stellar Objects, ed. D. S. Evans (Dordrecht: Reidel), p. 171.

I. Appenzeller and W. A. Hiltner, 1967, Ap. J. (Letters), 149, L17.

M. A. Arakelian, E. A. Dibai, V. F. Esipov, and B. E. Markarian, 1971, Astrofizika, 7, 177.

J. Arons, 1972, Ap. J., 172, 553.

J. Arons, R. M. Kulsrud, and J. P. Ostriker, 1975, Ap. J., 198, 687.

J. N. Bahcall, 1971, A. J., 76, 283.

J. N. Bahcall, 1975, Ap. J. (Letters), 200, L1.

J. N. Bahcall and U. Feldman, 1970, Ap. J., 161, 389.

J. N. Bahcall and S. Goldsmith, 1971, Ap. J., 170, 17.

J. N. Bahcall and P. C. Joss, 1973, Ap. J., 179, 381.

J. N. Bahcall and J. B. Oke, 1971, Ap. J., 163, 235.

J. N. Bahcall and P. J. E. Peebles, 1969, Ap. J. (Letters), 156, L7.

J. N. Bahcall and E. E. Salpeter, 1965, Ap. J., 142, 1677.

J. N. Bahcall and E. E. Salpeter, 1966, Ap. J., 144, 847.

J. N. Bahcall and L. Spitzer, 1969, Ap. J. (Letters), 156, L63.

J. N. Bahcall and R. A. Wolf, 1968, Ap. J., 152, 701.

J. N. Bahcall, P. C. Joss, and J. G. Cohen, 1973a, Ap. J., 184, 57.

J. N. Bahcall, P. C. Joss, and C. R. Lynds, 1973b, Ap. J. (Letters), 182, L95.

J. N. Bahcall, W. L. W. Sargent, and M. Schmidt, 1967, Ap. J. (Letters), 149, L11.

J. A. Baldwin, 1975, Ap. J., 201, 26.

J. A. Baldwin, E. M. Burbidge, C. Hazard, H. S. Murdoch, L. B. Robinson, and E. J. Wampler, 1973, Ap. J., 185, 739.

J. A. Baldwin, E. M. Burbidge, G. R. Burbidge, C. Hazard, L. B. Robinson, and E. J. Wampler, 1974, Ap. J., 193, 513.

D. Basu, 1973, Nature Phys. Sci., 241, 159.

G. S. Bisnovatyi-Kogan and Ya. B. Zel'dovich, 1969, Astrofizika, 5, 223.

G. M. Blake, 1972, M.N.R.A.S., 156, 67.

G. R. Blumenthal and W. G. Mathews, 1975, Ap. J., 198, 517.

A. Boksenberg and W. L. W. Sargent, 1975, Ap. J., 198, 31.

R. L. Brown and M. S. Roberts, 1973, Ap. J. (Letters), 184, L7.

E. M. Burbidge, 1967, Ann. Rev. Astr. and Ap., 5, 399.

E. M. Burbidge, 1972, Proc. IAU Symposium No. 44, External Galaxies and Quasi-Stellar Objects, ed. D. S. Evans (Dordrecht: Reidel), p. 109.

E. M. Burbidge and G. R. Burbidge, 1975, Ap. J., 202, 287.

G. R. Burbidge, 1970, Ann. Rev. Astr. and Ap., 8, 397.

G. R. Burbidge, 1973a, Nature Phys. Sci., 246, 17.

G. R. Burbidge, 1973b, Proc. IAU Symposium No. 55, X- and Gamma-Ray Astronomy, edited by H. Bradt and R. Giacconi (Dordrecht: Reidel), p. 199.

G. R. Burbidge and E. M. Burbidge, 1967, Quasi-Stellar Objects (San Francisco: W. H. Freeman).

G. R. Burbidge and E. M. Burbidge, 1969, Nature, 222, 735.

L. J. Caroff, P. D. Noerdlinger, and J. D. Scargle, 1972, Ap. J., 176, 439.

R. F. Carswell, P. A. Strittmatter, R. E. Williams, E. A. Beaver, and R. Harms, 1975, Ap. J., 195, 269.

J. P. Cassinelli and J. I. Castor, 1973, Ap. J., 179, 189.

Y.-W. T. Chan, 1974, Ph.D. thesis, University of California, San Diego.

Y.-W. T. Chan and E. M. Burbidge, 1971, Ap. J., 167, 213.

Y.-W. T. Chan and E. M. Burbidge, 1975, Ap. J., 198, 46.

S. Chandrasekhar, 1961, Hydrodynamic and Hydromagnetic Stability (Oxford: Clarendon).

R. A. Chevalier, 1974, Ap. J., 188, 501.

R. A. Chevalier, 1975a, Ap. J., 198, 355.

R. A. Chevalier, 1975b, Ap. J., 200, 698.

J. G. Cohen, 1973, Ap. J., 181, 619.

S. A. Colgate, J. D. Colvin, and A. G. Petschek, 1975, Ap. J. (Letters), 197, L105.

R. Courant, K. O. Friedrichs, and H. Lewy, 1928, Mathematische Annalen, 100, 32.

D. P. Cox and E. Daltabuit, 1971, Ap. J., 167, 113.

D. P. Cox and W. H. Tucker, 1969, Ap. J., 157, 1157.

E. Daltabuit and D. P. Cox, 1972, Ap. J. (Letters), 173, L13.

K. Davidson, 1972, Ap. J., 171, 213.

K. Davidson, 1973, Ap. J., 181, 1.

J. B. De Veny, W. H. Osborn, and K. Janes, 1971, Pub. Astron. Soc. Pacific, 83, 611.

D. S. De Young, 1971, Ap. J., 167, 541.

J. A. Eilek, 1975, Ph.D. thesis, University of British Columbia, Vancouver.

J. A. Eilek and L. J. Caroff, 1976, Ap. J., 208, 887.

J. Elliot and S. Shapiro, 1974, Ap. J. (Letters), 192, L3.

D. S. Evans, editor, 1972, Proc. IAU Symposium No. 44, External Galaxies and Quasi-Stellar Objects (Dordrecht: Reidel).

E. D. Fackerell, 1968, Ap. J., 153, 643.

D. W. Goldsmith and T. D. Kinman, 1965, Ap. J., 142, 1693.

R. H. Gordon, 1975, Ap. and Sp. Sci., 35, 197.

G. L. Grasdalen, 1976, Ap. J. (Letters), 208, L11.

M. Grewing and P. A. Strittmatter, 1973, Astr. and Ap., 28, 39.

B. J. Harris, 1972, Proc. IAU Symposium No. 44, External Galaxies and Quasi-Stellar Objects, ed. D. S. Evans (Dordrecht: Reidel), p. 232.

F. D. A. Hartwick, 1971, Ap. J. (Letters), 170, L127.

W. D. Hayes and R. F. Probstein, 1959, Hypersonic Flow Theory (New York: Academic Press).

F. M. Ipavich, 1975, Ap. J., 196, 107.

J. R. Ipser, 1969a, Ap. J., 156, 509.

J. R. Ipser, 1969b, Ap. J., 158, 17.

J. R. Ipser and K. S. Thorne, 1968, Ap. J., 154, 251.

D. L. Jones, 1962, NBS Technical Notes, No. 155 (Washington: Government Printing Office).

M. Jura, 1973, Ap. J., 181, 627.

K. I. Kellermann, 1972, Proc. IAU Symposium No. 44, External Galaxies and Quasi-Stellar Objects, ed. D. S. Evans (Dordrecht: Reidel), p. 190.

K. I. Kellermann and I. I. K. Pauliny-Toth, 1968, Ann. Rev. Astr. and Ap., 6, 417.

E. Y. Khachikian and D. W. Weedman, 1974, Ap. J., 192, 581.

T. D. Kinman, E. Lamla, T. Ciurla, E. Harlan, and C. A. Wirtanen, 1968, Ap. J., 152, 357.

R. Kippenhahn, L. Mestel, and J. J. Perry, 1975, Astr. and Ap., 44, 123.

R. Kippenhahn, J. J. Perry, and H.-J. Röser, 1974, Astr. and Ap., 34, 211.

J. Kristian, 1973, Ap. J. (Letters), 179, L61.

J. H. Krolik, 1976, preprint, University of California, Berkeley.

L. D. Landau and E. M. Lifshitz, 1959, Fluid Mechanics (Pergamon Press: London or Addison-Wesley: Reading, Mass.).

J. L. Lowrance, D. C. Morton, P. Zucchino, J. B. Oke, and M. Schmidt, 1972, Ap. J., 171, 233.

L. B. Lucy, 1971, Ap. J., 163, 95.

L. B. Lucy and P. M. Solomon, 1970, Ap. J., 159, 879.

C. R. Lynds, 1971, Ap. J. (Letters), 164, L73.

C. R. Lynds, 1972, Proc. IAU Symposium No. 44, External Galaxies and Quasi-Stellar Objects, ed. D. S. Evans (Dordrecht: Reidel), p. 127.

G. M. MacAlpine, 1972, Ap. J., 175, 11.

W. G. Mathews, 1974, Ap. J., 189, 23.

W. G. Mathews, 1976, Ap. J., 207, 351.

W. G. Mathews and J. C. Baker, 1971, Ap. J., 170, 241.

J. S. Mathis, 1970, Ap. J., 162, 761.

M. H. McCrea, 1968, Nature, 218, 257.

C. F. McKee and L. L. Cowie, 1975, Ap. J., 195, 715.

C. F. McKee and C. B. Tarter, 1975, Ap. J., 202, 306.

C. F. McKee, C. B. Tarter, and J. C. Weisheit, 1973, Ap. Letters, 13, 13.

W. W. Morgan, 1972, Proc. IAU Symposium No. 44, External Galaxies and Quasi-Stellar Objects, ed. D. S. Evans (Dordrecht: Reidel), p. 97.

D. C. Morton, 1967a, Ap. J., 147, 1017.

D. C. Morton, 1967b, Ap. J., 150, 535.

D. C. Morton and W. A. Morton, 1972, Ap. J., 174, 237.

D. C. Morton and D. O. Richstone, 1973, Ap. J., 184, 65.

D. C. Morton, E. B. Jenkins, and R. C. Bohlin, 1968, Ap. J., 154, 661.

D. C. Morton, E. B. Jenkins, T. A. Matilsky, and D. G. York, 1972, Ap. J., 177, 219.

R. F. Mushotzky, P. M. Solomon, and P. A. Strittmatter, 1972, Ap. J., 174, 7.

M. P. Nakada, 1973, Ap. J., 184, 551.

P. D. Noerdlinger, 1973, Ap. and Space Sci., 13, 70.

P. D. Noerdlinger, 1974, Ap. J., 192, 529.

P. D. Noerdlinger and G. B. Rybicki, 1974, Ap. J., 193, 651.

P. D. Noerdlinger and J. D. Scargle, 1972, Ap. J., 176, 463.

D. J. K. O'Connell, editor, 1971, Study Week on Nuclei of Galaxies (Amsterdam: North Holland).

A. Oemler and C. R. Lynds, 1975, Ap. J., 199, 958.

J. B. Oke, 1967, Ap. J., 147, 901.

J. B. Oke and J. E. Gunn, 1974, Ap. J. (Letters), 189, L5.

J. B. Oke and W. L. W. Sargent, 1968, Ap. J., 151, 807.

J. B. Oke, G. Neugebauer, and E. E. Becklin, 1970, Ap. J., 159, 341.

D. E. Osterbrock, 1971, Study Week on Nuclei of Galaxies, ed. D. J. K. O'Connell (Amsterdam: North Holland), p. 151.

D. E. Osterbrock and R. A. R. Parker, 1965, Ap. J., 141, 892.

D. E. Osterbrock, A. T. Koski, and M. M. Phillips, 1975, Ap. J. (Letters), 197, L41.

D. E. Osterbrock, A. T. Koski, and M. M. Phillips, 1976, Ap. J., 206, 898.

A. G. Pacholczyk and R. Weymann, editors, 1968, A. J., 73, 836.

P. J. E. Peebles, 1968, Ap. J. (Letters), 154, L121.

D. Potter, 1973, Computational Physics (London: Wiley).

M. J. Rees, 1970, Ap. J. (Letters), 160, L29.

P. J. Roache, 1972, Computational Fluid Dynamics (Los Angeles: Hermosa).

R. C. Roeder, 1972, Ap. J., 171, 451.

R. C. Roeder, and R. T. Verreault, 1968, Ap. J. (Letters), 153, L127.

D. K. Ross, 1973, Astr. and Ap., 24, 471.

A. Sandage, J. A. Westphal, and P. A. Strittmatter, 1966, Ap. J., 146, 322.

D. Sappenfield, 1969, Los Almos Scientific Lab. Rep. LA-4189-MS, University of California, Los Alamos, N.M.

J. D. Scargle, 1973, Ap. J., 179, 705.

J. D. Scargle, L. J. Caroff, and P. D. Noerdlinger, 1970, Ap. J. (Letters), 161, L115.

J. D. Scargle, L. J. Caroff, and C. B. Tarter, 1974, Ap. J., 189, 181.

M. Schmidt, 1969, Ann. Rev. Astr. and Ap., 7, 527.

L. I. Sedov, 1959, Similarity and Dimensional Methods in Mechanics, ed. M. Holt, trans. from Russian (New York: Academic).

G. A. Shields and J. B. Oke, 1975, Ap. J., 197, 5.

I. S. Shklovsky, 1967, Ap. J. (Letters), 150, L1.

A. M. Smith, 1972, Ap. J., 176, 405.

L. Spitzer, 1962, Physics of Fully Ionized Gases, 2nd ed. (New York: Interscience).

L. Spitzer, 1968, Diffuse Matter in Space (New York: Interscience).

J. R. Spreiter, A. L. Summers, and A. Y. Alksne, 1966, Planet. Space Sci., 14, 223.

T. P. Stecher, 1970, Ap. J., 159, 543.

W. A. Stein, S. L. O'Dell, and P. A. Strittmatter, 1976, Ann. Rev. Astr. and Ap., 14, 173.

A. N. Stockton and C. R. Lynds, 1966, Ap. J., 144, 451.

P. A. Strittmatter and R. E. Williams, 1976, Ann. Rev. Astr. and Ap., 14, 307.

P. A. Strittmatter, R. F. Carswell, E. M. Burbidge, C. Hazard, J. A. Baldwin, L. B. Robinson, and E. J. Wampler, 1973, Ap. J., 183, 767.

C. B. Tarter, 1975, private communication, Lawrence Livermore Laboratory, University of California, Livermore.

C. B. Tarter and C. F. McKee, 1973, Ap. J. (Letters), 186, L63 (TM).

C. B. Tarter, W. H. Tucker, and E. E. Salpeter, 1969, Ap. J., 156, 943.

G. Taylor, 1950, Proc. Royal Soc. London, 201A, 175.

P. A. Thompson, 1972, Compressible-Fluid Dynamics (New York: McGraw-Hill), p. 317.

N. Visvanathan, 1973, Ap. J., 179, 1.

J. von Neumann and R. D. Richtmyer, 1950, J. of Applied Physics, 21, 232.

R. V. Wagoner, 1967, Ap. J., 149, 465.

M. F. Walker, 1968a, A. J., 73, 854.

M. F. Walker, 1968b, Ap. J., 151, 71.

E. J. Wampler, L. Robinson, E. M. Burbidge, and J. A. Baldwin, 1975, Ap. J. (Letters), 198, L49.

R. J. Weymann, 1970, Ap. J., 160, 31.

R. J. Weymann, 1973, Comments Ap. and Space Phys., 5, 139.

R. J. Weymann, 1976, Ap. J., 208, 286.

R. E. Williams, 1967, Ap. J., 147, 556.

R. E. Williams, 1971, Ap. J. (Letters), 167, L27.

R. E. Williams, 1972, Ap. J., 178, 105.

R. E. Williams, P. A. Strittmatter, R. F. Carswell, and E. R. Craine, 1975, Ap. J., 202, 296.

D. W. Wingert, 1975, Ap. J., 198, 267.

A. M. Wolfe, 1974, Ap. J., 188, 243.

P. R. Woodward, 1975, preprint (abstract in Bull. A.A.S., 7, 528).

A. Yahil and J. P. Ostriker, 1973, Ap. J., 185, 787.

Ya. B. Zel'dovich and Yu. P. Raizer, 1966, Physics of Shock Waves and High-Temperature Hydrodynamic Phenomena, Vol. I (New York: Academic Press).

VIII. ACKNOWLEDGMENTS

I wish to thank my thesis advisor, Dr. Dennis K. Ross, for his continuing support, patience, and advice throughout my graduate career.

I am also particularly grateful to Dr. Lawrence J. Caroff for his direction and guidance throughout this work, as well as for his hospitality during my visits to the NASA/Ames Research Center, where most of the computer calculations were carried out. This thesis would not have been possible without his help, as well as that of many other friends at NASA/Ames. A special thanks goes to Dr. Jeffrey Scargle, Dr. Richard Durisen, Dr. Patrick Cassen, and Dr. Susan Lea for useful discussions; to Dr. Durisen and Dr. Scargle for sharing their respective homes with me during extended computer marathons; to Warren Van Camp for his assistance in programming and for the use of his contour routine; and to Brian Rainie for efficiently running many of my production programs via long distance directions.

I also wish to express my appreciation to Dr. David De Young for a very preliminary version of the present gasdynamic computer code and to Dr. Bruce Tarter for supplying the detailed results of his calculations on optically thin gases. I am indebted to Dr. Allen Grossman for his help in establishing my NASA/Ames contacts and for

his continuing interest in this work.

Last, but not least, I wish to thank my wife Kathleen for her ever present moral support, for her love and understanding, and for her endurance of the long separations necessitated by my trips to NASA/Ames. I also wish to thank my parents for many years of loving support, both moral and financial, and my son Robert for providing comic relief during the later phases of this work.

I gratefully acknowledge a dissertation research assistantship of the Graduate College of Iowa State University; this award allowed me to make my original trip to NASA/Ames. This work has also been supported by NASA/Ames through the provision of travel grants, computer facilities, and large amounts of computer time.

IX. APPENDIX A: COMPUTER CODE TESTS

A. Analytical-Numerical Comparisons

The computer code was used to generate numerical solutions to some problems with known analytical solutions. Comparison of the results establishes the code's credibility and permits estimates of its accuracy. For all of these tests the radiation pressure is turned off and the boundary conditions are modified when necessary. None of the tests require the large amounts of grid manipulation (Chapter IV.D) found necessary for evolving cloud models.

The first test solution is a static, spherically symmetric gas distribution surrounding a gravitating point mass M. It is governed by the differential equation

$$\frac{dP}{dr} = -\frac{GM}{r^2}\rho, \tag{9.1}$$

where P is the pressure, r is the radial distance from M, and ρ is the density. The isothermal solution for an ideal gas is

$$n(r) = n(r_o)\exp\{\frac{GM\mu m_o}{kT}(\frac{1}{r} - \frac{1}{r_o})\}, \tag{9.2}$$

where n is the atomic number density, μ is the mean molecular weight, m_o is the mass of 1 amu, T is the temperature, and r_o is the arbitrarily defined radius at which $n(r)$ is $n(r_o)$. A portion of this atmosphere was used as

a starting model for the code. The grid was positioned so that the lower left hand corner was at a distance of 10^{21} cm from the gravitating mass M, and the y-axis extended radially outward. There were 29 cells in the y-direction and 24 in the x-direction. The cell size in both directions was 10^{19} cm. The other initial conditions were $n(r_o = 10^{21}\ cm) = 10^4\ cm^{-3}$, $\mu = 0.618$, $T = 9.86 \times 10^3\ °K$, and $M = 10^8\ M_\odot$. The lower Lagrangian boundary was treated as in case 1b of Chapter IV.C. The calculation was done in all 696 cells at all times and an external pressure consistent with Equation 9.2 was applied as the upper Lagrangian boundary condition.

This model was evolved through 1000 time steps ($t = 1.76 \times 10^{15}$ sec) or about nine grid sound-crossing times. The gas remained virtually static throughout the evolution; no velocities greater than Mach 0.076 occurred. The atmosphere retained its initial density distribution (see Figure 40) and isothermality to within 1%. The internal energy of the entire grid remained constant to 0.16% and the kinetic energy (which should ideally remain identically zero) never exceeded 0.0017% of the internal energy.

The other three major code tests employ the Sedov (1959) similarity solutions for one-dimensional blast waves in n spatial dimensions (where n = 1, 2, or 3). These

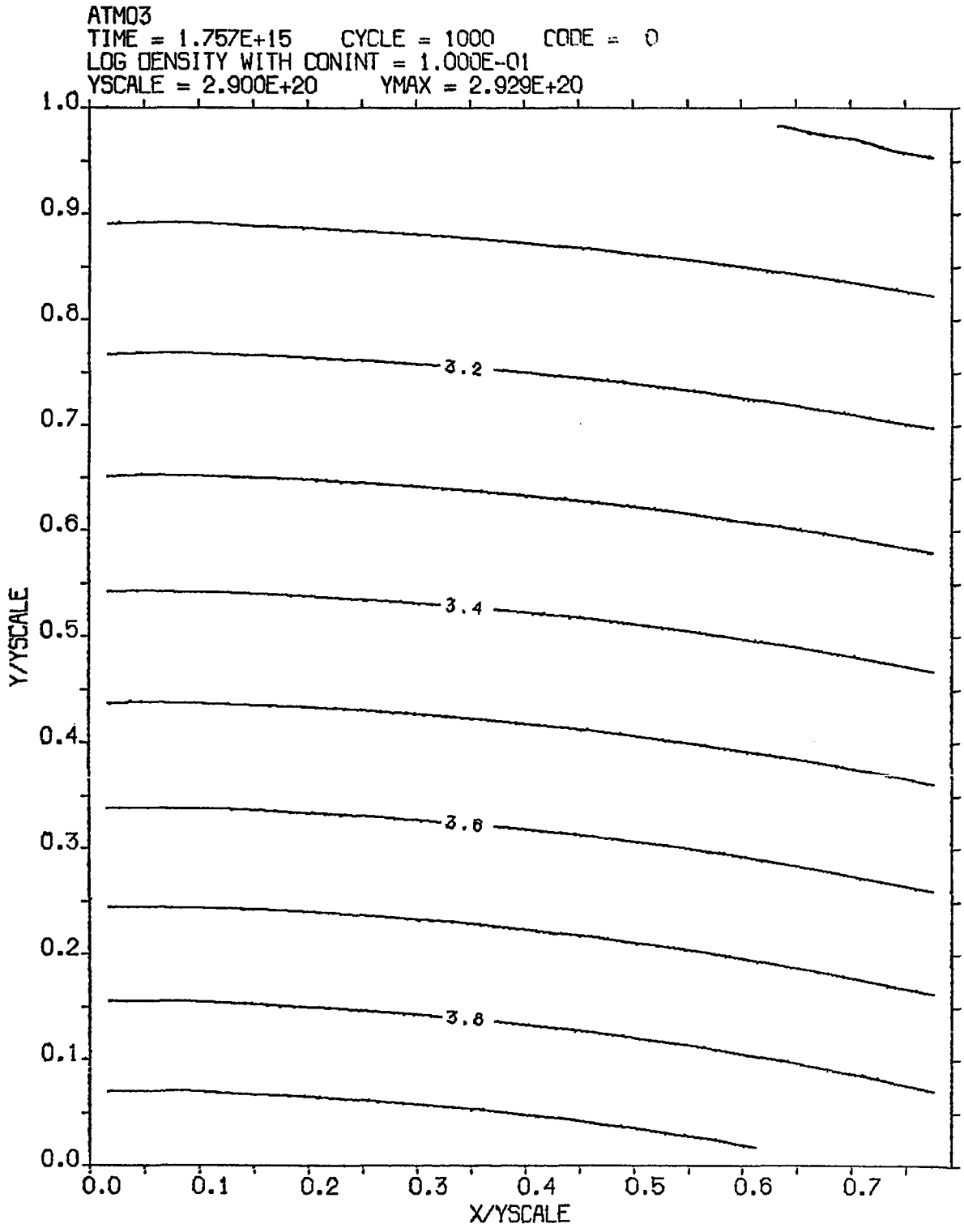

Figure 40. Contours of the logarithm of density (in particles/cm^3) at $t = 1.76 \times 10^{15}$ sec for a stratified atmosphere

solutions assume that the blasts are nonradiating and that the pressure of the external medium is negligible. The blasts are considered one-dimensional because their physical properties only depend on one spatial variable. The shock radius at time t is

$$r_s = (B_n E_s/\rho_o)^{\frac{1}{n+2}} t^{\frac{2}{n+2}} , \qquad (9.3)$$

where E_s is the blast wave energy and ρ_o is the density of the undisturbed gas. The constants B_n are calculated by Jones (1962) as functions of γ, the adiabatic index. The similarity solutions give analytical expressions for the run of density, temperature, and velocity behind the shock front. The jump conditions at the shock are specified by the Rankine-Hugoniot relations. These supersonic flows present a much more stringent test of the code than the static atmosphere discussed above.

Outside the blasts, the density was 10^{-6} g/cm^3 and the internal energy was 1 erg/g. The initial cell size in both the x- and y-directions was 2×10^3 cm. The blast energy for each geometry was picked so that the blast radius, r_s, was 1.2 km at t = 0.1 sec. Two very different ways of distributing the initial blast energy were tried. The first assumes that all the energy is thermal and deposits it in the smallest number of cells possible, while still maintaining the proper symmetry. This means that

for n = 1, corresponding to plane flow, the blast energy is put in the first Lagrangian zone of cells. The shock then propagates in the y-direction and involves only Lagrangian motion. For n = 2 the blast possesses cylindrical symmetry, so the energy is placed in the first Eulerian zone of cells and the resulting motion is purely Eulerian. The n = 3 solution is spherically symmetric and therefore involves both Eulerian and Lagrangian motion when treated in cylindrical coordinates. For the proper choice of the lower Lagrangian boundary (case 1a of Chapter IV.C), it is permissible to consider only one hemisphere of the flow. No choice of the blast-occupied cells has exact spherical symmetry, so the energy is simply dumped in the single cell in the lower, left hand corner of the grid. This initial condition is rather crude, but does mimic the similarity solution which has $r_s = 0$ at $t = 0$.

The second method of distributing the blast energy uses the similarity solutions to generate initial conditions for the code. The blast radius is taken as 4×10^4 cm (spans 20 cells) and the time since detonation is obtained from Equation 9.3. The run of density, internal energy, and velocity inside the blast is computed from Sedov's expressions, so the blast energy is correctly distributed as part kinetic and part thermal. For the n = 3

solution, this starting model approximates the desired symmetry vastly better than the one-cell model above. Even so, this case is still the most severe test of the code, and hence it is discussed in the most detail below.

For the n = 1 test the blast energy is 5.20×10^{10} ergs/cm^2 and the grid has 64 cells in the y-direction. The simple initial conditions prove adequate. At t = 0.1 sec the position of the blast wave agrees with Equation 9.3 to 1%. The density, internal energy, and velocity profiles all agree with the Sedov similarity solution to better than 20% except for oscillations near the shock front. Energy conservation is not assumed by the code, but volume integrals of the total energy are computed as a function of time to serve as a consistency check. This model conserves energy to four significant figures over the entire evolution. When the detailed initial conditions are used, the resulting numerical profiles are accurate to better than 10%.

For the n = 2, cylindrical solution the grid has 64 cells in the x-direction and the blast energy is 1.17×10^{16} ergs/cm. This purely Eulerian calculation is not as accurate as the Lagrangian one just discussed. The pressure is correct to 10%, but the inner regions are not sufficiently depleted of material. The density is too large by a factor of three and the internal energy is too low by a

similar factor. The shock position agrees with Equation 9.3 to within 3%, but the total energy is only conserved to 10%. As expected, the shock is less sharp than in the Lagrangian calculation. The accuracy is somewhat improved for models with increased resolution and is considerably improved for a model started from the n = 2 similarity solution. This latter model conserves energy to a fraction of a percent, and the density, internal energy, and velocity profiles at t = 0.1 sec are accurate to better than 25%. Hence the Eulerian differencing scheme also does an acceptable job when faced with a reasonable task.

As already noted, the n = 3 solution is spherically symmetric and thus involves both Eulerian and Lagrangian motion. It is not surprising that placing the total blast energy of 1.23×10^{21} ergs in the single cell in the lower, left hand corner of the grid leads to an extremely asymmetric expansion. Starting from the similarity solution at $t = 6.41 \times 10^{-3}$ sec gives good results. This model is computed on a grid of 50 by 50 cells and is terminated when the shock approaches the edge of the grid at $t = 4.82 \times 10^{-2}$ sec. Figures 41a and 41b display contour plots of the velocity and density distributions at this time. The plotting conventions are described in Appendix B. The individual contours are remarkably smooth and spherical

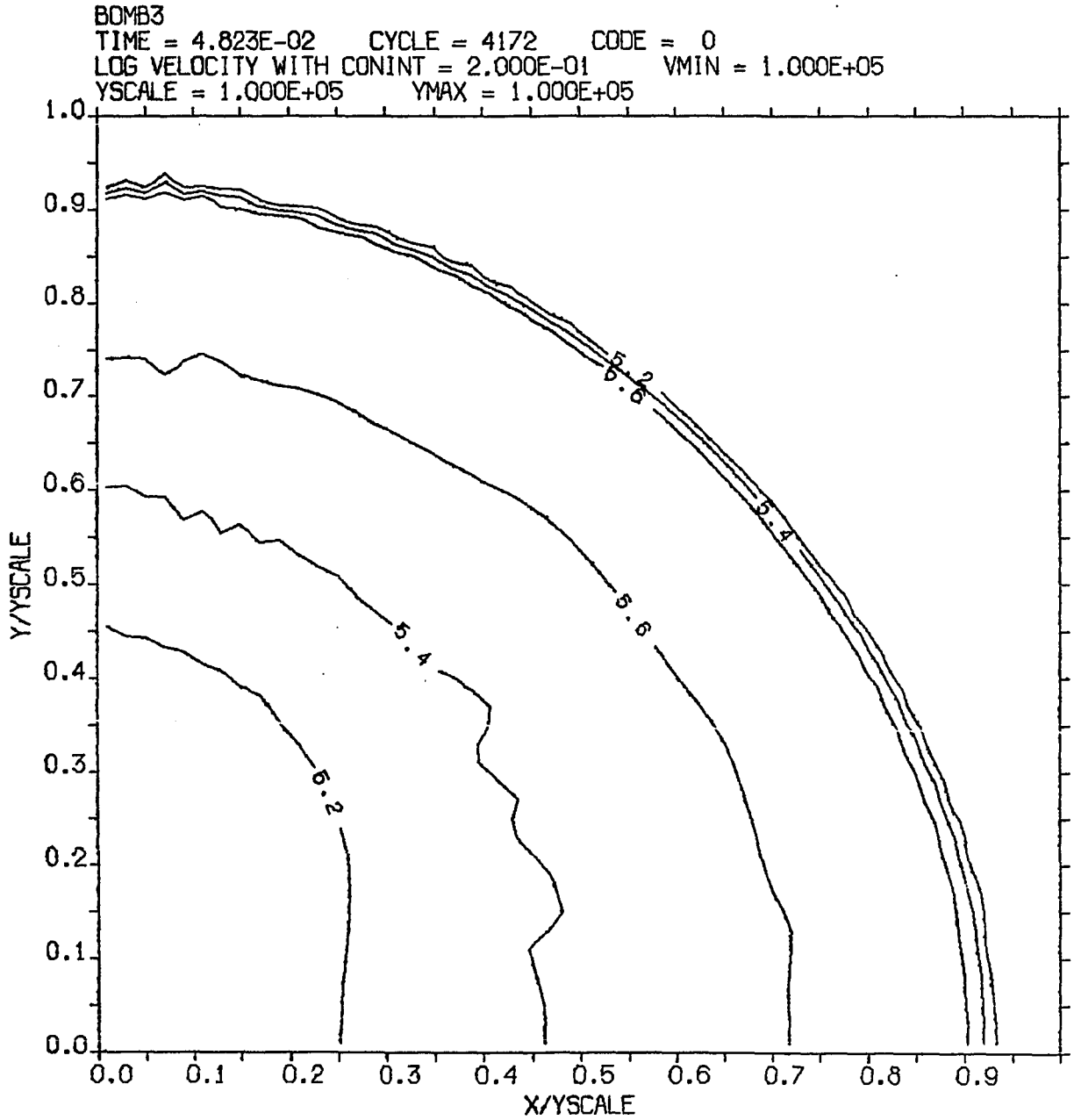

Figure 41a. Contours of the logarithm of velocity (in cm/sec) at $t = 4.82 \times 10^{-2}$ sec for a three-dimensional Sedov blast

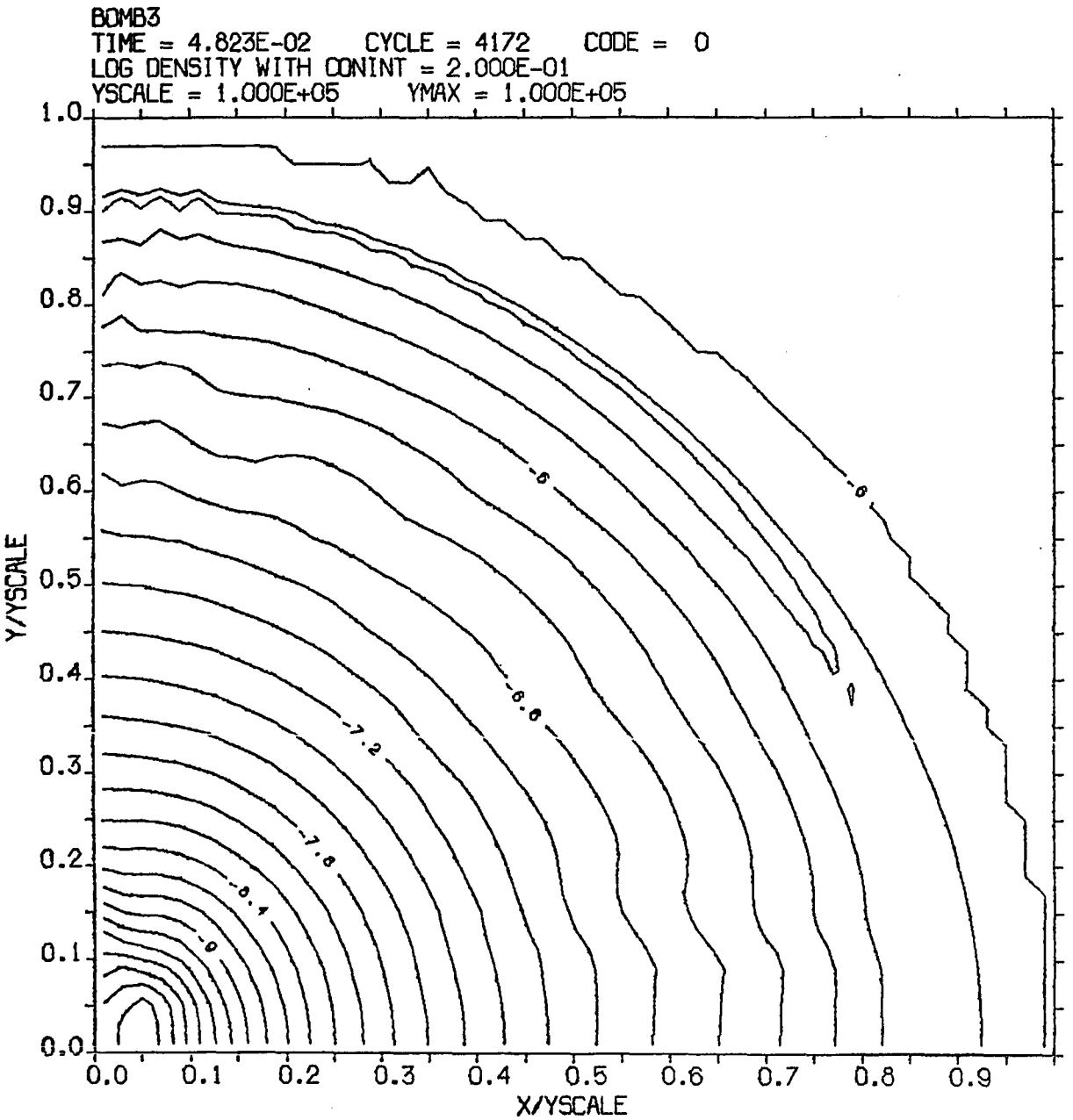

Figure 41b. Contours of the logarithm of density (in g/cm^3) at $t = 4.82 \times 10^{-2}$ sec for a three-dimensional Sedov blast

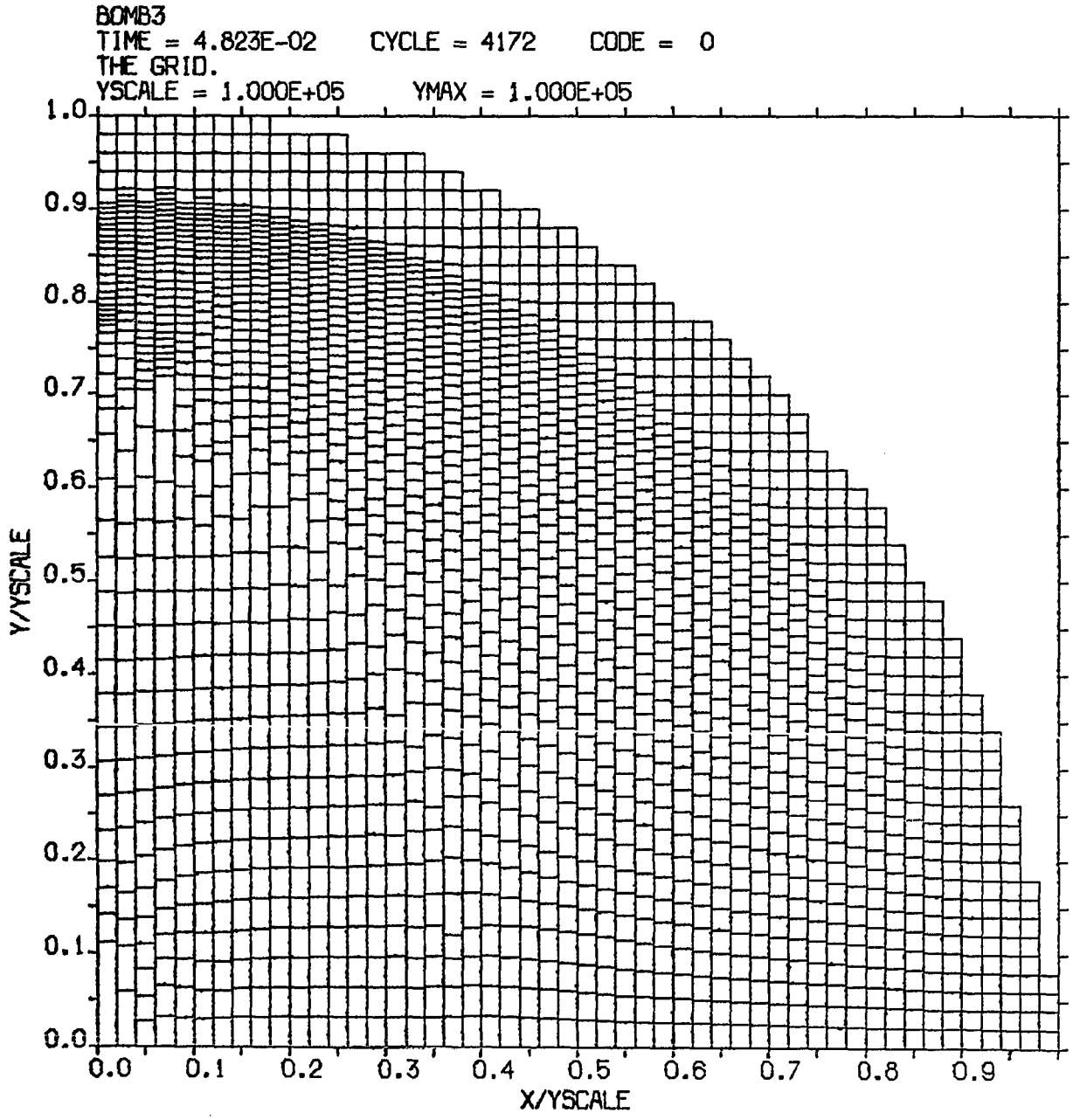

Figure 41c. The computational grid as it appears at $t = 4.82 \times 10^{-2}$ sec for a three-dimensional Sedov blast

except in the central region where the resolution is poor. A grid plot for the same time is presented in Figure 41c. Note the motion of the individual cells in the y-direction and the stationary Eulerian zones in the x-direction. No rezoning (see Chapter IV.D) was found necessary at the shock front, but a few cells were combined near the origin. Resolution is sacrificed here because these low mass cells severely restrict the size of the allowable time step (see Chapter IV.E).

Figures 42a-c compare the numerical solution (plotted points) along the y-axis (Lagrangian direction) with the similarity solution (solid curves). Similar plots along the x-axis (Eulerian direction) are given in Figures 43a-c. It should be emphasized that there are no free parameters with which to adjust the exact analytical solution to fit the numerical results. Again, the shock is sharper in the Lagrangian direction than in the Eulerian one, and its position in both directions agrees well with the predictions of Equation 9.3. Away from the origin, the density, internal energy, and pressure profiles remain accurate to within 25% throughout the evolution. The cause of the weak oscillation which develops at late times is unknown. Similar agreement for the x- and y-velocities is obtained at early times, but by $t = 4.82 \times 10^{-2}$ sec they have deviated substantially from the exact solution. Of course,

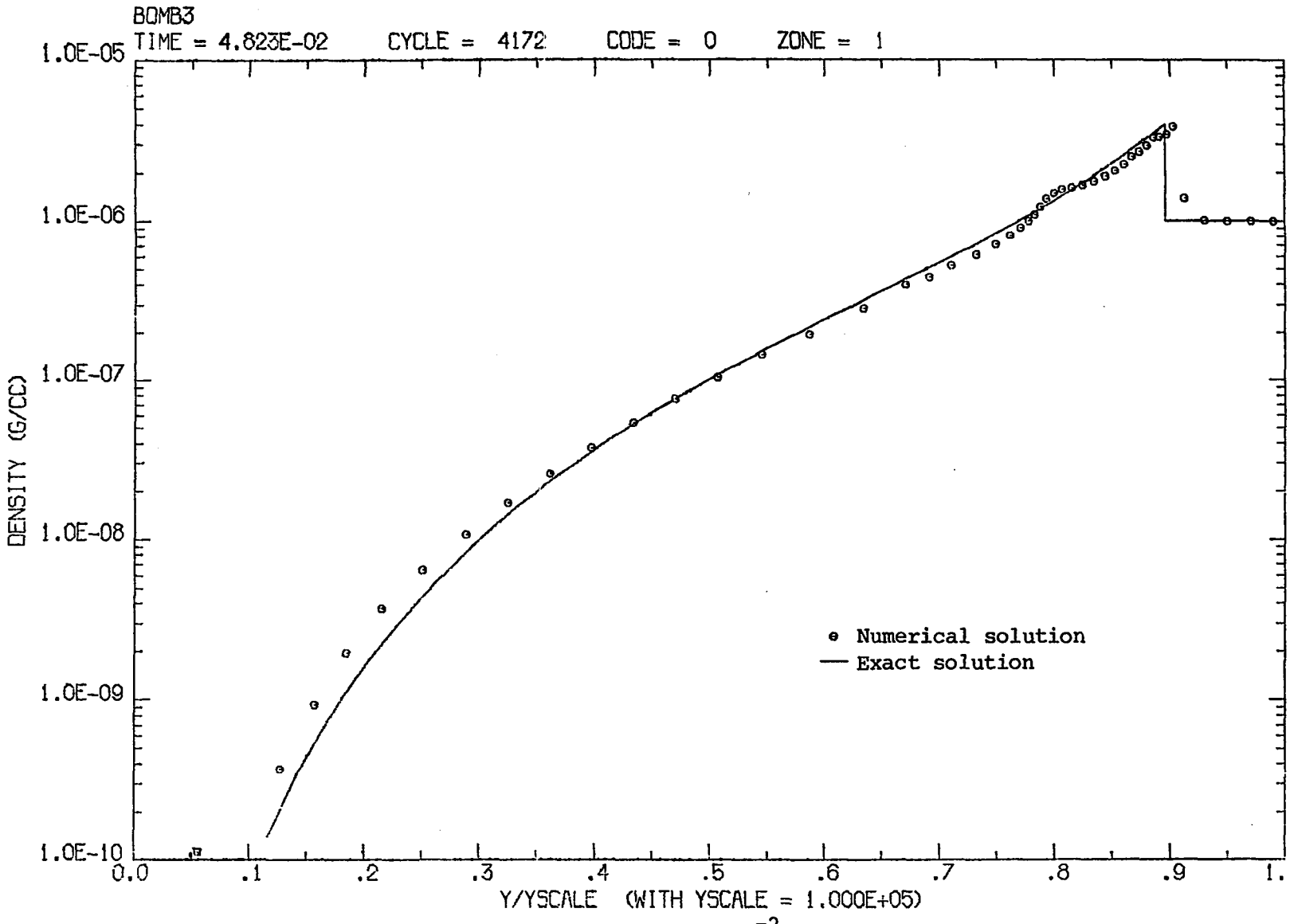

Figure 42a. The density along the y-axis at t = 4.82 x 10^{-2} sec for a three-dimensional Sedov blast

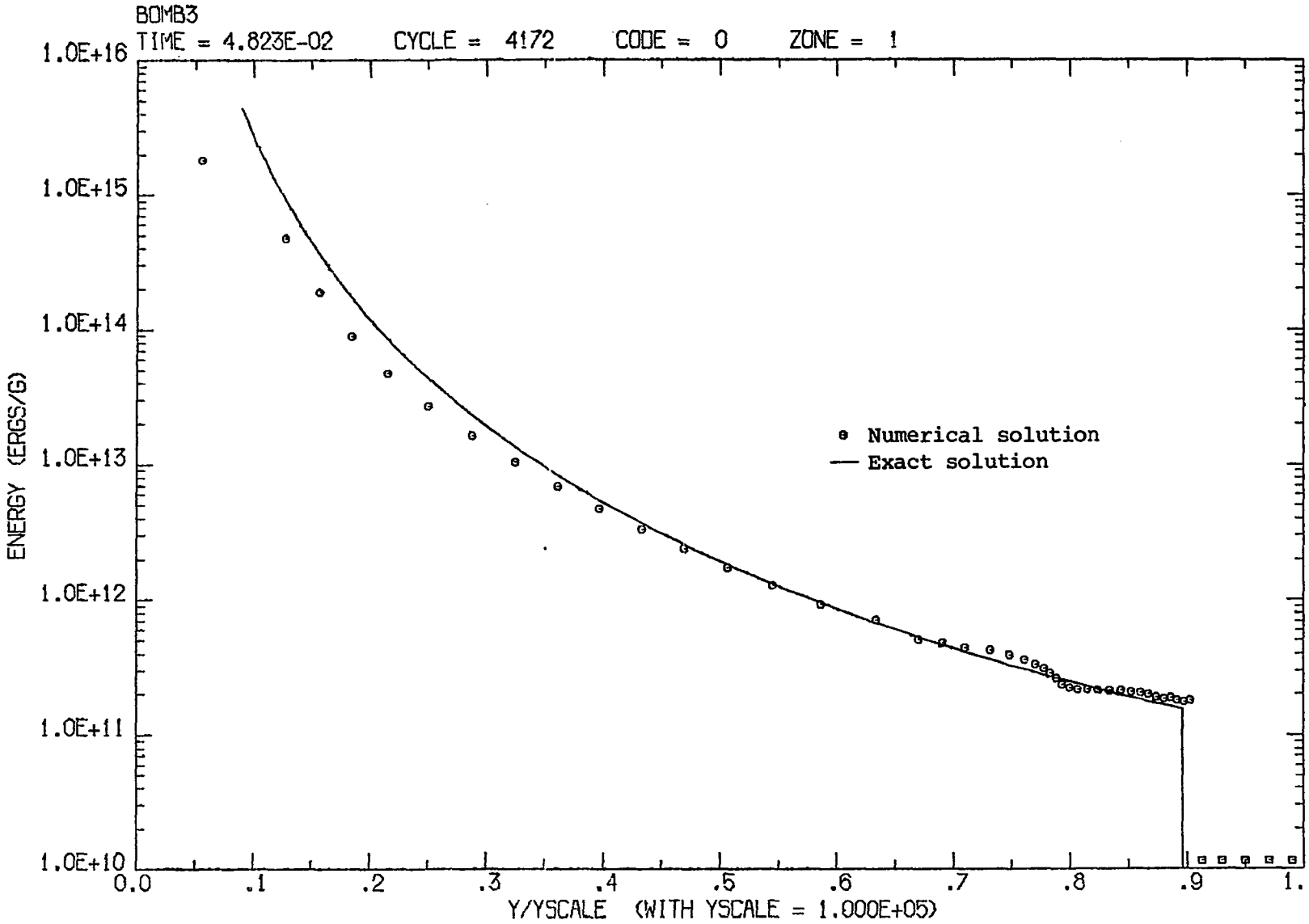

Figure 42b. The specific internal energy along the y-axis for a three-dimensional Sedov blast

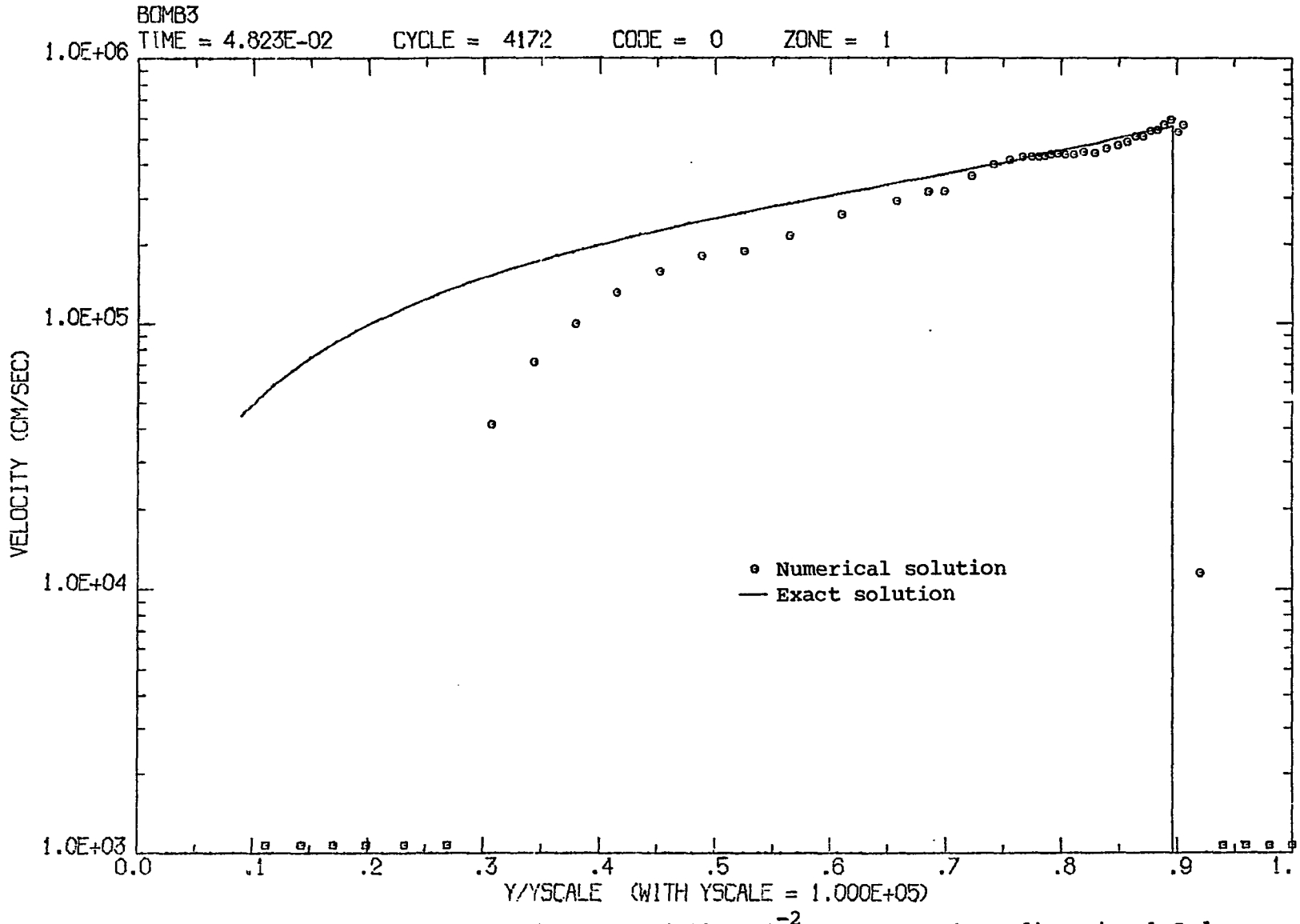

Figure 42c. The velocity along the y-axis at t = 4.82 x 10^{-2} sec for a three-dimensional Sedov blast

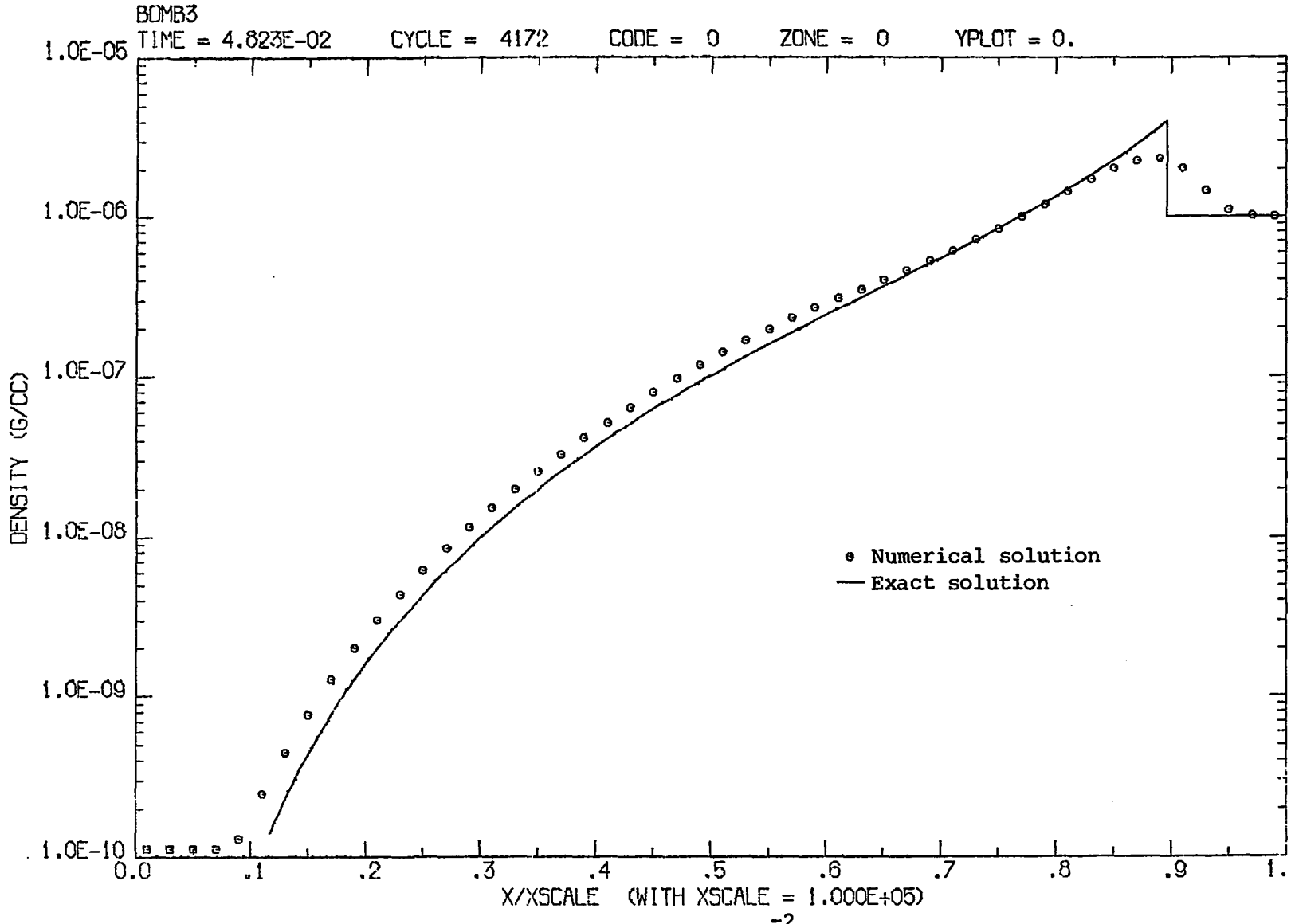

Figure 43a. The density along the x-axis at t = 4.82 x 10^{-2} sec for a three-dimensional Sedov blast

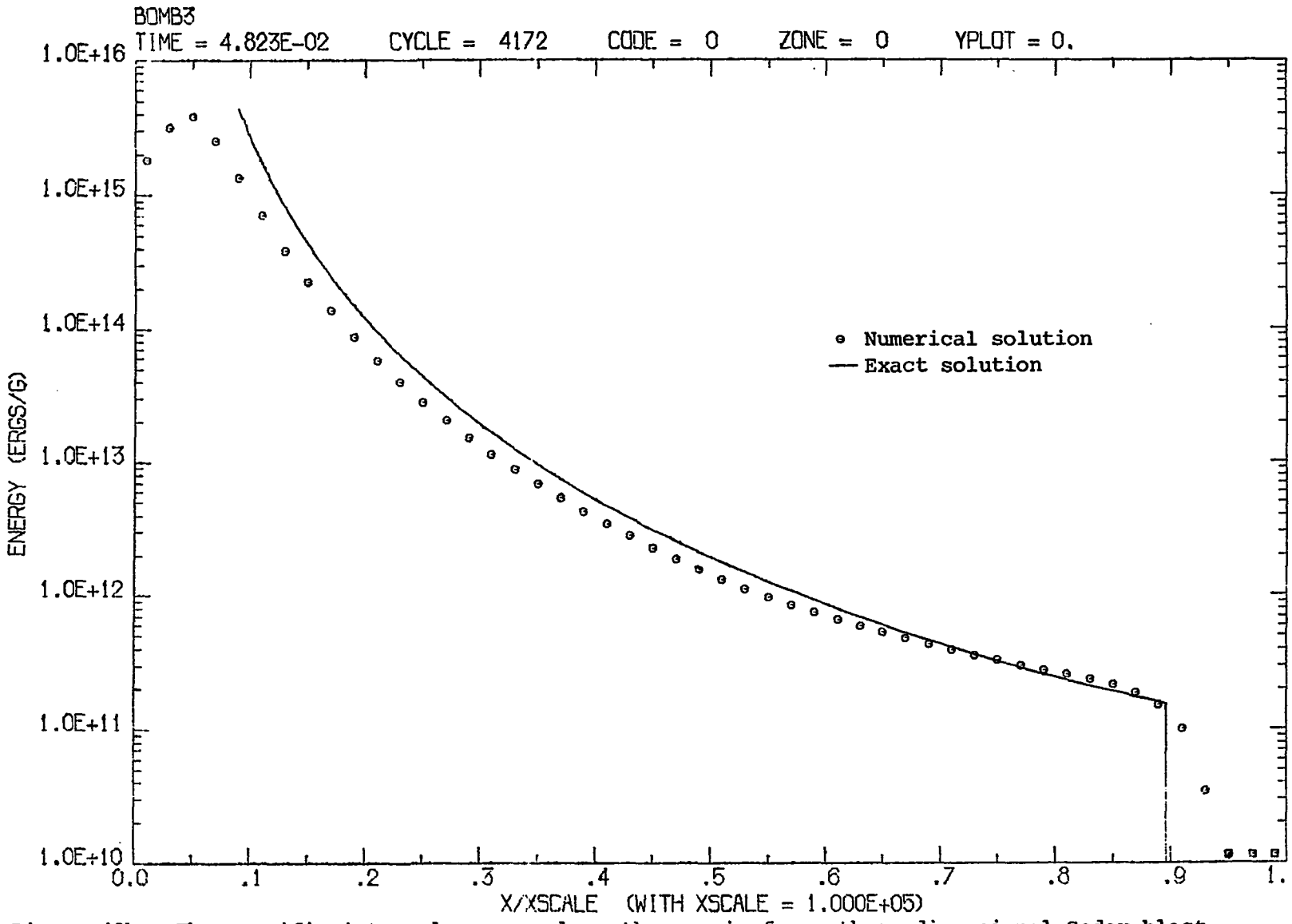

Figure 43b. The specific internal energy along the x-axis for a three-dimensional Sedov blast

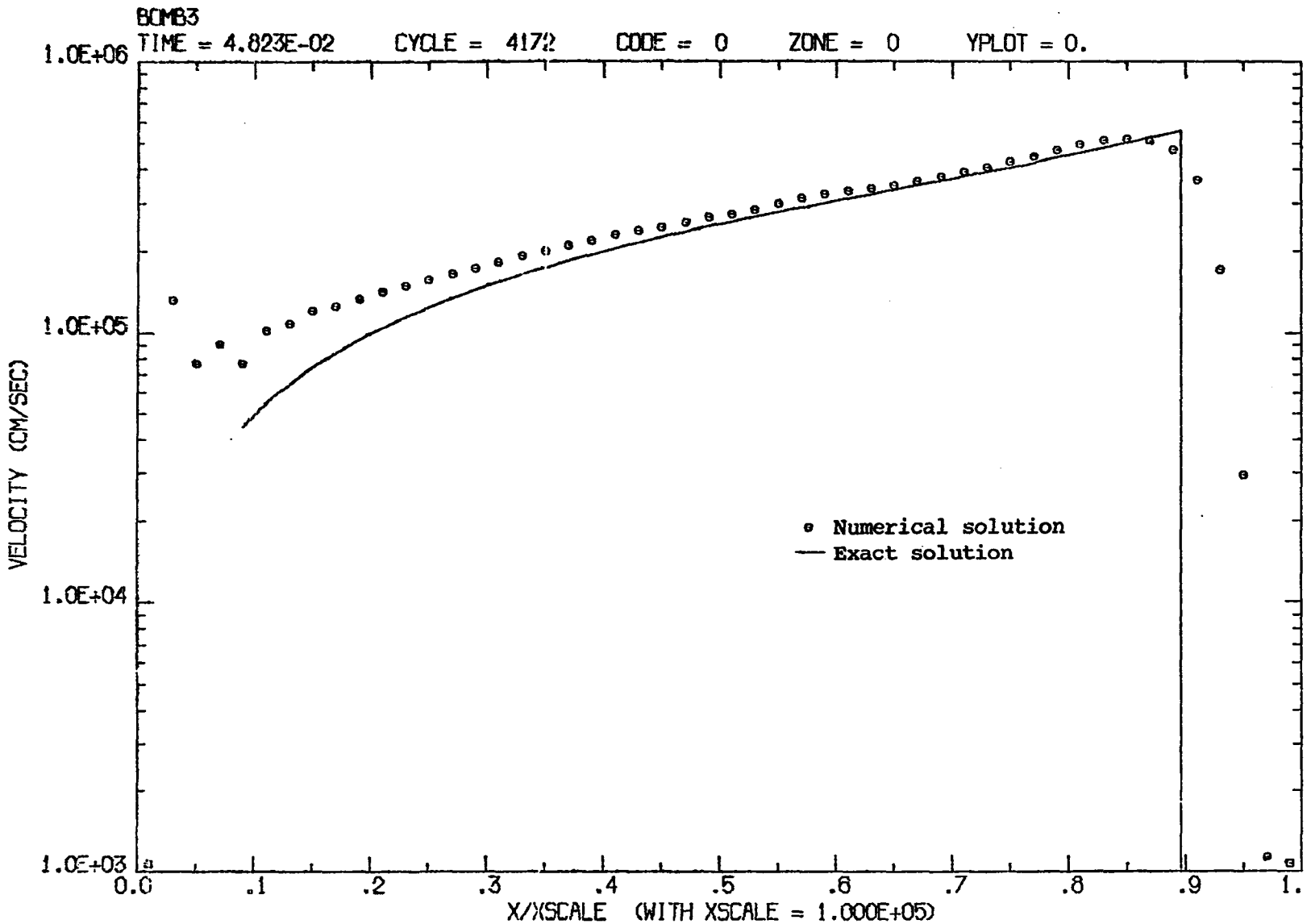

Figure 43c. The velocity along the x-axis at t = 4.82 x 10^{-2} sec for a three-dimensional Sedov blast

these differences appear exaggerated on the present logarithmic plots. This disagreement is probably a result of the failure to treat the central region with sufficient accuracy. In the exact solution the internal energy goes infinite and the density goes to zero at the origin. In a few of the central cells of the "20-cell starting model" the density was artificially raised and the internal energy suppressed (keeping the pressure constant) in order to avoid extremely low central densities. In addition, seven cells were combined into two during the first few iterations in order that more reasonably sized time steps could be taken. These cell manipulations produce errors which propagate outwards at the local sound speed, which is extremely large inside the blast. Such singularities are not encountered in the cloud models.

The volume integrals of internal energy, x-directed kinetic energy, and y-directed kinetic energy are computed throughout the evolution, and the total is conserved to 0.34%. By symmetry $\frac{1}{3}$ of the total kinetic energy should be y-directed and the remainder x-directed. The starting model has 35.3% y-directed (because the y-velocities are defined at the cell edge, while the x-velocities are defined at cell center), but by the end of the evolution it has dropped to 33.9%. Taylor (1950) has found that 74.6% of the total energy is thermal and the remainder

is kinetic. This result depends upon the numerical evaluation of some rather messy integrals and other authors have quoted slightly different values (Sappenfield 1969; Chevalier 1974). Here the internal energy comprises 70.4% of the total initially and 72.0% at the end. The overall accuracy of the n = 3 blast is quite good in view of the singularities at r = 0 and the large discontinuities at r = r_s (pressure and internal energy drop by 10 to 14 orders of magnitude).

B. Self-Consistency Checks

Of course no analytical solutions exist for comparison with the radiatively driven gas clouds. However a number of self-consistency checks establish confidence that the code continues to perform accurately here also. First, as mentioned above, energy conservation is not assumed by the code, but volume integrals of the total energy are computed every few hundred iterations. When radiation pressure is not included, the extent to which the energy remains constant serves as a check on code accuracy. The two ram-pressure-confined clouds with no radiation pressure (RQ334 and R0221, see Table 1) conserve energy to a fraction

of a percent over their entire evolutions.[1] The total grid mass is similarly conserved for all of the models.

Another indication that the code is performing properly is the fact that the cloud models appear physically reasonable. For example, the drag-decelerated clouds (R0334 and R022L) slow down at a rate consistent with theory (Figures 23 and 25). Also, a bow shock forms at the leading edge of the flow whenever the cloud motion is supersonic. The physical conditions directly in front of these clouds (behind the bow shocks) always agree with the stagnation conditions (Equations 5.1 and 5.2) for a blunt-nosed obstacle in a supersonic flow to within 30%.

None of the test solutions (Chapter IX.A) verify that the radiation pressure acceleration has been properly included. However radiation pressure and gravity are included at the same point in the code, and the latter is tested by the isothermal atmosphere (Equation 9.1). In addition, both the ram-pressure-confined clouds and the thermal-gas-pressure-confined clouds are accelerated at a rate consistent with the simple theory of constant-size clouds (Equation 2.17) at early times before they have expanded appreciably (Figures 17, 20, 35, 36, and 37).

[1] Corrections must be made to account for the new cells added at the top of the grid and for the chopping which occurs at the rear (Chapter IV.D).

Further confidence in the results comes from the fact that twiddling the "numerical knobs" makes the code run more efficiently, but does not significantly change the physics. For instance, changing the coefficient of the artificial viscous pressures (C_Q in Equations 4.6 and 4.7) from 1 to 2 results in insignificant changes in the variation of cloud length, velocity ($\bar{M}_n(s)$ in Equation 5.4), and column density with time. On the other hand, it results in a rather substantial savings in computation time ($\simeq$ 30-40%). Similarly, the models are relatively insensitive to changes in the structure of the computational grid. Both a uniform-cell grid (cf Figure 10) and one with increased resolution within the cloud (6 cells spanning the radius rather than 4) give comparable results.

Finally, the cell manipulation described in Chapter IV.D requires some discussion. Fine rezoning and cell splitting are primarily a trade-off between resolution and computation time. This has been verified for both the clouds and for the Sedov blasts (Chapter IX.A). The effects of chopping and course rezoning are not directly tested because all of the cloud models have some and none of the test solutions have any. However, these procedures are used primarily at late times ($s \gtrsim 2$) so that the clouds' behavior is well established before they are initiated. The fact that the physical variables such as cloud length,

velocity, and column density continue to vary reasonably smoothly after they are used suggests that they do not lead to serious error (see Chapter V model results).

X. APPENDIX B: PLOTTING CONVENTIONS

The output of the gasdynamic code is the x- and y-coordinates, the x- and y-velocities, the density, and the specific internal energy of each cell at each time step. Every few hundred time steps these arrays are used to create a series of printer plots to check on the model's progress. These arrays are also periodically stored on disk for later analysis and for use in producing computer-generated plots.

Contour plots of velocity, density, internal energy, and pressure (e.g., Figures 11a-d) and grid plots (e.g., Figure 9) are made. Of course, these plots represent a cross section of the actual grid, which possesses cylindrical symmetry (Chapter IV.A and B). The first line at the top of each of these plots gives the model name. The second line shows the TIME (elapsed time in seconds), CYCLE (number of iterations calculated), and CODE (number of grid manipulations performed, see Chapter IV.D). Line three identifies the quantity being plotted and specifies the contour interval (CONINT) for the contour plots. For the velocity contour plots, this line also gives VMIN (in cm/sec), the minimum velocity contoured. The final line gives the scaling factor for the y-axis (YSCALE) and the maximum y-value plotted (YMAX), both in centimeters.

The scaling for the x-axis is always a simple multiple of YSCALE, which is included in the axis label if different from unity. Notice that only a portion of the grid is usually plotted; it may extend to both larger and smaller y-values. The maximum y-value plotted corresponds to the present upper Lagrangian boundary (see Chapter IV.C) and the lower value is chosen so that YSCALE is a "nice" number. The lower boundary of the grid is not necessarily the same as it was at t = 0 because chopping may have occurred (Chapter IV.D).

Selected contours are labelled on each plot by the value of the logarithm of the quantity being contoured. The value of the unlabelled contours can usually be inferred from the labelled ones and CONINT, the contour interval. For the cloud models, the density which is plotted is atomic number density and the velocities are in cm/sec. The internal energy and pressure are normalized so that their values in the undisturbed medium are unity. For the blast wave solutions (Appendix A), cgs units are used throughout.

The contour routine requires that the x- and y-cell boundaries be continuous from cell to cell. The computational grid possesses such continuity for the x-cell boundaries but not for the y-cell boundaries (Figure 9). Thus a

linear interpolation onto a secondary grid with a uniform cell size in the y-direction ($\Delta y = \max\{YSCALE/100, \Delta x_1\}$, with Δx_1 = width of the first Eulerian zone) is performed. The contour routine then linearly interpolates along the sides of the cells in the secondary grid and draws only straight lines through individual cells. This double interpolation scheme results in smoothed contours which can be misleading because the actual computational grid has better resolution in some areas and worse in others.

Plots of velocity, density, internal energy, and pressure as a function of distance, either y-distance along the symmetry axis (e.g., Figures 12a-d and 42a-c) or x-distance for y = 0 (e.g., Figures 43a-c), are made. The variables TIME, CYCLE, CODE, YSCALE, and YMAX are defined as above and XSCALE is the variable analogous to YSCALE, but in the x-direction. The units for all distances are centimeters and the units for the quantities being plotted are given in the individual figures (on the ordinate). Points which would normally fall off the plot are boxed, rather than circled, and plotted 0.05 inches above the abscissa (e.g., Figure 43a).

XI. APPENDIX C: COMPUTER CODE LISTING

```
      PROGRAM MAIN( INPUT,OUTPUT,TAPE5=INPUT,TAPE6=OUTPUT,TAPE7,TAPE8)      MAIN.001
      IMPLICIT REAL (M)                                                     MAIN.002
      COMMON DY1,LEZ,ECHOP,EREZON,NOUT,IPRINT,ITAPE,GM,YZERO                MAIN.003
      DIMENSION Y(90,27),V(90,27),U(90,27),RHO(90,27),E(90,27),             MAIN.004
     1QE(90,27),QL(90,27),M(90,27),VOL(90,27),H(90,27),PPURE(90,27),        MAIN.005
     2P(90,27),Z(90,27),DELV(90,27),HDOT(90,27),MDOT(90,27),EDOT(90,27),    MAIN.006
     3LM1(27),LMAZ1(27),X(28),DXSQ(27),PI2X(27),DELX(27)                    MAIN.007
      DIMENSION Y2H(90,27),V2H(90,27),U2H(90,27),RHO2H(90,27),              MAIN.008
     1E2H(90,27),QE2H(90,27),QL2H(90,27)                                    MAIN.009
      COMMON /LCM/ Y2H,V2H,U2H,RHO2H,E2H,QE2H,QL2H                          MAIN.010
      LEVEL 2, Y2H,V2H,U2H,RHO2H,E2H,QE2H,QL2H                              MAIN.011
      DIMENSION ZI(51),GCL(51),GC(51),T(51),HI(51),MU(51),HIMU(51)          MAIN.012
C                                                                           MAIN.013
C*****THESE ARE TARTER'S BEST 1975 VALUES FOR THE RADIATION PRESSURE        MAIN.014
C*****ACCELERATION OF AN OPTICALLY THIN GAS.  GCL IS THE ACCELERATION/      MAIN.015
C*****DENSITY WHEN BOUND-FREE ABSORPTION, BOUND-BOUND ABSORPTION, AND       MAIN.016
C*****ELECTRON SCATTERING ARE INCLUDED.  GC IS THE ACCELERATION/DENSITY     MAIN.017
C*****WHEN ONLY BOUND-FREE ABSORPTION AND ELECTRON SCATTERING ARE           MAIN.018
C*****INCLUDED.                                                            MAIN.019
C                                                                           MAIN.020
      DATA GCL /2.222E+13,3.443E+13,5.150E+13,7.331E+13,1.011E+14,          MAIN.021
     11.350E+14,1.721E+14,2.093E+14,2.441E+14,2.756E+14,3.053E+14,          MAIN.022
     23.387E+14,3.805E+14,4.324E+14,4.918E+14,5.521E+14,6.032E+14,          MAIN.023
     36.403E+14,6.774E+14,7.145E+14,7.609E+14,8.259E+14,9.094E+14,          MAIN.024
     41.021E+15,1.132E+15,1.225E+15,1.285E+15,1.299E+15,1.271E+15,          MAIN.025
     51.211E+15,1.155E+15,1.188E+15,1.295E+15,1.392E+15,1.387E+15,          MAIN.026
     61.220E+15,1.179E+15,1.383E+15,1.926E+15,3.072E+15,4.965E+15,          MAIN.027
     77.285E+15,9.929E+15,1.434E+16,2.204E+16,3.503E+16,5.661E+16,          MAIN.028
     89.326E+16,1.531E+17,2.533E+17,4.181E+17/                              MAIN.029
      DATA GC  /5.279E+12,8.185E+12,1.223E+13,1.752E+13,2.429E+13,          MAIN.030
     13.248E+13,4.149E+13,5.072E+13,5.924E+13,6.658E+13,7.364E+13,          MAIN.031
     28.106E+13,8.966E+13,1.006E+14,1.126E+14,1.227E+14,1.306E+14,          MAIN.032
     31.343E+14,1.349E+14,1.339E+14,1.318E+14,1.300E+14,1.290E+14,          MAIN.033
     41.296E+14,1.307E+14,1.329E+14,1.360E+14,1.401E+14,1.455E+14,          MAIN.034
     51.526E+14,1.627E+14,1.834E+14,2.172E+14,2.606E+14,3.088E+14,          MAIN.035
     63.693E+14,5.044E+14,7.512E+14,1.158E+15,1.818E+15,2.887E+15,          MAIN.036
```

```
     74.632E+15,7.525E+15,1.236E+16,2.038E+16,3.367E+16,5.565E+16,      MAIN.037
     89.211E+16,1.524E+17,2.523E+17,4.176E+17/                          MAIN.038
      DATA ZI  /1.111E-05,1.840E-05,3.047E-05,5.047E-05,8.358E-05,      MAIN.039
     11.384E-04,2.292E-04,3.796E-04,6.287E-04,1.041E-03,1.724E-03,      MAIN.040
     22.856E-03,4.729E-03,7.832E-03,1.297E-02,2.148E-02,3.557E-02,      MAIN.041
     35.891E-02,9.756E-02,1.616E-01,2.676E-01,4.431E-01,7.339E-01,      MAIN.042
     41.215E+00,2.013E+00,3.333E+00,5.520E+00,9.142E+00,1.514E+01,      MAIN.043
     52.507E+01,4.152E+01,6.877E+01,1.139E+02,1.886E+02,3.124E+02,      MAIN.044
     65.173E+02,8.567E+02,1.419E+03,2.350E+03,3.891E+03,6.444E+03,      MAIN.045
     71.067E+04,1.767E+04,2.927E+04,4.847E+04,8.027E+04,1.329E+05,      MAIN.046
     82.202E+05,3.646E+05,6.038E+05,1.000E+06/                          MAIN.047
C                                                                       MAIN.048
C*****TARTER'S ELECTRON TEMPERATURES FOR AN OPTICALLY THIN GAS.          MAIN.049
C                                                                       MAIN.050
      DATA T   /1.346E+03,1.814E+03,2.648E+03,3.771E+03,4.697E+03,      MAIN.051
     15.388E+03,5.959E+03,6.451E+03,6.877E+03,7.265E+03,7.640E+03,      MAIN.052
     27.998E+03,8.346E+03,8.750E+03,9.287E+03,1.005E+04,1.112E+04,      MAIN.053
     31.237E+04,1.366E+04,1.494E+04,1.621E+04,1.751E+04,1.878E+04,      MAIN.054
     42.009E+04,2.155E+04,2.338E+04,2.593E+04,2.970E+04,3.569E+04,      MAIN.055
     54.625E+04,6.380E+04,8.193E+04,9.477E+04,1.076E+05,1.340E+05,      MAIN.056
     61.997E+05,2.565E+05,2.768E+05,2.819E+05,2.915E+05,3.263E+05,      MAIN.057
     74.191E+05,5.861E+05,7.080E+05,7.735E+05,7.999E+05,8.023E+05,      MAIN.058
     87.890E+05,7.694E+05,7.503E+05,1.831E+06/                          MAIN.059
C                                                                       MAIN.060
C*****THESE ARE TARTER'S VALUES FOR N(HI)/N(H).                         MAIN.061
C                                                                       MAIN.062
      DATA HI /8.53E-01,7.97E-01,7.16E-01,6.14E-01,5.09E-01,4.07E-01,   MAIN.063
     13.09E-01,2.23E-01,1.53E-01,1.01E-01,6.36E-02,3.93E-02,2.39E-02,   MAIN.064
     21.43E-02,8.44E-03,4.89E-03,2.78E-03,1.56E-03,8.82E-04,5.00E-04,   MAIN.065
     32.84E-04,1.62E-04,9.29E-05,5.33E-05,3.05E-05,1.73E-05,9.69E-06,   MAIN.066
     45.29E-06,2.80E-06,1.41E-06,6.91E-07,3.63E-07,2.04E-07,1.17E-07,   MAIN.067
     56.48E-08,3.00E-08,1.44E-08,8.10E-09,4.82E-09,2.82E-09,1.53E-09,   MAIN.068
     67.22E-10,3.09E-10,1.55E-10,8.54E-11,4.99E-11,3.00E-11,1.84E-11,   MAIN.069
     71.14E-11,7.08E-12,1.63E-12/                                       MAIN.070
C                                                                       MAIN.071
C*****TARTER'S VALUES OF MU.                                            MAIN.072
```

```
C                                                                       MAIN.073
      DATA MU  /1.133E-00,1.082E-00,1.014E-00,9.408E-01,8.750E-01,      MAIN.074
     18.188E-01,7.707E-01,7.325E-01,7.036E-01,6.831E-01,6.686E-01,      MAIN.075
     26.581E-01,6.508E-01,6.445E-01,6.389E-01,6.341E-01,6.296E-01,      MAIN.076
     36.262E-01,6.235E-01,6.215E-01,6.206E-01,6.200E-01,6.196E-01,      MAIN.077
     46.194E-01,6.193E-01,6.191E-01,6.190E-01,6.189E-01,6.187E-01,      MAIN.078
     56.186E-01,6.185E-01,6.184E-01,7*6.183E-01,12*6.182E-01/           MAIN.079
      DATA PI/3.141592653589 7/,NSAVE/4/,IW/0/,JW/0/,WITMAX/0.0/,       MAIN.080
     1TIME/0.0/,ICYCLE/0/                                               MAIN.081
      NOUT=1                                                            MAIN.082
      IPRINT=0                                                          MAIN.083
      ITAPE=0                                                           MAIN.084
      ECHOP=0.0                                                         MAIN.085
      EREZON=0.0                                                        MAIN.086
      EUNZON=0.0                                                        MAIN.087
    1 FORMAT(5H0LM1(I3,23H) HAS BEEN INCREASED TOI4,13H DURING CYCLE,I6) MAIN.088
    3 FORMAT(1H1,///,1X, 64HTHE PROGRAM HAS BEEN TERMINATED NORMALLY BEC MAIN.089
     1AUSE DT IS LESS THAN,1PE10.2,1H.)                                 MAIN.090
    4 FORMAT(1H1,///,1X, 78HTHE PROGRAM HAS BEEN TERMINATED NORMALLY BEC MAIN.091
     1AUSE YOU HAVE RUN OUT OF CPU TIME.)                               MAIN.092
    5 FORMAT(8H0CELLS (I3,1H,I3,7H) AND (I3,1H,I3,28H) WERE COMBINED AFT MAIN.093
     1ER CYCLE ,I5,15H WAS COMPLETED.)                                  MAIN.094
    6 FORMAT(19H0RESTART FROM CYCLE,I6,17H BECAUSE WITENO =,1PE10.3,10H MAIN.095
     1IN CELL (,I3,1H,I3,22H)   FOR PROPOSED CYCLE,I6,10H WHEN DT =,    MAIN.096
     2E12.5,1H.,/,15H COURANT PART =,E10.3,17H,   4(DVOL/VOL) =,        MAIN.097
     3E10.3,13H,   4(DM/M) =,E10.3)                                     MAIN.098
    7 FORMAT(7H0EINT =,1PE10.3,5X,7HEKINV =,E10.3,5X,7HEKINH =,E10.3,   MAIN.099
     15X,7HEGRAV =,E10.3,/,16H TOTAL ENERGY = ,                         MAIN.100
     2E10.3,11X,13HTOTAL MASS = ,E10.3,21X,15HTOTAL VOLUME = ,E10.3)    MAIN.101
    8 FORMAT(7H1TIME =,1PE14.7,5X,4HDT =,E14.7,5X,7HCYCLE =,I6,5X,      MAIN.102
     17HICODE =,I3,5X,7HWITMAX(,I3,1H,I3,3H) =,E10.3,///,               MAIN.103
     25X,1HI,2X,6HLM1(I),2X,8HLMAZ1(I),5X,4HX(I),//,                    MAIN.104
     3(3X,I3,3X,I3,6X,I3,5X,E10.3))                                     MAIN.105
    9 FORMAT(3X,I3,20X,1PE10.3,//,3X,5HLEZ =,I4)                        MAIN.106
   10 FORMAT(24H0MASS WAS LESS THAN MLIM)                               MAIN.107
   26 FORMAT(40H1JOB TERMINATED BECAUSE SPLITTING CELL (,I3,1H,I3,      MAIN.108
```

```
     142H) WOULD CAUSE LM1 TO BE LARGER THAN LMAZ1.)                    MAIN.109
  27  FORMAT(7H CELL (,I3,1H,I3,29H) HAS BEEN SPLIT DURING CYCLE,I5,7H,  MAIN.110
     1 LM1(,I3,11H) WENT FROM,I4,4H  TO,I4,12H  AND LMAZ1(,I3,6H) FROM,  MAIN.111
     1I4,4H  TO,I4,1H.)                                                 MAIN.112
  28  FORMAT(6H1ZI = ,1PE10.3,61H, SO PROGRAM CAN'T FIND T(ZI) FOR INTER MAIN.113
     1CLOUD MEDIUM IN TABLE.)                                           MAIN.114
  29  FORMAT(6H1ZI = ,1PE10.3,54H FOR THE CLOUD SO T(ZI) CAN'T BE FOUND  MAIN.115
     1FROM THE TABLE.)                                                  MAIN.116
  30  FORMAT(6X,I4,6X,I4,6X,I4,8X,I4)                                   MAIN.117
  31  FORMAT(4X,E10.3,8X,E10.3,7X,E10.3,8X,A10)                         MAIN.118
  32  FORMAT(8X,I4,8X,I4,7X,E10.3)                                      MAIN.119
  33  FORMAT(4X,E10.3,7X,E10.3,6X,E10.3,6X,E10.3,7X,E10.3)              MAIN.120
  34  FORMAT(6X,E10.3,7X,I4,6X,I4,6X,E10.3)                             MAIN.121
  35  FORMAT(8X,F5.2,8X,F5.2,4X,E10.3,4X,E10.3,7X,E10.3)                MAIN.122
  36  FORMAT(7X,E10.3,8X,E10.3)                                         MAIN.123
  37  FORMAT(4X,E10.3,5X,E10.3,7X,E10.3,7X,I4,7X,I4)                    MAIN.124
  40  FORMAT(1H1,    7X,70HTHIS MODEL STARTS FROM THE INITIAL CONDITIONS MAIN.125
     1 LISTED BELOW (ISTART=0).)                                        MAIN.126
  41  FORMAT(1H1,7X,42HTHIS MODEL IS A RESTART FROM TAPE (ISTART=,I3,2H) MAIN.127
     1.)                                                                MAIN.128
  42  FORMAT(8X,86HTHE GASDYNAMICS IS DONE IN ONLY THE FIRST LM1(I) CELL MAIN.129
     1S OF EACH VERTICAL ZONE (IALL=0).)                                MAIN.130
  43  FORMAT(8X,59HTHE GASDYNAMICS IS DONE IN ALL CELLS AT ALL TIMES (IA MAIN.131
     1LL=1).)                                                           MAIN.132
  44  FORMAT(//,8X,17HGRID INFORMATION:,15X,17HTIME INFORMATION:,15X,23H MAIN.133
     1PRINT/TAPE INFORMATION:,11X,26HMISCELLANEOUS INFORMATION:,//,12X, MAIN.134
     27HIMAX = I4,21X8HDT      =,1PE10.3,14X,9HIPRNT1 = ,I4,21X,7HCQ    =
     3E10.3,/,12X,7HJMAX = ,I4,21X,8HTIME    =,E10.3,14X,9HITAPE1 = ,I4,
     421X,7HVSQRT =,E10.3,/,44X,8HCYCLE  =,I5,53X,
     57HEMIN  =,E10.3,/,12X,8HRATIOX =,E10.3,/12X,8HRATIOY =,E10.3,
     614X,8HTIMLMT =,E10.3,/,44X,8HDTLIM  =,E10.3,10X,21HREZONING INFORM
     7ATION:,/,12X,8HDX     = ,E10.3,/12X8HDY     = ,E10.3,47X,7HMLIM  =,
     8E10.3,/,77X,7HDYLIM =,E10.3,/,12X,8HYZERO = ,E10.3,47X,7HDYMAX =,
     1E10.3)                                                            MAIN.142
  45  FORMAT(///,8X,33HPARAMETERS FOR INTERCLOUD MEDIUM:,19X,21HPARAMETE MAIN.143
     1RS FOR CLOUD:,//,12X,8HTZERO  =,1PE10.3,30X,6HTC    =,E10.3,4X,  MAIN.144
```

```
     28HICENT1 =,I4,/,12X,8HENZERO =,E10.3,30X,6HENC  =,E10.3,4X,8HIRAD    MAIN.145
     3 = ,I4,//,12X,8HRHOZRO =,E10.3,30X,6HRHOC =,                        MAIN.146
     4E10.3,/,60X,                        6HEC    =,E10.3//12X8HEZERO  =,E10.3,  MAIN.147
     530X,6HVC   =,E10.3,/,12X,8HAZRO   =,E10.3,30X,6HAC   =,E10.3,/,     MAIN.148
     660X,6HVC/A0=E10.3)                                                   MAIN.149
  46  FORMAT(//,8X,23HEXTERNAL ACCELERATIONS:,//,12X,7HEL46  =,1PE10.3,    MAIN.150
     1/,12X,7HLINES =,I4,/,12X,7HMASS  =,E10.3,/,12X,7HM/L   =,E10.3)      MAIN.151
  47  FORMAT(/,12X,8HZI      =,1PE10.3,30X,6HZI    =,E10.3)                MAIN.152
  48  FORMAT(///,8X,33HPARAMETERS FOR INTERCLOUD MEDIUM:,//,12X,8HTZERO     MAIN.153
     1 =,1PE10.3,/,12X,8HENZERO =,E10.3,//,12X,8HRHOZRO =,E10.3,           MAIN.154
     2              //,12X,8HEZERO  =,E10.3,/,12X,8HAZRO   =,E10.3)       MAIN.155
  49  FORMAT(/,18H COLUMN DENSITY = ,1PE10.3,9X,23HTAU(LYMAN CONTINUUM)     MAIN.156
     1 = ,E10.3,11X,19HTAU(LYMAN ALPHA) = ,E10.3)                          MAIN.157
  50  FORMAT(/,7H CELL (,I3,1H,I3,11H) HAS ZI = ,1PE10.3,2X,26HSO HI HAS    MAIN.158
     1 BEEN SET TO ONE.)                                                   MAIN.159
  51  FORMAT(/,12X,8HCOLDEN =,1PE10.3,30X,8HCOLDEN =,E10.3,/,               MAIN.160
     112X,8HTAU(C) =,E10.3,30X,8HTAU(C) =,E10.3,/,                         MAIN.161
     212X,8HTAU(L) =,E10.3,30X,8HTAU(L) =,E10.3)                           MAIN.162
  52  FORMAT(/,12X,8HCOLDEN =,1PE10.3,/,12X,8HTAU(C) =,E10.3,/,             MAIN.163
     112X,8HTAU(L) =,E10.3)                                                MAIN.164
  53  FORMAT(64H1CONGRATULATIONS. YOU HAVE REACHED EOF WITHOUT FINDING A    MAIN.165
     1NYTHING.)                                                            MAIN.166
  54  FORMAT(/,12X,8HZI      =,1PE10.3)                                     MAIN.167
  55  FORMAT(2I5,A10)                                                       MAIN.168
  57  FORMAT(9H0EGRAND =,1PE10.3,5X,8HEREZON =,E10.3,5X,8HEUNZON =,E10.3    MAIN.169
     1,5X,7HECHOP =,E10.3)                                                 MAIN.170
  58  FORMAT(26H0ADJUST CALLED WHEN TIME =,1PE10.3,5X,7HCYCLE =,I6,5X,      MAIN.171
     17HICODE =,I3)                                                        MAIN.172
C                                                                          MAIN.173
C*****READ IN THE REQUIRED CONSTANTS FROM CARDS.                           MAIN.174
C                                                                          MAIN.175
      READ(5,30) IMAX,JMAX,IALL,ISTART                                     MAIN.176
      READ(5,31) DT,TIMLMT,DTLIM,MODEL                                     MAIN.177
      READ(5,32) IPRNT1,ITAPE1,DYMAX                                       MAIN.178
      READ(5,33) CQ,VSQFR,EMIN,MLIN,DYLIM                                  MAIN.179
      READ(5,34) EL46,LINES,ITAU,MASS                                      MAIN.180
```

```
      READ(5,35) RATIOX,RATIOY,DX,DY,YZERO                              MAIN.181
      READ(5,36) TZERO,ENZERO                                           MAIN.182
      READ(5,37) TC,ENC,VCOA0,ICENT1,IRAD                               MAIN.183
C                                                                       MAIN.184
C*****ISTART = 0 IS INITIAL START, ISTART .GT. 0 IS RESTART FROM TAPE.  MAIN.185
C                                                                       MAIN.186
      IMAZ=IMAX-1                                                       MAIN.187
      IMAY=IMAX-2                                                       MAIN.188
      MOL=9.999E+99                                                     MAIN.189
      IF(EL46.GT.0.0) MOL=MASS*3.904E-13/EL46                           MAIN.190
      GM=6.67E-08*1.989E+33*MASS                                        MAIN.191
      ELUM=1.298*1.66043*EL46*1.0E+22                                   MAIN.192
      LOW=MAX0(ICENT1-IRAD+1,1)                                         MAIN.193
      LUP=ICENT1+IRAD                                                   MAIN.194
      MUZERO=0.6182                                                     MAIN.195
      MUC=0.6182                                                        MAIN.196
      DO 70 I=1,51                                                      MAIN.197
      HIMU(I)=HI(I)/SQRT(MU(I))                                         MAIN.198
   70 CONTINUE                                                          MAIN.199
      IF(ISTART.LE.0) GO TO 78                                          MAIN.200
      READ(5,55) ICYCLT,ICODT,TMODEL                                    MAIN.201
   72 READ(7) TIME,DT,ICYCLE,IMAZ,JMAX,LEZ,ICODE,WMODEL                 MAIN.202
      IF(EOF(7)) 74,75                                                  MAIN.203
   74 WRITE(6,53)                                                       MAIN.204
      STOP                                                              MAIN.205
   75 READ(7) LM1,LMAZ1,X,Y,V,U,RHO,E,QE,QL                             MAIN.206
      WRITE(8) TIME,DT,ICYCLE,IMAZ,JMAX,LEZ,ICODE,WMODEL                MAIN.207
      WRITE(8) LM1,LMAZ1,X,Y,V,U,RHO,E,QE,QL                            MAIN.208
      IF(ICYCLE.NE.ICYCLT) GO TO 72                                     MAIN.209
      IF(ICODE.NE.ICODT) GO TO 72                                       MAIN.210
      IF(WMODEL.NE.TMODEL) GO TO 72                                     MAIN.211
      GO TO 140                                                         MAIN.212
C                                                                       MAIN.213
C*****CALCULATE THE CELL BOUNDARIES.                                    MAIN.214
C        YZERO IS THE POSITION OF THE GRID RELATIVE TO THE QSO.         MAIN.215
C        DX IS THE CELL SIZE IN THE X DIRECTION INSIDE THE CLOUD.       MAIN.216
```

```
C         DY IS THE CELL SIZE IN THE Y DIRECTION INSIDE THE CLOUD.          MAIN.217
C         RATIOX IS (DX OF LAST CELL/DX OF FIRST CELL). RATIOX=1 GIVES      MAIN.218
C              LINEAR.                                                      MAIN.219
C         RATIOY IS (DY OF INTERCLOUD CELLS/DY OF CLOUD CELLS).             MAIN.220
C                                                                           MAIN.221
   78   X(1)=0.0                                                           MAIN.222
        IF(RATIOX.GT.1.0) DX1=ALOG(RATIOX)/FLOAT(IMAY-IRAD)                MAIN.223
        IF(RATIOX.GT.1.0) AX=DX/(EXP(DX1)-1.0)                             MAIN.224
        DO 80 I=1,IMAZ                                                     MAIN.225
        Y(1,I)=0.0                                                         MAIN.226
        LM1(I)=JMAX-1                                                      MAIN.227
        IF(IALL.NE.1) LM1(I)=IRAD+ICENT1+4                                 MAIN.228
        LEZ=IMAY                                                           MAIN.229
        IF(IALL.NE.1) LEZ=IRAD+4                                           MAIN.230
        LMAZ1(I)=JMAX-1                                                    MAIN.231
        X(I+1)=X(I)+DX                                                     MAIN.232
        IF(RATIOX.GT.1.0.AND.I.GT.IRAD) X(I+1)=X(IRAD+1)+AX*(EXP(FLOAT(I-I MAIN.233
       1RAD)*DX1)-1.0)                                                     MAIN.234
        DO 80 J=2,JMAX                                                     MAIN.235
        DY1=DY+DY*(RATIOY-1.0)*(0.5-SIGN(0.5,FLOAT((J-LOW-1)*(LUP-J+1))))  MAIN.236
        Y(J,I)=Y(J-1,I)+DY1                                                MAIN.237
   80   CONTINUE                                                           MAIN.238
C                                                                          MAIN.239
C*****CALCULATE RHOZRO, TZERO, AZRO, AND EZERO FOR THE INTERCLOUD MEDIUM   MAIN.240
C*****IF TZERO = 0, IT IS CALCULATED FROM THE TABLE.                       MAIN.241
C                                                                          MAIN.242
        RHOZRO=1.66043E-24*ENZERO*1.298                                    MAIN.243
        Z2=ELUM/(RHOZRO*YZERO**2)                                          MAIN.244
        IF(TZERO.GT.0.0) GO TO 90                                          MAIN.245
        IF(Z2.GT.ZI(1)) GO TO 84                                           MAIN.246
        WRITE(6,28) Z2                                                     MAIN.247
        STOP                                                               MAIN.248
   84   DO 86 N=2,51                                                       MAIN.249
        IF(Z2.LT.ZI(N)) GO TO 88                                           MAIN.250
   86   CONTINUE                                                           MAIN.251
        WRITE(6,28) Z2                                                     MAIN.252
```

```
      STOP                                                              MAIN.253
   88 TZERO=(T(N)-T(N-1))/(ZI(N)-ZI(N-1))*(Z2-ZI(N))+T(N)               MAIN.254
      MUZERO=(MU(N)-MU(N-1))/(ZI(N)-ZI(N-1))*(Z2-ZI(N))+MU(N)           MAIN.255
   90 EZERO=1.5*1.38054E-16*TZERO/(1.66043E-24*MUZERO)                  MAIN.256
      AZRO=SQRT(10./9.*EZERO)                                           MAIN.257
C                                                                       MAIN.258
C****INITIALIZE THE INDEPENDENT VARIABLES FOR THE INTERCLOUD MEDIUM.    MAIN.259
C                                                                       MAIN.260
      DO 100 I=1,IMAZ                                                   MAIN.261
      DO 100 J=1,JMAX                                                   MAIN.262
      V(J,I)=0.0                                                        MAIN.263
      U(J,I)=0.0                                                        MAIN.264
      QE(J,I)=0.0                                                       MAIN.265
      QL(J,I)=0.0                                                       MAIN.266
      E(J,I)=EZERO                                                      MAIN.267
      RHO(J,I)=RHOZRO                                                   MAIN.268
  100 CONTINUE                                                          MAIN.269
C                                                                       MAIN.270
C****FIND RHOC, TC, AC, AND EC FOR THE CLOUD IF ONE EXISTS.            MAIN.271
C****IF TC = 0, IT IS CALCULATED FROM THE TABLE.                        MAIN.272
C                                                                       MAIN.273
      IF(IRAD.LE.0) GO TO 116                                           MAIN.274
      RHOC=1.66043E-24*ENC*1.298                                        MAIN.275
      Z3=ELUM/(RHOC*(YZERO+0.5*(Y(LUP+1,1)+Y(LOW,1)))**2)               MAIN.276
      IF(TC.GT.0.0) GO TO 110                                           MAIN.277
      IF(Z3.GT.ZI(1)) GO TO 104                                         MAIN.278
      WRITE(6,29) Z3                                                    MAIN.279
      STOP                                                              MAIN.280
  104 DO 106 N=2,51                                                     MAIN.281
      IF(Z3.LT.ZI(N)) GO TO 108                                         MAIN.282
  106 CONTINUE                                                          MAIN.283
      WRITE(6,29) Z3                                                    MAIN.284
      STOP                                                              MAIN.285
  108 TC=(T(N)-T(N-1))/(ZI(N)-ZI(N-1))*(Z3-ZI(N))+T(N)                  MAIN.286
      MUC=(MU(N)-MU(N-1))/(ZI(N)-ZI(N-1))*(Z3-ZI(N))+MU(N)              MAIN.287
  110 EC=1.5*1.38054E-16*TC/(1.66043E-24*MUC)                           MAIN.288
```

```
      AC=SQRT(10./9.*EC)                                                    MAIN.289
      VC=VCOA0*AZRO                                                         MAIN.290
C                                                                           MAIN.291
C*****INITIALIZE THE INDEPENDENT VARIABLES FOR THE CLOUD IF ONE EXISTS.     MAIN.292
C                                                                           MAIN.293
      RAD=4.0*X(IRAD+1)**2                                                  MAIN.294
      DO 112 I=1,IRAD                                                       MAIN.295
      DO 112 J=LOW,LUP                                                      MAIN.296
      IF((((Y(J+1,I)+Y(J,I))-2.0*Y(ICENT1+1,1))**2+(X(I+1)+X(I))**2)        MAIN.297
     1.GT.RAD) GO TO 112                                                    MAIN.298
      RHO(J,I)=RHOC                                                         MAIN.299
      E(J,I)=EC                                                             MAIN.300
      V(J+1,I)=VC                                                           MAIN.301
      V(J,I)=VC                                                             MAIN.302
 112  CONTINUE                                                              MAIN.303
C                                                                           MAIN.304
C*****CALCULATE THE OPTICAL DEPTHS IF ITAU = 1.                             MAIN.305
C                                                                           MAIN.306
 116  IF(ITAU.EQ.0) GO TO 140                                               MAIN.307
      TAU1=0.0                                                              MAIN.308
      TAU2=0.0                                                              MAIN.309
      TAU3=0.0                                                              MAIN.310
      TAU4=0.0                                                              MAIN.311
      COLDEN=0.0                                                            MAIN.312
      C1=0.0                                                                MAIN.313
      I=1                                                                   MAIN.314
      L=LM1(I)                                                              MAIN.315
      DO 129 J=1,L                                                          MAIN.316
      IF(IRAD.LE.0) GO TO 124                                               MAIN.317
      Z4=ELUM/(RHO(J,1)*(YZERO+0.5*(Y(J,1)+Y(J+1,1)))**2)                   MAIN.318
      IF(Z4.GT.ZI(1)) GO TO 120                                             MAIN.319
      HI2=1.0                                                               MAIN.320
      HIMU2=1.27154                                                         MAIN.321
      WRITE(6,50) J,I,Z4                                                    MAIN.322
      GO TO 123                                                             MAIN.323
 120  DO 121 N=2,51                                                         MAIN.324
```

```
      IF(Z4.LT.ZI(N)) GO TO 122                                          MAIN.325
  121 CONTINUE                                                           MAIN.326
      HI2=0.0                                                            MAIN.327
      HIMU2=0.0                                                          MAIN.328
      GO TO 123                                                          MAIN.329
  122 HI2=(HI(N)-HI(N-1))/(ZI(N)-ZI(N-1))*(Z4-ZI(N))+HI(N)               MAIN.330
      HIMU2=(HIMU(N)-HIMU(N-1))/(ZI(N)-ZI(N-1))*(Z4-ZI(N))+HIMU(N)       MAIN.331
  123 CD=RHO(J,1)*(Y(J+1,1)-Y(J,1))                                      MAIN.332
      COLDEN=COLDEN+CD                                                   MAIN.333
      TAU1=TAU1+CD*HI2                                                   MAIN.334
      TAU2=TAU2+CD*HIMU2/SQRT(E(J,1))                                    MAIN.335
  124 Z4=ELUM/(RHOZRO*(YZERO+0.5*(Y(J,1)+Y(J+1,1)))**2)                  MAIN.336
      IF(Z4.GT.ZI(1)) GO TO 125                                          MAIN.337
      HI2=1.0                                                            MAIN.338
      HIMU2=1.27154                                                      MAIN.339
      WRITE(6,50) J,I,Z4                                                 MAIN.340
      GO TO 128                                                          MAIN.341
  125 DO 126 N=2,51                                                      MAIN.342
      IF(Z4.LT.ZI(N)) GO TO 127                                          MAIN.343
  126 CONTINUE                                                           MAIN.344
      HI2=0.0                                                            MAIN.345
      HIMU2=0.0                                                          MAIN.346
      GO TO 128                                                          MAIN.347
  127 HI2=(HI(N)-HI(N-1))/(ZI(N)-ZI(N-1))*(Z4-ZI(N))+HI(N)               MAIN.348
      HIMU2=(HIMU(N)-HIMU(N-1))/(ZI(N)-ZI(N-1))*(Z4-ZI(N))+HIMU(N)       MAIN.349
  128 CD=RHOZRO*(Y(J+1,1)-Y(J,1))                                        MAIN.350
      C1=C1+CD                                                           MAIN.351
      TAU3=TAU3+CD*HI2                                                   MAIN.352
      TAU4=TAU4+CD*HIMU2/SQRT(E(J,1))                                    MAIN.353
  129 CONTINUE                                                           MAIN.354
      COLDEN=COLDEN/(1.298*1.66043E-24)                                  MAIN.355
      C1=C1/(1.298*1.66043E-24)                                          MAIN.356
      TAU1=2.6542E+06*TAU1                                               MAIN.357
      TAU3=2.6542E+06*TAU3                                               MAIN.358
      TAU2=2.7770E+16*TAU2                                               MAIN.359
      TAU4=2.7770E+16*TAU4                                               MAIN.360
```

```
C                                                                       MAIN.361
C*****PRINT OUT THE TABLE OF INITIAL CONDITIONS.                        MAIN.362
C                                                                       MAIN.363
 140  IF(ISTART.EQ.0) WRITE(6,40)                                       MAIN.364
      IF(ISTART.GE.1) WRITE(6,41) ISTART                                MAIN.365
      IF(IALL.EQ.0) WRITE(6,42)                                         MAIN.366
      IF(IALL.EQ.1) WRITE(6,43)                                         MAIN.367
      VSQ=VSQFR**2*(10./9.)*E(JMAX,1)                                   MAIN.368
      VSQRT=SQRT(VSQ)                                                   MAIN.369
      WRITE(6,44) IMAX,DT,IPRNT1,CQ,JMAX,TIME,ITAPE1,VSQRT,ICYCLE,      MAIN.370
     1EMIN,RATIOX,RATIOY,TIMLMT,DTLIM,DX,DY,MLIM,DYLIM,YZERO,DYMAX      MAIN.371
      IF(IRAD.GT.0.AND.ISTART.EQ.0) WRITE(6,45) TZERO,TC,ICENT1,ENZERO, MAIN.372
     1ENC,IRAD,RHOZRO,RHOC,EC,EZERO,VC,AZRO,AC,VCOA0                    MAIN.373
      IF(IRAD.GT.0.AND.ISTART.EQ.0.AND.ELUM.NE.0.0) WRITE(6,47) Z2,Z3   MAIN.374
      IF(IRAD.LE.0.AND.ISTART.EQ.0) WRITE(6,48) TZERO,ENZERO,RHOZRO,    MAIN.375
     1EZERO,AZRO                                                        MAIN.376
      IF(IRAD.LE.0.AND.ISTART.EQ.0.AND.ELUM.NE.0.0) WRITE(6,54) Z2      MAIN.377
      IF(ITAU.EQ.1.AND.IRAD.GT.0.AND.ISTART.EQ.0) WRITE(6,51) C1,       MAIN.378
     1COLDEN,TAU3,TAU1,TAU4,TAU2                                        MAIN.379
      IF(ITAU.EQ.1.AND.IRAD.LE.0.AND.ISTART.EQ.0) WRITE(6,52) C1,TAU3,  MAIN.380
     1TAU4                                                              MAIN.381
      WRITE(6,46) EL46,LINES,MASS,MOL                                   MAIN.382
C                                                                       MAIN.383
C*****CHOOSE THE DESIRED ACCELERATION/DENSITY ACCORDING TO THE VALUE     MAIN.384
C*****   OF THE PARAMETER LINES.                                        MAIN.385
C*****     LINES = 1 GIVES ACC/RHO FOR LINES + CONTINUUM                MAIN.386
C*****     LINES = 0 GIVES ACC/RHO FOR CONTINUUM ONLY                   MAIN.387
C*****     LINES = -1 GIVES ACC/RHO = 0                                 MAIN.388
C                                                                       MAIN.389
      GSMALL=4.181E+11                                                  MAIN.390
      GLARGE=2.000E+18                                                  MAIN.391
      IF(LINES.EQ.0) GSMALL=4.176E+11                                   MAIN.392
      IF(LINES.EQ.0) GLARGE=4.751E+17                                   MAIN.393
      IF(LINES.EQ.-1) ELUM=0.0                                          MAIN.394
      IF(LINES.NE.0) GO TO 146                                          MAIN.395
      DO 144 I=1,51                                                     MAIN.396
```

```
      GCL(I)=GC(I)                                                          MAIN.397
  144 CONTINUE                                                              MAIN.398
  146 CONTINUE                                                              MAIN.399
C                                                                           MAIN.400
C*****CALCULATE THE DEPENDENT INITIAL QUANTITIES: VOL,M,H,PPURE,P,Z.       MAIN.401
C*****ALSO CALCULATE MTOTAL,VTOTAL,EINT,EKINH,EKINV.                       MAIN.402
C*****INITIALIZE MDOT, DELV, HDOT, AND EDOT TO ZERO.                       MAIN.403
C                                                                           MAIN.404
      LEZ=IMAZ                                                              MAIN.405
      IF(ISTART.LT.1) ICODE=0                                               MAIN.406
      DY1=DY*RATIOY                                                         MAIN.407
      DTT2=2.0*DT                                                           MAIN.408
      DT22=0.5*DT                                                           MAIN.409
      DT222=DT*DT*10./9.                                                    MAIN.410
      CQ=0.5*CQ                                                             MAIN.411
      MTOTAL=0.0                                                            MAIN.412
      VTOTAL=0.0                                                            MAIN.413
      EINT=0.0                                                              MAIN.414
      EKINH=0.0                                                             MAIN.415
      EKINV=0.0                                                             MAIN.416
      EGRAV=0.0                                                             MAIN.417
      DO 160 I=1,IMAZ                                                       MAIN.418
      DXSQ(I)=PI*(X(I+1)-X(I))*(X(I+1)+X(I))                               MAIN.419
      PI2X(I)=PI*2.0*X(I+1)                                                 MAIN.420
      DELX(I)=X(I+1)-X(I)                                                   MAIN.421
      L=LMAZ1(I)                                                            MAIN.422
      DO 160 J=1,L                                                          MAIN.423
      MDOT(J,I)=0.0                                                         MAIN.424
      EDOT(J,I)=0.0                                                         MAIN.425
      HDOT(J,I)=0.0                                                         MAIN.426
      DELV(J,I)=0.0                                                         MAIN.427
      VOL(J,I)=DXSQ(I)*(Y(J+1,I)-Y(J,I))                                    MAIN.428
      M(J,I)=RHO(J,I)*VOL(J,I)                                              MAIN.429
      PPURE(J,I)=2./3.*E(J,I)*RHO(J,I)                                      MAIN.430
      P(J,I)=PPURE(J,I)+QL(J,I)                                             MAIN.431
      Z(J,I)=PPURE(J,I)+QE(J,I)                                             MAIN.432
```

```
      IF(J.LT.L) GO TO 158                                                  MAIN.433
      DELV(J+1,I)=0.0                                                       MAIN.434
      MDOT(J+1,I)=0.0                                                       MAIN.435
      VOL(J+1,I)=VOL(J,I)                                                   MAIN.436
      M(J+1,I)=RHO(J+1,I)*VOL(J+1,I)                                        MAIN.437
      P(J+1,I)=(2./3.)*RHO(J+1,I)*E(J+1,I)                                  MAIN.438
 158  H(J,I)=M(J,I)*U(J,I)                                                  MAIN.439
      MTOTAL=MTOTAL+M(J,I)                                                  MAIN.440
      VTOTAL=VTOTAL+VOL(J,I)                                                MAIN.441
      EINT=EINT+E(J,I)*M(J,I)                                               MAIN.442
      EKINV=EKINV+M(J,I)*(V(J,I)**2+V(J+1,I)**2)*0.25                       MAIN.443
      EGRAV=EGRAV-GM*M(J,I)/SQRT((YZERO+0.5*(Y(J+1,I)+Y(J,I)))**2           MAIN.444
     1+0.25*(X(I+1)+X(I))**2)                                               MAIN.445
      EKINH=EKINH+M(J,I)*(U(J,I)**2)*0.5                                    MAIN.446
 160  CONTINUE                                                              MAIN.447
      ETOTAL=EINT+EKINV+EKINH+EGRAV                                         MAIN.448
C                                                                           MAIN.449
C*****PRINT OUT THE INITIAL DATA.  ************************************   MAIN.450
C                                                                           MAIN.451
      WRITE(6,8) TIME,DT,ICYCLE,ICODE,JW,IW,WITMAX,                         MAIN.452
     1(I,LM1(I),LMAZ1(I),X(I),I=1,IMAZ)                                     MAIN.453
      WRITE(6,9) IMAX,X(IMAX),LEZ                                           MAIN.454
      WRITE(6,7) EINT,EKINV,EKINH,EGRAV,ETOTAL,MTOTAL,VTOTAL                MAIN.455
      CALL OUT(IMAZ,JMAX,LM1,Y,V,U,RHO,E,QE,QL,PPURE,M)                     MAIN.456
      CALL PLOTER(IMAZ,JMAX,IMAX,LM1,LMAZ1,X,Y,V,U,RHO,E,PPURE,             MAIN.457
     1MDOT,HDOT,DELV,EDOT)                                                  MAIN.458
C                                                                           MAIN.459
C*****THIS IS THE START OF THE MAIN LOOP FOR DOING THE HYDRODYNAMICS.       MAIN.460
C*****IT RUNS FROM HERE THROUGH STATEMENT 420.                              MAIN.461
C                                                                           MAIN.462
 170  NSAVE=NSAVE+1                                                         MAIN.463
      IF(NSAVE.LT.4) GO TO 220                                              MAIN.464
      NSAVE=0                                                               MAIN.465
C                                                                           MAIN.466
C*****LOOP 188 DOES THE REZONING.  IT COMBINES CELLS THAT HAVE MASS         MAIN.467
C*****LESS THAN MLIM AND/OR Y DIMENSION LESS THAN DYLIM WITH AN             MAIN.468
```

```
C*****ADJOINING CELL.                                                    MAIN.469
C                                                                        MAIN.470
      DO 188 I=1,LEZ                                                     MAIN.471
      LMAZ=LM1(I)                                                        MAIN.472
      DO 174 N=2,LMAZ                                                    MAIN.473
      J=N-1                                                              MAIN.474
      L=N+1                                                              MAIN.475
      IF(Y(N,I)-Y(J,I).LT.DYLIM) GO TO 176                               MAIN.476
      IF(M(J,I).GT.MLIM) GO TO 174                                       MAIN.477
      WRITE(6,10)                                                        MAIN.478
      GO TO 176                                                          MAIN.479
 174  CONTINUE                                                           MAIN.480
      GO TO 188                                                          MAIN.481
C                                                                        MAIN.482
C*****COMBINE CELLS (N-1,I) AND (N,I).  **********************************MAIN.483
C                                                                        MAIN.484
 176  M12=M(J,I)+M(N,I)                                                  MAIN.485
      X1=1.0/M12                                                         MAIN.486
      Y(N,I)=Y(L,I)                                                      MAIN.487
      IF(V(N,I)*V(L,I).LT.0.0) GO TO 178                                 MAIN.488
      TEMP=((M12*V(N,I)**2+(M(N,I)+M(L,I))*V(L,I)**2                     MAIN.489
     1-M(N,I)*V(J,I)**2)/(M12+M(L,I)))                                   MAIN.490
      IF(TEMP.LT.0.0) GO TO 178                                          MAIN.491
      IF(V(N,I).GT.0.0.OR.V(L,I).GT.0.0) V(N,I)=SQRT(TEMP)               MAIN.492
      IF(V(N,I).LE.0.0.OR.V(L,I).LE.0.0)                                 MAIN.493
     1V(N,I)=-SQRT(TEMP)                                                 MAIN.494
      GO TO 180                                                          MAIN.495
 178  V(N,I)=(M12*V(N,I)+(M(N,I)+M(L,I))*V(L,I)-M(N,I)*V(J,I))           MAIN.496
     1/(M12+M(L,I))                                                      MAIN.497
 180  IF(U(J,I)*U(N,I).LT.0.0) GO TO 182                                 MAIN.498
      IF(U(J,I).GT.0.0.OR.U(N,I).GT.0.0)                                 MAIN.499
     1U(J,I)=SQRT((M(J,I)*U(J,I)**2+M(N,I)*U(N,I)**2)*X1)                MAIN.500
      IF(U(J,I).LE.0.0.OR.U(N,I).LE.0.0)                                 MAIN.501
     1U(J,I)=-SQRT((M(J,I)*U(J,I)**2+M(N,I)*U(N,I)**2)*X1)               MAIN.502
      GO TO 184                                                          MAIN.503
 182  U(J,I)=(M(J,I)*U(J,I)+M(N,I)*U(N,I))*X1                            MAIN.504
```

```
184   E(J,I)=(E(J,I)*M(J,I)+E(N,I)*M(N,I))*X1                    MAIN.505
      M(J,I)=M12                                                 MAIN.506
      VOL(J,I)=VOL(J,I)+VOL(N,I)                                 MAIN.507
      RHO(J,I)=M(J,I)/VOL(J,I)                                   MAIN.508
      H(J,I)=M(J,I)*U(J,I)                                       MAIN.509
      QE(J,I)=AMIN1(QE(J,I),QE(N,I))                             MAIN.510
      QL(J,I)=AMIN1(QL(J,I),QL(N,I))                             MAIN.511
      Z(J,I)=QE(J,I)+2./3.*E(J,I)*RHO(J,I)                       MAIN.512
      P(J,I)=QL(J,I)+2./3.*E(J,I)*RHO(J,I)                       MAIN.513
      LL=LMAZ1(I)                                                MAIN.514
      DO 186 N=L,LL                                              MAIN.515
      Y(N,I)=Y(N+1,I)                                            MAIN.516
      V(N,I)=V(N+1,I)                                            MAIN.517
      U(N-1,I)=U(N,I)                                            MAIN.518
      RHO(N-1,I)=RHO(N,I)                                        MAIN.519
      E(N-1,I)=E(N,I)                                            MAIN.520
      QE(N-1,I)=QE(N,I)                                          MAIN.521
      QL(N-1,I)=QL(N,I)                                          MAIN.522
      P(N-1,I)=P(N,I)                                            MAIN.523
      Z(N-1,I)=Z(N,I)                                            MAIN.524
      M(N-1,I)=M(N,I)                                            MAIN.525
      H(N-1,I)=H(N,I)                                            MAIN.526
186   VOL(N-1,I)=VOL(N,I)                                        MAIN.527
      Y(LL+1,I)=Y(LL+1,I)+DY1                                    MAIN.528
      V(LL+1,I)=0.0                                              MAIN.529
      U(LL,I)=0.0                                                MAIN.530
      RHO(LL,I)=RHO(JMAX,IMAZ)                                   MAIN.531
      E(LL,I)=E(JMAX,IMAZ)                                       MAIN.532
      QE(LL,I)=0.0                                               MAIN.533
      QL(LL,I)=0.0                                               MAIN.534
      P(LL,I)=(2./3.)*RHO(LL,I)*E(LL,I)                          MAIN.535
      Z(LL,I)=P(LL,I)                                            MAIN.536
      VOL(LL,I)=VOL(LL+1,I)                                      MAIN.537
      M(LL,I)=M(LL+1,I)                                          MAIN.538
      H(LL,I)=0.0                                                MAIN.539
      LM1(I)=LMAZ-1                                              MAIN.540
```

```
      EREZON=EREZON+M(LL,I)*(E(LL,I)-GM/SQRT((YZERO+0.5*(Y(LL+1,I)+Y(LL,    MAIN.541
     1I)))**2+0.25*(X(I+1)+X(I))**2))                                       MAIN.542
  188 CONTINUE                                                              MAIN.543
C                                                                           MAIN.544
C*****LOOP 208 SPLITS UP BIG CELLS WHERE EVER THEY MAY BE TO INCREASE       MAIN.545
C*****THE RESOLUTION IN EXPANDING PORTIONS OF THE GRID.                     MAIN.546
C                                                                           MAIN.547
      DO 208 I=1,LEZ                                                        MAIN.548
      LMAZ=LM1(I)                                                           MAIN.549
      DO 192 N=1,LMAZ                                                       MAIN.550
      L=N+1                                                                 MAIN.551
      IF(Y(N+1,I)-Y(N,I).GT.DYMAX) GO TO 194                                MAIN.552
  192 CONTINUE                                                              MAIN.553
      GO TO 208                                                             MAIN.554
  194 LL=LMAZ1(I)                                                           MAIN.555
      LM=LM1(I)                                                             MAIN.556
      LMLL=LL-L                                                             MAIN.557
      EUNZON=EUNZON+M(LL,I)*(E(LL,I)-GM/SQRT((YZERO+0.5*(Y(LL+1,I)+Y(LL,    MAIN.558
     1I)))**2+0.25*(X(I+1)+X(I))**2))                                       MAIN.559
      IF(JMAX-LL.LT.2) GO TO 195                                            MAIN.560
      LMAZ1(I)=LL+1                                                         MAIN.561
      Y(LL+2,I)=Y(LL+1,I)                                                   MAIN.562
      V(LL+2,I)=V(LL+1,I)                                                   MAIN.563
      U(LL+1,I)=U(LL,I)                                                     MAIN.564
      E(LL+1,I)=E(LL,I)                                                     MAIN.565
      M(LL+1,I)=M(LL,I)                                                     MAIN.566
      H(LL+1,I)=H(LL,I)                                                     MAIN.567
      P(LL+1,I)=P(LL,I)                                                     MAIN.568
      Z(LL+1,I)=Z(LL,I)                                                     MAIN.569
      RHO(LL+1,I)=RHO(LL,I)                                                 MAIN.570
      QE(LL+1,I)=QE(LL,I)                                                   MAIN.571
      QL(LL+1,I)=QL(LL,I)                                                   MAIN.572
      VOL(LL+1,I)=VOL(LL,I)                                                 MAIN.573
      GO TO 196                                                             MAIN.574
  195 IF(LM1(I).LT.LL) GO TO 196                                            MAIN.575
      WRITE(6,26) N,I                                                       MAIN.576
```

```
      GO TO 208                                                          MAIN.577
  196 LM1(I)=LM+1                                                        MAIN.578
      DO 198 J=1,LMLL                                                    MAIN.579
      Y(LL+2-J,I)=Y(LL+1-J,I)                                            MAIN.580
      V(LL+2-J,I)=V(LL+1-J,I)                                            MAIN.581
      U(LL+1-J,I)=U(LL-J,I)                                              MAIN.582
      RHO(LL+1-J,I)=RHO(LL-J,I)                                          MAIN.583
      E(LL+1-J,I)=E(LL-J,I)                                              MAIN.584
      QE(LL+1-J,I)=QE(LL-J,I)                                            MAIN.585
      QL(LL+1-J,I)=QL(LL-J,I)                                            MAIN.586
      M(LL+1-J,I)=M(LL-J,I)                                              MAIN.587
      VOL(LL+1-J,I)=VOL(LL-J,I)                                          MAIN.588
      H(LL+1-J,I)=H(LL-J,I)                                              MAIN.589
      P(LL+1-J,I)=P(LL-J,I)                                              MAIN.590
      Z(LL+1-J,I)=Z(LL-J,I)                                              MAIN.591
  198 CONTINUE                                                           MAIN.592
      Y(L+1,I)=Y(L,I)                                                    MAIN.593
      Y(L,I)=0.5*(Y(L,I)+Y(L-1,I))                                       MAIN.594
      M(L,I)=0.5*M(L-1,I)                                                MAIN.595
      M(L-1,I)=M(L,I)                                                    MAIN.596
      E(L,I)=E(L-1,I)                                                    MAIN.597
      RHO(L,I)=RHO(L-1,I)                                                MAIN.598
      U(L,I)=U(L-1,I)                                                    MAIN.599
      V(L+1,I)=V(L,I)                                                    MAIN.600
      IF(V(L-1,I)*V(L,I).GE.0.0) GO TO 200                               MAIN.601
      GO TO 204                                                          MAIN.602
  200 IF(V(L,I).GT.0.0) GO TO 202                                        MAIN.603
      V(L,I)=-SQRT(0.5*(V(L-1,I)**2+V(L,I)**2))                          MAIN.604
      GO TO 206                                                          MAIN.605
  202 V(L,I)=SQRT(0.5*(V(L-1,I)**2+V(L,I)**2))                           MAIN.606
      GO TO 206                                                          MAIN.607
  204 V(L,I)=0.5*(V(L,I)+V(L-1,I))                                       MAIN.608
  206 H(L,I)=M(L,I)*U(L,I)                                               MAIN.609
      H(L-1,I)=H(L,I)                                                    MAIN.610
      VOL(L,I)=0.5*VOL(L-1,I)                                            MAIN.611
      VOL(L-1,I)=VOL(L,I)                                                MAIN.612
```

```
      QE(L,I)=QE(L-1,I)                                                 MAIN.613
      QL(L,I)=AMAX1(0.0,CQ*RHO(L,I)*SQRT(10./9.*E(L,I))*(V(L,I)-V(L+1,I)  MAIN.614
     1))                                                                MAIN.615
      QL(L-1,I)=AMAX1(0.0,CQ*RHO(L-1,I)*SQRT(10./9.*E(L-1,I))*(V(L-1,I)-  MAIN.616
     1V(L,I)))                                                          MAIN.617
      P(L,I)=(2./3.)*E(L,I)*RHO(L,I)+QL(L,I)                            MAIN.618
      P(L-1,I)=(2./3.)*E(L-1,I)*RHO(L-1,I)+QL(L-1,I)                    MAIN.619
      Z(L,I)=Z(L-1,I)                                                   MAIN.620
 208  CONTINUE                                                          MAIN.621
C                                                                       MAIN.622
C*****LOOP 210 SAVES THE INDEPENDENT VARIABLES IN THE 2H VARIABLES FOR  MAIN.623
C*****RESTARTING WHEN WITMAX .GT. 0.6.                                 MAIN.624
C                                                                       MAIN.625
      DT2H=DT                                                           MAIN.626
      TIME2H=TIME                                                       MAIN.627
      ICYC2H=ICYCLE                                                     MAIN.628
      DO 210 I=1,LEZ                                                    MAIN.629
      L=LM1(I)                                                          MAIN.630
      Y2H(1,I)=Y(1,I)                                                   MAIN.631
      V2H(1,I)=V(1,I)                                                   MAIN.632
      DO 210 J=1,L                                                      MAIN.633
      Y2H(J+1,I)=Y(J+1,I)                                               MAIN.634
      V2H(J+1,I)=V(J+1,I)                                               MAIN.635
      U2H(J,I)=U(J,I)                                                   MAIN.636
      RHO2H(J,I)=RHO(J,I)                                               MAIN.637
      E2H(J,I)=E(J,I)                                                   MAIN.638
      QE2H(J,I)=QE(J,I)                                                 MAIN.639
 210  QL2H(J,I)=QL(J,I)                                                 MAIN.640
C                                                                       MAIN.641
C*****LOOP 280 CALCULATES THE TIME RATE OF CHANGE OF M,P,H, AND E       MAIN.642
C*****(IE, MDOT, DELV, HDOT, AND EDOT) FOR EACH CELL.                  MAIN.643
C                                                                       MAIN.644
 220  DO 280 I=1,IMAZ                                                  MAIN.645
      K=1                                                               MAIN.646
      LMAZ=LM1(I)                                                       MAIN.647
      LMAY=LM1(I+1)+1                                                   MAIN.648
```

```
      DO 280 J=1,LMAZ                                                    MAIN.649
      IF(I.GT.IMAY) GO TO 270                                            MAIN.650
C                                                                        MAIN.651
C*****LOOP 230 DETERMINES WHICH CELLS ADJOIN CELL (J,I).  **************  MAIN.652
C                                                                        MAIN.653
      DO 230 L=K,LMAY                                                    MAIN.654
      IF(Y(L,I+1).GE.Y(J+1,I)) GO TO 240                                 MAIN.655
  230 CONTINUE                                                           MAIN.656
      L=LMAY                                                             MAIN.657
  240 L=L-1                                                              MAIN.658
      DO 260 N=K,L                                                       MAIN.659
C                                                                        MAIN.660
C*****SET UP THE ARTIFICIAL CELL BOUNDARIES.  ***************************  MAIN.661
C                                                                        MAIN.662
      VK4=AMIN1(Y(J+1,I),Y(N+1,I+1))-AMAX1(Y(J,I),Y(N,I+1))              MAIN.663
      IF(VK4.LE.0.0) GO TO 260                                           MAIN.664
      M1=RHO(J,I)*DXSQ(I)*VK4                                            MAIN.665
      M2=RHO(N,I+1)*DXSQ(I+1)*VK4                                        MAIN.666
      CA=PI2X(I)*VK4                                                     MAIN.667
      M12=1.0/(M1+M2)                                                    MAIN.668
      X3=CA*(Z(J,I)-Z(N,I+1))*M12                                        MAIN.669
      CA=CA*((M1*U(J,I)+M2*U(N,I+1))*M12+X3*DT22)                        MAIN.670
      IF(CA.LT.0.0) GO TO 250                                            MAIN.671
C                                                                        MAIN.672
C*****MASS FLOW FROM CELL (J,I) TO CELL (N,I+1).  **********************  MAIN.673
C                                                                        MAIN.674
      X1=RHO(J,I)*CA                                                     MAIN.675
      MDOT(J,I)=MDOT(J,I)-X1                                             MAIN.676
      MDOT(N,I+1)=MDOT(N,I+1)+X1                                         MAIN.677
      VBAR=0.5*(V(J,I)+V(J+1,I))                                         MAIN.678
      X2=X1*E(J,I)                                                       MAIN.679
      EDOT(N,I+1)=EDOT(N,I+1)+0.5*X1*((0.5*(V(N,I+1)+V(N+1,I+1))-VBAR)   MAIN.680
     1**2+(U(N,I+1)-U(J,I))**2)+X2+Z(N,I+1)*CA                           MAIN.681
      EDOT(J,I)=EDOT(J,I)-X2-Z(J,I)*CA                                   MAIN.682
      VBAR=0.5*X1*VBAR                                                   MAIN.683
      X1=X1*U(J,I)                                                       MAIN.684
```

```
      HDOT(J,I)=HDOT(J,I)+M1*X3-X1                                          MAIN.685
      HDOT(N,I+1)=HDOT(N,I+1)+M2*X3+X1                                      MAIN.686
      IF(J.GT.1) GO TO 247                                                  MAIN.687
      DELV(2,I)=DELV(2,I)-2.0*VBAR                                          MAIN.688
      GO TO 248                                                             MAIN.689
 247  DELV(J,I)=DELV(J,I)-VBAR                                              MAIN.690
      DELV(J+1,I)=DELV(J+1,I)-VBAR                                          MAIN.691
 248  IF(N.GT.1) GO TO 249                                                  MAIN.692
      DELV(2,I+1)=DELV(2,I+1)+2.0*VBAR                                      MAIN.693
      GO TO 260                                                             MAIN.694
 249  DELV(N,I+1)=DELV(N,I+1)+VBAR                                          MAIN.695
      DELV(N+1,I+1)=DELV(N+1,I+1)+VBAR                                      MAIN.696
      GO TO 260                                                             MAIN.697
C                                                                           MAIN.698
C*****MASS FLOW FROM CELL (N,I+1) TO CELL (J,I).  **********************    MAIN.699
C                                                                           MAIN.700
 250  X1=-RHO(N,I+1)*CA                                                     MAIN.701
      MDOT(J,I)=MDOT(J,I)+X1                                                MAIN.702
      MDOT(N,I+1)=MDOT(N,I+1)-X1                                            MAIN.703
      VBAR=0.5*(V(N,I+1)+V(N+1,I+1))                                        MAIN.704
      X2=X1*E(N,I+1)                                                        MAIN.705
      EDOT(J,I)=EDOT(J,I)+0.5*X1*((0.5*(V(J,I)+V(J+1,I))-VBAR)**2           MAIN.706
     1+(U(J,I)-U(N,I+1))**2)+X2-Z(J,I)*CA                                   MAIN.707
      EDOT(N,I+1)=EDOT(N,I+1)-X2+Z(N,I+1)*CA                                MAIN.708
      VBAR=0.5*X1*VBAR                                                      MAIN.709
      X1=X1*U(N,I+1)                                                        MAIN.710
      HDOT(N,I+1)=HDOT(N,I+1)+M2*X3-X1                                      MAIN.711
      HDOT(J,I)=HDOT(J,I)+M1*X3+X1                                          MAIN.712
      IF(J.GT.1) GO TO 257                                                  MAIN.713
      DELV(2,I)=DELV(2,I)+2.0*VBAR                                          MAIN.714
      GO TO 258                                                             MAIN.715
 257  DELV(J,I)=DELV(J,I)+VBAR                                              MAIN.716
      DELV(J+1,I)=DELV(J+1,I)+VBAR                                          MAIN.717
 258  IF(N.GT.1) GO TO 259                                                  MAIN.718
      DELV(2,I+1)=DELV(2,I+1)-2.0*VBAR                                      MAIN.719
      GO TO 260                                                             MAIN.720
```

```
 259  DELV(N,I+1)=DELV(N,I+1)-VBAR                                          MAIN.721
      DELV(N+1,I+1)=DELV(N+1,I+1)-VBAR                                      MAIN.722
 260  CONTINUE                                                              MAIN.723
      K=L                                                                   MAIN.724
      IF(Y(L+1,I+1).NE.Y(J+1,I)) GO TO 270                                  MAIN.725
      IF(L.LT.LMAY-1) K=K+1                                                 MAIN.726
C                                                                           MAIN.727
C*****EXTERNAL ACCELERATIONS ARE ADDED IN HERE.                             MAIN.728
C                                                                           MAIN.729
 270  X1=0.5*(X(I+1)+X(I))                                                  MAIN.730
      X3=X1**2+(YZERO+0.5*(Y(J+1,I)+Y(J,I)))**2                             MAIN.731
      Z2=ELUM/(RHO(J,I)*X3)                                                 MAIN.732
      IF(Z2.GT.ZI(1)) GO TO 271                                             MAIN.733
      G=GLARGE*Z2                                                           MAIN.734
      GO TO 274                                                             MAIN.735
 271  DO 272 N=2,51                                                         MAIN.736
      IF(Z2.LT.ZI(N)) GO TO 273                                             MAIN.737
 272  CONTINUE                                                              MAIN.738
      G=GSMALL*Z2                                                           MAIN.739
      GO TO 274                                                             MAIN.740
 273  G=(GCL(N)-GCL(N-1))/(ZI(N)-ZI(N-1))*(Z2-ZI(N))+GCL(N)                 MAIN.741
 274  HDOT(J,I)=HDOT(J,I)+(G*RHO(J,I)-GM/X3)*M(J,I)*X1/SQRT(X3)             MAIN.742
      X2=YZERO+Y(J+1,I)                                                     MAIN.743
      X3=X1**2+X2**2                                                        MAIN.744
      Z2=ELUM/((RHO(J,I)+RHO(J+1,I))*0.5*X3)                                MAIN.745
      IF(Z2.GT.ZI(1)) GO TO 275                                             MAIN.746
      G=GLARGE*Z2                                                           MAIN.747
      GO TO 278                                                             MAIN.748
 275  DO 276 N=2,51                                                         MAIN.749
      IF(Z2.LT.ZI(N)) GO TO 277                                             MAIN.750
 276  CONTINUE                                                              MAIN.751
      G=GSMALL*Z2                                                           MAIN.752
      GO TO 278                                                             MAIN.753
 277  G=(GCL(N)-GCL(N-1))/(ZI(N)-ZI(N-1))*(Z2-ZI(N))+GCL(N)                 MAIN.754
 278  DELV(J+1,I)=DELV(J+1,I)+(P(J,I)-P(J+1,I))*DXSQ(I)+(G*(M(J+1,I)+       MAIN.755
     1M(J,I))/(VOL(J+1,I)+VOL(J,I))-GM/X3)*0.5*(M(J+1,I)+M(J,I))*X2/        MAIN.756
```

```
     1SQRT(X3)                                                          MAIN.757
 280  CONTINUE                                                          MAIN.758
      WITMAX=0.0                                                        MAIN.759
C                                                                       MAIN.760
C*****LOOP 305 ADVANCES THE HYDRODYNAMICS ONE TIME STEP.  **************MAIN.761
C                                                                       MAIN.762
      DO 305 I=1,LEZ                                                    MAIN.763
      LMAZ=LM1(I)                                                       MAIN.764
      K=1                                                               MAIN.765
      DO 305 J=1,LMAZ                                                   MAIN.766
      IF(J.GT.1) GO TO 300                                              MAIN.767
      MOLD2=M(1,I)                                                      MAIN.768
      M(1,I)=MOLD2+DT*MDOT(1,I)                                         MAIN.769
 300  MOLD1=MOLD2                                                       MAIN.770
      MOLD2=M(J+1,I)                                                    MAIN.771
      VOLD=V(J+1,I)                                                     MAIN.772
      IF(J.GE.LMAZ) GO TO 302                                           MAIN.773
      M(J+1,I)=MOLD2+DT*MDOT(J+1,I)                                     MAIN.774
      V(J+1,I)=((MOLD1+MOLD2)*VOLD+DTT2*DELV(J+1,I))/(M(J,I)+M(J+1,I))  MAIN.775
      Y(J+1,I)=Y(J+1,I)+DT22*(VOLD+V(J+1,I))                            MAIN.776
 302  DELV(J+1,I)=0.0                                                   MAIN.777
      VOLOLD=VOL(J,I)                                                   MAIN.778
      DELY=Y(J+1,I)-Y(J,I)                                              MAIN.779
      VOL(J,I)=DXSQ(I)*DELY                                             MAIN.780
      DVOL=VOL(J,I)-VOLOLD                                              MAIN.781
      X2=1.0/VOL(J,I)                                                   MAIN.782
      IF(J.LT.2) GO TO 306                                              MAIN.783
      RHO(J,I)=M(J,I)*X2                                                MAIN.784
      X3=1.0/M(J,I)                                                     MAIN.785
      E(J,I)=AMAX1((E(J,I)*MOLD1+DT*EDOT(J,I)-P(J,I)*DVOL)*X3,EMIN)     MAIN.786
      GO TO 307                                                         MAIN.787
 306  M(1,I)=RHO(1,I)*VOL(1,I)                                          MAIN.788
      X3=1.0/M(1,I)                                                     MAIN.789
 307  EDOT(J,I)=0.0                                                     MAIN.790
      H(J,I)=H(J,I)+DT*HDOT(J,I)                                        MAIN.791
      HDOT(J,I)=0.0                                                     MAIN.792
```

```
      U(J,I)=H(J,I)*X3                                                  MAIN.793
      ASQRT=SQRT(10./9.*E(J,I))                                         MAIN.794
      QE(J,I)=AMAX1(0.0,CQ*ASQRT*MDOT(J,I)/(PI2X(I)*DELY))              MAIN.795
      MDOT(J,I)=0.0                                                     MAIN.796
      QL(J,I)=AMAX1(0.0,CQ*ASQRT*RHO(J,I)*(V(J,I)-V(J+1,I)))            MAIN.797
      PPURE(J,I)=(2./3.)*RHO(J,I)*E(J,I)                                MAIN.798
      P(J,I)=PPURE(J,I)+QL(J,I)                                         MAIN.799
      Z(J,I)=PPURE(J,I)+QE(J,I)                                         MAIN.800
      WITENO=DT222*E(J,I)/((AMIN1(DELY,DELX(I)))**2)                    MAIN.801
     1+4.0*(ABS((MOLD1-M(J,I))*X3)+ABS(DVOL*X2))                        MAIN.802
      IF(WITENO.LE.WITMAX) GO TO 305                                    MAIN.803
      IW=I                                                              MAIN.804
      JW=J                                                              MAIN.805
      WITMAX=WITENO                                                     MAIN.806
      IF(WITMAX.GT.0.6) GO TO 430                                       MAIN.807
  305 CONTINUE                                                          MAIN.808
C                                                                       MAIN.809
C*****ADJUST THE TIME STEP AND ADVANCE THE COUNTER QUANTITIES.  ********MAIN.810
C                                                                       MAIN.811
      TIME=TIME+DT                                                      MAIN.812
      DTS=DT                                                            MAIN.813
      IF(WITMAX.GT.0.20) GO TO 360                                      MAIN.814
      DT=1.5*DT                                                         MAIN.815
      DTT2=2.0*DT                                                       MAIN.816
      DT22=0.5*DT                                                       MAIN.817
      DT222=DT*DT*10./9.                                                MAIN.818
  360 IPRINT=IPRINT+1                                                   MAIN.819
      ITAPE=ITAPE+1                                                     MAIN.820
      ICYCLE=ICYCLE+1                                                   MAIN.821
C                                                                       MAIN.822
C*****CHECK TO SEE IF THE HYDRODYNAMICS HAS EXPANDED INTO ANY NEW CELLS.MAIN.823
C                                                                       MAIN.824
      IF(IALL.GT.0) GO TO 385                                           MAIN.825
  368 DO 380 I=1,LEZ                                                    MAIN.826
      L=LM1(I)                                                          MAIN.827
      IF(V(L-2,I)**2+U(L-3,I)**2.LT.VSQ) GO TO 380                      MAIN.828
```

```
      IF(L.GT.LMAZ1(I)-2) GO TO 370                                      MAIN.829
      LM1(I)=L+1                                                         MAIN.830
      NSAVE=4                                                            MAIN.831
      GO TO 380                                                          MAIN.832
  370 CONTINUE                                                           MAIN.833
      WRITE(6,58) TIME,ICYCLE,ICODE                                      MAIN.834
      WRITE(8) TIME,DTS,ICYCLE,IMAZ,JMAX,LEZ,ICODE,MODEL                 MAIN.835
      WRITE(8) LM1,LMAZ1,X,Y,V,U,RHO,E,QE,QL                             MAIN.836
      CALL ADJUST(IMAZ,JMAX,IMAX,LM1,LMAZ1,X,Y,V,U,RHO,E,QE,QL,M,VOL,H,  MAIN.837
     1PPURE,P,Z)                                                         MAIN.838
      NSAVE=4                                                            MAIN.839
      ICODE=ICODE+1                                                      MAIN.840
      IPRINT=IPRNT1                                                      MAIN.841
      ITAPE=ITAPE1                                                       MAIN.842
  380 CONTINUE                                                           MAIN.843
C                                                                        MAIN.844
C*****CHECK THE TIME REMAINING IN THIS JOB.  ****************************MAIN.845
C                                                                        MAIN.846
  385 CALL SECOND(X1)                                                    MAIN.847
      IF(X1.GT.TIMLMT) GO TO 450                                         MAIN.848
C                                                                        MAIN.849
C*****TO PUT IT ON TAPE, OR NOT TO PUT IT ON TAPE. THAT IS THE QUESTION. MAIN.850
C                                                                        MAIN.851
  390 IF(ITAPE.LT.ITAPE1) GO TO 400                                      MAIN.852
      WRITE(8) TIME,DTS,ICYCLE,IMAZ,JMAX,LEZ,ICODE,MODEL                 MAIN.853
      WRITE(8) LM1,LMAZ1,X,Y,V,U,RHO,E,QE,QL                             MAIN.854
      ITAPE=0                                                            MAIN.855
C                                                                        MAIN.856
C*****TO PRINT, OR NOT TO PRINT, THAT IS NOW THE QUESTION.  ************MAIN.857
C                                                                        MAIN.858
  400 IF(IPRINT.LT.IPRNT1) GO TO 170                                     MAIN.859
      IPRINT=0                                                           MAIN.860
C                                                                        MAIN.861
C*****LOOP 410 CALCULATES THE VARIOUS ENERGIES AND THE MASS OF THE       MAIN.862
C*****SYSTEM.  IT ALSO CALCULATES THE OPTICAL DEPTHS IF ITAU = 1.        MAIN.863
C                                                                        MAIN.864
```

```
      MTOTAL=0.0                                                                MAIN.865
      VTOTAL=0.0                                                                MAIN.866
      EINT=0.0                                                                  MAIN.867
      EKINH=0.0                                                                 MAIN.868
      EKINV=0.0                                                                 MAIN.869
      EGRAV=0.0                                                                 MAIN.870
      TAU1=0.0                                                                  MAIN.871
      TAU2=0.0                                                                  MAIN.872
      COLDEN=0.0                                                                MAIN.873
      DO 410 I=1,IMAZ                                                           MAIN.874
      LMAZ=LMAZ1(I)                                                             MAIN.875
      L=LM1(I)                                                                  MAIN.876
      DO 410 J=1,LMAZ                                                           MAIN.877
      IF(I.NE.1.OR.ITAU.EQ.0.OR.J.GT.L) GO TO 405                               MAIN.878
      Z2=ELUM/(RHO(J,1)*(YZERO+0.5*(Y(J,1)+Y(J+1,1)))**2)                       MAIN.879
      IF(Z2.GT.ZI(1)) GO TO 401                                                 MAIN.880
      HI2=1.0                                                                   MAIN.881
      HIMU2=1.27154                                                             MAIN.882
      WRITE(6,50) J,I,Z2                                                        MAIN.883
      GO TO 404                                                                 MAIN.884
401   DO 402 N=2,51                                                             MAIN.885
      IF(Z2.LT.ZI(N)) GO TO 403                                                 MAIN.886
402   CONTINUE                                                                  MAIN.887
      HI2=0.0                                                                   MAIN.888
      HIMU2=0.0                                                                 MAIN.889
      GO TO 404                                                                 MAIN.890
403   HI2=(HI(N)-HI(N-1))/(ZI(N)-ZI(N-1))*(Z2-ZI(N))+HI(N)                      MAIN.891
      HIMU2=(HIMU(N)-HIMU(N-1))/(ZI(N)-ZI(N-1))*(Z2-ZI(N))+HIMU(N)              MAIN.892
404   CD=RHO(J,1)*(Y(J+1,1)-Y(J,1))                                             MAIN.893
      COLDEN=COLDEN+CD                                                          MAIN.894
      TAU1=TAU1+CD*HI2                                                          MAIN.895
      TAU2=TAU2+CD*HIMU2/SQRT(E(J,1))                                           MAIN.896
405   CONTINUE                                                                  MAIN.897
      MTOTAL=MTOTAL+M(J,I)                                                      MAIN.898
      VTOTAL=VTOTAL+VOL(J,I)                                                    MAIN.899
      EINT=EINT+M(J,I)*E(J,I)                                                   MAIN.900
```

```
      EKINH=EKINH+M(J,I)*U(J,I)**2                                      MAIN.901
      EGRAV=EGRAV-M(J,I)/SQRT((YZERO+0.5*(Y(J+1,I)+Y(J,I)))**2          MAIN.902
     1+0.25*(X(I+1)+X(I))**2)                                           MAIN.903
 410  EKINV=EKINV+M(J,I)*(V(J,I)**2+V(J+1,I)**2)                        MAIN.904
      EKINH=EKINH*0.5                                                   MAIN.905
      EKINV=EKINV*0.25                                                  MAIN.906
      EGRAV=EGRAV*GM                                                    MAIN.907
      ETOTAL=EINT+EKINV+EKINH+EGRAV                                     MAIN.908
      EGRAND=ETOTAL-EREZON+EUNZON+ECHOP                                 MAIN.909
C                                                                       MAIN.910
C*****PRINT OUT THE HYDRODYNAMIC QUANTITIES.  **************************MAIN.911
C                                                                       MAIN.912
      WRITE(6,8) TIME,DTS,ICYCLE,ICODE,JW,IW,WITMAX,                    MAIN.913
     1(I,LM1(I),LMAZ1(I),X(I),I=1,IMAZ)                                 MAIN.914
      WRITE(6,9) IMAX,X(IMAX),LEZ                                       MAIN.915
      WRITE(6,7) EINT,EKINV,EKINH,EGRAV,ETOTAL,MTOTAL,VTOTAL            MAIN.916
      WRITE(6,57) EGRAND,EREZON,EUNZON,ECHOP                            MAIN.917
      IF(ITAU.EQ.0) GO TO 415                                           MAIN.918
      COLDEN=COLDEN/(1.298*1.66043E-24)                                 MAIN.919
      TAU1=2.6542E+06*TAU1                                              MAIN.920
      TAU2=2.7770E+16*TAU2                                              MAIN.921
      WRITE(6,49) COLDEN,TAU1,TAU2                                      MAIN.922
 415  CONTINUE                                                          MAIN.923
      CALL OUT(IMAZ,JMAX,LM1,Y,V,U,RHO,E,QE,QL,PPURE,M)                 MAIN.924
      CALL PLOTER(IMAZ,JMAX,IMAX,LM1,LMAZ1,X,Y,V,U,RHO,E,PPURE,         MAIN.925
     1MDOT,HDOT,DELV,EDOT)                                              MAIN.926
 420  IF(NOUT.LT.2) GO TO 170                                           MAIN.927
      STOP                                                              MAIN.928
C                                                                       MAIN.929
C*****FROM HERE TO STATEMENT 450 PREPARES FOR A RESTART AFTER BOMBING   MAIN.930
C*****OUT DUE TO WITMAX .GT. 0.6.                                       MAIN.931
C                                                                       MAIN.932
 430  DVOLV=4.0*DVOL*X2                                                 MAIN.933
      DELMM=4.0*(MOLD1-M(JW,IW))*X3                                     MAIN.934
      C1=DT222*E(JW,IW)/((AMIN1(DELY,DELX(IW)))**2)                     MAIN.935
      ICYCLE=ICYCLE+1                                                   MAIN.936
```

```
      WRITE(6,6) ICYC2H,WITENO,JW,IW,ICYCLE,DT,C1,DVOLV,DELMM                MAIN.937
      DT=DT2H/1.5                                                            MAIN.938
      DTS=DT2H                                                               MAIN.939
      DT2H=DT                                                                MAIN.940
      DTT2=2.0*DT                                                            MAIN.941
      DT22=0.5*DT                                                            MAIN.942
      DT222=DT*DT*10./9.                                                     MAIN.943
      NSAVE=0                                                                MAIN.944
      TIME=TIME2H                                                            MAIN.945
      ICYCLE=ICYC2H                                                          MAIN.946
      DO 440 I=1,LEZ                                                         MAIN.947
      L=LM1(I)                                                               MAIN.948
      Y(1,I)=Y2H(1,I)                                                        MAIN.949
      V(1,I)=V2H(1,I)                                                        MAIN.950
      DO 440 J=1,L                                                           MAIN.951
      Y(J+1,I)=Y2H(J+1,I)                                                    MAIN.952
      V(J+1,I)=V2H(J+1,I)                                                    MAIN.953
      U(J,I)=U2H(J,I)                                                        MAIN.954
      E(J,I)=E2H(J,I)                                                        MAIN.955
      RHO(J,I)=RHO2H(J,I)                                                    MAIN.956
      QE(J,I)=QE2H(J,I)                                                      MAIN.957
      QL(J,I)=QL2H(J,I)                                                      MAIN.958
      VOL(J,I)=DXSQ(I)*(Y(J+1,I)-Y(J,I))                                     MAIN.959
      M(J,I)=RHO(J,I)*VOL(J,I)                                               MAIN.960
      P(J,I)=QL(J,I)+2./3.*RHO(J,I)*E(J,I)                                   MAIN.961
      Z(J,I)=QE(J,I)+2./3.*RHO(J,I)*E(J,I)                                   MAIN.962
      H(J,I)=M(J,I)*U(J,I)                                                   MAIN.963
      MDOT(J,I)=0.0                                                          MAIN.964
      EDOT(J,I)=0.0                                                          MAIN.965
      HDOT(J,I)=0.0                                                          MAIN.966
440   DELV(J+1,I)=0.0                                                        MAIN.967
      IF(DT.LT.DTLIM) GO TO 460                                              MAIN.968
      CALL SECOND(X1)                                                        MAIN.969
      IF(X1.LT.TIMLMT) GO TO 220                                             MAIN.970
450   WRITE(6,4)                                                             MAIN.971
      GO TO 470                                                              MAIN.972
```

```
460   WRITE(6,3) DTLIM                                          MAIN.973
470   NOUT=2                                                    MAIN.974
      ITAPE=ITAPE1                                              MAIN.975
      IPRINT=IPRNT1                                             MAIN.976
      GO TO 390                                                 MAIN.977
      END                                                       MAIN.978
```

```
      SUBROUTINE ADJUST(IMAZ,JMAX,IMAX,LM1,LMAZ1,X,Y,V,U,RHO,E,QE,QL,M,   ADJUST.001
     1VOL,H,PPURE,P,Z)                                                    ADJUST.002
C                                                                         ADJUST.003
C*****THIS SUBROUTINE CONTROLS THE GRID MANIPULATION.                     ADJUST.004
C*****IT CALLS THE SUBROUTINES WHICH ACTUALLY DO THE COURSE REZONING       ADJUST.005
C*****AND CHOPPING.  IT CHECKS ON THE POSITION OF THE CLOUD RELATIVE TO   ADJUST.006
C*****YCHOP.                                                              ADJUST.007
C                                                                         ADJUST.008
      IMPLICIT REAL(M)                                                    ADJUST.009
      DIMENSION LM1(IMAZ),LMAZ1(IMAZ),X(IMAX),Y(JMAX,IMAZ),V(JMAX,IMAZ),  ADJUST.010
     1U(JMAX,IMAZ),RHO(JMAX,IMAZ),E(JMAX,IMAZ),QE(JMAX,IMAZ),            ADJUST.011
     2QL(JMAX,IMAZ),M(JMAX,IMAZ),VOL(JMAX,IMAZ),H(JMAX,IMAZ),            ADJUST.012
     3PPURE(JMAX,IMAZ),P(JMAX,IMAZ),Z(JMAX,IMAZ)                         ADJUST.013
      COMMON DY1,LEZ,ECHOP,EREZON,NOUT,IPRINT,ITAPE,GM,YZERO              ADJUST.014
      DATA IREAD/1/                                                       ADJUST.015
C                                                                         ADJUST.016
C*****COMBINE SMALL CELLS IN PAIRS OR QUADRUPLES.                         ADJUST.017
C                                                                         ADJUST.018
      CALL REZONE(1,IMAZ,JMAX,IMAX,LM1,LMAZ1,X,Y,V,U,RHO,E,QE,QL,M,VOL,   ADJUST.019
     1H,PPURE,P,Z)                                                        ADJUST.020
      ILG=0                                                               ADJUST.021
      DO 20 I=2,LEZ                                                       ADJUST.022
      CALL REZONE(I,IMAZ,JMAX,IMAX,LM1,LMAZ1,X,Y,V,U,RHO,E,QE,QL,M,VOL,   ADJUST.023
     1H,PPURE,P,Z)                                                        ADJUST.024
      IF(LM1(I).GT.LM1(1))                                                ADJUST.025
     1CALL REZONE(I,IMAZ,JMAX,IMAX,LM1,LMAZ1,X,Y,V,U,RHO,E,QE,QL,M,VOL,  ADJUST.026
     1H,PPURE,P,Z)                                                        ADJUST.027
      IF(LM1(I).LT.ILG) GO TO 20                                          ADJUST.028
      NLG=I                                                               ADJUST.029
      ILG=LM1(I)                                                          ADJUST.030
   20 CONTINUE                                                            ADJUST.031
C                                                                         ADJUST.032
C*****CHECK TO SEE IF CHOPPING IS NECESSARY TO CONTINUE THE EVOLUTION,    ADJUST.033
C*****OR IF REZONING WAS ENOUGH.                                          ADJUST.034
C                                                                         ADJUST.035
      IF(IREAD.GT.0) READ(5,30) FCHOP,CHECK,LEFT                          ADJUST.036
```

```
   30   FORMAT(2E10.3,I5)                                                    ADJUST.037
        IREAD=0                                                              ADJUST.038
        WRITE(6,31) FCHOP,CHECK,LEFT                                         ADJUST.039
   31   FORMAT(8H0FCHOP =,1PE10.3,5X,7HCHECK =,E10.3,5X,6HLEFT =,I3)         ADJUST.040
        IF(LMAZ1(NLG)-ILG.GT.LEFT) RETURN                                    ADJUST.041
C                                                                            ADJUST.042
C*****CHECK TO SEE IF CHOPPING CAN OCCUR WITHOUT AFFECTING CLOUD.            ADJUST.043
C                                                                            ADJUST.044
        YCHOP=FCHOP*(Y(LM1(1)+1,1)-Y(1,1))+Y(1,1)                            ADJUST.045
        YCHECK=CHECK*(Y(LM1(1)+1,1)-Y(1,1))+Y(1,1)                           ADJUST.046
        LL=LMAZ1(1)                                                          ADJUST.047
        DO 40 J=1,LL                                                         ADJUST.048
        IF(YCHECK.LT.Y(J,1)) GO TO 41                                        ADJUST.049
        JS=J                                                                 ADJUST.050
   40   CONTINUE                                                             ADJUST.051
   41   IF(RHO(JS,1).LT.RHO(JMAX,IMAZ)) GO TO 60                             ADJUST.052
        WRITE(6,42) YCHOP                                                    ADJUST.053
   42   FORMAT(22H1CHOPPING WITH YCHOP =,1PE10.3,32H MAY GET TOO CLOSE TO    ADJUST.054
       1THE CLOUD.)                                                          ADJUST.055
        NOUT=2                                                               ADJUST.056
        IPRINT=1000000                                                       ADJUST.057
        ITAPE=1000000                                                        ADJUST.058
        RETURN                                                               ADJUST.059
C                                                                            ADJUST.060
C*****CHOP OFF THE BACK END OF THE GRID.                                     ADJUST.061
C                                                                            ADJUST.062
   60   WRITE(6,61) YCHOP                                                    ADJUST.063
        CALL CHOP(YCHOP,IMAZ,JMAX,IMAX,LM1,LMAZ1,X,Y,V,U,RHO,E,QE,QL,M,VOL   ADJUST.064
       1,H,PPURE,P,Z)                                                        ADJUST.065
   61   FORMAT(26H0ENTERED CHOP WITH YCHOP =,1PE10.3)                        ADJUST.066
        RETURN                                                               ADJUST.067
        END                                                                  ADJUST.068
```

```
      SUBROUTINE REZONE(I,IMAZ,JMAX,IMAX,LM1,LMAZ1,X,Y,V,U,RHO,E,QE,QL,  REZONE.001
     1M,VOL,H,PPURE,P,Z)                                                 REZONE.002
C                                                                        REZONE.003
C*****THIS SUBROUTINE DOES THE COURSE REZONING.                          REZONE.004
C                                                                        REZONE.005
      IMPLICIT REAL (M)                                                  REZONE.006
      DIMENSION LM1(IMAZ),LMAZ1(IMAZ),X(IMAX),Y(JMAX,IMAZ),V(JMAX,IMAZ), REZONE.007
     1U(JMAX,IMAZ),RHO(JMAX,IMAZ),E(JMAX,IMAZ),QE(JMAX,IMAZ),            REZONE.008
     2QL(JMAX,IMAZ),M(JMAX,IMAZ),VOL(JMAX,IMAZ),H(JMAX,IMAZ),            REZONE.009
     3PPURE(JMAX,IMAZ),P(JMAX,IMAZ),Z(JMAX,IMAZ)                         REZONE.010
      COMMON DY1,LEZ,ECHOP,EREZON,NOUT,IPRINT,ITAPE,GM,YZERO             REZONE.011
      LMAZ=LMAZ1(I)                                                      REZONE.012
      DYLIM1=0.55*DY1                                                    REZONE.013
C                                                                        REZONE.014
C*****REZONING.                                                          REZONE.015
C                                                                        REZONE.016
      INUM=0                                                             REZONE.017
      ILM1=0                                                             REZONE.018
      DO 174 J=1,LMAZ                                                    REZONE.019
      JS=J                                                               REZONE.020
      IF(Y(J+1+INUM,I)-Y(J+INUM,I).LT.DYLIM1) GO TO 1                    REZONE.021
C                                                                        REZONE.022
C*****SHIFT CELLS INUM SPACES DOWN IN THE ARRAYS.                        REZONE.023
C                                                                        REZONE.024
      Y(J+1,I)=Y(J+1+INUM,I)                                             REZONE.025
      V(J+1,I)=V(J+1+INUM,I)                                             REZONE.026
      U(J,I)=U(J+INUM,I)                                                 REZONE.027
      RHO(J,I)=RHO(J+INUM,I)                                             REZONE.028
      E(J,I)=E(J+INUM,I)                                                 REZONE.029
      QE(J,I)=QE(J+INUM,I)                                               REZONE.030
      QL(J,I)=QL(J+INUM,I)                                               REZONE.031
      H(J,I)=H(J+INUM,I)                                                 REZONE.032
      P(J,I)=P(J+INUM,I)                                                 REZONE.033
      Z(J,I)=Z(J+INUM,I)                                                 REZONE.034
      M(J,I)=M(J+INUM,I)                                                 REZONE.035
      PPURE(J,I)=PPURE(J+INUM,I)                                         REZONE.036
```

```
      VOL(J,I)=VOL(J+INUM,I)                                                    REZONE.037
      GO TO 3                                                                   REZONE.038
C                                                                               REZONE.039
C*****COMBINE CELLS (J+INUM,I) AND (J+1+INUM,I).                                REZONE.040
C                                                                               REZONE.041
    1 M12=M(J+1+INUM,I)+M(J+INUM,I)                                             REZONE.042
      X1=1.0/M12                                                                REZONE.043
      Y(J+1,I)=Y(J+2+INUM,I)                                                    REZONE.044
      IF(V(J+1+INUM,I)*V(J+2+INUM,I).LE.0.0) GO TO 178                          REZONE.045
      TEMP=((M12*V(J+1+INUM,I)**2                                               REZONE.046
     1+(M(J+1+INUM,I)+M(J+2+INUM,I))*V(J+2+INUM,I)**2                           REZONE.047
     1-M(J+1+INUM,I)*V(J+INUN,I)**2)/(M12+M(J+2+INUM,I)))                       REZONE.048
      IF(TEMP.LT.0.0) GO TO 178                                                 REZONE.049
      IF(V(J+1+INUM,I).GT.0..OR.V(J+2+INUM,I).GT.0.) V(J+1,I)=SQRT(TEMP)        REZONE.050
      IF(V(J+1+INUM,I).LE.0.0) V(J+1,I)=-SQRT(TEMP)                             REZONE.051
      GO TO 180                                                                 REZONE.052
  178 V(J+1,I)=(M12*V(J+1+INUM,I)+(M(J+1+INUM,I)+M(J+2+INUM,I))                 REZONE.053
     1*V(J+2+INUM,I)-M(J+1+INUM,I)*V(J+INUM,I))/(M12+M(J+2+INUM,I))             REZONE.054
  180 IF(U(J+INUM,I)*U(J+1+INUM,I).LT.0.0) GO TO 182                            REZONE.055
      IF(U(J+INUM,I).GT.0.0.OR.U(J+1+INUM,I).GT.0.0) U(J,I)=SQRT((              REZONE.056
     1M(J+INUM,I)*U(J+INUM,I)**2+M(J+1+INUM,I)*U(J+1+INUM,I)**2)*X1)            REZONE.057
      IF(U(J+INUM,I).LE.0.0) U(J,I)=-SQRT((                                     REZONE.058
     1M(J+INUM,I)*U(J+INUM,I)**2+M(J+1+INUM,I)*U(J+1+INUM,I)**2)*X1)            REZONE.059
      GO TO 184                                                                 REZONE.060
  182 U(J,I)=(M(J+INUM,I)*U(J+INUM,I)+M(J+1+INUM,I)*U(J+1+INUM,I))*X1           REZONE.061
  184 E(J,I)=(E(J+INUM,I)*M(J+INUM,I)+E(J+1+INUM,I)*M(J+1+INUM,I))*X1           REZONE.062
      VOL(J,I)=VOL(J+INUM,I)+VOL(J+1+INUM,I)                                    REZONE.063
      M(J,I)=M12                                                                REZONE.064
      RHO(J,I)=M12/VOL(J,I)                                                     REZONE.065
      H(J,I)=M12*U(J,I)                                                         REZONE.066
      QE(J,I)=AMIN1(QE(J+INUM,I),QE(J+1+INUM,I))                                REZONE.067
      QL(J,I)=AMIN1(QL(J+INUM,I),QL(J+1+INUM,I))                                REZONE.068
      PPURE(J,I)=(2./3.)*RHO(J,I)*E(J,I)                                        REZONE.069
      P(J,I)=PPURE(J,I)+QL(J,I)                                                 REZONE.070
      Z(J,I)=PPURE(J,I)+QE(J,I)                                                 REZONE.071
      INUM=INUM+1                                                               REZONE.072
```

```
      IF(J+INUM.LT.LM1(I)) ILM1=ILM1+1                                  REZONE.073
    3 IF(J+INUM+2.GT.LMAZ) GO TO 4                                      REZONE.074
  174 CONTINUE                                                          REZONE.075
C                                                                       REZONE.076
C*****ADD ON NEW CELLS TO THE TOP OF THE GRID.                          REZONE.077
C                                                                       REZONE.078
    4 JS=JS+1                                                           REZONE.079
      DO 5 J=JS,LMAZ                                                    REZONE.080
      Y(J+1,I)=Y(J,I)+DY1                                               REZONE.081
      V(J+1,I)=0.0                                                      REZONE.082
      U(J,I)=0.0                                                        REZONE.083
      RHO(J,I)=RHO(JMAX,1)                                              REZONE.084
      E(J,I)=E(JMAX,1)                                                  REZONE.085
      QE(J,I)=0.0                                                       REZONE.086
      QL(J,I)=0.0                                                       REZONE.087
      PPURE(J,I)=(2./3.)*E(J,I)*RHO(J,I)                                REZONE.088
      P(J,I)=PPURE(J,I)                                                 REZONE.089
      Z(J,I)=PPURE(J,I)                                                 REZONE.090
      VOL(J,I)=3.1415926535897*(X(I+1)+X(I))*(X(I+1)-X(I))*(Y(J+1,I)-Y(J REZONE.091
     1,I))                                                              REZONE.092
      M(J,I)=VOL(J,I)*RHO(J,I)                                          REZONE.093
      H(J,I)=0.0                                                        REZONE.094
      EREZON=EREZON+M(J,I)*(E(J,I)-GM/SQRT((YZERO+0.5*(Y(J+1,I)+Y(J,I))) REZONE.095
     1**2+0.25*(X(I+1)+X(I))**2))                                       REZONE.096
    5 CONTINUE                                                          REZONE.097
      VOL(JMAX,I)=3.1415926535897*(X(I+1)+X(I))*(X(I+1)-X(I))*DY1       REZONE.098
      M(JMAX,I)=RHO(JMAX,I)*VOL(JMAX,I)                                 REZONE.099
      LM1(I)=LM1(I)-ILM1                                                REZONE.100
      RETURN                                                            REZONE.101
      END                                                               REZONE.102
```

```
      SUBROUTINE CHOP(YCHOP,IMAZ,JMAX,IMAX,LM1,LMAZ1,X,Y,V,U,RHO,E,QE,QL    CHOP.001
     1,M,VOL,H,PPURE,P,Z)                                                  CHOP.002
C                                                                          CHOP.003
C*****THIS SUBROUTINE DOES THE CHOPPING.                                   CHOP.004
C                                                                          CHOP.005
      IMPLICIT REAL(M)                                                     CHOP.006
      DIMENSION LM1(IMAZ),LMAZ1(IMAZ),X(IMAX),Y(JMAX,IMAZ),V(JMAX,IMAZ),   CHOP.007
     1U(JMAX,IMAZ),RHO(JMAX,IMAZ),E(JMAX,IMAZ),QE(JMAX,IMAZ),              CHOP.008
     2QL(JMAX,IMAZ),M(JMAX,IMAZ),VOL(JMAX,IMAZ),H(JMAX,IMAZ),              CHOP.009
     3PPURE(JMAX,IMAZ),P(JMAX,IMAZ),Z(JMAX,IMAZ)                           CHOP.010
      COMMON DY1,LEZ,ECHOP,EREZON,NOUT,IPRINT,ITAPE,GM,YZERO               CHOP.011
      DO 10 I=1,IMAZ                                                       CHOP.012
C                                                                          CHOP.013
C*****FIND WHICH CELL YCHOP CROSSES.                                       CHOP.014
C                                                                          CHOP.015
      L=LMAZ1(I)                                                           CHOP.016
      LLL=L-4                                                              CHOP.017
      IF(Y(1,I).LT.YCHOP) GO TO 2                                          CHOP.018
      WRITE(6,4) I                                                         CHOP.019
   4  FORMAT(5H0Y(1,,I3,24H) IS GREATER THAN YCHOP.)                       CHOP.020
      NOUT=2                                                               CHOP.021
      IPRINT=1000000                                                       CHOP.022
      ITAPE=1000000                                                        CHOP.023
      RETURN                                                               CHOP.024
   2  DO 1 J=1,LLL                                                         CHOP.025
      JCHOP=J                                                              CHOP.026
      IF(Y(J+1,I).GT.YCHOP) GO TO 3                                        CHOP.027
   1  CONTINUE                                                             CHOP.028
      WRITE(6,5) J,I                                                       CHOP.029
   5  FORMAT(3H0Y(,I3,1H,I3,21H) IS LESS THAN YCHOP.)                      CHOP.030
      NOUT=2                                                               CHOP.031
      IPRINT=1000000                                                       CHOP.032
      ITAPE=1000000                                                        CHOP.033
      RETURN                                                               CHOP.034
C                                                                          CHOP.035
C*****KEEP TRACK OF THE ENERGY LOST DUE TO CHOPPING.                       CHOP.036
```

```
C                                                                       CHOP.037
    3  DO 9 J=1,JCHOP                                                   CHOP.038
       MASS=M(J,I)                                                      CHOP.039
       VTOP=V(J+1,I)                                                    CHOP.040
       YTOP=Y(J+1,I)                                                    CHOP.041
       IF(J.LT.JCHOP) GO TO 12                                          CHOP.042
       MASS=M(J,I)*(YCHOP-Y(J,I))/(Y(J+1,I)-Y(J,I))                     CHOP.043
       VTOP=(V(JCHOP+1,I)-V(JCHOP,I))/(Y(JCHOP+1,I)                     CHOP.044
      1-Y(JCHOP,I))*(YCHOP-Y(JCHOP+1,I))+V(JCHOP+1,I)                   CHOP.045
       YTOP=YCHOP                                                       CHOP.046
   12  CONTINUE                                                         CHOP.047
       ECHOP=ECHOP+MASS*(E(J,I)+0.5*U(J,I)**2+0.25*(V(J,I)**2+VTOP**2   CHOP.048
      1)-GM/SQRT((YZERO+0.5*(YTOP+Y(J,I)))**2+0.25*(X(I+1)+X(I))**2))  CHOP.049
    9  CONTINUE                                                         CHOP.050
C                                                                       CHOP.051
C*****MOVE OLD CELLS DOWN IN THE ARRAYS.                                CHOP.052
C                                                                       CHOP.053
       Y(1,I)=YCHOP                                                     CHOP.054
       V(1,I)=VTOP                                                      CHOP.055
       Y(2,I)=Y(JCHOP+2,I)                                              CHOP.056
       V(2,I)=V(JCHOP+2,I)                                              CHOP.057
       RATIO=((Y(JCHOP+1,I)-YCHOP)/(Y(JCHOP+1,I)-Y(JCHOP,I)))           CHOP.058
       VOL(1,I)=VOL(JCHOP+1,I)+VOL(JCHOP,I)*RATIO                       CHOP.059
       M(1,I)=M(JCHOP+1,I)+M(JCHOP,I)*RATIO                             CHOP.060
       RHO(1,I)=M(1,I)/VOL(1,I)                                         CHOP.061
       E(1,I)=(M(JCHOP+1,I)*E(JCHOP+1,I)+M(JCHOP,I)*RATIO*E(JCHOP,I))/  CHOP.062
      1M(1,I)                                                           CHOP.063
       U(1,I)=(M(JCHOP+1,I)*U(JCHOP+1,I)+M(JCHOP,I)*RATIO*U(JCHOP,I))/  CHOP.064
      1M(1,I)                                                           CHOP.065
       QE(1,I)=AMIN1(QE(JCHOP+1,I),QE(JCHOP,I))                         CHOP.066
       QL(1,I)=AMIN1(QL(JCHOP+1,I),QL(JCHOP,I))                         CHOP.067
       H(1,I)=M(1,I)*U(1,I)                                             CHOP.068
       PPURE(1,I)=(2./3.)*E(1,I)*RHO(1,I)                               CHOP.069
       P(1,I)=PPURE(1,I)+QL(1,I)                                        CHOP.070
       Z(1,I)=PPURE(1,I)+QE(1,I)                                        CHOP.071
       JC=JCHOP+2                                                       CHOP.072
```

```
      DO 6 J=JC,L                                                        CHOP.073
      Y(J+1-JCHOP,I)=Y(J+1,I)                                            CHOP.074
      V(J+1-JCHOP,I)=V(J+1,I)                                            CHOP.075
      U(J-JCHOP,I)=U(J,I)                                                CHOP.076
      RHO(J-JCHOP,I)=RHO(J,I)                                            CHOP.077
      E(J-JCHOP,I)=E(J,I)                                                CHOP.078
      QE(J-JCHOP,I)=QE(J,I)                                              CHOP.079
      QL(J-JCHOP,I)=QL(J,I)                                              CHOP.080
      PPURE(J-JCHOP,I)=PPURE(J,I)                                        CHOP.081
      P(J-JCHOP,I)=P(J,I)                                                CHOP.082
      Z(J-JCHOP,I)=Z(J,I)                                                CHOP.083
      VOL(J-JCHOP,I)=VOL(J,I)                                            CHOP.084
      M(J-JCHOP,I)=M(J,I)                                                CHOP.085
      H(J-JCHOP,I)=H(J,I)                                                CHOP.086
    6 CONTINUE                                                           CHOP.087
C                                                                        CHOP.088
C*****ADD NEW CELLS AT THE TOP OF THE GRID.                              CHOP.089
C                                                                        CHOP.090
      LP1=L+1                                                            CHOP.091
      LPC=L+JCHOP                                                        CHOP.092
      DO 7 J=LP1,LPC                                                     CHOP.093
      Y(J+1-JCHOP,I)=Y(J-JCHOP,I)+DY1                                    CHOP.094
      V(J+1-JCHOP,I)=0.0                                                 CHOP.095
      U(J-JCHOP,I)=0.0                                                   CHOP.096
      RHO(J-JCHOP,I)=RHO(JMAX,IMAZ)                                      CHOP.097
      E(J-JCHOP,I)=E(JMAX,IMAZ)                                          CHOP.098
      QE(J-JCHOP,I)=0.0                                                  CHOP.099
      QL(J-JCHOP,I)=0.0                                                  CHOP.100
      PPURE(J-JCHOP,I)=(2./3.)*RHO(JMAX,IMAZ)*E(JMAX,IMAZ)               CHOP.101
      P(J-JCHOP,I)=PPURE(J-JCHOP,I)                                      CHOP.102
      Z(J-JCHOP,I)=PPURE(J-JCHOP,I)                                      CHOP.103
      VOL(J-JCHOP,I)=VOL(L+1,I)                                          CHOP.104
      M(J-JCHOP,I)=M(L+1,I)                                              CHOP.105
      H(J-JCHOP,I)=0.0                                                   CHOP.106
      ECHOP=ECHOP-M(J-JCHOP,I)*(E(JMAX,IMAZ)-GM/((YZERO+0.5*(Y(J+1-JCHOP CHOP.107
     1,I)+Y(J-JCHOP,I)))**2+0.25*(X(I+1)+X(I))**2))                      CHOP.108
```

```
    7  CONTINUE                                                    CHOP.109
       LM1(I)=MAX0(LM1(I)-JCHOP,4)                                 CHOP.110
   10  CONTINUE                                                    CHOP.111
       RETURN                                                      CHOP.112
       END                                                         CHOP.113
```

```
      SUBROUTINE PLOTER(IMAZ,JMAX,IMAX,LM1,LMAZ1,X,Y,V,U,RHO,E,PPURE,    PLOTER.001
     1RHOP,VP,YP,EP)                                                     PLOTER.002
C                                                                        PLOTER.003
C*****THIS SUBROUTINE PREPS THE DATA FOR MAKING PRINTER PLOTS AND ALSO   PLOTER.004
C*****DOES THE ACTUAL PRINTING.                                          PLOTER.005
C                                                                        PLOTER.006
      DIMENSION LM1(IMAZ),LMAZ1(IMAZ),Y(JMAX,IMAZ),V(JMAX,IMAZ),         PLOTER.007
     1U(JMAX,IMAZ),RHO(JMAX,IMAZ),E(JMAX,IMAZ),PPURE(JMAX,IMAZ),        PLOTER.008
     2RHOP(JMAX,IMAZ),VP(JMAX,IMAZ),EP(JMAX,IMAZ),                      PLOTER.009
     3X(IMAX),YP(JMAX,IMAZ)                                             PLOTER.010
      DIMENSION YGRID(127),F(127,40)                                     PLOTER.011
      COMMON DY1,LEZ                                                     PLOTER.012
C                                                                        PLOTER.013
C*****FIND THE MAXIMUM Y AND THE MAXIMUM LMAZ1(I).                       PLOTER.014
C                                                                        PLOTER.015
      LMX2=0                                                             PLOTER.016
      YMAX=0.0                                                           PLOTER.017
      DO 10 I=1,IMAZ                                                     PLOTER.018
      YMAX=AMAX1(YMAX,Y(LM1(I)+1,I))                                     PLOTER.019
      LMX2=MAX0(LMX2,LMAZ1(I))                                           PLOTER.020
   10 CONTINUE                                                           PLOTER.021
C                                                                        PLOTER.022
C*****READ IN A CARD CONTAINING PLOT INFORMATION.                        PLOTER.023
C                                                                        PLOTER.024
      DATA IREAD/1/                                                      PLOTER.025
      IF(IREAD.GT.0) READ(5,15) NSYM,LOGV,LOGRHO,LOGE,LOGP,VMIN          PLOTER.026
   15 FORMAT(5I5,E10.3)                                                  PLOTER.027
      IREAD=0                                                            PLOTER.028
C                                                                        PLOTER.029
C*****PREP THE DATA.                                                     PLOTER.030
C                                                                        PLOTER.031
      ASQ=SQRT(E(JMAX,IMAZ)*10./9.)*VMIN                                 PLOTER.032
      DO 20 I=1,IMAZ                                                     PLOTER.033
      DO 20 J=1,LMX2                                                     PLOTER.034
      YP(J,I)=0.5*(Y(J,I)+Y(J+1,I))                                      PLOTER.035
      VP(J,I)=AMAX1(ASQ,SQRT(U(J,I)**2+0.5*(V(J+1,I)**2+V(J,I)**2)))     PLOTER.036
```

```
      IF(LOGV.GT.0) VP(J,I)=ALOG10(VP(J,I))                              PLOTER.037
      RHOP(J,I)=RHO(J,I)/(1.298*1.66043E-24)                             PLOTER.038
      IF(LOGRHO.GT.0) RHOP(J,I)=ALOG10(RHOP(J,I))                        PLOTER.039
      EP(J,I)=E(J,I)/E(JMAX,IMAZ)                                        PLOTER.040
      IF(LOGE.GT.0) EP(J,I)=ALOG10(EP(J,I))                              PLOTER.041
   20 CONTINUE                                                           PLOTER.042
C                                                                        PLOTER.043
C*****PRINT OUT THE PLOT INFORMATION.                                    PLOTER.044
C                                                                        PLOTER.045
      WRITE(6,41) YMAX,Y(1,1),NSYM                                       PLOTER.046
   41 FORMAT(7H0YMAX =,1PE10.3,5X,6HYMIN =,E10.3,5X,30HNUMBER OF DIFFERE PLOTER.047
     1NT SYMBOLS IS,I3)                                                  PLOTER.048
C                                                                        PLOTER.049
C*****SET UP THE EULERIAN GRID.                                          PLOTER.050
C                                                                        PLOTER.051
      DY=X(2)-X(1)                                                       PLOTER.052
      LMX1=IFIX(((YMAX-Y(1,1))/DY)+0.5)                                  PLOTER.053
      IF(LMX1.LT.128) GO TO 25                                           PLOTER.054
      WRITE(6,42)                                                        PLOTER.055
   42 FORMAT(45H0THE Y AXIS IS COMPRESSED TO FIT ON THE PAGE.)           PLOTER.056
      DY=(YMAX-Y(1,1))/127.0                                             PLOTER.057
      LMX1=127                                                           PLOTER.058
   25 CONTINUE                                                           PLOTER.059
      YGRID(1)=Y(1,1)+0.5*DY                                             PLOTER.060
      DO 30 J=2,LMX1                                                     PLOTER.061
      YGRID(J)=YGRID(J-1)+DY                                             PLOTER.062
   30 CONTINUE                                                           PLOTER.063
C                                                                        PLOTER.064
C*****PLOT THE VELOCITIES ON THE PRINTER.                                PLOTER.065
C                                                                        PLOTER.066
      CALL REGRID(IMAZ,JMAX,IMAZ,LMX1,LMAZ1,YP,YGRID,VP,F)              PLOTER.067
      CALL PRPL(IMAZ,LMX1,F,FMAX,FMIN,NSYM)                              PLOTER.068
      IF(LOGV.GT.0) WRITE(6,50) FMAX,FMIN                                PLOTER.069
   50 FORMAT(26H1LOG VELOCITY WITH MAX OF ,1PE10.3,9H, MIN OF ,E10.3,/)  PLOTER.070
      IF(LOGV.LT.1) WRITE(6,51) FMAX,FMIN                                PLOTER.071
   51 FORMAT(22H1VELOCITY WITH MAX OF ,1PE10.3,9H, MIN OF ,E10.3,/)      PLOTER.072
```

```
      DO 52 I=1,IMAZ                                                    PLOTER.073
      WRITE(6,53) I,(F(J,I),J=1,LMX1)                                   PLOTER.074
   52 CONTINUE                                                          PLOTER.075
   53 FORMAT(1X,I2,1X,127A1)                                            PLOTER.076
C                                                                       PLOTER.077
C*****PLOT THE DENSITIES ON THE PRINTER.                                PLOTER.078
C                                                                       PLOTER.079
      CALL REGRID(IMAZ,JMAX,IMAZ,LMX1,LMAZ1,YP,YGRID,RHOP,F)            PLOTER.080
      CALL PRPL(IMAZ,LMX1,F,FMAX,FMIN,NSYM)                             PLOTER.081
      IF(LOGRHO.GT.0) WRITE(6,60) FMAX,FMIN                             PLOTER.082
   60 FORMAT(25H1LOG DENSITY WITH MAX OF ,1PE10.3,9H, MIN OF ,E10.3,/)  PLOTER.083
      IF(LOGRHO.LT.1) WRITE(6,61) FMAX,FMIN                             PLOTER.084
   61 FORMAT(21H1DENSITY WITH MAX OF ,1PE10.3,9H, MIN OF ,E10.3,/)      PLOTER.085
      DO 62 I=1,IMAZ                                                    PLOTER.086
      WRITE(6,53) I,(F(J,I),J=1,LMX1)                                   PLOTER.087
   62 CONTINUE                                                          PLOTER.088
C                                                                       PLOTER.089
C*****PLOT THE ENERGIES ON THE PRINTER.                                 PLOTER.090
C                                                                       PLOTER.091
      CALL REGRID(IMAZ,JMAX,IMAZ,LMX1,LMAZ1,YP,YGRID,EP,F)              PLOTER.092
      CALL PRPL(IMAZ,LMX1,F,FMAX,FMIN,NSYM)                             PLOTER.093
      IF(LOGE.GT.0) WRITE(6,70) FMAX,FMIN                               PLOTER.094
   70 FORMAT(24H1LOG ENERGY WITH MAX OF ,1PE10.3,9H, MIN OF ,E10.3,/)   PLOTER.095
      IF(LOGE.LT.1) WRITE(6,71) FMAX,FMIN                               PLOTER.096
   71 FORMAT(20H1ENERGY WITH MAX OF ,1PE10.3,9H, MIN OF ,E10.3,/)       PLOTER.097
      DO 72 I=1,IMAZ                                                    PLOTER.098
      WRITE(6,53) I,(F(J,I),J=1,LMX1)                                   PLOTER.099
   72 CONTINUE                                                          PLOTER.100
C                                                                       PLOTER.101
C*****PLOT THE PRESSURES ON THE PRINTER.                                PLOTER.102
C                                                                       PLOTER.103
      DO 75 I=1,IMAZ                                                    PLOTER.104
      DO 75 J=1,LMX2                                                    PLOTER.105
      EP(J,I)=PPURE(J,I)*3.0/(2.0*RHO(JMAX,IMAZ)*E(JMAX,IMAZ))          PLOTER.106
      IF(LOGP.GT.0) EP(J,I)=ALOG10(EP(J,I))                             PLOTER.107
   75 CONTINUE                                                          PLOTER.108
```

```
      CALL REGRID(IMAZ,JMAX,IMAZ,LMX1,LMAZ1,YP,YGRID,EP,F)                PLOTER.109
      CALL PRPL(IMAZ,LMX1,F,FMAX,FMIN,NSYM)                               PLOTER.110
      IF(LOGP.GT.0) WRITE(6,80) FMAX,FMIN                                 PLOTER.111
   80 FORMAT(26H1LOG PRESSURE WITH MAX OF ,1PE10.3,9H, MIN OF ,E10.3,/)   PLOTER.112
      IF(LOGP.LT.1) WRITE(6,81) FMAX,FMIN                                 PLOTER.113
   81 FORMAT(22H1PRESSURE WITH MAX OF ,1PE10.3,9H, MIN OF ,E10.3,/)       PLOTER.114
      DO 82 I=1,IMAZ                                                      PLOTER.115
      WRITE(6,53) I,(F(J,I),J=1,LMX1)                                     PLOTER.116
   82 CONTINUE                                                            PLOTER.117
      DO 90 I=1,IMAZ                                                      PLOTER.118
      DO 90 J=1,LMX2                                                      PLOTER.119
      VP(J,I)=0.0                                                         PLOTER.120
      RHOP(J,I)=0.0                                                       PLOTER.121
      EP(J,I)=0.0                                                         PLOTER.122
      YP(J,I)=0.0                                                         PLOTER.123
   90 CONTINUE                                                            PLOTER.124
      RETURN                                                              PLOTER.125
      END                                                                 PLOTER.126
```

```
      SUBROUTINE REGRID(IMAZ,JMAX,IPTS,JPTS,LMAZ1,Y,YGRID,F,Q)          REGRID.001
C                                                                       REGRID.002
C*****THIS SUBROUTINE REGRIDS THE DATA FOR MAKING PRINTER PLOTS.        REGRID.003
C                                                                       REGRID.004
      DIMENSION Y(JMAX,IMAZ),YGRID(JPTS),F(JMAX,IMAZ),LMAZ1(IMAZ),      REGRID.005
     1Q(127,IPTS)                                                       REGRID.006
      DO 100 I=1,IPTS                                                   REGRID.007
      L=LMAZ1(I)                                                        REGRID.008
      DO 100 J=1,JPTS                                                   REGRID.009
      IF(YGRID(J).GT.Y(1,I)) GO TO 50                                   REGRID.010
      Q(J,I)=F(1,I)                                                     REGRID.011
      GO TO 100                                                         REGRID.012
   50 DO 53 K=2,L                                                       REGRID.013
      IF(YGRID(J).LT.Y(K,I)) GO TO 55                                   REGRID.014
   53 CONTINUE                                                          REGRID.015
      Q(J,I)=F(L,I)                                                     REGRID.016
      GO TO 100                                                         REGRID.017
   55 Q(J,I)=(F(K,I)-F(K-1,I))/(Y(K,I)-Y(K-1,I))*(YGRID(J)-Y(K,I))+F(K,I REGRID.018
     1)                                                                 REGRID.019
  100 CONTINUE                                                          REGRID.020
      RETURN                                                            REGRID.021
      END                                                               REGRID.022
```

```
      SUBROUTINE PRPL(IPTS,JPTS,F,FMAX,FMIN,NSYM)                       PRPL.001
      DIMENSION F(127,IPTS)                                             PRPL.002
C                                                                       PRPL.003
C*****TAKES F(JPTS,IPTS) AND FINDS FMAX AND FMIN.                       PRPL.004
C*****THEN REPLACES NUMERICAL VALUES OF F WITH THE PROPER SYMBOLS FOR    PRPL.005
C*****USE IN MAKING PRINTER PLOTS.                                      PRPL.006
C*****NSYM IS THE NUMBER OF DIFFERENT SYMBOLS USED.                     PRPL.007
C                                                                       PRPL.008
      FMIN= 1.00E+100                                                   PRPL.009
      FMAX=-1.00E+100                                                   PRPL.010
      DO 100 I=1,IPTS                                                   PRPL.011
      DO 100 J=1,JPTS                                                   PRPL.012
      FMIN=AMIN1(FMIN,F(J,I))                                           PRPL.013
      FMAX=AMAX1(FMAX,F(J,I))                                           PRPL.014
 100  CONTINUE                                                          PRPL.015
C                                                                       PRPL.016
C                                                                       PRPL.017
      IF(FMAX.GT.FMIN) CONST=(FLOAT(NSYM-1)/(FMAX-FMIN))                PRPL.018
      IF(FMAX.LE.FMIN) CONST=1.0                                        PRPL.019
C                                                                       PRPL.020
C                                                                       PRPL.021
      DO 120 I=1,IPTS                                                   PRPL.022
      DO 120 J=1,JPTS                                                   PRPL.023
      INDEX=INT((F(J,I)-FMIN)*CONST+1.0E-12)+1                          PRPL.024
      GO TO (1,2,3,4,5,6,7,8,9,10,11,12,13,14,15,16,17,18,19,20,21,22,  PRPL.025
     123,24,25,26),INDEX                                                PRPL.026
   1  F(J,I)=1HA                                                        PRPL.027
      GO TO 120                                                         PRPL.028
   2  F(J,I)=1HB                                                        PRPL.029
      GO TO 120                                                         PRPL.030
   3  F(J,I)=1HC                                                        PRPL.031
      GO TO 120                                                         PRPL.032
   4  F(J,I)=1HD                                                        PRPL.033
      GO TO 120                                                         PRPL.034
   5  F(J,I)=1HE                                                        PRPL.035
      GO TO 120                                                         PRPL.036
```

```
 6  F(J,I)=1HF                                                    PRPL.037
    GO TO 120                                                     PRPL.038
 7  F(J,I)=1HG                                                    PRPL.039
    GO TO 120                                                     PRPL.040
 8  F(J,I)=1HH                                                    PRPL.041
    GO TO 120                                                     PRPL.042
 9  F(J,I)=1HI                                                    PRPL.043
    GO TO 120                                                     PRPL.044
10  F(J,I)=1HJ                                                    PRPL.045
    GO TO 120                                                     PRPL.046
11  F(J,I)=1HK                                                    PRPL.047
    GO TO 120                                                     PRPL.048
12  F(J,I)=1HL                                                    PRPL.049
    GO TO 120                                                     PRPL.050
13  F(J,I)=1HM                                                    PRPL.051
    GO TO 120                                                     PRPL.052
14  F(J,I)=1HN                                                    PRPL.053
    GO TO 120                                                     PRPL.054
15  F(J,I)=1HO                                                    PRPL.055
    GO TO 120                                                     PRPL.056
16  F(J,I)=1HP                                                    PRPL.057
    GO TO 120                                                     PRPL.058
17  F(J,I)=1HQ                                                    PRPL.059
    GO TO 120                                                     PRPL.060
18  F(J,I)=1HR                                                    PRPL.061
    GO TO 120                                                     PRPL.062
19  F(J,I)=1HS                                                    PRPL.063
    GO TO 120                                                     PRPL.064
20  F(J,I)=1HT                                                    PRPL.065
    GO TO 120                                                     PRPL.066
21  F(J,I)=1HU                                                    PRPL.067
    GO TO 120                                                     PRPL.068
22  F(J,I)=1HV                                                    PRPL.069
    GO TO 120                                                     PRPL.070
23  F(J,I)=1HW                                                    PRPL.071
    GO TO 120                                                     PRPL.072
```

```
 24   F(J,I)=1HX                                              PRPL.073
      GO TO 120                                               PRPL.074
 25   F(J,I)=1HY                                              PRPL.075
      GO TO 120                                               PRPL.076
 26   F(J,I)=1HZ                                              PRPL.077
120   CONTINUE                                                PRPL.078
      RETURN                                                  PRPL.079
      END                                                     PRPL.080
```

```
      SUBROUTINE OUT(IMAZ,JMAX,LM1,Y,V,U,RHO,E,QE,QL,PPURE,M)                OUT.001
C                                                                            OUT.002
C*****THIS SUBROUTINE OUTPUTS NUMERICAL DATA TO THE PRINTER.                 OUT.003
C                                                                            OUT.004
      IMPLICIT REAL (M)                                                      OUT.005
      DIMENSION LM1(IMAZ),Y(JMAX,IMAZ),V(JMAX,IMAZ),U(JMAX,IMAZ),            OUT.006
     1RHO(JMAX,IMAZ),E(JMAX,IMAZ),QE(JMAX,IMAZ),QL(JMAX,IMAZ),              OUT.007
     2PPURE(JMAX,IMAZ),M(JMAX,IMAZ)                                          OUT.008
   11 FORMAT(14H1Y COORDINATES,//,(I4,2X,1P12E10.3))                         OUT.009
   12 FORMAT(20H1VERTICAL VELOCITIES,//,(I4,2X,1P12E10.3))                   OUT.010
   13 FORMAT(22H1HORIZONTAL VELOCITIES,//,(I4,2X,1P12E10.3))                 OUT.011
   14 FORMAT(8H1DENSITY,//,(I4,2X,1P12E10.3))                                OUT.012
   15 FORMAT(16H1INTERNAL ENERGY,//,(I4,2X,1P12E10.3))                       OUT.013
   16 FORMAT(7H1MASSES,//,(I4,2X,1P12E10.3))                                 OUT.014
   17 FORMAT(10H1PRESSURES,//,(I4,2X,1P12E10.3))                             OUT.015
   18 FORMAT(38H1EULERIAN ARTIFICIAL VISCOUS PRESSURES,//,(I4,2X,1P12E10     OUT.016
     1.3))                                                                   OUT.017
   19 FORMAT(40H1LAGRANGIAN ARTIFICIAL VISCOUS PRESSURES,//,(I4,2X,1P12E     OUT.018
     110.3))                                                                 OUT.019
   23 FORMAT(*ISECOND HALF:*,//,(I4,2X,1P12E10.3))                           OUT.020
      L1=MAX0(LM1(1),LM1(2),LM1(3),LM1(4),LM1(5),LM1(6),LM1(7),LM1(8),       OUT.021
     1LM1(9),LM1(10),LM1(11),LM1(12))+1                                      OUT.022
      L2=LM1(13)+1                                                           OUT.023
      WRITE(6,11) (J,(Y(J,I),I=1,12),J=1,L1)                                 OUT.024
      WRITE(6,23) (J,(Y(J,I),I=13,24),J=1,L2)                                OUT.025
      WRITE(6,12) (J,(V(J,I),I=1,12),J=1,L1)                                 OUT.026
      WRITE(6,23) (J,(V(J,I),I=13,24),J=1,L2)                                OUT.027
      WRITE(6,13) (J,(U(J,I),I=1,12),J=1,L1)                                 OUT.028
      WRITE(6,23) (J,(U(J,I),I=13,24),J=1,L2)                                OUT.029
      WRITE(6,14) (J,(RHO(J,I),I=1,12),J=1,L1)                               OUT.030
      WRITE(6,23) (J,(RHO(J,I),I=13,24),J=1,L2)                              OUT.031
      WRITE(6,15) (J,(E(J,I),I=1,12),J=1,L1)                                 OUT.032
      WRITE(6,23) (J,(E(J,I),I=13,24),J=1,L2)                                OUT.033
      WRITE(6,17) (J,(PPURE(J,I),I=1,12),J=1,L1)                             OUT.034
      WRITE(6,23) (J,(PPURE(J,I),I=13,24),J=1,L2)                            OUT.035
      WRITE(6,18) (J,(QE(J,I),I=1,12),J=1,L1)                                OUT.036
```

```
      WRITE(6,23) (J,(QE(J,I),I=13,24),J=1,L2)                    OUT.037
      WRITE(6,19) (J,(QL(J,I),I=1,12),J=1,L1)                     OUT.038
      WRITE(6,23) (J,(QL(J,I),I=13,24),J=1,L2)                    OUT.039
      WRITE(6,16) (J,(M(J,I),I=1,12),J=1,L1)                      OUT.040
      WRITE(6,23) (J,(M(J,I),I=13,24),J=1,L2)                     OUT.041
      RETURN                                                      OUT.042
      END                                                         OUT.043
```